

PURDUE UNIVERSITY
GRADUATE SCHOOL
Thesis/Dissertation Acceptance

This is to certify that the thesis/dissertation prepared

By Damon Russell Fick

Entitled

Experimental Investigation of a Full-Scale Flat-Plate Reinforced Concrete Structure Subjected to Cyclic Lateral Loading in the Inelastic Range of Response

For the degree of Doctor of Philosophy

Is approved by the final examining committee:

Mete A. Sozen

Co- Chair

Michael E. Kreger

Co-Chair

Antonio Bobet

Arvid Johnson

To the best of my knowledge and as understood by the student in the *Research Integrity and Copyright Disclaimer (Graduate School Form 20)*, this thesis/dissertation adheres to the provisions of Purdue University's "Policy on Integrity in Research" and the use of copyrighted material.

Approved by Major Professor(s): Mete A. Sozen

Michael E. Kreger

Approved by: Rao S. Govindaraju

Head of the Graduate Program

June 18, 2008

Date

**PURDUE UNIVERSITY
GRADUATE SCHOOL**

Research Integrity and Copyright Disclaimer

Title of Thesis/Dissertation:

Experimental Investigation of a Full-Scale Flat-Plate Reinforced Concrete Structure Subjected to Cyclic Lateral Loading in the Inelastic Range of Response

For the degree of Doctor of Philosophy

I certify that in the preparation of this thesis, I have observed the provisions of *Purdue University Executive Memorandum No. C-22*, September 6, 1991, *Policy on Integrity in Research*.*

Further, I certify that this work is free of plagiarism and all materials appearing in this thesis/dissertation have been properly quoted and attributed.

I certify that all copyrighted material incorporated into this thesis/dissertation is in compliance with the United States' copyright law and that I have received written permission from the copyright owners for my use of their work, which is beyond the scope of the law. I agree to indemnify and save harmless Purdue University from any and all claims that may be asserted or that may arise from any copyright violation.

Damon Russell Fick

Signature of Candidate

June 18, 2008

Date

*Located at http://www.purdue.edu/policies/pages/teach_res_outreach/c_22.html

EXPERIMENTAL INVESTIGATION OF A FULL-SCALE FLAT-PLATE
REINFORCED CONCRETE STRUCTURE SUBJECTED TO CYCLIC LATERAL
LOADING IN THE INELASTIC RANGE OF RESPONSE

A Dissertation

Submitted to the Faculty

of

Purdue University

by

Damon R. Fick

In Partial Fulfillment of the
Requirements for the Degree

of

Doctor of Philosophy

August 2008

Purdue University

West Lafayette, Indiana

ACKNOWLEDGMENTS

The writer is grateful for the support and guidance of Professors Mete A. Sozen and Michael E. Kreger throughout the study. Special acknowledgement is given to Professors Antonio Bobet and Arvid M. Johnson for serving on the advisory committee.

The author would like to thank the U.S. Army's Construction Engineering Research Laboratory, Hunt Construction, and Jack and Kay Hockema for their generous contributions toward the construction of the test specimen. The assistance of Harry Tidrick in the lab and Sally Shriver in the business office was greatly appreciated. The effort by Matthew Schroeder of Shore Western Manufacturing was a notable contribution to the success of the testing program.

Special recognition is also deserved of many of the author's friends and fellow students in civil engineering. The support of Fabian Consuegra during all phases of instrumentation and testing was invaluable. Preparing the test specimen and data collection during the testing program was made possible by the willing efforts of Jeff Rautenberg, Matt Murray, Rucha Watve, and Tyler Krahn.

Finally the writer would like to sincerely acknowledge the endless support and encouragement from his wife, Andrea.

TABLE OF CONTENTS

| | Page |
|---|------|
| LIST OF TABLES | vi |
| LIST OF FIGURES | vii |
| ABSTRACT | xii |
| CHAPTER 1. INTRODUCTION | 1 |
| 1.1. Background | 1 |
| 1.2. Object and Scope | 1 |
| 1.3. Organization | 2 |
| CHAPTER 2. PREVIOUS RESEARCH | 3 |
| 2.1. Introduction | 3 |
| 2.2. Analysis Methods | 3 |
| 2.2.1. Eccentric Shear Stress | 3 |
| 2.2.2. Beam Analogy | 4 |
| 2.3. Comparisons of Measured and Calculated Data | 5 |
| 2.4. Experimental Observations | 6 |
| CHAPTER 3. CYCLIC LATERAL-LOAD TEST | 8 |
| 3.1. Introductory Remarks | 8 |
| 3.2. First Cycle (0.2% Roof Drift Ratio) | 9 |
| 3.3. Second Cycle (0.4% Roof Drift Ratio) | 10 |
| 3.3.1. Flexural Cracking in the Columns | 10 |
| 3.3.2. Cracking in the Floor Slab | 10 |
| 3.4. Third Cycle (1.5% Roof Drift Ratio) | 11 |
| 3.4.1. Flexural Cracking in the Columns | 11 |
| 3.4.2. Cracking in the Floor Slab | 11 |
| 3.5. Fourth Cycle (3.0% Roof Drift Ratio) | 12 |
| 3.5.1. Flexural Cracking in the Columns | 12 |
| 3.5.2. Cracking in the Floor Slab | 13 |
| 3.6. Observations at Limiting Drift | 13 |
| 3.7. Load and Displacement Data | 14 |
| 3.7.1. Base Shear vs. Displacement | 14 |
| 3.7.2. Load and Displacement Profiles | 15 |
| 3.7.3. Story Displacements and Shears | 15 |
| 3.8. Strains Measured on Slab and Column Surfaces | 15 |
| 3.8.1. Slab Strains | 15 |
| 3.8.2. Column Strains | 16 |
| 3.9. Crack Measurements | 16 |

| | Page |
|--|------|
| 3.9.1. Crack Widths | 16 |
| 3.9.2. Crack Maps | 17 |
| CHAPTER 4. ANALYSIS | 18 |
| 4.1. Introduction | 18 |
| 4.2. Limit State Analysis | 18 |
| 4.3. Trilinear Model | 19 |
| 4.3.1. Cracked Section Properties | 19 |
| 4.3.2. Yielding Properties | 19 |
| 4.3.3. Analysis | 20 |
| 4.4. Nonlinear Frame Analysis | 21 |
| 4.5. Limiting Drift Condition | 21 |
| 4.6. Evaluation of Small-Scale Data | 22 |
| CHAPTER 5. ESTIMATION OF DRIFT RESPONSE | 24 |
| 5.1. Introduction | 24 |
| 5.2. Bilinear Hysteresis Model | 24 |
| 5.3. Generalized Single Degree of Freedom System | 25 |
| 5.4. Earthquake Records | 26 |
| 5.5. Analysis | 26 |
| 5.6. Concluding Remarks | 27 |
| CHAPTER 6. SUMMARY AND CONCLUSIONS | 28 |
| 6.1. Summary | 28 |
| 6.1.1. Object and Scope | 28 |
| 6.1.2. Cyclic Lateral-load Test | 28 |
| 6.1.3. Analysis | 29 |
| 6.1.4. Estimation of Story Drift | 30 |
| 6.2. Conclusions | 30 |
| TABLES | 31 |
| FIGURES | 45 |
| LIST OF REFERENCES | 131 |
| APPENDICES | |
| Appendix A. Experimental Program | 136 |
| A.1. Introduction | 136 |
| A.2. Materials | 136 |
| A.2.1. Concrete | 136 |
| A.2.2. Steel | 136 |
| A.3. Design | 137 |
| A.4. Construction | 138 |
| A.5. Instrumentation | 139 |
| A.5.1. Encoders | 140 |
| A.5.2. LVDT Measurements | 140 |
| A.5.3. Concrete Surface Strains | 140 |
| A.5.4. Actuator Load and Displacement | 141 |
| A.5.5. Data Acquisition | 141 |
| A.6. Load Frames | 142 |

| | Page |
|--------------------------|------|
| A.7. Test Sequence | 142 |
| VITA | 170 |

LIST OF TABLES

| Table | Page |
|---|------|
| Table 2-1 Experimental Programs | 31 |
| Table 3-1 Experimental Program Summary..... | 33 |
| Table 3-2 Load and Displacement Summary | 34 |
| Table 3-3 Story Shear and Displacement Summary..... | 34 |
| Table 3-4 Normalized Story Drift Ratios | 35 |
| Table 3-5 Limiting Drift Values..... | 35 |
| Table 3-6 Crack Width Measurements in Inches | 36 |
| Table 4-1 Cracking and Yield Moments..... | 39 |
| Table 4-2 Trilinear Analysis Summary..... | 39 |
| Table 4-3 Nonlinear Analysis Frame Section Properties | 39 |
| Table 4-4 Nonlinear Analysis Rotation Hinge Properties..... | 40 |
| Table 4-5 Nonlinear Analysis Properties | 40 |
| Table 5-1 SDOF System Properties | 41 |
| Table 5-2 Original Ground Motion Records | 41 |
| Table 5-3 Scaled Ground Motion Records | 42 |
| Table 5-4 Calculated Displacements | 43 |
| Table 5-5 Calculated Story Drifts..... | 44 |
| Appendix Table | |
| Table A.1 Concrete Mix Designs | 165 |
| Table A.2 Concrete Cylinder 28-Day Strengths..... | 166 |
| Table A.3 Concrete Cylinder Test Strengths, psi..... | 167 |
| Table A.4 Reinforcement Tensile Tests, ksi | 168 |
| Table A.5 Concrete Placement Dates | 168 |
| Table A.6 Instrumentation Accuracy | 169 |

LIST OF FIGURES

| Figure | Page |
|--|------|
| Figure 2-1 Assumed Eccentric Shear Stress Distribution (ACI 318-2005)..... | 45 |
| Figure 2-2 Beam Analogy (Hawkins and Corley 1971)..... | 45 |
| Figure 2-3 Isolated Slab-Column Test Specimen..... | 46 |
| Figure 2-4 Calculated Moments using the Eccentric Shear Method..... | 46 |
| Figure 2-5 Calculated Moments using the Beam Analogy..... | 47 |
| Figure 2-6 Small-Scale Slab-Column Test Data..... | 47 |
| Figure 3-1 Specimen Plan View..... | 48 |
| Figure 3-2 Specimen Elevation View..... | 48 |
| Figure 3-3 Load Distribution and Control Schematic..... | 49 |
| Figure 3-4 Distribution of 55-gallon Barrels of Water..... | 49 |
| Figure 3-5 Specimen Elevation View..... | 50 |
| Figure 3-6 Specimen Plan View..... | 50 |
| Figure 3-7 Column Flexural Cracks..... | 51 |
| Figure 3-8 Cracks Extending Across Full-Slab Width..... | 52 |
| Figure 3-9 Flexural Crack Widths Frame A, North 3% Roof Drift..... | 52 |
| Figure 3-10 Flexural Crack Widths Frame B, North 3% Roof Drift..... | 53 |
| Figure 3-11 Flexural Crack Widths Frame A, South 3% Roof Drift..... | 53 |
| Figure 3-12 Flexural Crack Widths Frame B, South 3% Roof Drift..... | 54 |
| Figure 3-13 Frame B Failure Location..... | 54 |
| Figure 3-14 Slab-Column Connection Failure..... | 55 |
| Figure 3-15 Slab Column Connection Failure..... | 55 |
| Figure 3-16 Failure Perimeter..... | 56 |
| Figure 3-17 Failure Section..... | 56 |
| Figure 3-18 Vertical Slab Separation Frame A, North 3% Roof Drift..... | 57 |
| Figure 3-19 Vertical Slab Separation Frame B, North 3% Roof Drift..... | 57 |
| Figure 3-20 Vertical Slab Separation Frame A, South 3% Roof Drift..... | 58 |
| Figure 3-21 Vertical Slab Separation Frame B, South 3% Roof Drift..... | 58 |
| Figure 3-22 Vertical Slab Separation (North 3% Roof Drift Ratio)..... | 59 |
| Figure 3-23 Vertical Slab Separation (South 3% Roof Drift Ratio, Column 3-2B-N)..... | 59 |
| Figure 3-24 Base Shear vs. Roof Displacement..... | 60 |
| Figure 3-25 Base Shear vs. Level 3 Displacement..... | 60 |
| Figure 3-26 Base Shear vs. Level 2 Displacement..... | 61 |
| Figure 3-27 Normalized Load and Displacement Profiles (0.2% and 0.4% Roof Drift Ratio)..... | 62 |

| Figure | Page |
|--|------|
| Figure 3-28 Normalized Load and Displacement Profiles (1.5% and 3.0% Roof Drift Ratio) | 63 |
| Figure 3-29 Level 1 Story Shear vs. Story Displacement | 64 |
| Figure 3-30 Level 2 Story Shear vs. Story Displacement | 64 |
| Figure 3-31 Level 3 Story Shear vs. Story Displacement | 65 |
| Figure 3-32 Column 2-2A Strains in Slab Surface (North 3% Roof Drift Ratio)..... | 66 |
| Figure 3-33 Column 2-2A Strains in Slab Surface (South 3% Roof Drift Ratio)..... | 67 |
| Figure 3-34 Column 3-2A Strains in Slab Surface (North 3% Roof Drift Ratio)..... | 68 |
| Figure 3-35 Column 3-2A Strains in Slab Surface (South 3% Roof Drift Ratio)..... | 69 |
| Figure 3-36 Column R-2A Strains in Slab Surface (North 3% Roof Drift Ratio)..... | 70 |
| Figure 3-37 Column R-2A Strains in Slab Surface (South 3% Roof Drift Ratio)..... | 71 |
| Figure 3-38 Column 1-2B Surface Strain Measurements | 72 |
| Figure 3-39 Locations of Measured Maximum Crack Widths (Level 2) | 73 |
| Figure 3-40 Locations of Measured Maximum Crack Widths (Level 3) | 74 |
| Figure 3-41 Locations of Measured Maximum Crack Widths (Roof) | 75 |
| Figure 3-42 Level 2-1A Crack Width vs. Roof Drift..... | 76 |
| Figure 3-43 Level 2-2A Crack-Width vs. Roof Drift..... | 76 |
| Figure 3-44 Level 2-3A Crack-Width vs. Roof Drift..... | 77 |
| Figure 3-45 Level 2-1B Crack-Width vs. Roof Drift..... | 77 |
| Figure 3-46 Level 2-2B Crack-Width vs. Roof Drift..... | 78 |
| Figure 3-47 Level 2-3B Crack-Width vs. Roof Drift..... | 78 |
| Figure 3-48 Level 3-1A Crack-Width vs. Roof Drift..... | 79 |
| Figure 3-49 Level 3-2A Crack-Width vs. Roof Drift..... | 79 |
| Figure 3-50 Level 3-3A Crack-Width vs. Roof Drift..... | 80 |
| Figure 3-51 Level 3-1B Crack-Width vs. Roof Drift..... | 80 |
| Figure 3-52 Level 3-2B Crack-Width vs. Roof Drift..... | 81 |
| Figure 3-53 Level 3-3B Crack-Width vs. Roof Drift..... | 81 |
| Figure 3-54 Level R-1A Crack-Width vs. Roof Drift | 82 |
| Figure 3-55 Level R-2A Crack-Width vs. Roof Drift | 82 |
| Figure 3-56 Level R-3A Crack-Width vs. Roof Drift | 83 |
| Figure 3-57 Level R-1B Crack-Width vs. Roof Drift | 83 |
| Figure 3-58 Level R-2B Crack-Width vs. Roof Drift | 84 |
| Figure 3-59 Level R-3B Crack-Width vs. Roof Drift | 84 |
| Figure 3-60 Locations of Measured Crack Widths (Level 2) | 85 |
| Figure 3-61 Locations of Measured Crack Widths (Level 3)..... | 86 |
| Figure 3-62 Locations of Measured Crack Widths (Roof) | 87 |
| Figure 3-63 Level 3-2A and 2B Initial Top of Slab Cracks | 88 |

| Figure | Page |
|---|------|
| Figure 3-64 Level 3-2A and 2B Top of Slab Cracks (North 0.4% Roof Drift)..... | 88 |
| Figure 3-65 Level 3-2A and 2B Top of Slab Cracks (South 0.4% Roof Drift)..... | 88 |
| Figure 3-66 Level 3-2A and 2B Top Slab Cracks (North 1.5% Roof Drift) | 89 |
| Figure 3-67 Level 3-2A and 2B Top Slab Cracks (South 1.5% Roof Drift) | 89 |
| Figure 3-68 Level 3-2A and 2B Top Slab Cracks (North 3% Roof Drift) | 89 |
| Figure 3-69 Level 3-2A and 2B Top Slab Cracks (South 3% Roof Drift) | 90 |
| Figure 3-70 Level 3-2A and 2B Bottom Slab Cracks (North 1.5% Roof Drift)..... | 90 |
| Figure 3-71 Level 3-2A and 2B Bottom Slab Cracks (South 1.5% Roof Drift)..... | 90 |
| Figure 3-72 Level 3-2A and 2B Bottom Slab Cracks (North 3% Roof Drift) | 91 |
| Figure 3-73 Level 3-2A and 2B Bottom Slab Cracks (South 3% Roof Drift) | 91 |
| Figure 3-74 Level 2 Column 2A South Initial Cracks | 92 |
| Figure 3-75 Level 2 Column 2A South Final Cracks..... | 92 |
| Figure 3-76 Level 2 Column 3A South Initial Cracks | 93 |
| Figure 3-77 Level 2 Column 3A South Final Cracks..... | 93 |
| Figure 3-78 Level 2 Column 2B South Initial Cracks | 94 |
| Figure 3-79 Level 2 Column 2B South Final Cracks..... | 94 |
| Figure 3-80 Level 2 Column 3B South Initial Cracks | 95 |
| Figure 3-81 Level 2 Column 3B South Final Cracks..... | 95 |
| Figure 3-82 Level 3 Column 2A South Initial Cracks | 96 |
| Figure 3-83 Level 3 Column 2A South Final Cracks..... | 96 |
| Figure 3-84 Level 3 Column 3A South Initial Cracks | 97 |
| Figure 3-85 Level 3 Column 3A South Final Cracks..... | 97 |
| Figure 3-86 Level 3 Column 2B South Initial Cracks | 98 |
| Figure 3-87 Level 3 Column 2B South Final Cracks..... | 98 |
| Figure 3-88 Level 3 Column 3B South Initial Cracks | 99 |
| Figure 3-89 Level 3 Column 3B South Final Cracks..... | 99 |
| Figure 3-90 Roof Column 2A South Initial Cracks | 100 |
| Figure 3-91 Roof Column 2A South Final Cracks..... | 100 |
| Figure 3-92 Roof Column 3A South Initial Cracks | 101 |
| Figure 3-93 Roof Column 3A South Final Cracks..... | 101 |
| Figure 3-94 Roof Column 2B South Initial Cracks | 102 |
| Figure 3-95 Roof Column 2B South Final Cracks..... | 102 |
| Figure 3-96 Roof Column 3B South Initial Cracks | 103 |
| Figure 3-97 Roof Column 3B South Final Cracks..... | 103 |
| Figure 3-98 Level 2 Column 1A North Initial Cracks..... | 104 |
| Figure 3-99 Level 2 Column 1A North Final Cracks | 104 |
| Figure 3-100 Level 2 Column 2A North Initial Cracks..... | 105 |
| Figure 3-101 Level 2 Column 2A North Final Cracks | 105 |
| Figure 3-102 Level 2 Column 1B North Initial Cracks..... | 106 |
| Figure 3-103 Level 2 Column 1B North Final Cracks | 106 |

| Figure | Page |
|--|------|
| Figure 3-104 Level 2 Column 2B North Initial Cracks | 107 |
| Figure 3-105 Level 2 Column 2B North Final Cracks | 107 |
| Figure 3-106 Level 3 Column 1A North Initial Cracks | 108 |
| Figure 3-107 Level 3 Column 1A North Final Cracks | 108 |
| Figure 3-108 Level 3 Column 2A North Initial Cracks | 109 |
| Figure 3-109 Level 3 Column 2A North Final Cracks | 109 |
| Figure 3-110 Level 3 Column 1B North Initial Cracks | 110 |
| Figure 3-111 Level 3 Column 1B North Final Cracks | 110 |
| Figure 3-112 Level 3 Column 2B North Initial Cracks | 111 |
| Figure 3-113 Level 3 Column 2B North Final Cracks | 111 |
| Figure 3-114 Roof Column 1A North Initial Cracks | 112 |
| Figure 3-115 Roof Column 1A North Final Cracks | 112 |
| Figure 3-116 Roof Column 2A North Initial Cracks | 113 |
| Figure 3-117 Roof Column 2A North Final Cracks | 113 |
| Figure 3-118 Roof Column 1B North Initial Cracks | 114 |
| Figure 3-119 Roof Column 1B North Final Cracks | 114 |
| Figure 3-120 Roof Column 2B North Initial Cracks | 115 |
| Figure 3-121 Roof Column 2B North Final Cracks | 115 |
| Figure 4-1 Limit State Analysis Results | 116 |
| Figure 4-2 Trilinear Model Segments | 116 |
| Figure 4-3 Trilinear Model with Hinges | 117 |
| Figure 4-4 Trilinear Model Comparison | 117 |
| Figure 4-5 Nonlinear Analysis Frame Dimensions and Loading | 118 |
| Figure 4-6 Nonlinear Static Analysis Comparison | 118 |
| Figure 4-7 Flat-Plate Comparison with Previous Data | 119 |
| Figure 5-1 Bilinear Model Segments | 120 |
| Figure 5-2 Bilinear Model Comparison | 120 |
| Figure 5-3 Castic N21E Acceleration History and Displacement Spectrum | 121 |
| Figure 5-4 Tarzana NS Acceleration History and Displacement Spectrum | 122 |
| Figure 5-5 Lolloe N10E Acceleration History and Displacement Spectrum | 123 |
| Figure 5-6 El Centro NS Acceleration History and Displacement Spectrum | 124 |
| Figure 5-7 Kobe NS Acceleration History and Displacement Spectrum | 125 |
| Figure 5-8 Taft N21E Acceleration History and Displacement Spectrum | 126 |
| Figure 5-9 Seattle S02W Acceleration History and Displacement Spectrum | 127 |
| Figure 5-10 Sendai NS Acceleration History and Displacement Spectrum | 128 |
| Figure 5-11 Santa Barbara S48E Acceleration History and Displacement Spectrum | 129 |

| Figure | Page |
|---|------|
| Figure 5-12 Hachinohe EW Acceleration History and Displacement Spectrum | 130 |
| Appendix Figure | |
| Figure A-1 Concrete Cylinder Strength Data | 144 |
| Figure A-2 Stress Strain Plot, No. 4. Bottom Reinforcing Bars | 144 |
| Figure A-3 Stress Strain Plot, No. 4 Top Reinforcing Bars | 145 |
| Figure A-4 Stress Strain Plot, No. 7 Column Longitudinal Bars | 145 |
| Figure A-5 Longitudinal Reinforcement | 146 |
| Figure A-6 Transverse Reinforcement..... | 147 |
| Figure A-7 Reinforcement Depths | 147 |
| Figure A-8 Structural Mechanism | 148 |
| Figure A-9 Loading Distribution | 148 |
| Figure A-10 Column Reinforcement | 149 |
| Figure A-11 Footing Reinforcement..... | 150 |
| Figure A-12 Level 1 Column Cage and Forms | 150 |
| Figure A-13 Level 1 Slab Shoring..... | 151 |
| Figure A-14 Slab Reinforcement | 151 |
| Figure A-15 Concrete Placement | 152 |
| Figure A-16 Concrete Finishing | 152 |
| Figure A-17 Completed Specimen..... | 153 |
| Figure A-18 Roof Instrumentation Plan | 153 |
| Figure A-19 Level 3 Instrumentation Plan | 154 |
| Figure A-20 Level 2 Instrumentation Plan | 154 |
| Figure A-21 Frame A Instrumentation Elevation..... | 155 |
| Figure A-22 Frame B Instrumentation Elevation..... | 155 |
| Figure A-23 Upper Diagonal Encoder String Connection | 156 |
| Figure A-24 Lower Diagonal Encoder Connection..... | 156 |
| Figure A-25 Lateral Displacement Encoder | 157 |
| Figure A-26 Diagonal Displacement Encoder..... | 157 |
| Figure A-27 Column Rotation LVDTs | 158 |
| Figure A-28 Load Frame Channel-Slab Connection LVDT..... | 158 |
| Figure A-29 Footing Movement LVDT | 159 |
| Figure A-30 Column Rotation LVDT | 159 |
| Figure A-31 Footing Movement LVDT | 160 |
| Figure A-32 Load Frame Channel-Slab Connection LVDT Photo | 160 |
| Figure A-33 Longitudinal Concrete Surface Strain Measurements..... | 161 |
| Figure A-34 Transverse Concrete Surface Strain Measurements | 161 |
| Figure A-35 Column Surface Strain Measurements | 162 |
| Figure A-36 Electronic Whittemore Gage | 162 |
| Figure A-37 Electronic Whittemore Measurement..... | 163 |
| Figure A-38 Load Frame Connection | 163 |
| Figure A-39 Load Frame Connection Details | 164 |

ABSTRACT

Fick, Damon R. Ph.D., Purdue University, August 2008. Experimental Investigation of a Full-Scale Flat-Plate Reinforced Concrete Structure Subjected to Cyclic Lateral Loading in the Inelastic Range of Response. Major Professors: Michael E. Kreger and Mete A. Sozen.

Reinforced concrete flat-plate construction is a popular building type because of the simple formwork required for construction and the clearance that is provided for mechanical and electrical equipment. During the period 1950 through 1980, buildings using the flat-plate for the lateral-force resisting system have been built in seismic regions. The displacement response of these structures during credible earthquakes results in concentrations of shear, flexure, and torsion at the slab-column connection that can lead to brittle failures. Proper evaluation of this response is a matter of importance for the economy and for public safety. Included in this study is the (a) construction, instrumentation, and cyclic lateral-load testing of a full-scale three-story flat-plate structure, (b) development of analysis methods to determine the limiting strength and drift capacities of flat-plate structures, and (c) the definition of a hysteresis model to estimate the dynamic response of the flat-plate structure subjected to selected strong ground motions.

CHAPTER 1. INTRODUCTION

1.1. Background

During the period 1950 through 1980, buildings using the flat plate for the lateral-force resisting system have been built in seismic regions. The flat-plate structure resists the displacements during an earthquake by transferring flexure, shear and torsion from the slab to the column. Detailing practices for flat plates did not include requirements that protect against collapse of the floor slab after a connection failure. Proper evaluation of this response is a matter of importance for the economy and for public safety.

The overall earthquake response of flat-plate structures depends on the hysteretic properties of the slab-column connection. The current understanding of the behavior is based largely on the experiments of small-scale isolated slab-column assemblies. The results contain a wide range of maximum drift ratios and failure modes that create uncertainty in evaluation of their behavior during strong ground motion.

1.2. Object and Scope

The object and scope of the study included (a) the construction, instrumentation, and cyclic lateral-load testing of a full-scale three-story flat-plate structure, (b) development of analysis methods to determine the limiting strength and drift capacities of flat-plate structures, and (c) the definition of a hysteresis model to estimate the dynamic response of the flat-plate structure subjected to selected strong ground motions.

1.3. Organization

Chapter 2 is a description of common analysis methods used to determine the limiting strength of slab-column connections subjected to shear and moment transfer. A review of the test data from small-scale isolated slab-column tests is included.

Chapter 3 is a description of the cyclic lateral-load test and the data that were recorded. Observations made during each cycle of loading are provided.

Chapter 4 discusses the analysis methods used to reproduce the load-displacement response of the flat-plate structure. The limiting drift condition is described and a method to estimate the drift capacity of flat-plate structures is presented.

Chapter 5 includes the description of a procedure to estimate the dynamic response of flat-plate structures. Ten ground motions are selected and the results of the dynamic response are discussed.

Summary and conclusions are presented in Chapter 6

CHAPTER 2. PREVIOUS RESEARCH

2.1. Introduction

The early information on slab-column connections came from research related to reinforced concrete footings. The following summary was made by Hognestad (1953) about a new design approach related to the shear strength of footings:

“At present, it is hardly possible to evaluate the shearing strength of a slab through a rational theory based on fundamental principles, since they are not fully understood. The alternative is an approach of empirical nature which recognizes all the important known facts.”

Determining the “important known facts” has been the subject of many investigations of slab-column connections. A review of the analysis methods and experimental data is presented below.

2.2. Analysis Methods

A slab-column connection subjected to lateral displacements creates bending in the slab. This bending must be transferred to the column through contributions of flexure, shear, and torsion. Two techniques to analyze this behavior include the eccentric-shear-stress method and the beam analogy.

2.2.1. Eccentric Shear Stress

The form of the eccentric shear stress method in the current ACI Building Code was based on the work by Di Stasio and Van Buren (1960). It is assumed that

the shear stress from the unbalanced moment varies linearly along the sides of the column (Figure 2-1). The maximum shear stress is related to the shear force, V , the unbalanced moment, M , and the effective depth of the reinforcement, d , by the following equation:

$$v = \frac{V}{A_o} \pm \frac{\gamma_v \cdot M \cdot c_{ab}}{J_c} \quad \text{Eq. 2.1}$$

where

$$A_c = 2d(c_1 + c_2 + 2d) \quad \text{Eq. 2.2}$$

is the area of the assumed critical section and

$$J_c = \frac{d(c_1 + d)^3}{6} + \frac{(c_1 + d)d^3}{6} + \frac{d(c_2 + d)(c_1 + d)^2}{2} \quad \text{Eq. 2.3}$$

is the property analogous to the polar moment of inertia for the assumed critical section. The variable γ_v is the fraction of unbalanced moment transferred to the slab by eccentric shear stresses and was assumed by Moe (1961) to be a constant evaluated empirically from test data. Square column tests done by Hanson and Hanson (1968) concluded that 40% of the moment should be included in the calculation of shear stresses. For rectangular and edge columns, the current ACI Building Code (ACI 318-2005) assigns a value of γ_v based on the critical sections of each column face.

2.2.2. Beam Analogy

Beam analogies for analyzing slab-column connections have been proposed by Andersson (1963), Tasker (1963), Hawkins and Corley (1971), and Zaghlool (1973). These beam analogies idealize the slab as beams framing into the

column. One of the methods used to convert the slab into four beams framing into each side of an interior column is shown in Figure 2-2 (Hawkins 1974). In this model, each beam is assumed to develop the full flexural, torsional, and shear capacity at the connection to the column. The stresses that exceed the capacity of an individual beam are distributed to adjacent beams. The limiting condition occurs when the flexure, shear, and torsion capacities are exceeded on three of the four beam connections for an interior column.

2.3. Comparisons of Measured and Calculated Data

Nineteen investigations (Table 2-1) have been conducted on isolated slab-column assemblies to study the response of slab-column connections subjected to lateral displacements. Figure 2-3 shows the range of specimen dimensions for the most common test assembly. Summaries of the specimen properties have been done by Pan and Moehle (1989), Megally and Ghali (1994), Luo and Durrani (1995), and more recently by Hueste et al. (2007).

The eccentric-shear method can be used to solve for the maximum unbalanced moment by substituting the applied gravity-shear, V , into Eq. 2.1. The beam analogy described above can also be used to calculate a maximum unbalanced moment by using torsional and shear strengths assumed by Hawkins (1974) from the 1971 ACI Building Code (ACI 318-1971).

The maximum moment measured during the test of each specimen is shown in Table 2-1. A comparison of the calculated and maximum test moments are shown in Figure 2-4 and Figure 2-5. The scatter is about the same for both calculations. The values from Hawkins beam analogy appear overly conservative, however improvements could be made by changing the width of the idealized beams or the strengths attributed to shear and torsion.

2.4. Experimental Observations

An important piece of information from the experimental data is the maximum rotation of the slab-column connection or drift ratio of the test structure at failure. The maximum displacement measured at failure is divided by the height of the test specimen to obtain the peak drift ratio. The peak drift (Table 2-1) is useful because it can be related to performance of flat-plate structures during earthquakes.

Tests of one-third scale slab-column assemblies by Morrison (1983) identified the reinforcement ratio as a contributing variable. Specimens with lower reinforcement ratios were able to develop the full flexural strength of the slab without failing in shear. All specimens failed in flexure. Drift ratio capacities of the specimens ranged from 2.8 to 4.8%.

Gravity-shear was recognized as a primary variable for drift capacity by testing three-fifths scale slab-column assemblies (Pan and Moehle 1989; 1992). Specimens with higher gravity loads were found more likely to fail in shear before reaching the flexural strength of the slab. Drift ratio capacities of the specimens ranged from 1.5 to 3.7%.

The trend of reduced drift capacity for higher loads was observed in the study by Pan and Moehle (1989; 1992) by plotting the gravity shear ratio (γ) vs. the story drift ratio (SDR). The gravity shear ratio was defined as the applied gravity load on the slab-column connection divided by the nominal shear capacity. The nominal shear capacity for an interior column for the condition of no moment transfer is defined by the current ACI Building Code (ACI 318-2005) as:

$$4\sqrt{f'_c}b_o d$$

Eq. 2.4

where f'_c is the concrete strength, b_o is the perimeter of the assumed critical section (Figure 2-1), and d is the effective depth of the reinforcement.

Figure 2-6 is a plot of gravity shear ratio, γ , vs. story drift ratio, SDR for the nineteen investigations listed in Table 2-1. The trend of reduced story drift ratio for higher gravity shears observed by Pan and Moehle (1989; 1992) is present for the experimental data considered in this study.

CHAPTER 3. CYCLIC LATERAL-LOAD TEST

3.1. Introductory Remarks

The test specimen was a full-scale two-span three-story reinforced concrete flat-plate structure consisting of six columns spaced at 20 ft in each direction supporting a 7 in. thick slab (Figure 3-1 and Figure 3-2). There was a 5 ft cantilevered slab around the perimeter of the building. The footing dimensions were 4 ft-6 in. square by 2 ft-6 in. thick. Each footing was post-tensioned to the 33 in. thick laboratory strong floor with four 1-3/8 in. Dywidag Threadbars[®], each post-tensioned to 100 kips. Details of the design, construction, and instrumentation of the specimen are presented in Appendix A.

Six 110-kip hydraulic actuators (2 per floor) were used to apply lateral load to the test structure. The actuators were connected to a strong wall and applied load to each floor level through a steel load frame (Appendix A) bolted to the slab. The test was controlled by the two roof-level actuators operating in displacement control. The load from these actuators was multiplied by a linear ratio and used to control the actuators on Level 3 and Level 2 in load control. Figure 3-3 is a schematic showing the applied load distribution and the control strategy.

A superimposed load was added to the structure by filling 55 gallon barrels with water. Each barrel weighed approximately 500 lbs. Forty barrels per floor resulted in a distributed load of 13.3 psf. The layout of the barrels on each slab is shown in Figure 3-4.

The cyclic lateral-load test included four cycles of loading. Values of displacements and loads are positive for loading in the north direction (Figure 3-3). Loading was paused at each of the target displacements and at intermediate loading points during cycles 3 and 4 to observe and document the response of the structure. Data collected included electronic Whittemore strain measurements, crack widths made with a crack comparator, slab elevation measurements with a surveying level, crack maps, and photographs. Table 3-1 shows the details of the loading cycles and the data collected.

The discussion of the observed response of the test specimen at each loading cycle includes specific references to individual slab-column connections. The connections are labeled with a format that contains four identifiers. The first (a number) refers to the level (Figure 3-5), the second (a number) and third (a letter) refer to the grid lines of the column (Figure 3-6) and the fourth (a letter) identifies the face of column. Slab-column connection 3-2B-N, for example, refers to the third level, grid location 2B, and the north face.

After the first cycle of loading, 108 cracks in the slab near the column were selected for width measurement at peak displacements of subsequent cycles. They are referred to as “selected crack widths” and do not necessarily represent the maximum crack width of the slab at a particular connection.

Reference is also made to the base shear coefficient (C_b), which is the ratio of the total base shear to the total weight of the structure assuming a reinforced concrete weight of 150 lb/ft³. The total weight of the test structure above the footings, including the applied distributed gravity load, was 509 kips.

3.2. First Cycle (0.2% Roof Drift Ratio)

The first cycle roof displacement was 0.7 in. (0.2% roof drift ratio). The peak base shear was 54 kips ($C_b = 0.11$). The cycle was performed primarily to test

the servo-hydraulic control equipment and to verify all instrumentation was working properly. Electronic Whittmore readings and survey of slab elevations was performed to evaluate the measuring process and the time required for the manual data collection operations. Cracks were observed but not mapped or measured. They were wider on the tension side of the slab. Cracks were not visible in the columns.

3.3. Second Cycle (0.4% Roof Drift Ratio)

The maximum roof displacements in the second cycle were ± 1.5 in. (0.4% roof drift ratio). The peak base shear was 80 kips ($C_b = 0.16$). Maxima are listed in Table 3-2.

3.3.1. Flexural Cracking in the Columns

Story 1: Cracks were observed in the bottom 36 in. of the first-story columns (Figure 3-7). Cracks were not visible in the first-story columns below the level 2 slab.

Story 2: Cracks were observed in the bottom 12 in. of columns above the level 2 floor slab (Figure 3-7). Cracks were not visible below the level 3 slab.

Story 3: No cracks were visible in the columns.

3.3.2. Cracking in the Floor Slab

A small number (0-4) of new cracks and extended cracks were observed in the slab. Maximum selected crack widths in the slab were .030 and .035 in. at connection 2-2B-N and 2-2B-S (Figure 3-5 and Figure 3-6).

3.4. Third Cycle (1.5% Roof Drift Ratio)

The maximum roof displacements in the third cycle were ± 5.4 in. (1.5% roof drift ratio). The peak base shear was 137 kips ($C_b = 0.27$). Approximately 6 cracks were “heard” while loading in the north and south directions, beginning at about 4 in. of displacement and continuing randomly to the peak displacement. Some of the cracking sounds were associated with a small (less than 1 kip) drop in base shear.

3.4.1. Flexural Cracking in the Columns

Story 1: The observed deflected shape of the first-story columns resembled that of a cantilever fixed at Level 1. The observed crack distribution 74 in. above the base of the first story confirmed this impression (Figure 3-7). Cracking was not visible in the first-story column below the level 2 slab.

Story 2: The crack pattern in the second-story columns reflected “double bending.” The cracks opening at the bottom and top of the columns were on opposite faces of the column. Cracking was observed in the bottom of columns 32 in. above the level 2 slab and in the top of the columns 25 in. below the level 3 slab.

Story 3: No cracks were visible above the level 3 slab. Cracks were observed in the top of the columns 45 in. below the roof-level slab.

3.4.2. Cracking in the Floor Slab

Cracks in the slabs, such as those shown in Figure 3-8, extended across the entire slab width on top and bottom surfaces of the slab. At the peak north displacement the slab-column connections at column line 3 had more cracks near the column. At the peak south displacement, the slab-column connections at column line 1 exhibited similar cracking characteristics. In general, the cracks

extended from random shrinkage cracks that existed around each column prior to testing. These crack extensions tended to align perpendicular to the direction of loading as expected for flexural behavior. Maximum selected crack widths for loading in the north direction exceeded 0.060 in. at connections 2-3A-S and 3-2A-S, and column 2-2B-N for loading in the south direction.

3.5. Fourth Cycle (3.0% Roof Drift Ratio)

The maximum roof displacements in the fourth cycle were ± 10.8 in. (3.0% roof drift ratio). The peak base shear was 161 kips ($C_b = 0.32$). Cracking was heard at north and south roof displacements of approximately 9 in. and resulted in a drop in base shear of 1 kip. Loading in the south direction was paused briefly after a larger drop in base shear occurred at a roof displacement of 10.5 in. Loading continued 4 minutes later until the target roof displacement was reached.

3.5.1. Flexural Cracking in the Columns

Story 1: The nearly cantilever response of the first-story columns was more pronounced than it was in the previous cycle. Cracking was observed in the bottom 80 in. of the first-story columns (Figure 3-7). Cracks at the top of the columns near the level 2 slab were not visible. Spalling was observed at the base of all columns during load application to the north. Only one first-story column (1-1A-N) had spalling at its base during loading to the south.

Story 2: Cracking was observed in the bottom of the columns a distance of 45 in. above the top of the level 2 slab and in the top of the columns 25 in. below the level 3 slab.

Story 3: Cracking in the columns was not observed above the level 3 slab. Cracking was observed in the top of the columns 45 in. below the roof slab.

3.5.2. Cracking in the Floor Slab

Cracking in the slab increased significantly during the fourth cycle (3.0% roof drift ratio). Several full-width cracks appeared on top and bottom surfaces of the slab. Additional cracking occurred near the column. The maximum crack widths in the slab at each connection were recorded and are shown in Figure 3-9 through Figure 3-12.

3.6. Observations at Limiting Drift

A failure occurred at slab-column connection 3-2B (Figure 3-13) during loading in the south direction of cycle 4 (3.0% roof drift ratio). The roof displacement at failure was 10.5 in. (2.9% roof drift ratio). The peak base shear was 154 kips ($C_b = 0.30$). The failure occurred suddenly without any forewarning in the load-displacement curve. On its occurrence, the measured base shear dropped 18 kips to 136 kips ($C_b = 0.27$). Loading in the south direction was resumed 4 minutes later until the roof displacement was 10.8 in (3.0% roof drift ratio). The corresponding base shear was 140 kips ($C_b = 0.28$). The story shears and displacements immediately before the failure are shown in Table 3-5. Photographs of the failure are shown in Figure 3-14 and Figure 3-15. The perimeter of the failure is shown in Figure 3-16 and a section sketch with an estimated failure surface is shown in Figure 3-17.

In cycle 4 when the displacement reached the maximum in both directions, a vertical separation of the slab ranging from 1/16 to 5/16-in. on both the bottom and top surfaces of the slab was observed. The locations and depths of these measurements are identified in Figure 3-18 through Figure 3-21. Figure 3-22 and Figure 3-23 are representative photographs of the vertical slab separation.

The number of vertical slab separations observed in Frame A (Figure 3-6) was more than in Frame B. At the peak north displacement, the crack widths for slab-column connections 2-3B-S and 3-3B-S (Figure 3-9) were 50% larger than those

in Frame B. The single and largest vertical separation in Frame B occurred at slab-column connection R-2B.

3.7. Load and Displacement Data

3.7.1. Base Shear vs. Displacement

Base shear vs. roof, level 3, and level 2 displacements are shown in Figure 3-24 through Figure 3-26. The maximum and minimum values of the load and displacement figures are listed in Table 3-2. The displacements in the figures are the averages of the two displacement measurements made at each level. The drop in base shear in cycles 3 and 4 occurred when the loading was stopped and data measurements were made (Table 3-1). The data collection process lasted from 3 to 5 hours.

The data-acquisition system stopped functioning at the peak north displacement of cycle 2 (0.4% roof drift ratio). As a result, lateral displacements were not recorded while unloading. A straight line from the peak load and displacement to the manually recorded displacement at zero load is represented in the figures. The problem with the data acquisition system was identified and resolved for all other loading cycles.

A reduction in base shear of approximately 1 kip occurred near the peak displacements of cycle 3 (1.5% roof drift ratio) and cycle 4 (3.0% roof drift ratio). The drop is noticeable in the load-displacement plots at all levels and for both frames. Because the drop is evident on all levels, slipping of an individual load frame connection is unlikely. Based on the cracking that was heard during the loading process and the crack maps, the cause may be due to cracks extending across the full width of the slab. Many of the full-width slab cracks on top of the slab were observed at the peaks of cycle 3, and a majority of the cracks on the

bottom of the slab that extended the full width of the slab were observed during cycle 4 peaks.

3.7.2. Load and Displacement Profiles

Load and displacement profiles normalized by the values at the roof for each cycle are shown in Figure 3-27 and Figure 3-28. The load ratios shown in the profiles confirm the desired load distribution was achieved.

The displacement profiles were approximately the same for the first two cycles of loading. Displacement reductions of approximately 5% at level three and 7% at level two occurred at the peak displacement of the third cycle (1.5% roof drift ratio). The fourth cycle loading resulted in a displacement increase of approximately 7% at level two.

3.7.3. Story Displacements and Shears

Story shear vs. story displacement data are shown in Figure 3-29 through Figure 3-31. Maximum and minimum values are provided in Table 3-3. The shape and characteristics are similar to the load-displacement responses described above. The largest story drift occurred consistently at the second story. Table 3-4 lists the story drift ratios normalized with the first story drift. The second story drift is largest during the third cycle (1.5% roof drift ratio) of loading.

3.8. Strains Measured on Slab and Column Surfaces

3.8.1. Slab Strains

Surface strains were measured with an electronic Whittemore gage (Section A.5.3) along the centerlines of each column and across each face in the

longitudinal direction (Figure A-33). The distribution of strains across slab-column connections 2-2B, 3-2B, and R-2B for cycle four (3.0% roof drift ratio) are shown in Figure 3-32 through Figure 3-37. Tension strains are positive.

The so-called measured concrete surface strains were largely dependent on the location of cracks in the slab. Surface strain measurements were mostly crack openings divided by the Whittemore gage length. Because the crack density decreases away from the columns, the strain measurements further away from the column are more variable. The cases where the strain value drops to nearly zero are consistently locations where a crack does not pass between measurement locations.

3.8.2. Column Strains

Longitudinal strains related to shrinkage and creep were measured on four sides of each column in the first story (Figure A-35). Measurements began during construction and continued for 118 weeks. Negative strain values represent compression and are shown for column 1-2B in Figure 3-38.

The last concrete column surface strain measurement recorded on March 23, 2007 was approximately .0004, which is in the range of predictions that can be made for the material properties, construction methods, and weight of the flat-plate structure.

3.9. Crack Measurements

3.9.1. Crack Widths

Three cracks in the slab were randomly selected in front of the north and south faces of the column. The three cracks were labeled c1, c2, and c3. At the

displacement peaks of each cycle, the cracks on the tension side of the column were measured with a crack comparator. Locations of the cracks with the largest measured width are shown in Figure 3-39 through Figure 3-41. The maximum measured widths are plotted against the roof drift ratio in Figure 3-42 through Figure 3-59. Most of the selected cracks showed an increase in width as the roof drift ratio increased. The maximum measured crack width was 0.17 in. All crack width measurements are listed in Table 3-6 and the locations of cracks with widths less than the widths of the maximum are shown in Figure 3-60 through Figure 3-62.

The maximum crack width on the tension side of the slab and column bases was measured at peak displacements of cycle 4 (3.0% roof drift ratio) and is shown in Figure 3-9 through Figure 3-12.

3.9.2. Crack Maps

Crack maps were drawn for slab-column connections 3-2A and 3-2B for each loading cycle (Figure 3-63 through Figure 3-73). Most of the new crack growth during cycle 2 (0.4% roof drift ratio) was extension of the existing cracks. Full slab width cracks occurred during cycle 3 (1.5% roof drift ratio). Most of the full-width cracks on the bottom of the slab occurred during cycle 4 (3.0% roof drift ratio).

Photographs of the initial and final crack patterns for each column are shown in Figure 3-74 through Figure 3-121.

CHAPTER 4. ANALYSIS

4.1. Introduction

The load and displacement records from the full-scale three-story flat-plate structure provide directly useful data for testing the feasibility of determining: (1) the limiting base shear capacity; (2) the relationship between base-shear force and roof displacement at various stages of response; and (3) the conditions leading to the limiting drift. In analyzing the relationship between base shear and roof displacement, two different approaches were used. In the first approach, the force-displacement curve was reproduced in three linear segments. In the second approach, a step-by-step procedure was used.

4.2. Limit State Analysis

A limit state analysis was used to approximate the base shear capacity of the flat-plate structure. The magnitude of the base shear is found by setting the work done by the external loads equal to the internal work by the frame members. A description of the assumed failure mechanism (Figure A-8) used in this analysis can be found in Section A.3.

Base shear coefficients calculated using strengths of the entire slab width (15 ft) and the column strip (10 ft) are shown with the envelope of the flat-plate test data in Figure 4-1. The measured strength of the flat-plate test structure was between the two values. Because the 15 ft width is asymmetric about the column and because it is preferable to underestimate the base shear strength in design analyses, a slab width of 10 ft is selected.

4.3. Trilinear Model

A two-dimensional linear-elastic frame analysis program was used to analyze the frame along one of the N-S column centerlines. The width of the frame was equal to the column strip dimension (10 ft).

4.3.1. Cracked Section Properties

The cracking moments for the slab and columns were assumed to occur when the tensile stress of the gross section reached a modulus of rupture of $7.5\sqrt{f'_c}$ based on the mean compressive strength for the concrete in the slabs and the columns. Concrete strengths used for this computation are listed in Table A.3. Calculated cracking moments in the column included the contribution of an assumed uniform axial stress from gravity loading. Calculated moduli of rupture (f_r) and cracking moments are listed in Table 4-1.

Transformed properties of the cracked sections were used to calculate the corresponding moments of inertia. Calculated and approximated values used in the incremental analysis are listed in Table 4-1.

4.3.2. Yielding Properties

Yielding capacities of the slabs and columns were calculated using the mean material properties shown in Table A.3 and Table A.4. A rectangular compressive stress distribution (Whitney 1937) was assumed for the concrete.

To determine the effective depth of the reinforcement after the experimental program, concrete cover on the top reinforcement and slab thicknesses were checked at 7 locations near the slab-column connections. The average slab thickness was 7-3/8 in. and the average rebar cover was 1-1/4 in. The effective depth was assumed to be 5-7/8 in. for the top reinforcement. The cover on the

bottom reinforcement was checked before casting and found to be 3/4 in. at all critical sections. Based on the average slab thickness near the slab-column connections, the effective depth of the bottom reinforcement was assumed to be 6-3/8 in. The nominal depths of the reinforcement are shown in Figure A-7.

4.3.3. Analysis

The load-displacement curve was constructed in three linear segments. The first segment was limited by cracking at the base of the first-story columns. The corresponding displacement was computed assuming the entire structure to be uncracked. The calculated roof drift was 0.4 in. (0.1% roof drift ratio) and the base shear for two frames is 39 kips ($C_b=0.08$). Cracked-section properties are listed in Table 4-1 and the calculated load and displacement for the first segment are shown in Figure 4-2.

The next segment was limited by the development of the yield moment at the bases of the first-story columns. At that stage, the maximum moments at the level 2 and level 3 slabs were within 5% of their calculated yield moments. The corresponding displacement was determined assuming all columns to have one-third and all slabs to have one-fifth of their uncracked moments of inertia. The calculated roof displacement is 5.7 in. (1.6% roof drift ratio) and a base shear of 146 kips ($C_b=0.29$).

To determine the slope of the third segment a structure with hinges at the base of the first story columns and at all slab-column joints of levels two and three (Figure 4-3) was analyzed with the member stiffnesses used for the second segment. The maximum load was limited when the roof level slab-column joints yielded and the structural mechanism was formed (Figure A-8). The calculated roof displacement is 16.8 in. (4.7% roof drift ratio) and a base shear of 171 kips ($C_b=0.34$).

Properties of the trilinear model are listed in Table 4-2 and a comparison with the envelope of the flat-plate test data is shown in Figure 4-4.

4.4. Nonlinear Frame Analysis

Nonlinear-static step-by-step frame analysis programs are used by practicing engineers to evaluate the inelastic response of structures. It is of interest to input the parameters established for the bilinear hysteresis model (Section 5.2) and the material properties from the flat-plate specimen to a commercially available software program.

A two-dimensional frame was created in SAP 2000 (Computers and Structures 2004) A slab width of 10 ft was used for the beam. Moments of inertia assigned to the slab and column members were one-half gross section properties. The concrete strengths were 4000 psi and the reinforcement yield stress was 66 ksi for the column reinforcement and 68 ksi for the slab reinforcement. Strain hardening in the reinforcement was assumed to reach 1.25 times the yield stress. The analysis included geometric nonlinearity effects. Properties used in the analysis are shown in Table 4-3 through Table 4-5 and Figure 4-5. A comparison of the flat-plate load-displacement envelope and the nonlinear static analysis is shown in Figure 4-6.

4.5. Limiting Drift Condition

The structure was loaded in four cycles of increasing roof displacement. The target roof drift ratio for the fourth cycle was 3%. Failure of slab-column connection 3-2B was observed while loading in the south direction in cycle 4 (Table 3-1). This event occurred at a drift ratio of 2.9%. Upon inspection, it was found that other connections failed during loading to 3% roof drift ratio in the north direction, but there had been no indication of it in the load-displacement curve.

As described in Section 3.6, vertical slab separations were observed in five different slab-column connections of Frame A compared with one location in Frame B (Figure 3-18, Figure 3-19). Vertical separation was observed at each slab level of column 2A (Figure 3-1). In addition to the separations in column 2A, the crack widths at level 2 and 3 of column 3A were 50% larger than the crack widths in Frame B (Figure 3-9 and Figure 3-10). The observations suggest damage in the slab surrounding column 2A was driven by the rotation demand at the slab-column connections to column 3A. The redistribution of rotations continued while loading in the south direction of cycle 4 and contributed to the slab-column connection failure in Frame B (Figure 3-13).

Another characteristic of the flat-plate structure near the limiting drift condition is the near-zero slope of the load-displacement curve. The base shear increased only five kips over the last one-half percent roof drift ratio.

4.6. Evaluation of Small-Scale Data

An incentive for testing the full-scale flat-plate structure was to compare the results with previous investigations of small-scale isolated slab-column specimens (Table 2-1). The effects of slab-column connections in multiple stories and frames to the failure of a single connection make the comparison useful.

The isolated test assemblies represent slab-column connections of a prototype structure. The peak drifts of these specimens are compared with the second story drift ratio (3.4%, Table 3-3) recorded at the level of the connection failure.

As described in Section 2.4, a trend of reduced drift in slab-column connections is observed for higher gravity-shear ratios (Pan and Moehle 1989; 1992). The gravity shear on the flat-plate structure includes 88 psf self weight and 13 psf

superimposed loading. This loading distributed over the tributary area of an interior column (300 ft²) produces 30 kips of shear at the connection. The assumed critical section for the flat-plate test structure is 576 in² (Figure 2-1) which provides a nominal shear capacity of 146 kips for a condition of no moment transfer (Section 2.4). From these values, the gravity-shear ratio, γ , for the flat-plate structure is calculated to be 0.21.

Results of the available tests of slab-column connections are plotted in Figure 4-7. The y-axis is the gravity shear ratio, γ , the x-axis is the story drift ratio, SDR. The story drift limit is well within the trend of the data.

It is interesting and relevant to note that a “best estimate” representative of the data would be the simple expression:

$$SDR(\%) = 5 - 8\gamma \quad \text{Eq. 4.1}$$

A safe “lower-bound” that would be suitable for design is:

$$SDR(\%) = 4 - 8\gamma \quad \text{Eq. 4.2}$$

CHAPTER 5. ESTIMATION OF DRIFT RESPONSE

5.1. Introduction

Drift response was estimated by generalizing the three-story flat-plate structure as a single-degree-of-freedom (SDOF) system. A bilinear hysteresis model is constructed to represent the recorded load-displacement curve with two linear segments. Properties of the hysteresis model were used with a numerical procedure to calculate the approximate response of the SDOF system subjected to selected ground-motion records.

5.2. Bilinear Hysteresis Model

The linear-elastic analysis method described in Section 4.3 was used to select moments of inertia for the slab and column members to define the first segment of the bilinear model. The first segment was limited by the location at which first yielding occurred in the slab or column members.

Moments of inertia of the slab and column members were selected to be one-half their gross section properties. Calculated first yielding occurred at the level-two slab-column connections (Figure 5-1). The calculated roof displacement was 2.4 in. (0.7 roof drift ratio) and a base shear of 125 kips ($C_b=0.25$).

The calculated stiffness (k) of the two-dimensional frame model for the first linear segment is 53 kips/in. The second linear segment is assigned a stiffness of $53/14 = 4$ kips/in. A limiting drift condition was not defined in the bilinear model. A comparison of the model to the flat-plate test envelope is shown in Figure 5-2.

5.3. Generalized Single Degree of Freedom System

The three-story flat-plate structure was transformed to a single-degree-of-freedom (SDOF) system based on conservation of energy principles developed in 1873 by Lord Rayleigh (Rayleigh 1945). To determine the total potential and kinetic energy of the system, assumptions about the story stiffness must be made.

A simple procedure to approximate the story stiffness that includes the flexibility of the slab can be made with the following equation (Schultz 1992):

$$K_s = \frac{24E}{H^2} \frac{1}{\frac{2}{\sum k_c} + \frac{1}{\sum k_{ga}} + \frac{1}{\sum k_{gb}}} \quad \text{Eq. 5.1}$$

where:

H = clear story height

E = concrete modulus of elasticity

k_c = column stiffness = $\frac{I_{col}}{H}$

k_{ga} = slab stiffness above story = $\frac{I_{slab}}{L}$

k_{gb} = slab stiffness below story = $\frac{I_{slab}}{L}$

Moments of inertia of the slab and column members are assumed to be the same as the bilinear model (one-half gross section properties). Because the first story columns connect directly to the footings, the last term in the denominator of Eq. 5.1 is not included in the first story computation. To include the reduced stiffness in the third story due to the discontinuous column at the roof, the numerator in Eq. 5.1 is reduced by the quantity $\frac{k_c}{55 \cdot k_s}$ (Schultz 1992). Properties used to generalize the three-story structure as a SDOF system are listed in Table 5-1.

5.4. Earthquake Records

Ground motions from ten different sites were used in the calculations to estimate the maximum nonlinear displacements of the generalized single-degree-of-freedom system described above. Characteristics of the original ground motions (not scaled) are listed in Table 5-2.

The same ten ground motions were used by Lepage (1997) to develop a method of estimating nonlinear response of buildings to earthquake motions. The ground motions used in the study by Lepage were normalized to the idealized displacement response of the El Centro 1940 NS record scaled to an acceleration of 0.5g. The same scaling procedure was applied in this study. Maximum scaled accelerations are shown in Table 5-3. Acceleration histories and displacement spectra are shown in Figure 5-3 through Figure 5-12.

5.5. Analysis

Nonlinear displacements of the generalized single-degree-of-freedom system were calculated using the Newmark Beta Method (1959) with a beta value of 1/6. The method is a time-step procedure that evaluates the dynamic response of a SDOF system and can be modified to include properties of a defined hysteresis model (Section 5.2).

The maximum calculated nonlinear displacement of the SDOF system is multiplied by the participation factor of 1.24 calculated for the flat-plate structure to determine the equivalent roof displacements (Table 5-4). The roof displacements were multiplied by the assumed mode shape of the structure (Table 5-1) to determine the story displacements. Story drift values are shown in Table 5-5.

5.6. Concluding Remarks

Results of the dynamic analysis suggest the maximum story drift recorded in the flat-plate structure (Table 3-3) would not be exceeded in 7 of the 10 strong ground motions considered. A relationship between peak acceleration or velocity to the calculated response is not apparent.

The analysis of the experimental data demonstrated that the relationship between base shear and roof drift could be determined using credible assumptions about the stiffness and flexural strength of the structure. The procedure for determining the load-displacement relationship is sufficiently explicit for general application.

With the convenience provided by easy modeling of the flat-plate structure for dynamic analysis and a failure criterion provided by:

$$SDR(\%) = 4(1 - 2\gamma) \text{ for } \gamma \leq 0.5 \quad \text{Eq. 4.2}$$

a study was made of the drift response from the ten strong ground motion results (Table 5-5). Comparing the failure criterion (Eq. 4.2) for the flat-plate test structure of 2.3% ($\gamma = 0.21$) with the calculated response reveals acceptable performance in 7 of the 10 records. Results of the study confirm the plausibility of defining a lower bound to the limiting drift condition.

CHAPTER 6. SUMMARY AND CONCLUSIONS

6.1. Summary

6.1.1. Object and Scope

The object and scope of the study included (a) the construction, instrumentation, and cyclic lateral-load testing of a full-scale three-story flat-plate structure, (b) development of analysis methods to determine the limiting strength and drift capacities of flat-plate structures, and (c) the definition of a hysteresis model to estimate the dynamic response of the flat-plate structure subjected to selected strong ground motions.

6.1.2. Cyclic Lateral-load Test

A cyclic lateral-load test was conducted of a three-story full-scale reinforced concrete flat-plate structure. A superimposed load of 13.3 psf was applied to the structure to represent a permanent loading condition for a typical building. The self weight of the slabs was estimated to be 87.5 psf. Four cycles of loading produced roof drift ratios of 0.2, 0.4, 1.5, and 3.0%.

Initiation of failure at slab-column connections was indicated by small changes (1/16 to 5/16 in.) in elevation of the slab near the column (Figure 3-22 and Figure 3-23). Loading in the north direction (Figure 3-2) to a roof drift ratio of 3.0% produced vertical separations at 6 of the 18 slab-column connections (Figure 3-9 and Figure 3-10). A reduction in base shear did not accompany the observed damage in the slab-column connections.

Loading in the south direction resulted in a slab-column connection failure at 2.9% roof drift ratio. An 11% drop in base shear occurred immediately after the limiting drift condition was reached.

Damage observed while loading in the north direction did not result in complete failure of an individual slab-column connection because of the inherent redundancy of the three-story flat-plate structure.

6.1.3. Analysis

Three different approaches were used in analyzing the flat-plate test structure to test the feasibility of determining the limiting base shear capacity and the relationship between base-shear force and roof displacement.

- 1) The base shear capacity of the flat-plate structure was calculated using a limit state analysis. The recorded strength of the flat-plate structure was bounded by the limiting conditions based on the full slab width (15 ft) and a slab width that included only the column strip (10 ft).
- 2) A linear step-by-step analysis was used to reconstruct the recorded load-displacement response with three linear segments. The characteristics of the three individual segments were related to the gross and cracked stiffness properties of the slabs and columns limited by their yield capacities.
- 3) A two-dimensional nonlinear step-by-step analysis with commercially available software was used to reconstruct the load-displacement behavior of the flat-plate structure. Measured material properties and a slab width that included only the column strip were used in the model. The calculated load-displacement response is an acceptable approximation to the recorded data.

6.1.4. Estimation of Story Drift

A bilinear hysteresis model was constructed to reproduce the recorded load-displacement envelope. An equivalent single-degree-of-freedom (SDOF) system was defined to represent the flat-plate structure. A nonlinear step-by-step analysis was used to determine the maximum displacements of the SDOF system subjected to ten selected strong ground motions.

6.2. Conclusions

Based on the experimental observations of the full-scale flat-plate test structure, the following conclusions are made:

1. A lower bound estimate to the base shear strength of the three-story flat-plate structure includes the moment capacities of the slab-column connections for the width of the column strip (10 ft).
2. The recorded load-displacement response of the flat-plate structure can be defined by segments from a linear analysis based on the stiffness and strengths of slab and column members.
3. The limiting drift condition of the full-scale flat-plate structure falls within the bounds of test data from small-scale isolated slab-column tests.
4. A lower bound to the limiting story drift ratio (SDR) for slab-column connections can be estimated with the following equation:

$$SDR(\%) = 4(1 - 2\gamma) \quad \text{Eq. 4.2}$$

where:

$$\gamma = \text{gravity shear ratio, } \frac{V_g}{V_o} \leq 0.5$$

V_g = gravity shear carried by slab-column connection

V_o = nominal shear capacity for slab-column connection defined by the current ACI Building Code

5. A procedure to estimate the nonlinear dynamic response of the flat-plate structure suggests calculated maximum story drifts were acceptable for 7 of the 10 strong ground motions studied.

TABLES

Table 2-1 Experimental Programs

| | Label | γ | Peak Drift [%] | Failure | Test Moment [k-in] |
|------------------------------|---------------|----------|----------------|---------|--------------------|
| (Durrani et al. 1995) | DNY 1 | 0.20 | 3.0 | F | 220 |
| | DNY 2 | 0.30 | 2.0 | P | 194 |
| | DNY 3 | 0.24 | 2.0 | F | 206 |
| | DNY 4 | 0.28 | 2.6 | F-P | 220 |
| (Elgabry and Ghali 1987) | 1 | 0.46 | N/A | P | 1152 |
| (Farhey et al. 1993) | 1 | 0.04 | 4.8 | F | 292 |
| | 2 | 0.04 | 4.0 | F | 292 |
| | 3 | 0.26 | 3.6 | P | 168 |
| | 4 | 0.30 | 2.4 | P | 133 |
| (Ghali et al. 1976) | SM 0.5 | 0.31 | 6.0 | F | 888 |
| | SM 1.0 | 0.33 | 2.7 | F-P | 1128 |
| | SM 1.5 | 0.30 | 2.7 | F-P | 1176 |
| (Hanson and Hanson 1968) | A12 | 0.29 | N/A | P | 181 |
| | A13L | 0.29 | N/A | P | 176 |
| | B16 | 0.29 | N/A | P | 242 |
| | B7 | 0.04 | 3.8 | F-P | 316 |
| | C17 | 0.24 | N/A | F-P | 219 |
| | C8 | 0.05 | 5.8 | F | 278 |
| (Hawkins et al. 1974) | S1 | 0.33 | 3.8 | P | 1280 |
| | S2 | 0.45 | 2.0 | P | 778 |
| | S3 | 0.45 | 2.0 | P | 475 |
| | S4 | 0.40 | 2.6 | P | 1110 |
| (Hwang and Moehle 2000) | 4 Int. Joints | 0.24 | 4.0 | N/A | N/A |
| (Islam and Park 1976) | 1 | 0.25 | 3.7 | P | 270 |
| | 2 | 0.23 | 3.3 | P | 334 |
| | 3C | 0.23 | 4.0 | F-P | 317 |
| (Robertson and Johnson 2006) | ND1C | 0.23 | 3.0 to 5.0 | F-P | 375 |
| | ND4LL | 0.28 | 3.0 | F-P | 394 |
| | ND5XL | 0.47 | 1.5 | P | 288 |
| | ND6HR | 0.29 | 3.0 | P | 519 |
| | NC7LR | 0.26 | 3.0 | F-P | 265 |
| | ND8BU | 0.26 | 3.0 | F-P | 520 |
| (Luo and Durrani 1995) | I.I | 0.08 | 5.0 | F | 348 |
| | INT 1 | 0.43 | N/A | P | 347 |
| | INT 2 | 0.50 | N/A | P | 280 |
| (Megally and Ghali 2000) | MG-2A | 0.58 | 1.2 | P | 576 |
| | MG-7 | 0.29 | 3.1 | F-P | 641 |
| | MG-8 | 0.42 | 2.3 | F-P | 679 |
| | MG-9 | 0.36 | 2.2 | F-P | 758 |

Table 2-1 Experimental Programs (Continued)

| | Label | γ | Peak Drift [%] | Failure | Test Moment [k-in] |
|------------------------------|-------|----------|----------------|---------|--------------------|
| (Morrison et al. 1983) | S1 | 0.03 | 4.7 | F | 302 |
| | S2 | 0.03 | 2.8 | F | 343 |
| | S3 | 0.03 | 4.2 | F | 363 |
| | S4 | 0.07 | 4.5 | F | 314 |
| | S5 | 0.15 | 4.8 | F | 332 |
| (Pan and Moehle 1989) | AP 1 | 0.37 | 1.6 | F-P | 468 |
| | AP 2 | 0.36 | 1.5 | F-P | 396 |
| | AP 3 | 0.18 | 3.7 | F-P | 720 |
| | AP 4 | 0.19 | 3.5 | F-P | 684 |
| (Pan and Moehle 1992) | 1 | 0.35 | 1.5 | P | 468 |
| | 2 | 0.35 | 1.5 | P | 396 |
| | 3 | 0.22 | 3.1 | F-P | 720 |
| | 4 | 0.22 | 3.2 | P | 684 |
| (Robertson and Durrani 1990) | 1 | 0.21 | 2.8 | F | 573 |
| | 2C | 0.22 | 3.5 | F-P | 586 |
| | 3SE | 0.19 | 3.5 | F | 640 |
| | 5SO | 0.21 | 3.5 | F | 591 |
| | 6LL | 0.54 | 0.9 | P | 227 |
| | 7L | 0.40 | 1.5 | P | 353 |
| | 8I | 0.18 | 3.5 | F-P | 590 |
| (Robertson et al. 2002) | 1C | 0.17 | 3.5 | P | 517 |
| (Symonds et al. 1976) | S6 | 0.86 | 1.1 | P | 644 |
| | S7 | 0.81 | 1.0 | P | 376 |
| (Wey and Durrani 1992) | SC 0 | 0.25 | 3.5 | P | 549 |
| (Zee and Moehle 1984) | INT | 0.21 | 3.3 | F-P | N/A |

Table 3-1 Experimental Program Summary

| | Date | Roof Displacement [in] | Roof Drift [%] | Position | Data Collected | | | |
|-----------|-----------|------------------------|----------------|--------------|------------------------|------------|--------------|-------------|
| | | | | | Whittemore Strain Data | Crack Maps | Crack Widths | Slab Survey |
| 1st Cycle | 7-Sep-07 | 0.7 | 0.2 | Initial | x | x | | x |
| | | | | + Peak | x | | | x |
| | 8-Sep-07 | -0.7 | -0.2 | Zero | | | | |
| | | | | Initial | x | | | |
| 2nd Cycle | 11-Sep-07 | 1.5 | 0.4 | + Peak | x | | | |
| | | | | Zero | | | | |
| | 12-Sep-07 | -1.5 | -0.4 | Initial | x | | | x |
| | | | | - Peak | x | x | x | x |
| 3rd Cycle | 13-Sep-07 | 3.0 | 0.8 | Final | x | | | x |
| | | | | Initial | | | | |
| | 14-Sep-07 | -3.0 | -0.8 | Intermediate | x | x | x | x |
| | | | | + Peak | x | x | x | x |
| 3rd Cycle | 14-Sep-07 | -5.4 | -1.5 | Zero | x | | | x |
| | | | | Initial | | | | |
| 4th Cycle | 28-Nov-07 | 5.4 | 1.5 | Intermediate | x | x | x | x |
| | | | | + Peak | x | x | x | x |
| | 29-Nov-07 | -5.4 | -1.5 | Zero | x | | | x |
| | | | | Initial | | | | |
| 4th Cycle | 29-Nov-07 | -10.8 | -3.0 | Intermediate | x | x | x | x |
| | | | | - Peak | x | x | x | x |
| | | | | Final | x | | | x |

Table 3-2 Load and Displacement Summary

| | Base Shear, kips | | Maximum Coefficient | Roof Displacement, in. | | Maximum Roof Drift, % |
|------------------|------------------|-------|---------------------|------------------------|--------|-----------------------|
| | North | South | | North | South | |
| 1st Cycle | 52 | -54 | 0.11 | 0.68 | -0.70 | 0.2 |
| 2nd Cycle | 80 | -80 | 0.16 | 1.51 | -1.51 | 0.4 |
| 3rd Cycle | 137 | -134 | 0.27 | 5.41 | -5.41 | 1.5 |
| 4th Cycle | 161 | -154 | 0.32 | 10.81 | -10.83 | 3.0 |

Table 3-3 Story Shear and Displacement Summary

| Cycle | Story | Story Shear, kips | | Story Displacement, in. | | Maximum Drift, % |
|--------------------------------------|----------|-------------------|-------|-------------------------|-------|------------------|
| | | North | South | North | South | |
| 1st Cycle 0.2% Roof Drift | 3 | 9 | -9 | 0.23 | -0.23 | 0.19 |
| | 2 | 35 | -36 | 0.28 | -0.28 | 0.23 |
| | 1 | 52 | -54 | 0.18 | -0.19 | 0.16 |
| 2nd Cycle 0.4% Roof Drift | 3 | 13 | -13 | 0.49 | -0.49 | 0.42 |
| | 2 | 53 | -54 | 0.61 | -0.62 | 0.51 |
| | 1 | 80 | -80 | 0.42 | -0.41 | 0.35 |
| 3rd Cycle 1.5% Roof Drift | 3 | 23 | -22 | 1.92 | -1.90 | 1.60 |
| | 2 | 92 | -89 | 2.16 | -2.14 | 1.80 |
| | 1 | 137 | -134 | 1.35 | -1.37 | 1.14 |
| 4th Cycle 3.0% Roof Drift | 3 | 27 | -26 | 3.84 | -3.89 | 3.24 |
| | 2 | 107 | -103 | 4.12 | -4.09 | 3.43 |
| | 1 | 161 | -154 | 2.86 | -2.88 | 2.40 |

Table 3-4 Normalized Story Drift Ratios

| Cycle | Level | Story Drift, % | | Maximum Normalized Drift [%] |
|--------------------------------------|-------|----------------|-------|------------------------------|
| | | North | South | |
| 1st Cycle 0.2% Roof Drift | 3 | 0.19 | -0.19 | 1.28 |
| | 2 | 0.23 | -0.23 | 1.56 |
| | 1 | 0.15 | -0.16 | 1.00 |
| 2nd Cycle 0.4% Roof Drift | 3 | 0.41 | -0.41 | 1.17 |
| | 2 | 0.51 | -0.52 | 1.45 |
| | 1 | 0.35 | -0.34 | 1.00 |
| 3rd Cycle 1.5% Roof Drift | 3 | 1.60 | -1.58 | 1.42 |
| | 2 | 1.80 | -1.78 | 1.60 |
| | 1 | 1.13 | -1.14 | 1.00 |
| 4th Cycle 3.0% Roof Drift | 3 | 3.20 | -3.24 | 1.34 |
| | 2 | 3.43 | -3.41 | 1.44 |
| | 1 | 2.38 | -2.40 | 1.00 |

Table 3-5 Limiting Drift Values

| Level | Shear [kips] | Story Shear [kips] | Displacement [in] | Story Displacement [in] | Roof Drift [%] | Story Drift [%] |
|-------|--------------|--------------------|-------------------|-------------------------|----------------|-----------------|
| 3 | 76.9 | 25.6 | 10.54 | 3.70 | 2.93 | 3.08 |
| 2 | 51.3 | 103 | 6.84 | 3.97 | | 3.31 |
| 1 | 25.6 | 154 | 2.87 | 2.87 | | 2.39 |

Table 3-6 Crack Width Measurements in Inches

| Column | Column Face | Crack Label | Roof Drift Ratio | | | | | | | | | | |
|--------|-------------|-------------|------------------|--------|-----------|--------|--------|--------|-----------|--------|--------|--------|-------|
| | | | 2nd Cycle | | 3rd Cycle | | | | 4th Cycle | | | | |
| | | | + 0.4% | - 0.4% | + 0.8% | + 1.5% | - 0.8% | - 1.5% | + 1.5% | + 3.0% | - 1.5% | - 3.0% | |
| 2-1A | N | c1 | | 0.010 | | | | 0.005 | | | | 0.005 | 0.005 |
| | | c2 | | 0.016 | | | | 0.016 | 0.025 | | | 0.016 | 0.020 |
| | | c3 | | 0.016 | | | | 0.020 | 0.030 | | | 0.030 | 0.040 |
| | S | c1 | 0.013 | | 0.005 | 0.005 | | | | 0.007 | 0.009 | | |
| | | c2 | 0.007 | | 0.009 | 0.009 | | | | 0.013 | 0.010 | | |
| | | c3 | 0.005 | | 0.005 | 0.009 | | | | 0.007 | 0.005 | | |
| 2-2A | N | c1 | | 0.009 | | | | 0.01 | 0.013 | | | 0.013 | 0.016 |
| | | c2 | | 0.013 | | | | 0.016 | 0.02 | | | 0.025 | 0.025 |
| | | c3 | | 0.013 | | | | 0.013 | 0.02 | | | 0.025 | 0.066 |
| | S | c1 | 0.005 | | 0.013 | 0.02 | | | | 0.025 | 0.03 | | |
| | | c2 | 0.013 | | 0.016 | 0.04 | | | | 0.04 | 0.1 | | |
| | | c3 | 0.010 | | 0.01 | 0.02 | | | | 0.025 | 0.05 | | |
| 2-3A | N | c1 | | 0.007 | | | | 0.009 | 0.013 | | | 0.016 | 0.009 |
| | | c2 | | 0.005 | | | | 0.005 | 0.007 | | | 0.009 | 0.009 |
| | | c3 | | | | | | | | | | | |
| | S | c1 | 0.010 | | 0.013 | 0.013 | | | | 0.016 | 0.050 | | |
| | | c2 | 0.016 | | 0.035 | 0.060 | | | | 0.060 | 0.150 | | |
| | | c3 | 0.013 | | 0.020 | 0.016 | | | | 0.020 | 0.050 | | |
| 2-1B | N | c1 | | 0.016 | | | | 0.025 | 0.030 | | | 0.030 | 0.035 |
| | | c2 | | 0.016 | | | | 0.020 | 0.025 | | | 0.030 | 0.025 |
| | | c3 | | 0.007 | | | | 0.007 | 0.009 | | | 0.005 | 0.005 |
| | S | c1 | | | 0.007 | 0.005 | | | | 0.010 | 0.005 | | |
| | | c2 | | | 0.007 | 0.007 | | | | 0.010 | 0.010 | | |
| | | c3 | | | 0.005 | 0.005 | | | | 0.007 | 0.005 | | |
| 2-2B | N | c1 | | 0.013 | | | | 0.013 | 0.025 | | | 0.030 | 0.060 |
| | | c2 | | 0.035 | | | | 0.050 | 0.060 | | | 0.060 | 0.125 |
| | | c3 | | 0.016 | | | | 0.016 | 0.016 | | | 0.025 | 0.025 |
| | S | c1 | 0.020 | | 0.025 | 0.016 | | | | 0.030 | 0.050 | | |
| | | c2 | 0.030 | | 0.035 | 0.060 | | | | 0.060 | 0.125 | | |
| | | c3 | 0.013 | | 0.013 | 0.020 | | | | 0.025 | 0.025 | | |
| 2-3B | N | c1 | | | | | | | | | | | |
| | | c2 | | 0.007 | | | | 0.009 | 0.010 | | | 0.013 | 0.020 |
| | | c3 | | 0.016 | | | | 0.013 | 0.016 | | | 0.020 | 0.020 |
| | S | c1 | | | 0.016 | 0.020 | | | | 0.025 | 0.030 | | |
| | | c2 | | | 0.025 | 0.050 | | | | 0.040 | 0.100 | | |
| | | c3 | | | 0.016 | 0.016 | | | | 0.025 | 0.025 | | |

Table 3-6 Crack Width Measurements in Inches (Continued)

| | | | | | | | | | | | | |
|------|---|----|-------|-------|-------|-------|-------|-------|-------|-------|-------|-------|
| 3-1A | N | c1 | | 0.005 | | | 0.010 | 0.007 | | | 0.005 | 0.007 |
| | | c2 | | 0.020 | | | 0.020 | 0.020 | | | 0.025 | 0.035 |
| | | c3 | | 0.005 | | | 0.005 | 0.010 | | | 0.010 | 0.050 |
| | S | c1 | 0.005 | | 0.005 | 0.005 | | | 0.005 | 0.005 | | |
| | | c2 | 0.007 | | 0.009 | 0.013 | | | 0.007 | 0.013 | | |
| | | c3 | 0.005 | | 0.005 | 0.005 | | | 0.005 | 0.000 | | |
| 3-2A | N | c1 | | 0.013 | | | 0.013 | 0.030 | | | 0.030 | 0.010 |
| | | c2 | | 0.016 | | | 0.016 | 0.020 | | | 0.013 | 0.025 |
| | | c3 | | 0.007 | | | 0.013 | 0.010 | | | 0.009 | 0.040 |
| | S | c1 | | | 0.016 | 0.016 | | | 0.020 | 0.100 | | |
| | | c2 | | | 0.040 | 0.060 | | | 0.060 | 0.170 | | |
| | | c3 | | | 0.016 | 0.020 | | | 0.016 | 0.025 | | |
| 3-3A | N | c1 | | 0.009 | | | 0.007 | 0.009 | | | 0.005 | 0.007 |
| | | c2 | | 0.005 | | | 0.010 | 0.010 | | | 0.013 | 0.013 |
| | | c3 | | | | | | | | | | |
| | S | c1 | 0.007 | | 0.013 | 0.016 | | | 0.016 | 0.010 | | |
| | | c2 | 0.016 | | 0.020 | 0.025 | | | 0.025 | 0.025 | | |
| | | c3 | 0.007 | | 0.010 | 0.013 | | | 0.013 | 0.025 | | |
| 3-1B | N | c1 | | 0.016 | | | 0.020 | 0.030 | | | 0.030 | 0.030 |
| | | c2 | | 0.013 | | | 0.010 | 0.016 | | | 0.013 | 0.013 |
| | | c3 | | 0.010 | | | 0.016 | 0.025 | | | 0.025 | 0.020 |
| | S | c1 | 0.007 | | 0.009 | 0.010 | | | 0.009 | 0.005 | | |
| | | c2 | 0.010 | | 0.005 | 0.005 | | | 0.005 | 0.005 | | |
| | | c3 | 0.005 | | | | | | | | | |
| 3-2B | N | c1 | | 0.013 | | | 0.013 | 0.025 | | | 0.010 | |
| | | c2 | | 0.016 | | | 0.016 | 0.020 | | | 0.020 | |
| | | c3 | | 0.010 | | | 0.016 | 0.020 | | | 0.010 | |
| | S | c1 | 0.016 | | 0.016 | 0.020 | | | 0.025 | 0.070 | | |
| | | c2 | 0.025 | | 0.030 | 0.060 | | | 0.060 | 0.125 | | |
| | | c3 | 0.013 | | 0.016 | 0.016 | | | 0.016 | 0.030 | | |
| 3-3B | N | c1 | | | | | | | | | | |
| | | c2 | | 0.005 | | | 0.005 | 0.010 | | | 0.010 | 0.020 |
| | | c3 | | 0.010 | | | 0.009 | 0.013 | | | 0.010 | 0.009 |
| | S | c1 | | | 0.013 | 0.025 | | | 0.030 | 0.045 | | |
| | | c2 | | | 0.016 | 0.016 | | | 0.020 | 0.025 | | |
| | | c3 | | | 0.013 | 0.016 | | | 0.016 | 0.050 | | |

Table 3-6 Crack Width Measurements in Inches (Continued)

| | | | | | | | | | | | | |
|------|---|----|-------|-------|-------|-------|-------|-------|-------|-------|-------|-------|
| R-1A | N | c1 | | 0.005 | | | 0.007 | 0.010 | | | 0.010 | 0.013 |
| | | c2 | | 0.009 | | | 0.010 | 0.016 | | | 0.010 | 0.013 |
| | | c3 | | 0.010 | | | 0.013 | 0.016 | | | 0.010 | 0.020 |
| | S | c1 | 0.005 | | 0.005 | 0.010 | | | 0.009 | 0.010 | | |
| | | c2 | 0.005 | | 0.007 | 0.009 | | | 0.013 | 0.009 | | |
| | | c3 | 0.005 | | 0.009 | 0.013 | | | 0.007 | 0.009 | | |
| R-2A | N | c1 | | 0.016 | | | 0.025 | 0.020 | | | 0.020 | 0.016 |
| | | c2 | | 0.020 | | | 0.016 | 0.016 | | | 0.005 | 0.007 |
| | | c3 | | 0.009 | | | 0.013 | 0.013 | | | 0.020 | 0.020 |
| | S | c1 | | | 0.009 | 0.010 | | | 0.010 | 0.016 | | |
| | | c2 | | | 0.030 | 0.040 | | | 0.060 | 0.070 | | |
| | | c3 | | | 0.005 | 0.010 | | | 0.007 | 0.010 | | |
| R-3A | N | c1 | | 0.007 | | | 0.007 | 0.005 | | | 0.007 | 0.005 |
| | | c2 | | 0.007 | | | 0.007 | 0.007 | | | 0.005 | 0.010 |
| | | c3 | | | | | | | | | | |
| | S | c1 | 0.010 | | 0.016 | 0.013 | | | 0.016 | 0.030 | | |
| | | c2 | 0.020 | | 0.035 | 0.040 | | | 0.030 | 0.050 | | |
| | | c3 | 0.007 | | 0.009 | 0.013 | | | 0.013 | 0.016 | | |
| R-1B | N | c1 | | 0.010 | | | 0.013 | 0.013 | | | 0.013 | 0.013 |
| | | c2 | | 0.009 | | | 0.007 | 0.007 | | | 0.005 | 0.005 |
| | | c3 | | 0.010 | | | 0.020 | 0.025 | | | 0.030 | 0.020 |
| | S | c1 | 0.007 | | 0.007 | 0.007 | | | 0.007 | 0.010 | | |
| | | c2 | 0.005 | | 0.013 | 0.016 | | | 0.013 | 0.013 | | |
| | | c3 | 0.005 | | 0.005 | 0.005 | | | 0.005 | 0.005 | | |
| R-2B | N | c1 | | 0.009 | | | 0.010 | 0.009 | | | 0.016 | 0.013 |
| | | c2 | | 0.013 | | | 0.025 | 0.020 | | | 0.030 | 0.040 |
| | | c3 | | 0.016 | | | 0.016 | 0.016 | | | 0.013 | 0.016 |
| | S | c1 | 0.013 | | 0.016 | 0.025 | | | 0.016 | 0.020 | | |
| | | c2 | 0.020 | | 0.025 | 0.020 | | | 0.030 | 0.035 | | |
| | | c3 | 0.010 | | 0.010 | 0.013 | | | 0.010 | 0.007 | | |
| R-3B | N | c1 | | | | | 0.009 | | | | | |
| | | c2 | | 0.010 | | | 0.010 | 0.010 | | | 0.010 | 0.016 |
| | | c3 | | 0.005 | | | | 0.020 | | | 0.016 | 0.025 |
| | S | c1 | | | 0.010 | 0.016 | | | 0.013 | 0.013 | | |
| | | c2 | | | 0.020 | 0.030 | | | 0.030 | 0.035 | | |
| | | c3 | | | 0.010 | 0.013 | | | 0.010 | 0.016 | | |

Table 4-1 Cracking and Yield Moments

| | I_g [in ⁴] | I_{cr} [in ⁴] | | f_r [psi] | M_{cr} [kip-in] | M_y [kip-in] |
|-----------------------|--------------------------|-----------------------------|-----------------|-------------|-------------------|----------------|
| | | Calculated | Trilinear Model | | | |
| Column ⁽¹⁾ | 8750 | 2630 | $1/3 I_g$ | 460 | 660 | 2780 |
| Slab | 3430 | 720 | $1/5 I_g$ | 470 | 460 | 2080 |

⁽¹⁾ Calculated column moments are the average of three columns in the frame

Table 4-2 Trilinear Analysis Summary

| Moments of Inertia | Base Shear | | Roof Displacement [in] | Roof Drift Ratio [%] |
|---|------------|-------------|------------------------|----------------------|
| | [kips] | Coefficient | | |
| $I_{col} = I_g$ $I_{slab} = I_g$ | 39 | 0.08 | 0.4 | 0.1 |
| $I_{col} = 1/3 I_g$ $I_{slab} = 1/5 I_g$ | 146 | 0.29 | 5.7 | 1.6 |
| $I_{col} = 1/3 I_g$ $I_{slab} = 1/5 I_g$ | 171 | 0.34 | 16.8 | 4.7 |

Table 4-3 Nonlinear Analysis Frame Section Properties

| | Width [in] | Thickness [in] | Moment of Inertia [in ⁴] | Cover to Rebar Center [in] | f'_c [psi] | f_y [ksi] |
|--------|------------|----------------|--------------------------------------|----------------------------|--------------|-------------|
| Column | 18 | 18 | $1/2 I_g$ | 2.3 | 4.0 | 66.0 |
| Beam | 120 | 7 | $1/2 I_g$ | 1 | 4.0 | 68.0 |

Table 4-4 Nonlinear Analysis Rotation Hinge Properties

| | M_y [k-in] | M_u [k-in] | θ_y [rad] | θ_u [rad] |
|------------------|-----------------|-----------------|---------------------|---------------------|
| Column | 2850 | 3560 | 0 | 0.03 |
| Beam (top steel) | 1350 | 1680 | 0 | 0.03 |
| Beam (bot steel) | 750 | 940 | 0 | 0.03 |

Table 4-5 Nonlinear Analysis Properties

| | |
|------------------------|-------------------------|
| Selfweight Load | 87.5 psf |
| Superimposed Load | 13.3 |
| Analysis Case Type | Static Nonlinear |
| Load Application | Displacement Control |
| Geometric Nonlinearity | P-Delta |
| Hinge Unloading | Local Redistribution |

Table 5-1 SDOF System Properties

| | Story | Stiffness [k/in] | Mass [k*sec ² /in] | Calculated Mode Shape | Period [sec] |
|-------------------------|-------|---------------------|----------------------------------|--------------------------|--------------------|
| SDOF | | 53 | 0.7 | | 0.7 |
| Flat-Plate Structure | 3 | 110 | 0.442 | 1.0 | 0.5 ⁽¹⁾ |
| | 2 | 122 | 0.442 | 0.72 | |
| | 1 | 212 | 0.442 | 0.29 | |

⁽¹⁾ Gross section properties assumed

Table 5-2 Original Ground Motion Records

| Earthquake | Station | Component | Peak Ground Acceleration [g] | Record Duration [sec] |
|---------------------------------|---|-----------|------------------------------------|-----------------------------|
| San Fernando 2/9/1971 | Castaic Old Ridge Route, California ⁽¹⁾ | N21E | 0.32 | 30 |
| Northridge 1/17/1994 | Tarzana Cedar Hills Nursery, California ⁽²⁾ | NS | 0.99 | 30 |
| Chili 3/3/1985 | Llolleo D.I.C., Chili ⁽³⁾ | N10E | 0.71 | 75 |
| Emperial Valley 5/18/1940 | El Centro Irrigation District, California ⁽⁴⁾ | NS | 0.35 | 45 |
| Hyogo-Ken-Nanbu 1/17/1995 | Kobe KMMO, Japan ⁽⁵⁾ | NS | 0.83 | 30 |
| Kern County 7/21/1952 | Taft Lincoln School Tunnel, California ⁽⁴⁾ | N21E | 0.16 | 45 |
| Western Washington 4/13/1949 | Seattle Army Base, Washington ⁽⁶⁾ | S02W | 0.07 | 65 |
| Miyagi-Ken-Okii 6/12/1978 | Sendai Tohoku University, Japan ⁽⁷⁾ | NS | 0.26 | 40 |
| Kern County 7/21/1952 | Santa Barbara Courthouse, California ⁽⁴⁾ | S48E | 0.13 | 60 |
| Tokachi-Okii 5/16/1968 | Hachinohe Harbor, Japan ⁽⁷⁾ | EW | 0.19 | 35 |

^(a) Cut from original record at 25 sec.

Information Sources:

⁽¹⁾ CALTECH. (1973c)

⁽²⁾ CSMIP (1994)

⁽³⁾ Saragoni et. al (1985)

⁽⁴⁾ CALTECH. (1971)

⁽⁵⁾ JMA (1995)

⁽⁶⁾ (1973a)

⁽⁷⁾ Mori and Crouse (1981)

Table 5-3 Scaled Ground Motion Records

| | Maximum Scaled Acceleration [g] | Peak Ground Velocity [in/sec] |
|--|--|--|
| San Fernando, 1971 Castic N21E | 0.78 | 19.5 |
| Northridge, 1994 Tarzana NS | 0.62 | 19.2 |
| Chili, 1985 Llolleo N10E | 0.55 | 12.6 |
| Emperial Valley, 1940 El Centro NS | 0.50 | 21.5 |
| Hyogo-Ken-Nanbu, 1995 Kobe NS | 0.39 | 17.0 |
| Kern County, 1952 Taft N21E | 0.38 | 17.5 |
| Western Washington, 1949 Seattle S02W | 0.31 | 13.9 |
| Miyagi-Ken-Oki, 1978 Sendai NS | 0.29 | 16.2 |
| Kern County, 1952 Santa Barabara S48E | 0.27 | 15.8 |
| Tokachi-Oki, 1968 Hachinohe EW | 0.24 | 21.8 |

Table 5-4 Calculated Displacements

| | Maximum Scaled Acceleration [g] | Peak Ground Velocity [in/sec] | Maximum Roof Displacement [in] | Roof Drift Ratio [%] |
|--|--|--------------------------------------|---------------------------------------|-----------------------------|
| San Fernando, 1971 Castic N21E | 0.78 | 19.5 | 5.0 | 1.4 |
| Northridge, 1994 Tarzana NS | 0.62 | 19.2 | 6.2 | 1.7 |
| Chili, 1985 Llolleo N10E | 0.55 | 12.6 | 4.7 | 1.3 |
| Emperial Valley, 1940 El Centro NS | 0.50 | 21.5 | 5.1 | 1.4 |
| Hyogo-Ken-Nanbu, 1995 Kobe NS | 0.39 | 17.0 | 5.7 | 1.6 |
| Kern County, 1952 Taft N21E | 0.38 | 17.5 | 9.4 | 2.6 |
| Western Washington, 1949 Seattle S02W | 0.31 | 13.9 | 10.5 | 2.9 |
| Miyagi-Ken-Oki, 1978 Sendai NS | 0.29 | 16.2 | 11.3 | 3.1 |
| Kern County, 1952 Santa Barabara S48E | 0.27 | 15.8 | 3.7 | 1.0 |
| Tokachi-Oki, 1968 Hachinohe EW | 0.24 | 21.8 | 4.7 | 1.3 |

Table 5-5 Calculated Story Drifts

| Record | Story | Displacement [in] | Story Displacement [in] | Story Drift Ratio [%] | Roof Drift Ratio [%] |
|--|--------------|------------------------------|--|--|---|
| San Fernando, 1971 Catic N21E | 3 | 5.0 | 1.3 | 1.0 | 1.4 |
| | 2 | 3.8 | 2.3 | 1.9 | |
| | 1 | 1.5 | 1.5 | 1.3 | |
| Northridge, 1994 Tarzana NS | 3 | 6.2 | 1.6 | 1.3 | 1.7 |
| | 2 | 4.7 | 2.8 | 2.3 | |
| | 1 | 1.9 | 1.9 | 1.6 | |
| Chili, 1985 Llolleo N10E | 3 | 4.7 | 1.2 | 1.0 | 1.3 |
| | 2 | 3.5 | 2.1 | 1.8 | |
| | 1 | 1.4 | 1.4 | 1.2 | |
| Emperial Valley, 1940 EI Centro NS | 3 | 5.1 | 1.3 | 1.1 | 1.4 |
| | 2 | 3.8 | 2.3 | 1.9 | |
| | 1 | 1.5 | 1.5 | 1.3 | |
| Hyogo-Ken-Nanbu, 1995 Kobe NS | 3 | 5.7 | 1.4 | 1.2 | 1.6 |
| | 2 | 4.3 | 2.6 | 2.1 | |
| | 1 | 1.7 | 1.7 | 1.4 | |
| Kern County, 1952 Taft N21E | 3 | 9.4 | 2.4 | 2.0 | 2.6 |
| | 2 | 7.1 | 4.2 | 3.5 | |
| | 1 | 2.8 | 2.8 | 2.4 | |
| Western Washington, 1949 Seattle S02W | 3 | 10.5 | 2.6 | 2.2 | 2.9 |
| | 2 | 7.9 | 4.7 | 3.9 | |
| | 1 | 3.2 | 3.2 | 2.6 | |
| Miyagi-Ken-Oki, 1978 Sendai NS | 3 | 11.3 | 2.8 | 2.4 | 3.1 |
| | 2 | 8.5 | 5.1 | 4.2 | |
| | 1 | 3.4 | 3.4 | 2.8 | |
| Kern County, 1952 Santa Barabara S48E | 3 | 3.7 | 0.9 | 0.8 | 1.0 |
| | 2 | 2.8 | 1.7 | 1.4 | |
| | 1 | 1.1 | 1.1 | 0.9 | |
| Tokachi-Oki, 1968 Hachinohe EW | 3 | 4.7 | 1.2 | 1.0 | 1.3 |
| | 2 | 3.5 | 2.1 | 1.8 | |
| | 1 | 1.4 | 1.4 | 1.2 | |

FIGURES

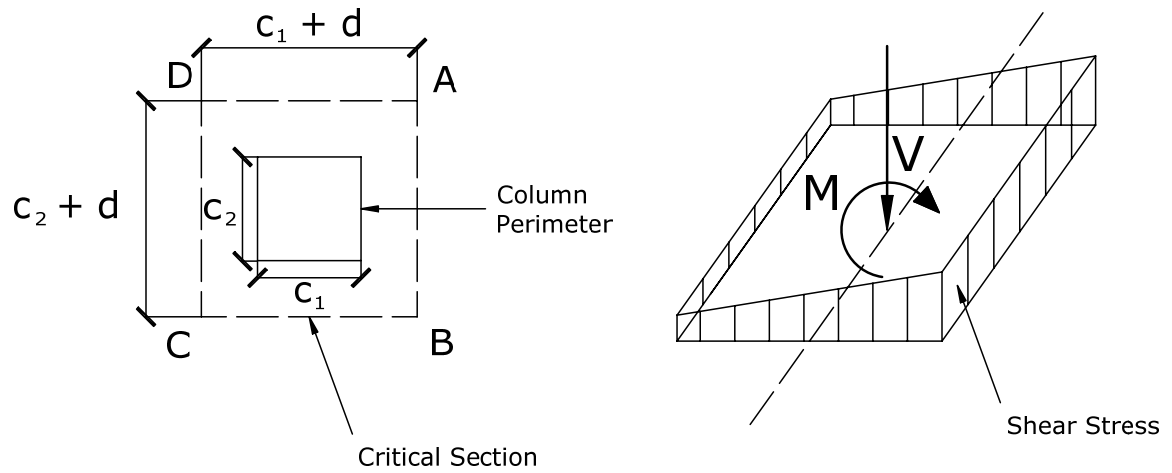


Figure 2-1 Assumed Eccentric Shear Stress Distribution (ACI 318-2005)

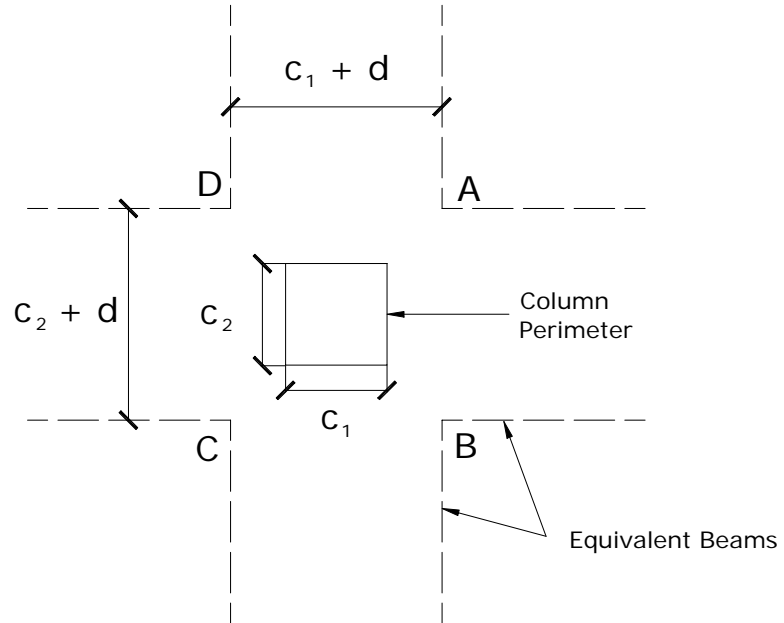


Figure 2-2 Beam Analogy (Hawkins and Corley 1971)

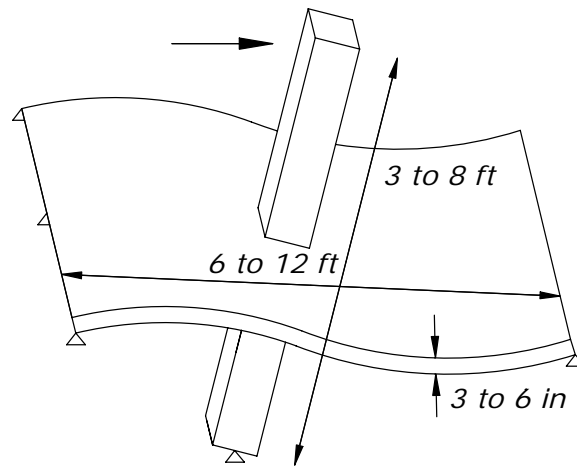


Figure 2-3 Isolated Slab-Column Test Specimen

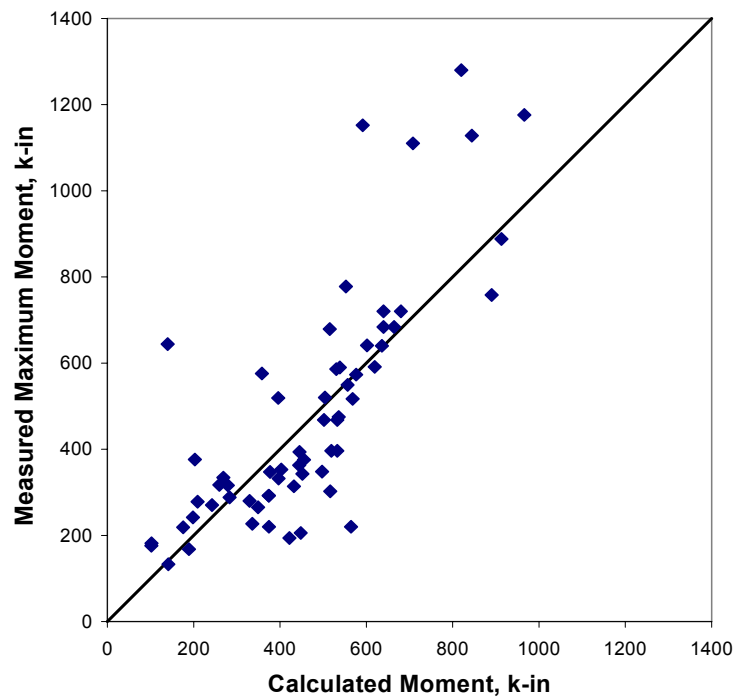


Figure 2-4 Calculated Moments using the Eccentric Shear Method

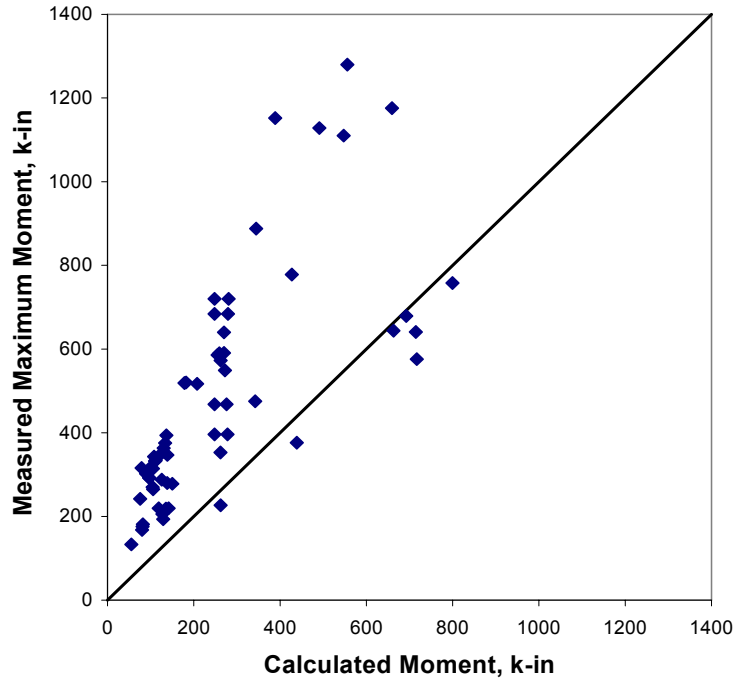


Figure 2-5 Calculated Moments using the Beam Analogy

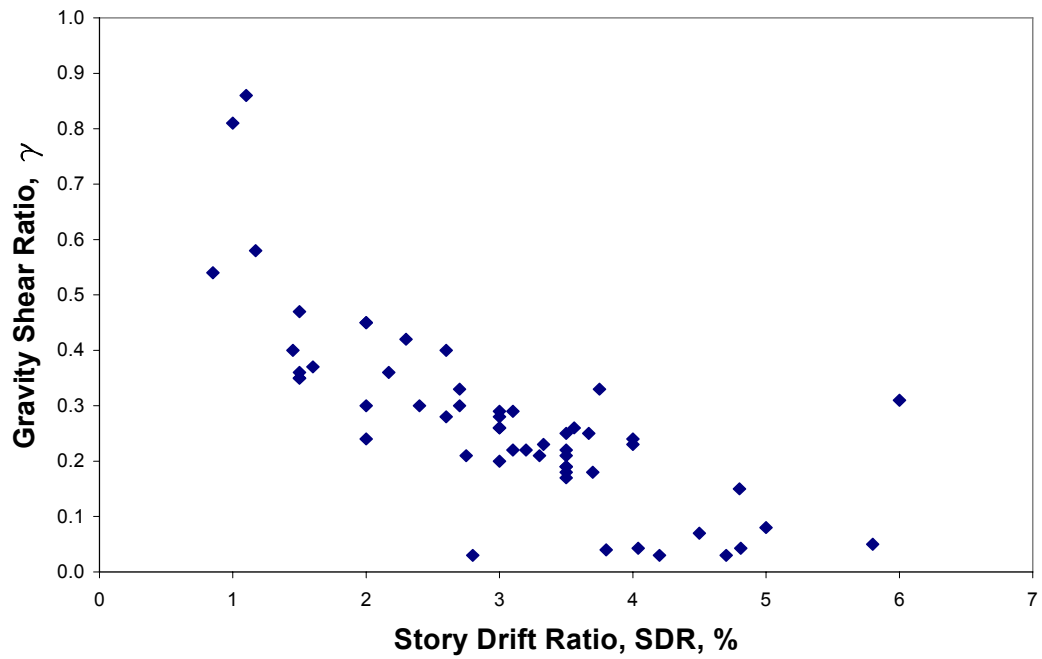
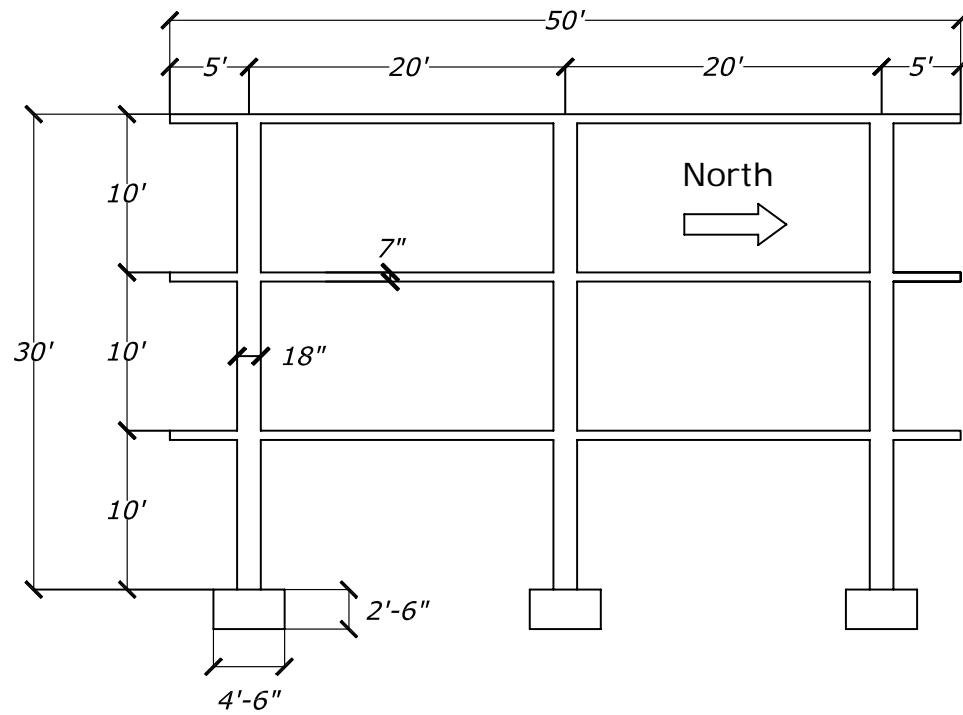
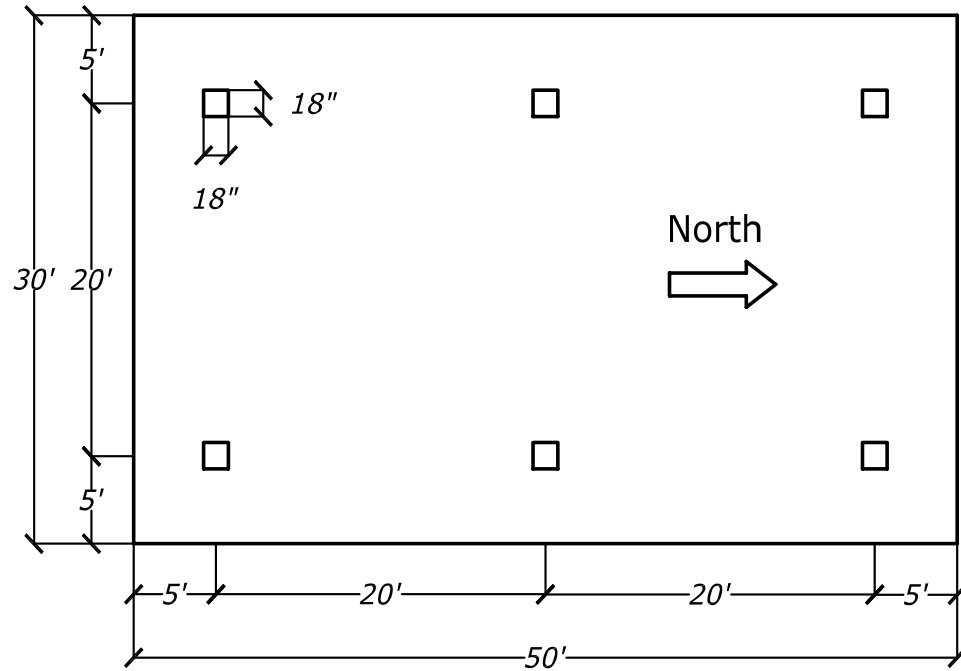


Figure 2-6 Small-Scale Slab-Column Test Data



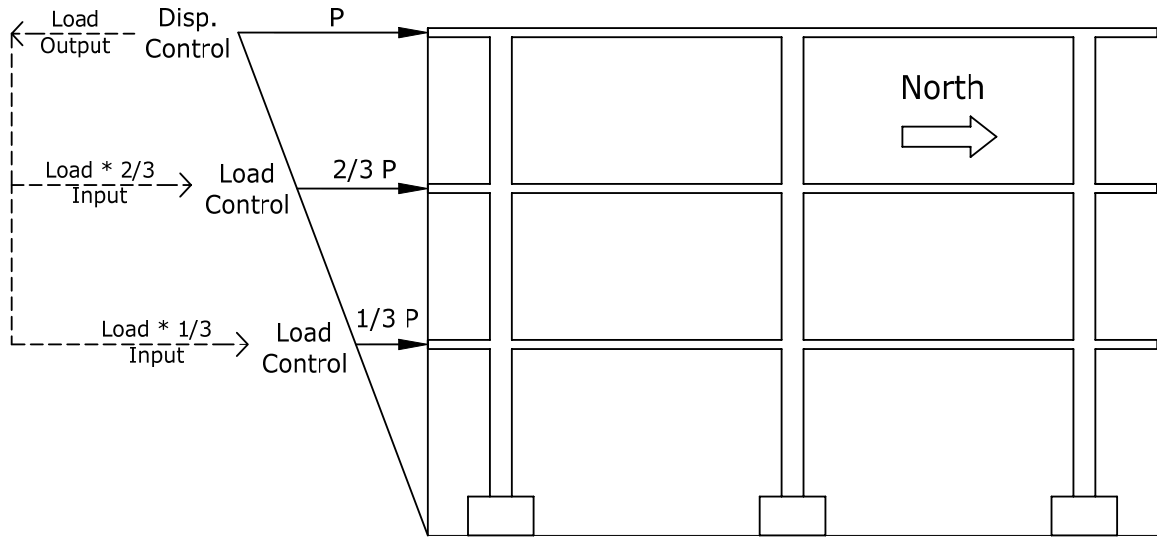


Figure 3-3 Load Distribution and Control Schematic

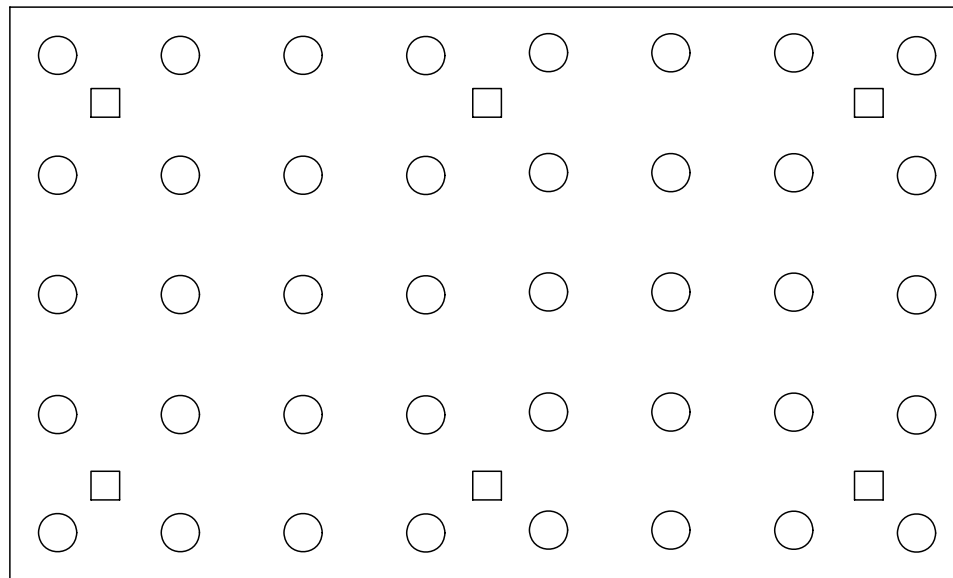


Figure 3-4 Distribution of 55-gallon Barrels of Water

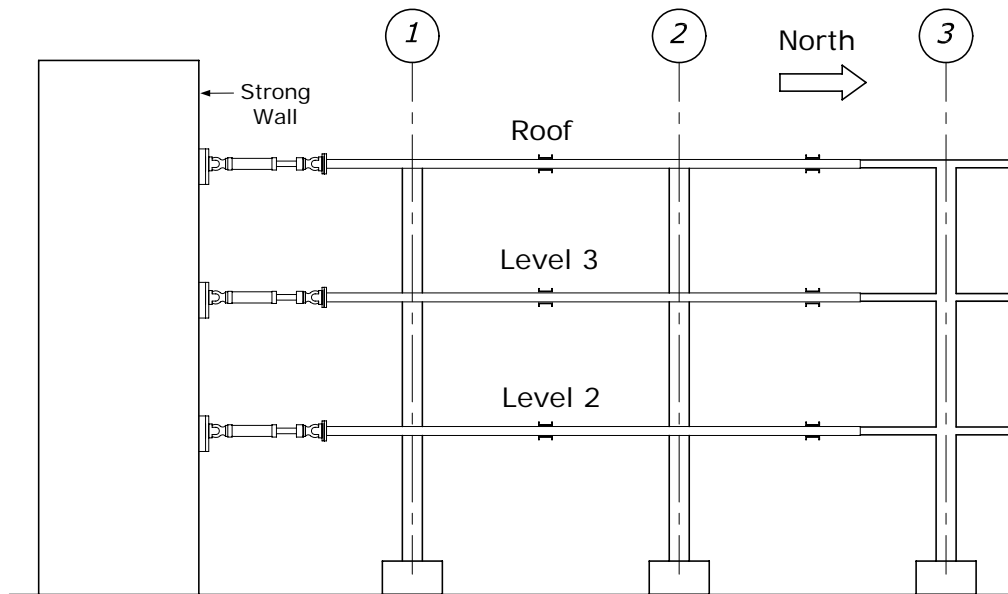


Figure 3-5 Specimen Elevation View

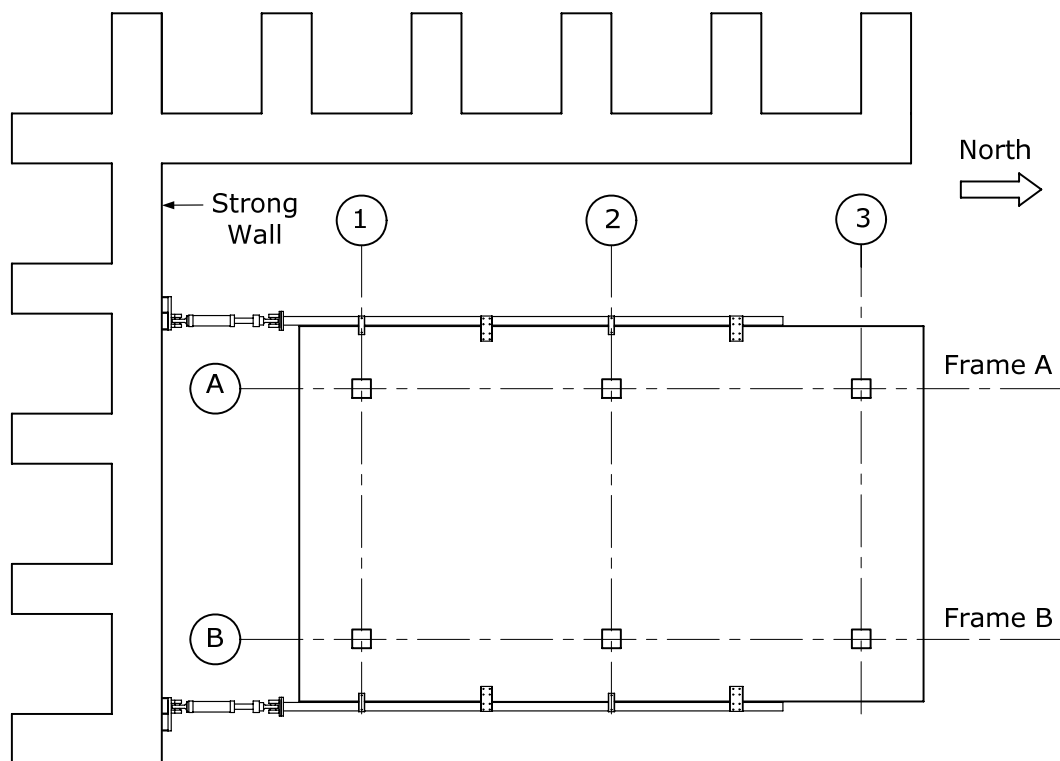


Figure 3-6 Specimen Plan View

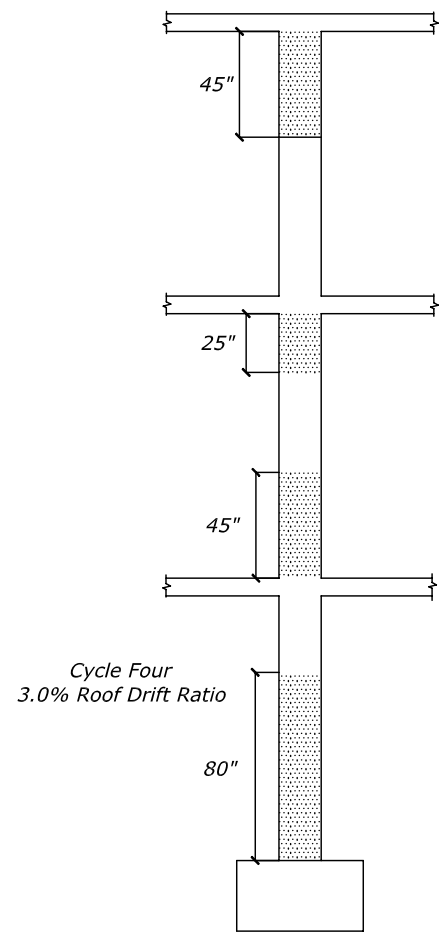
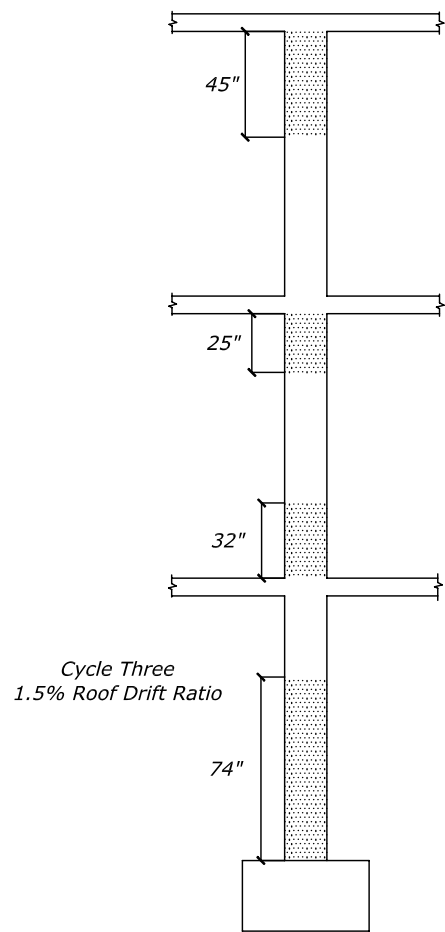
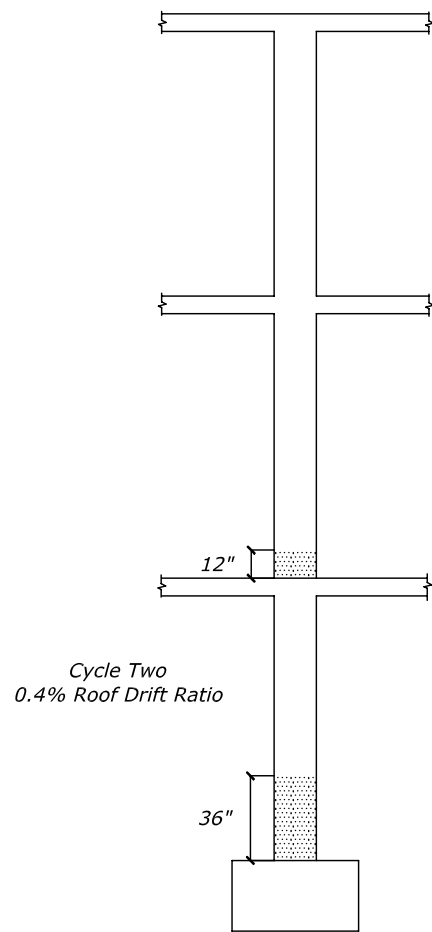


Figure 3-7 Column Flexural Cracks

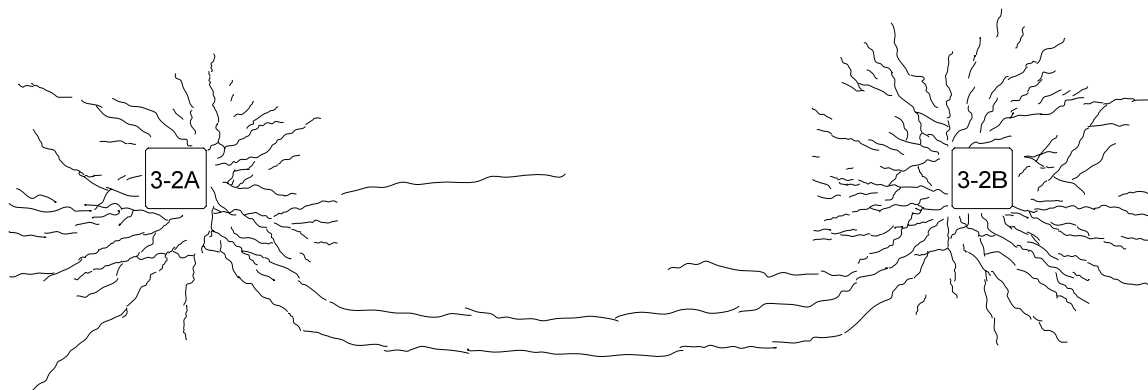


Figure 3-8 Cracks Extending Across Full-Slab Width

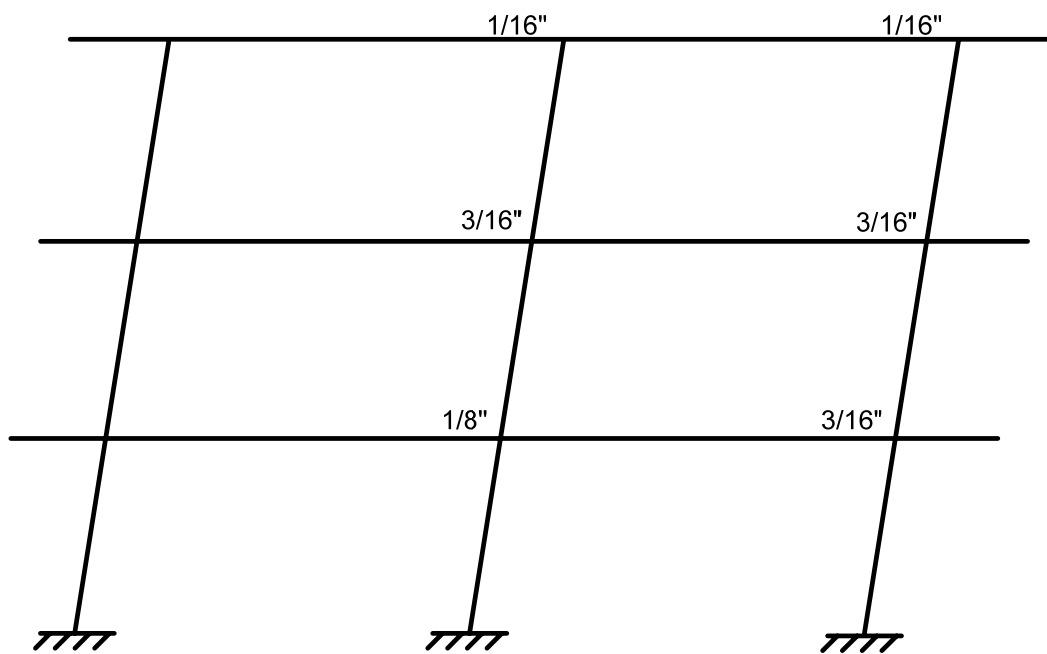


Figure 3-9 Flexural Crack Widths Frame A, North 3% Roof Drift

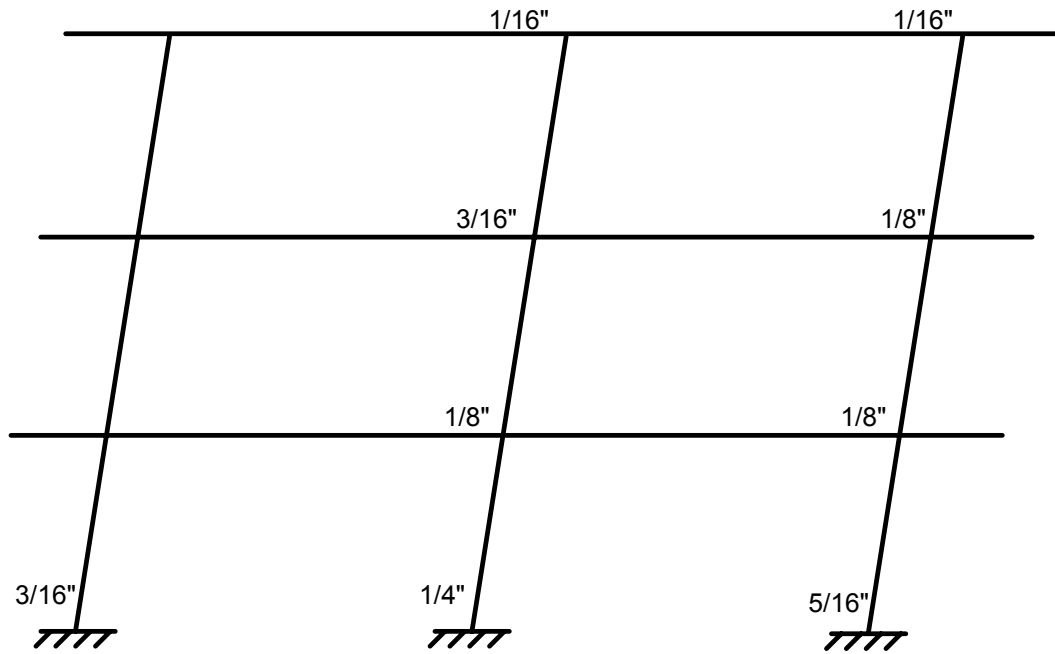


Figure 3-10 Flexural Crack Widths Frame B, North 3% Roof Drift

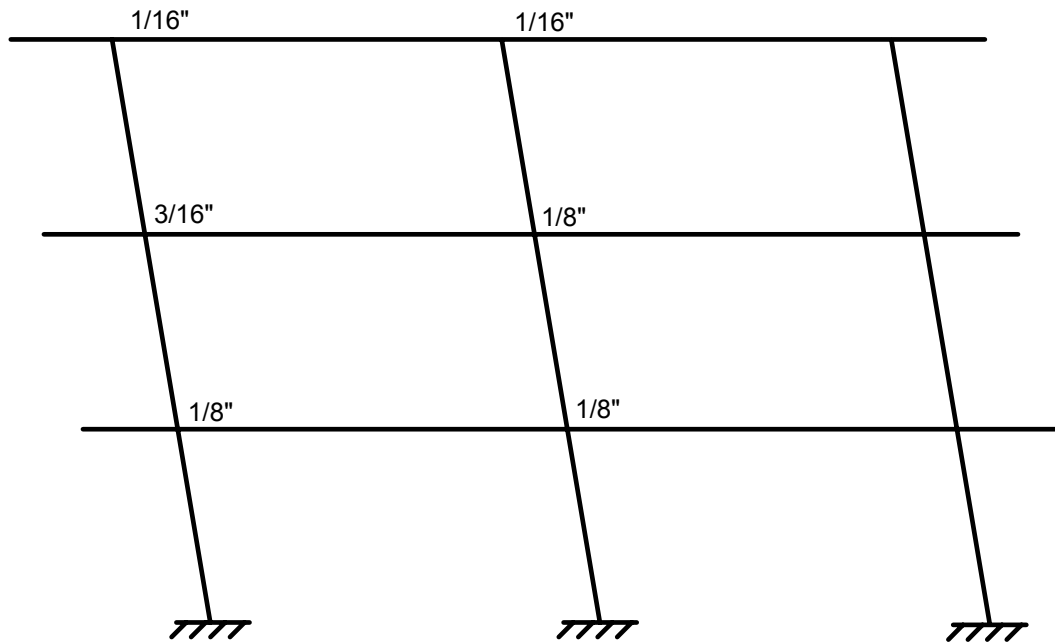


Figure 3-11 Flexural Crack Widths Frame A, South 3% Roof Drift

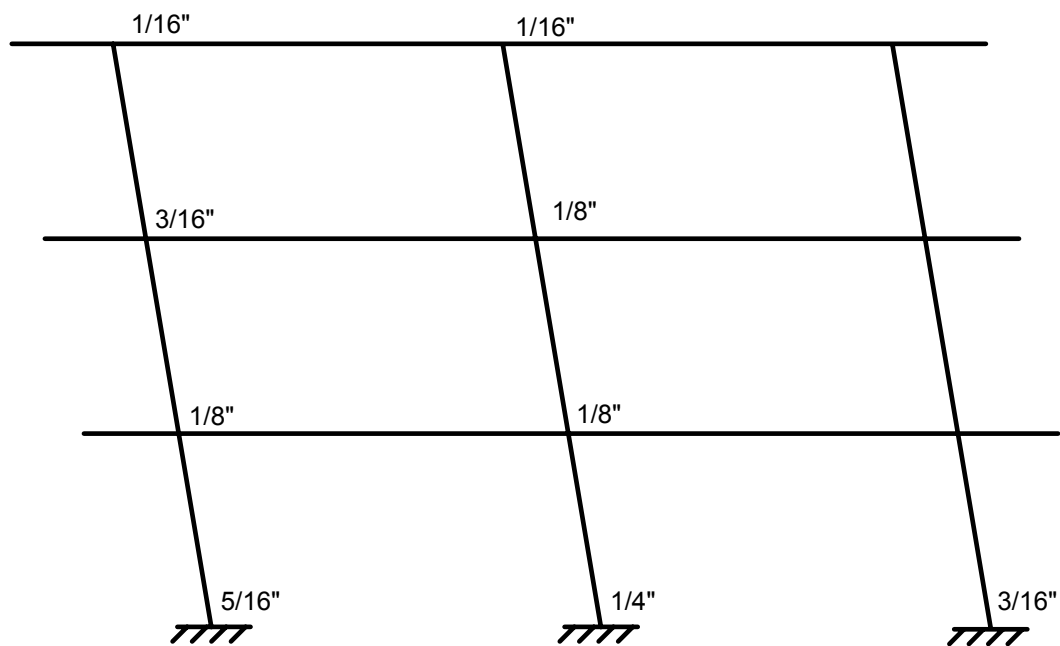


Figure 3-12 Flexural Crack Widths Frame B, South 3% Roof Drift

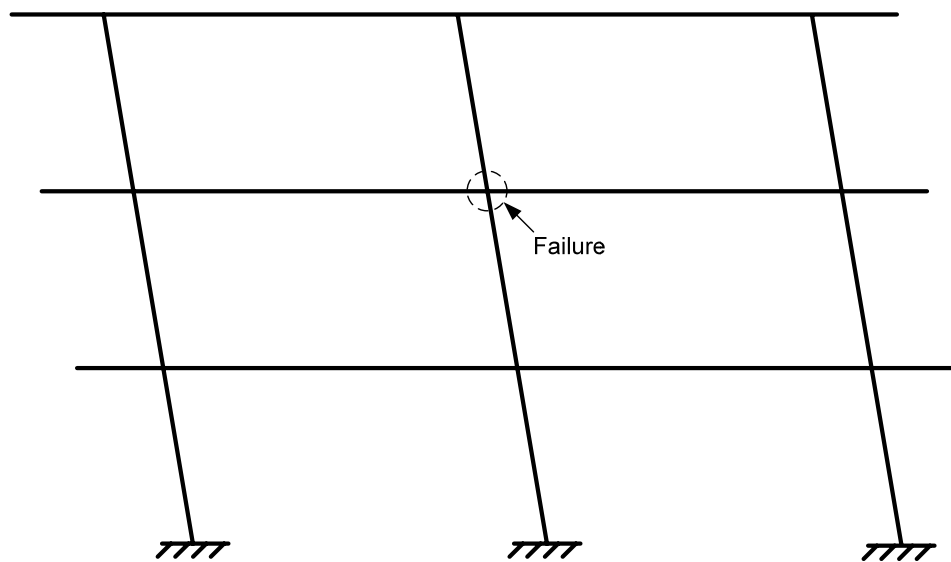


Figure 3-13 Frame B Failure Location



Figure 3-14 Slab-Column Connection Failure



Figure 3-15 Slab Column Connection Failure

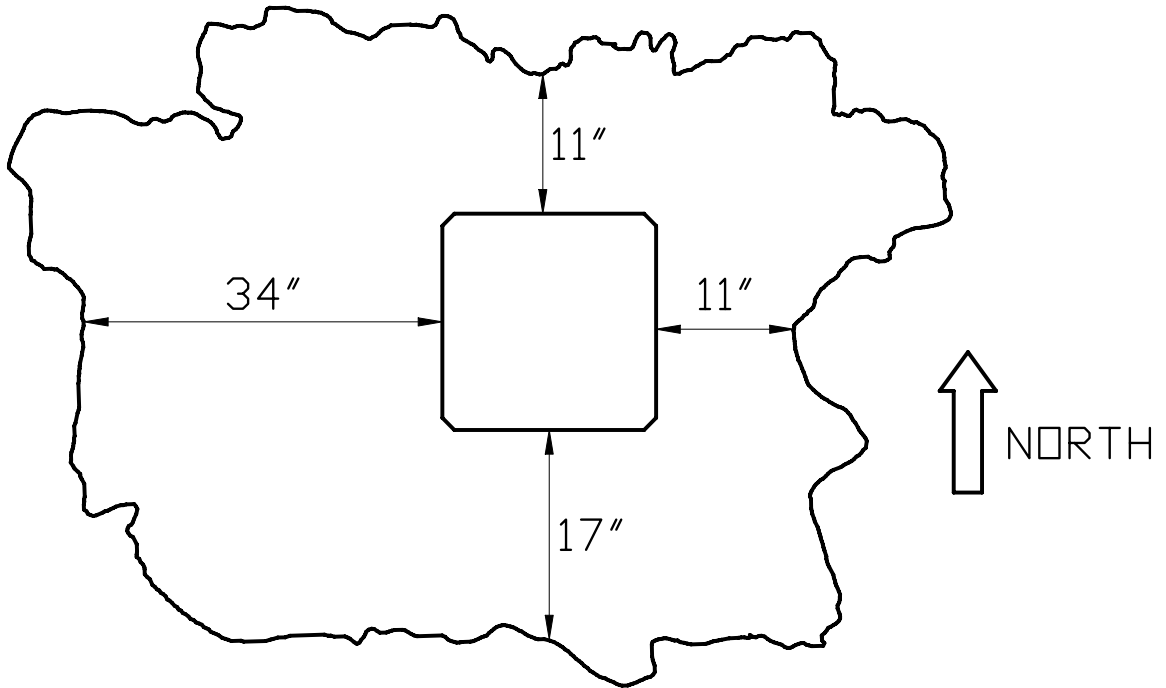


Figure 3-16 Failure Perimeter

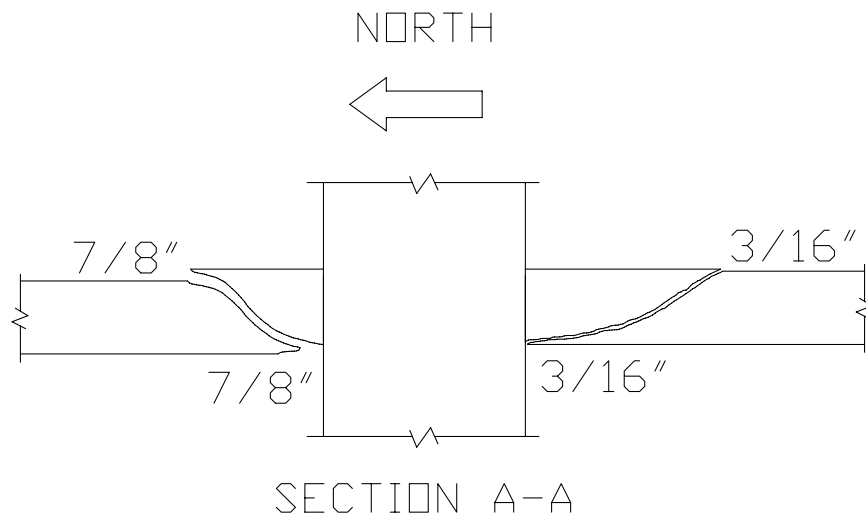


Figure 3-17 Failure Section

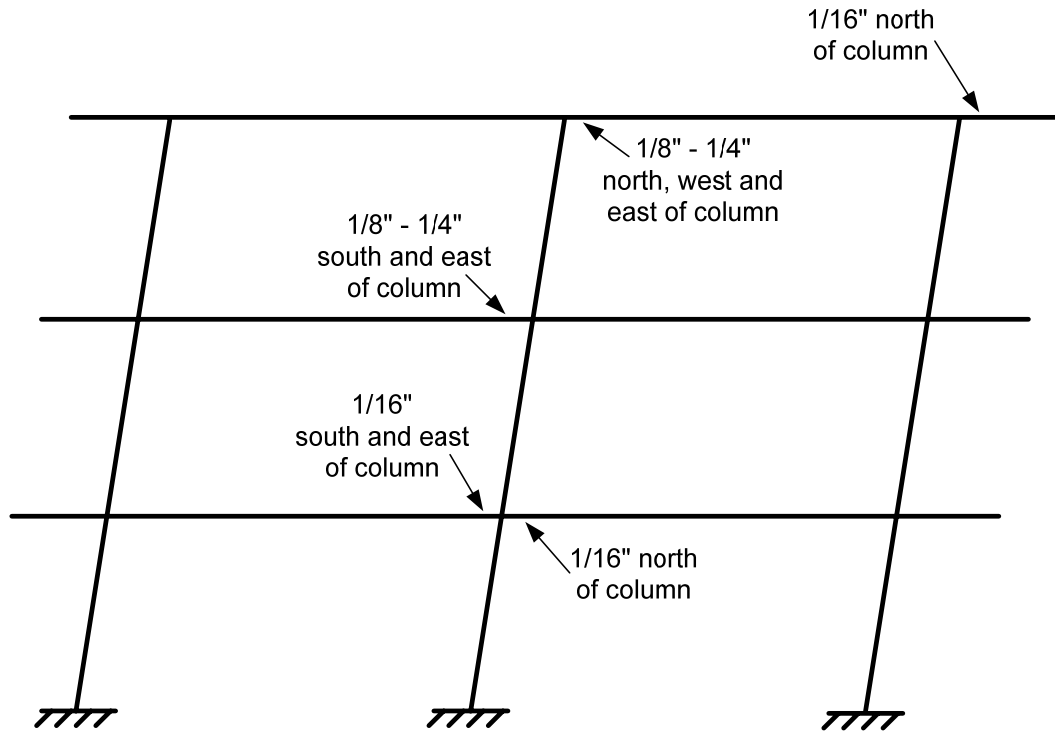


Figure 3-18 Vertical Slab Separation Frame A, North 3% Roof Drift

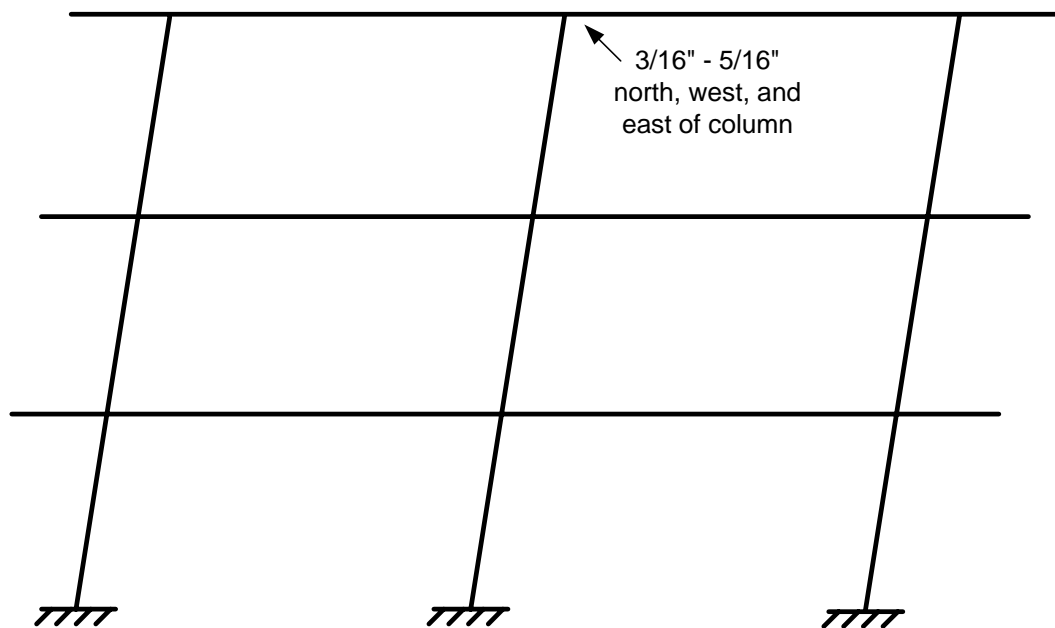


Figure 3-19 Vertical Slab Separation Frame B, North 3% Roof Drift

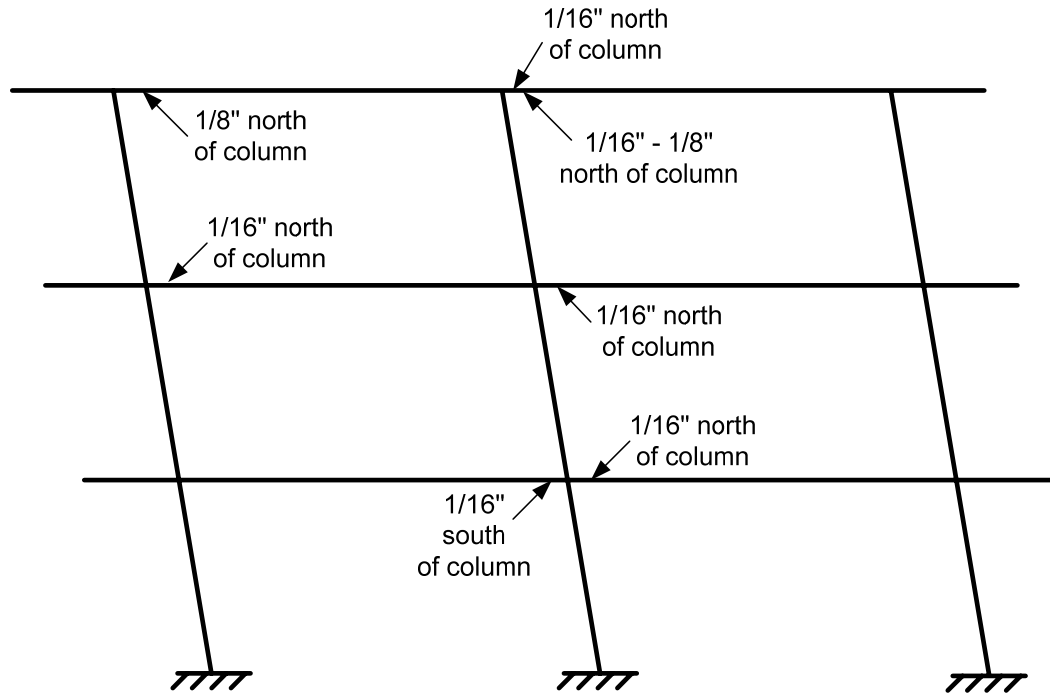


Figure 3-20 Vertical Slab Separation Frame A, South 3% Roof Drift

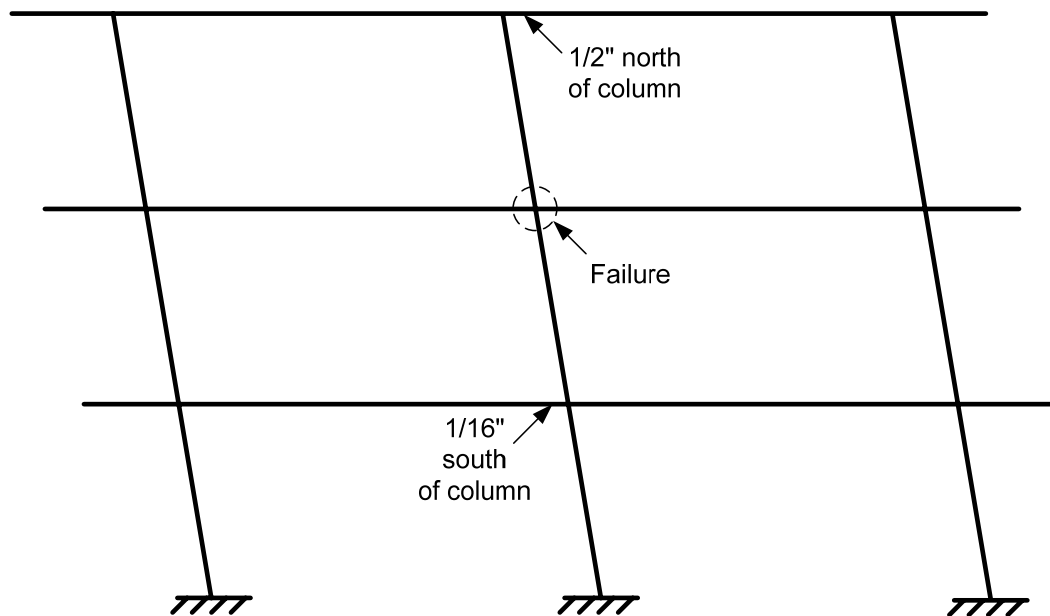


Figure 3-21 Vertical Slab Separation Frame B, South 3% Roof Drift



Figure 3-22 Vertical Slab Separation (North 3% Roof Drift Ratio)



Figure 3-23 Vertical Slab Separation (South 3% Roof Drift Ratio, Column 3-2B-N)

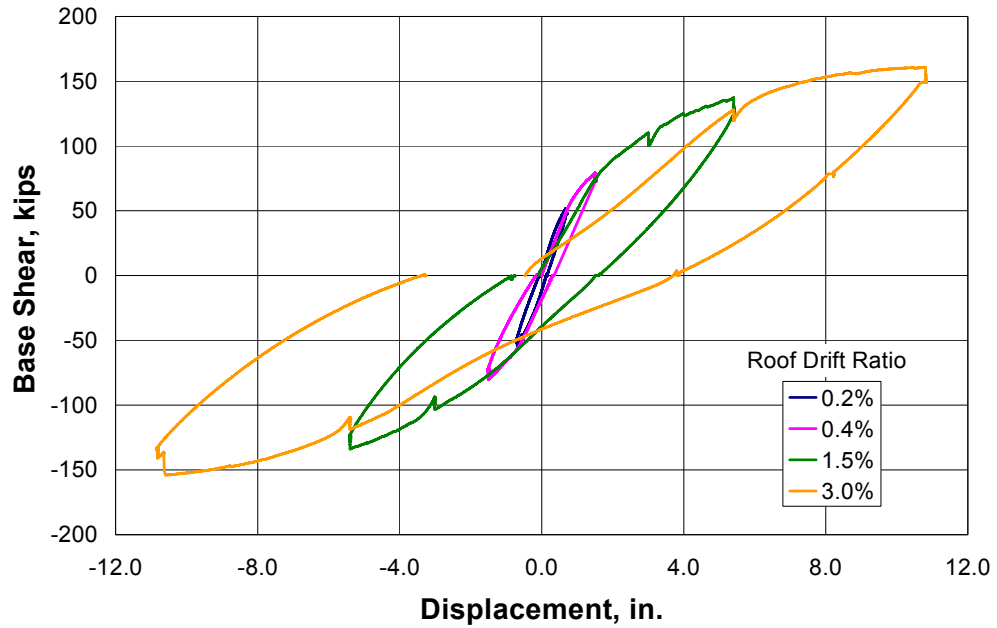


Figure 3-24 Base Shear vs. Roof Displacement
(See Table 3-2 for Peak Values)

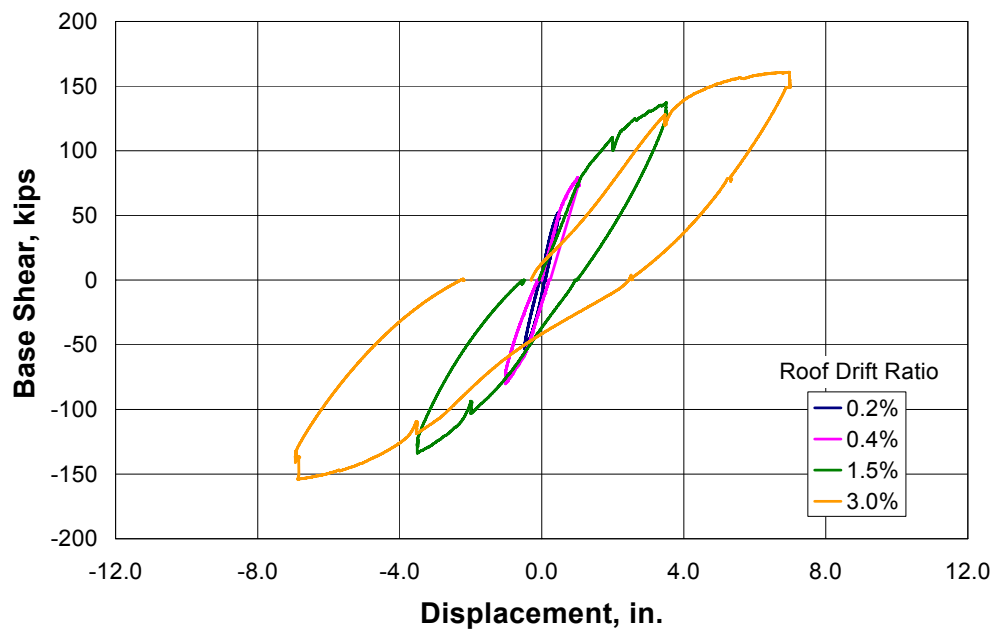


Figure 3-25 Base Shear vs. Level 3 Displacement
(See Table 3-2 for Peak Values)

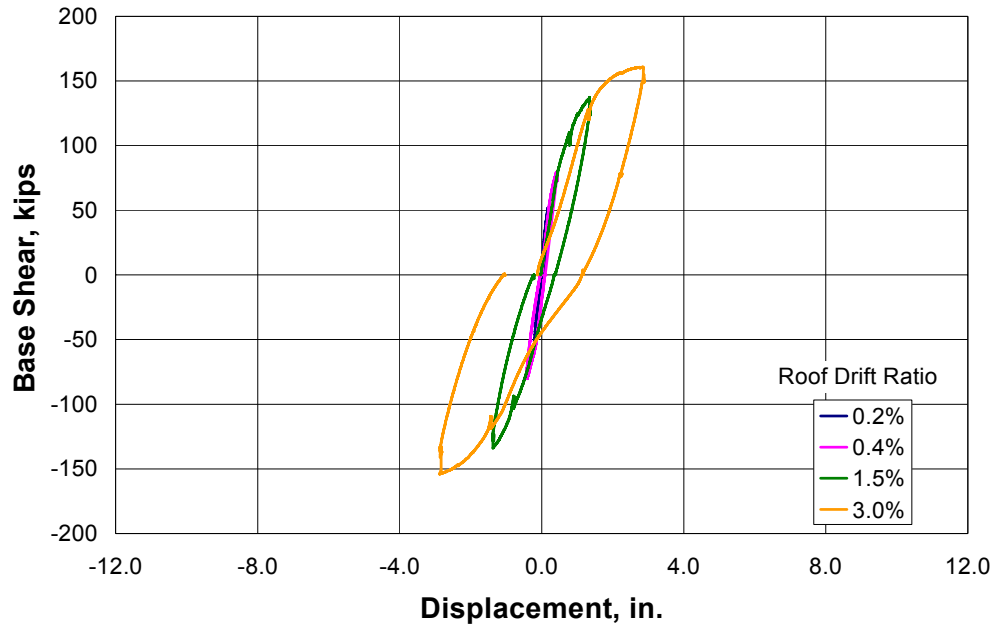


Figure 3-26 Base Shear vs. Level 2 Displacement
(See Table 3-2 for Peak Values)

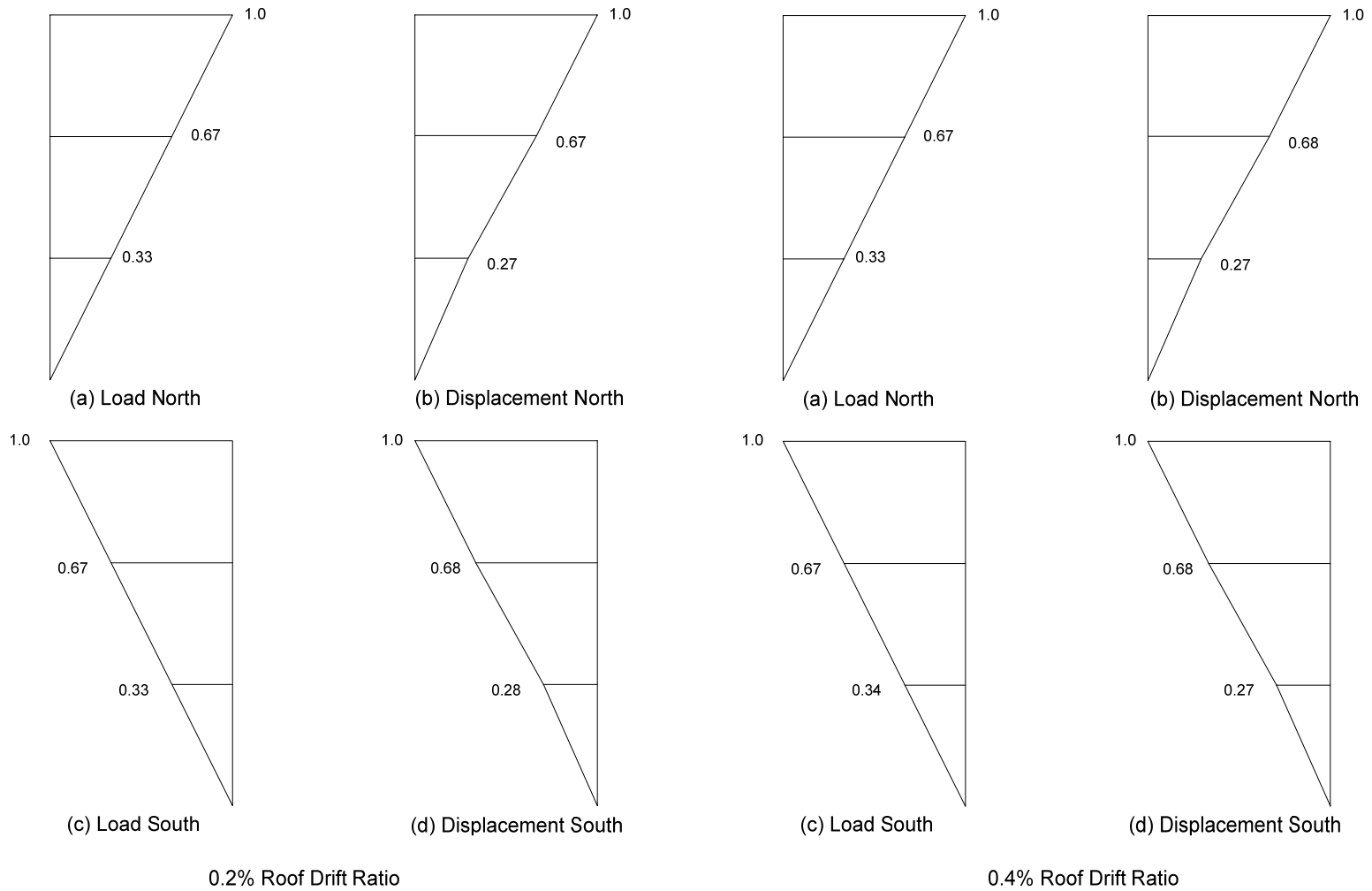


Figure 3-27 Normalized Load and Displacement Profiles (0.2% and 0.4% Roof Drift Ratio)

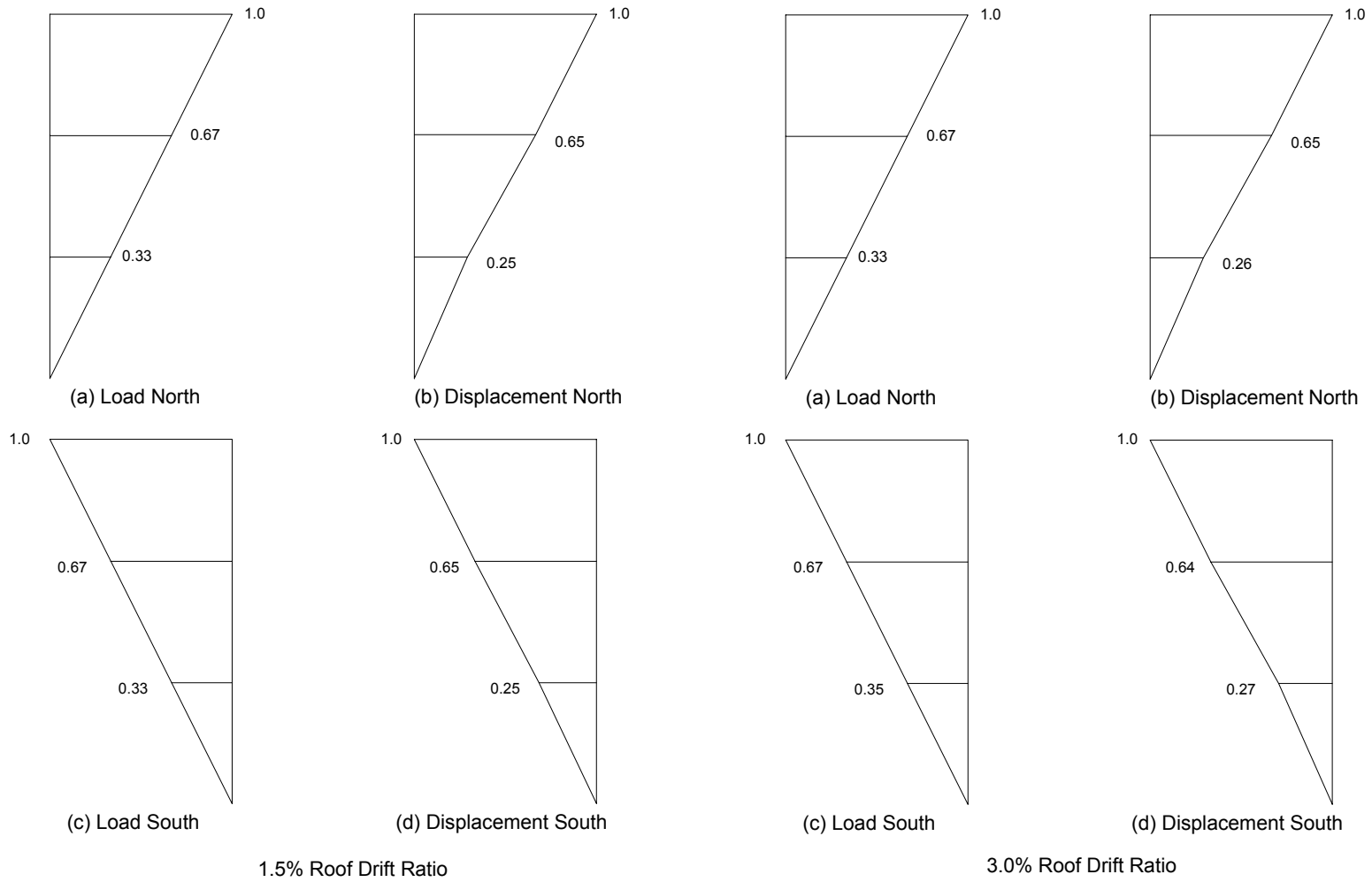


Figure 3-28 Normalized Load and Displacement Profiles (1.5% and 3.0% Roof Drift Ratio)

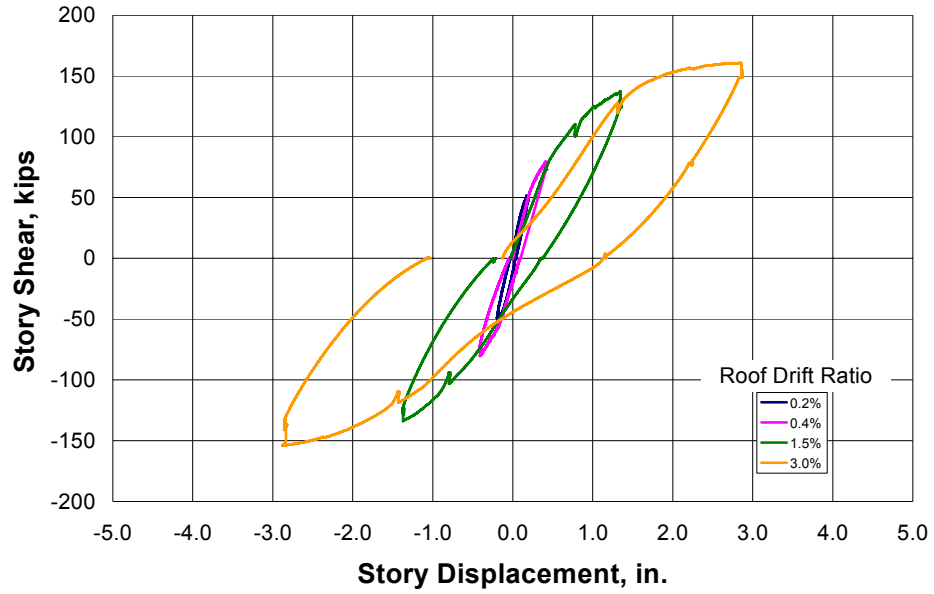


Figure 3-29 Level 1 Story Shear vs. Story Displacement
(See Table 3-3 for Peak Values)

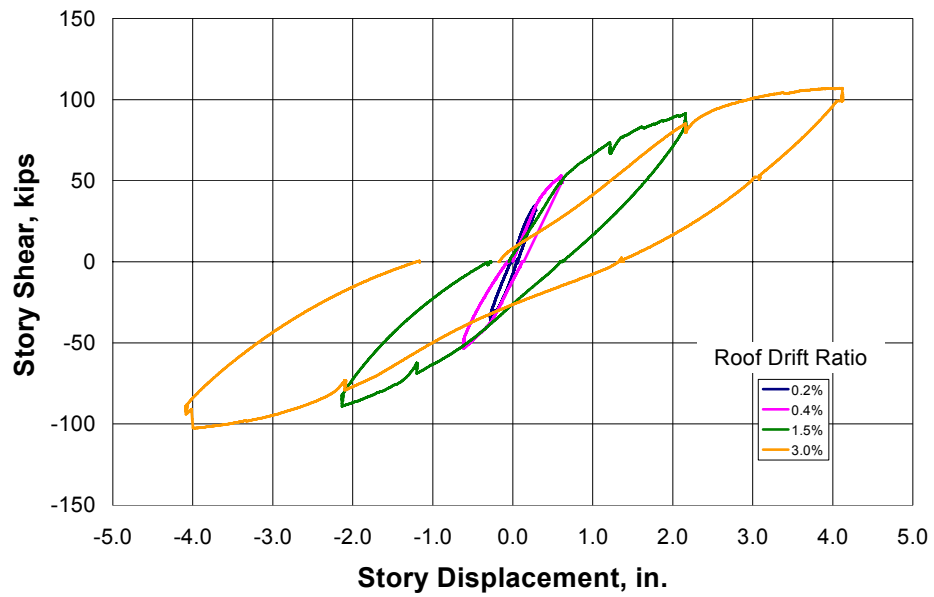


Figure 3-30 Level 2 Story Shear vs. Story Displacement
(See Table 3-3 for Peak Values)

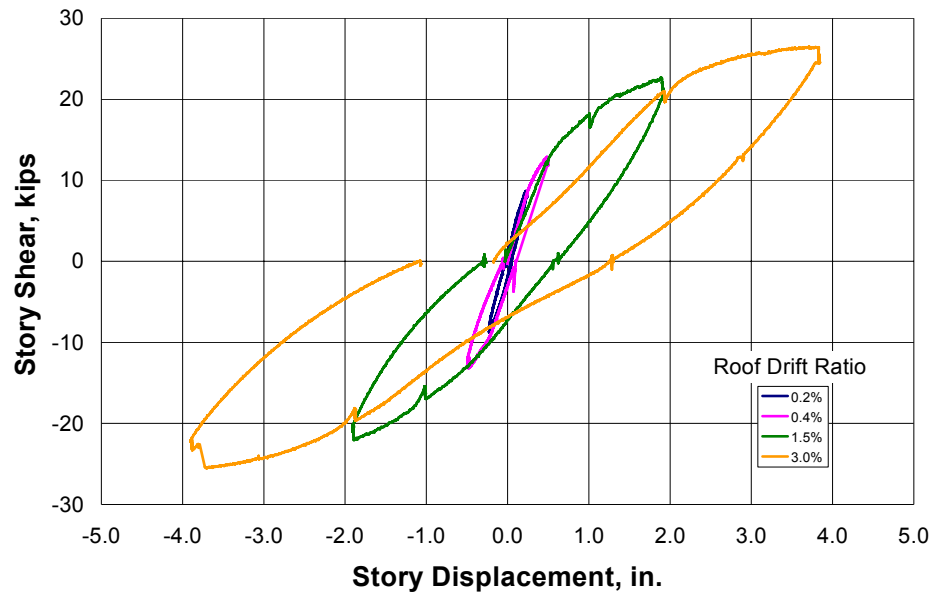


Figure 3-31 Level 3 Story Shear vs. Story Displacement
(See Table 3-3 for Peak Values)

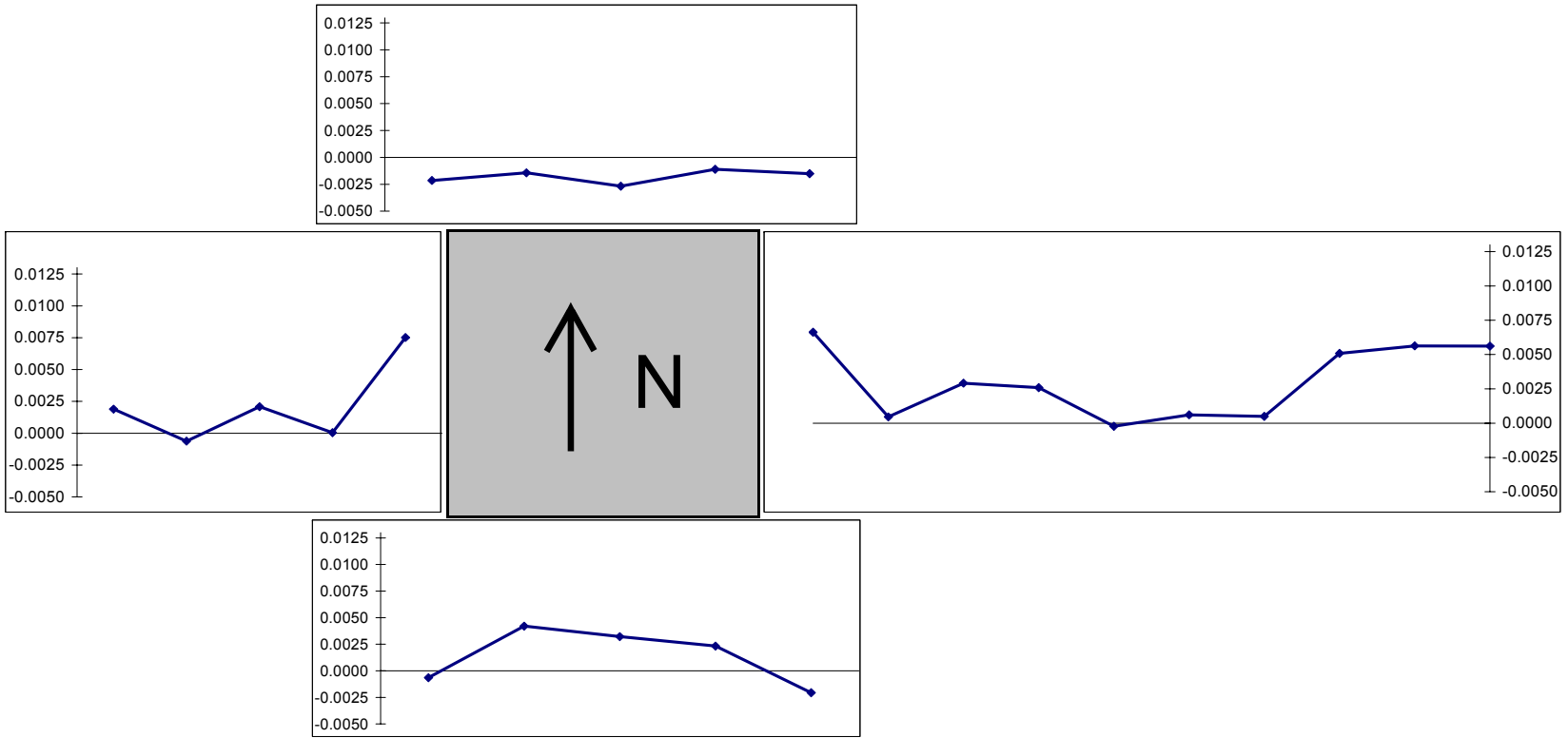


Figure 3-32 Column 2-2A Strains in Slab Surface (North 3% Roof Drift Ratio)
 (See Figure A-33 for Measurement Locations)

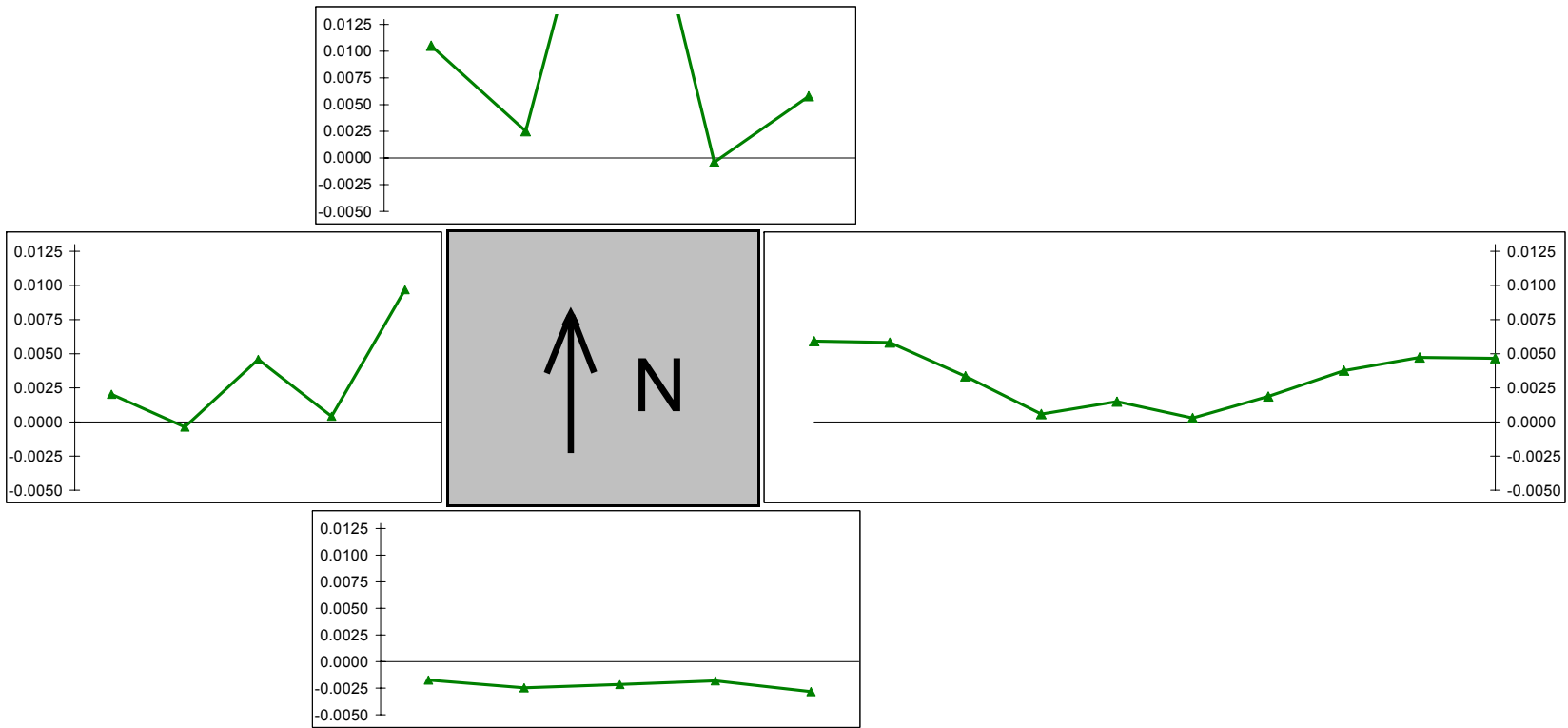


Figure 3-33 Column 2-2A Strains in Slab Surface (South 3% Roof Drift Ratio)
 (See Figure A-33 for Measurement Locations)

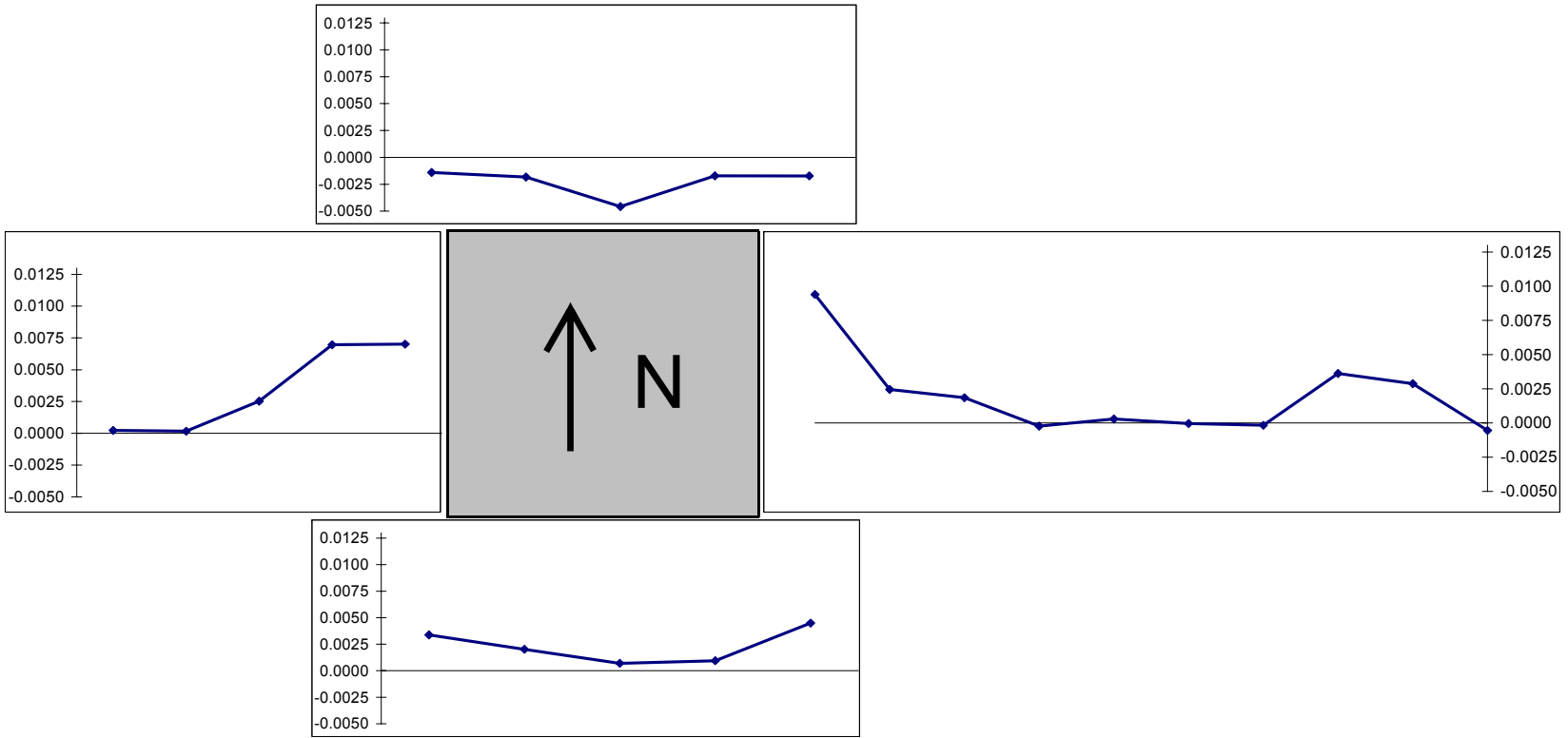


Figure 3-34 Column 3-2A Strains in Slab Surface (North 3% Roof Drift Ratio)
 (See Figure A-33 for Measurement Locations)

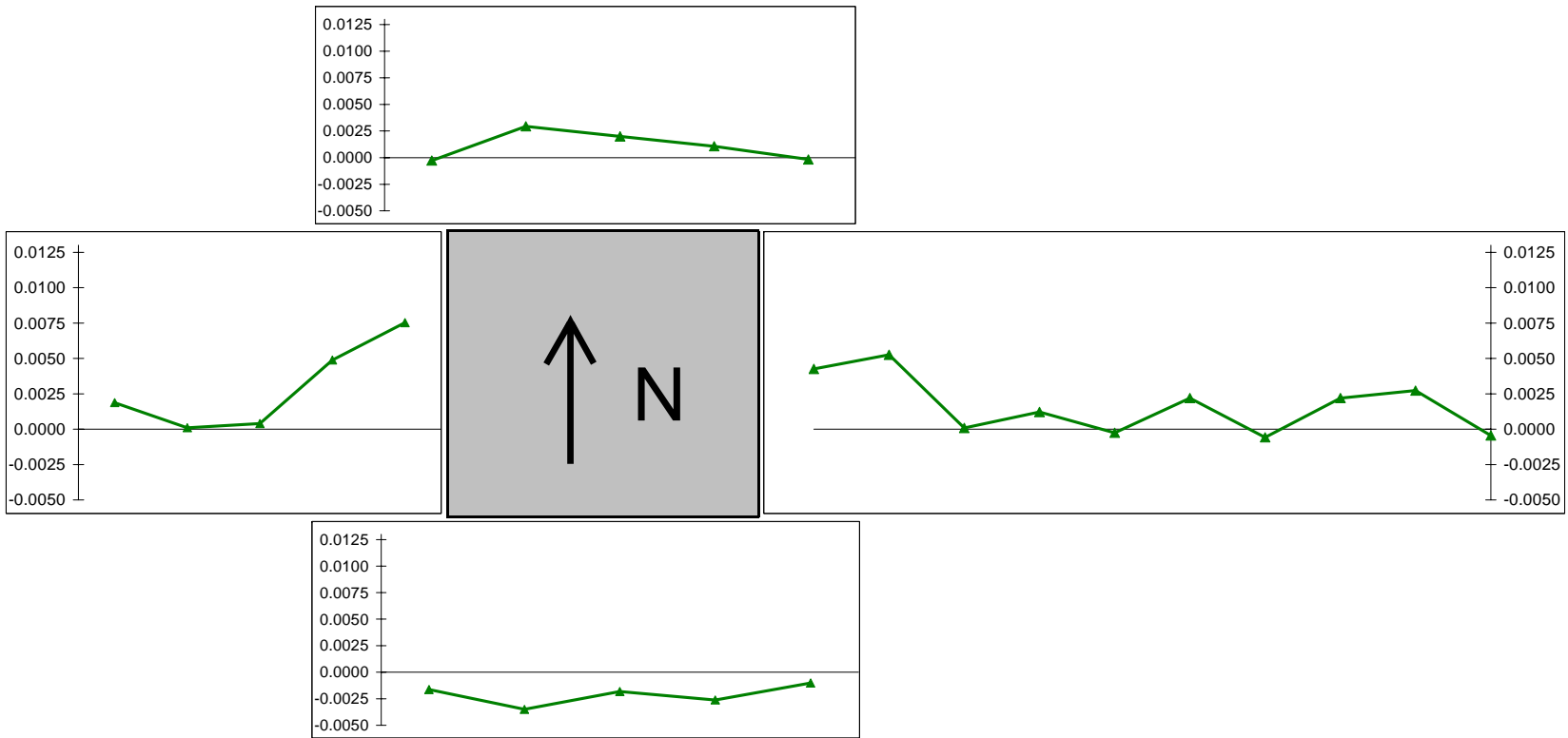


Figure 3-35 Column 3-2A Strains in Slab Surface (South 3% Roof Drift Ratio)
 (See Figure A-33 for Measurement Locations)

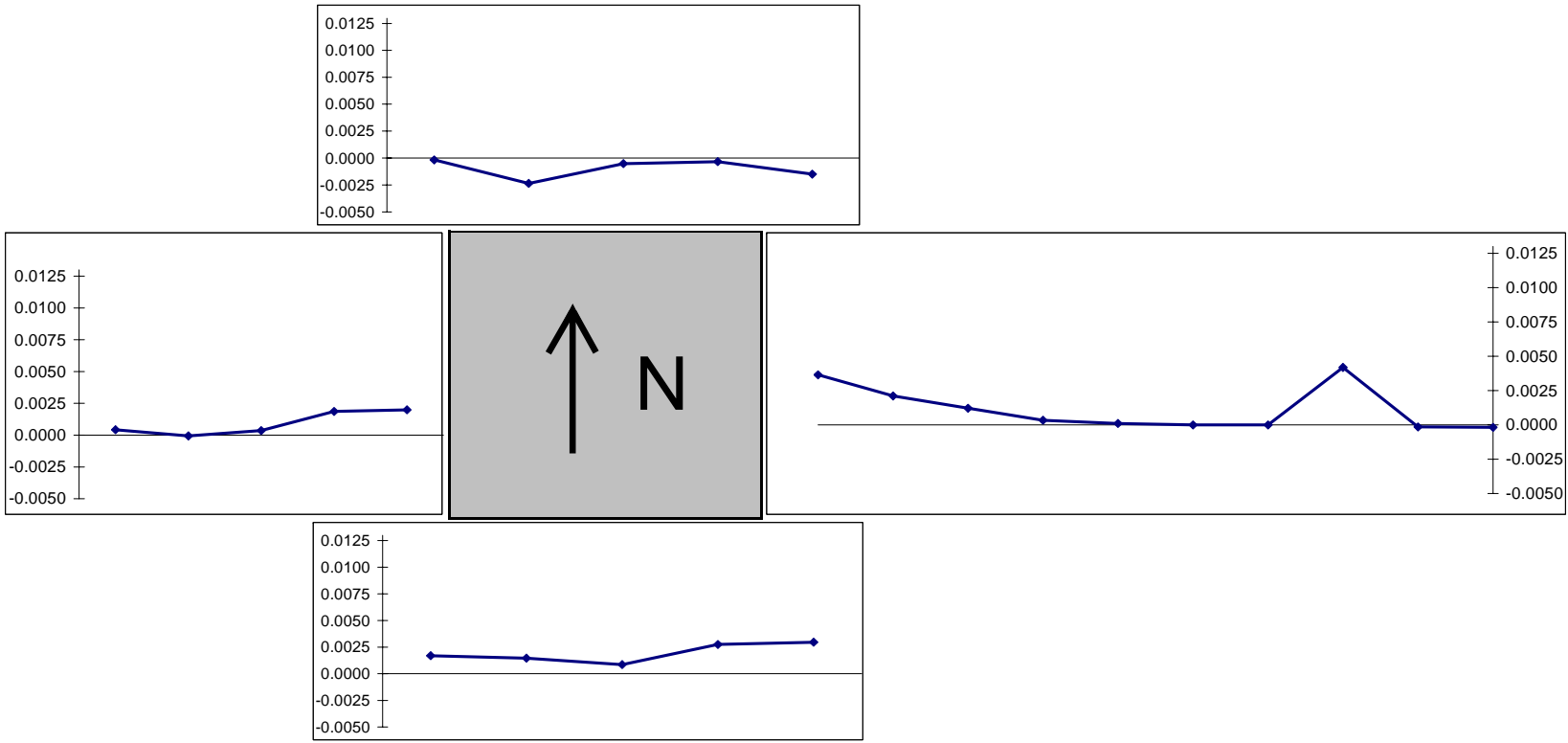


Figure 3-36 Column R-2A Strains in Slab Surface (North 3% Roof Drift Ratio)
 (See Figure A-33 for Measurement Locations)

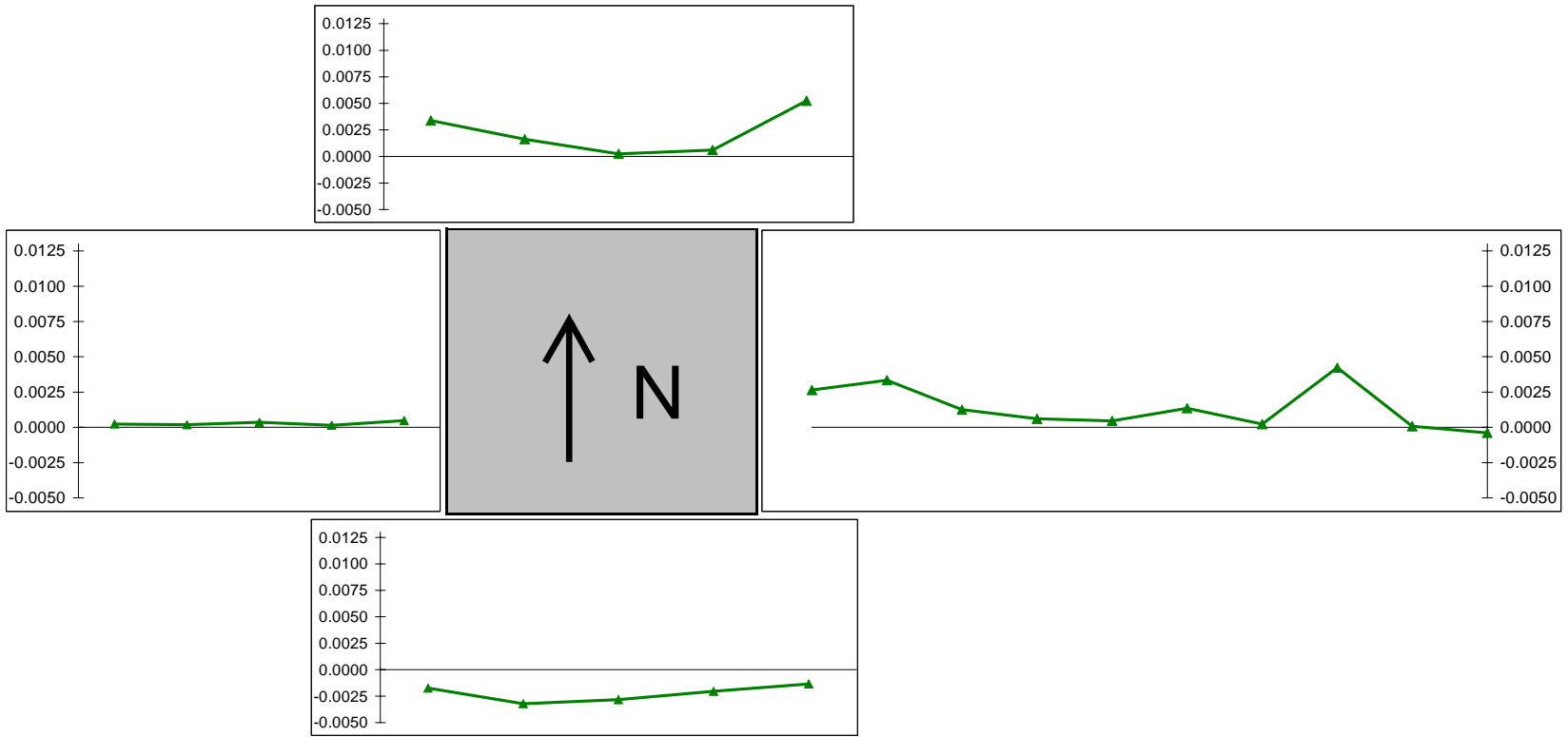


Figure 3-37 Column R-2A Strains in Slab Surface (South 3% Roof Drift Ratio)
 (See Figure A-33 for Measurement Locations)

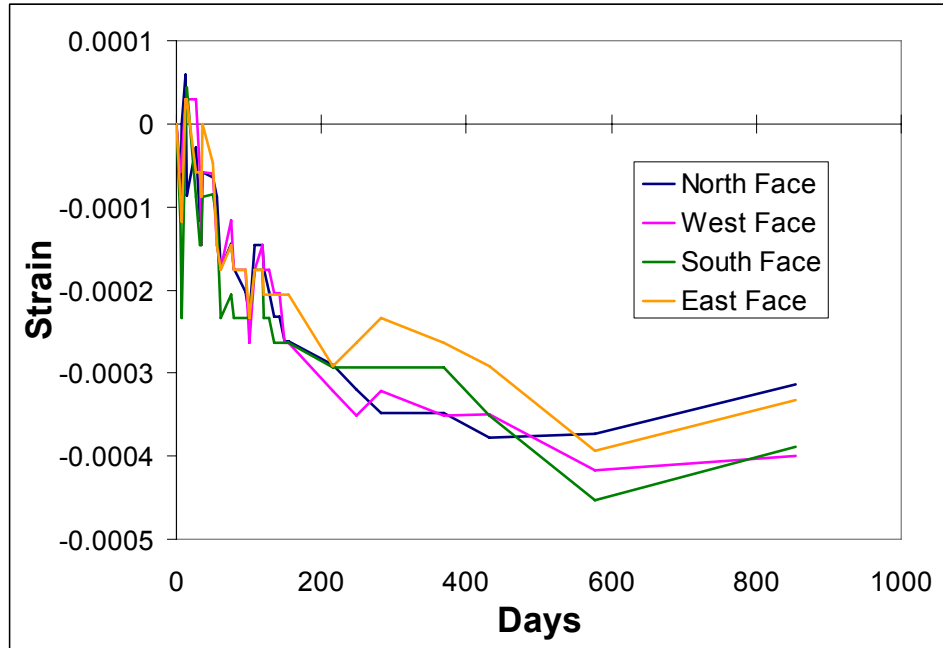


Figure 3-38 Column 1-2B Surface Strain Measurements

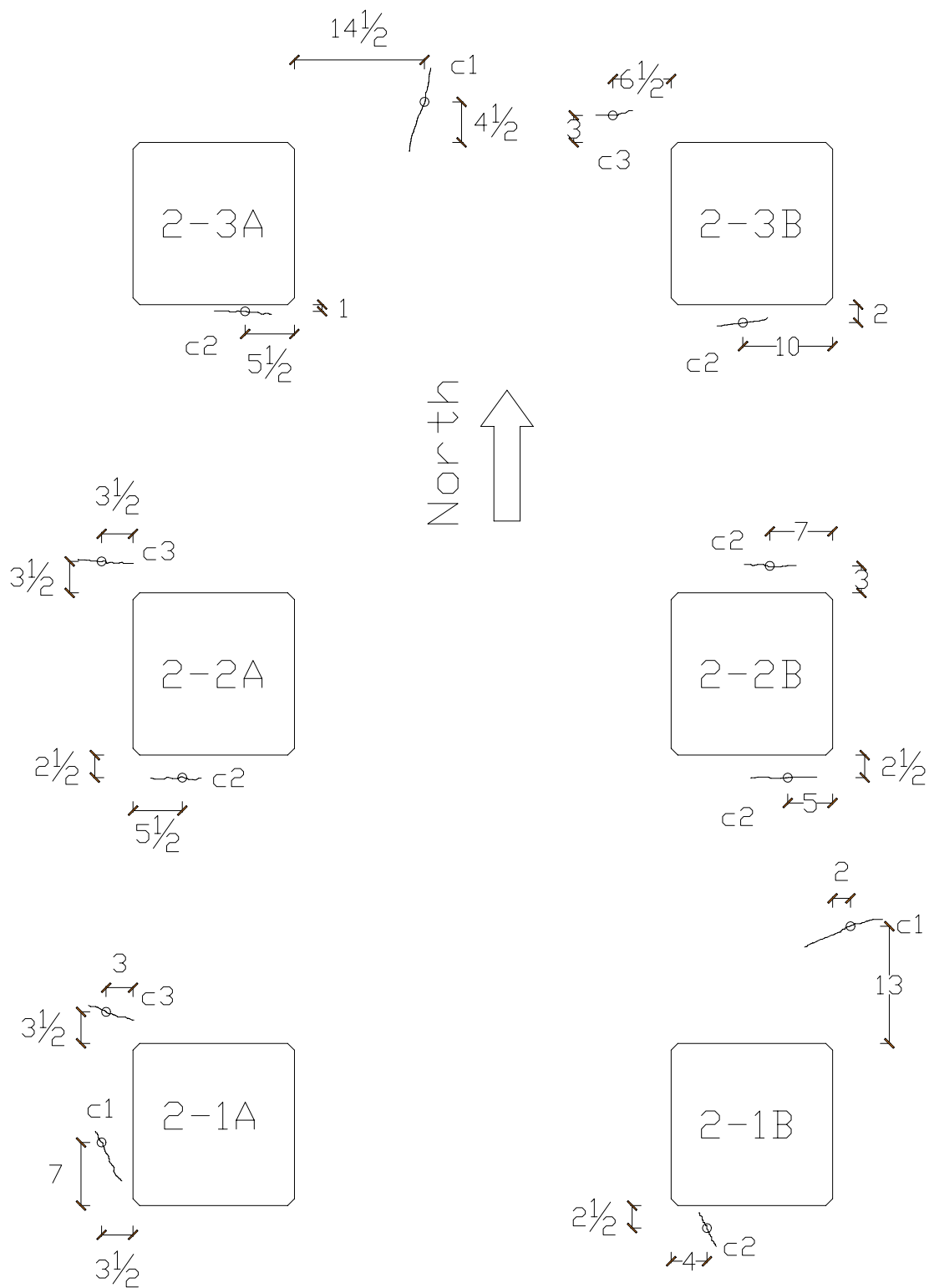


Figure 3-39 Locations of Measured Maximum Crack Widths (Level 2)
(Dimensions in Inches)

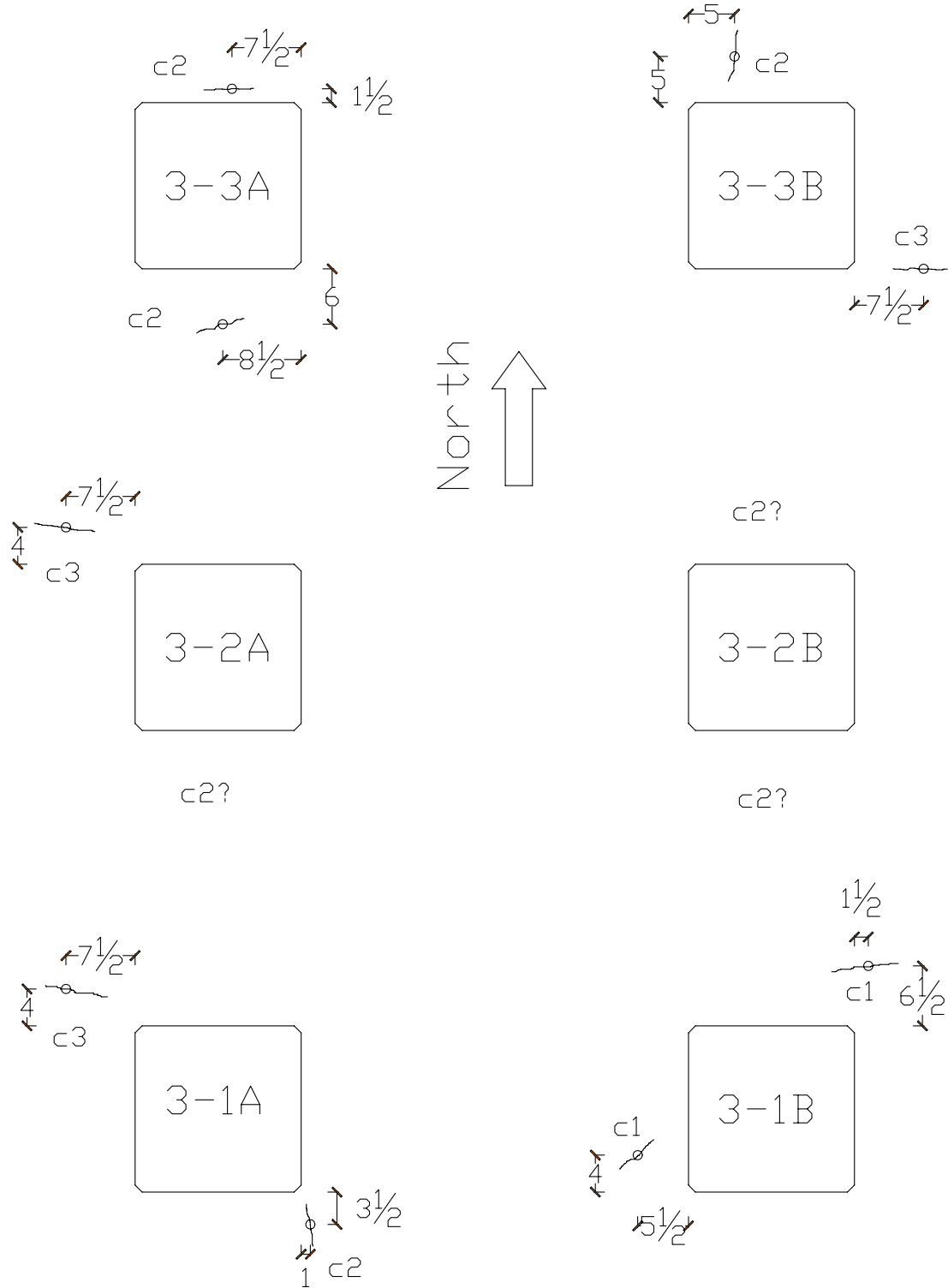


Figure 3-40 Locations of Measured Maximum Crack Widths (Level 3)
(Dimensions in Inches)

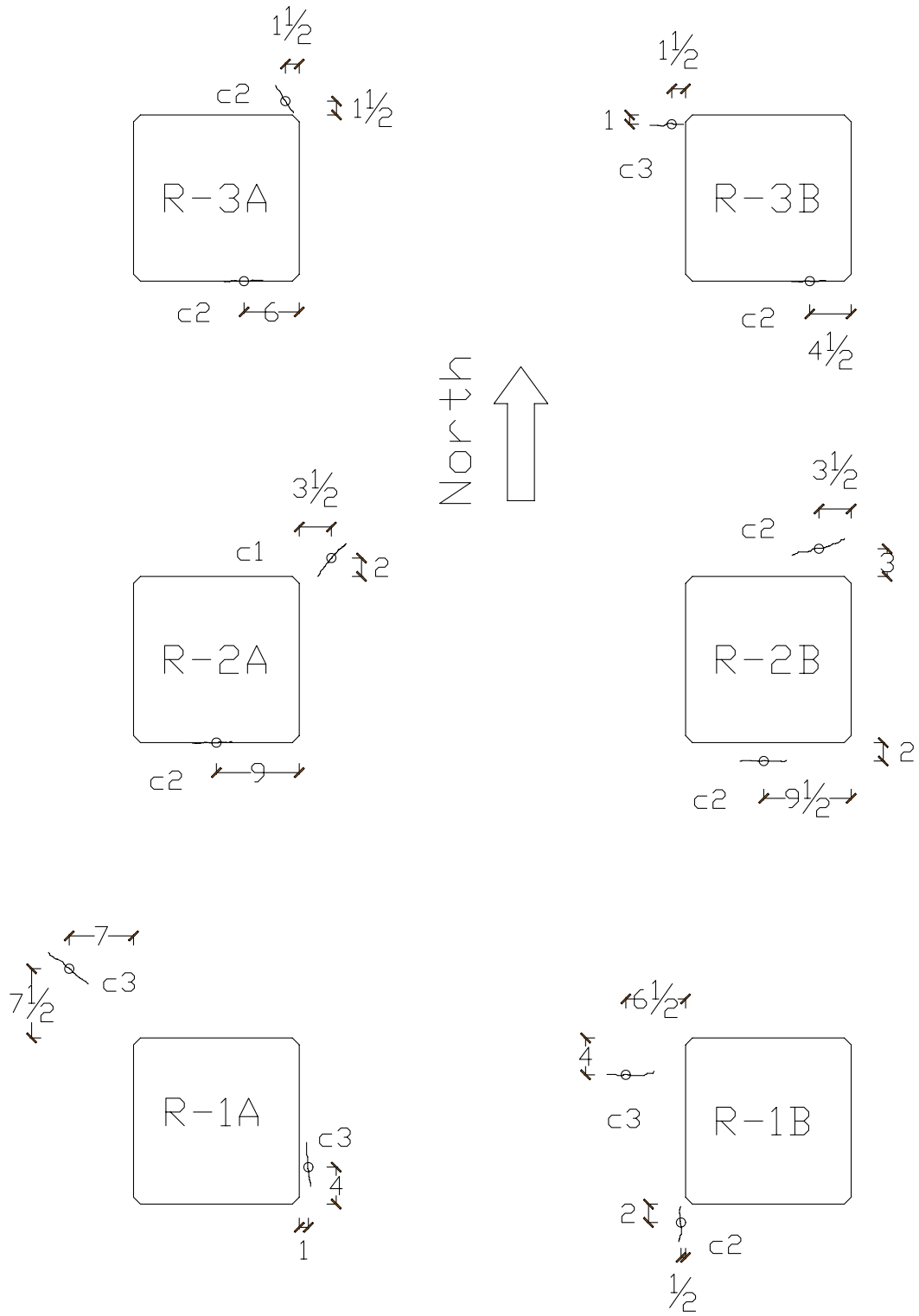


Figure 3-41 Locations of Measured Maximum Crack Widths (Roof)
(Dimensions in Inches)

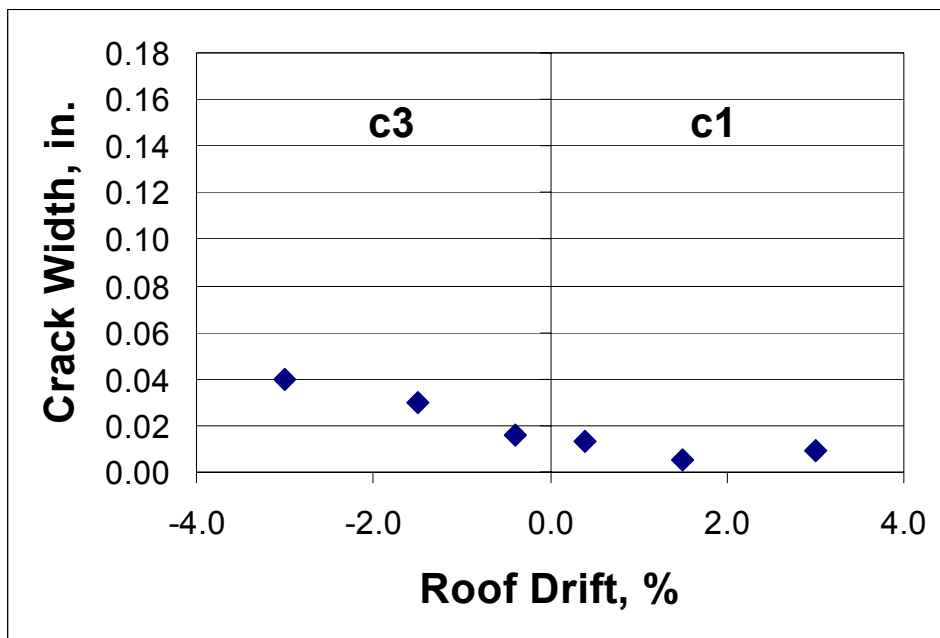


Figure 3-42 Level 2-1A Crack Width vs. Roof Drift

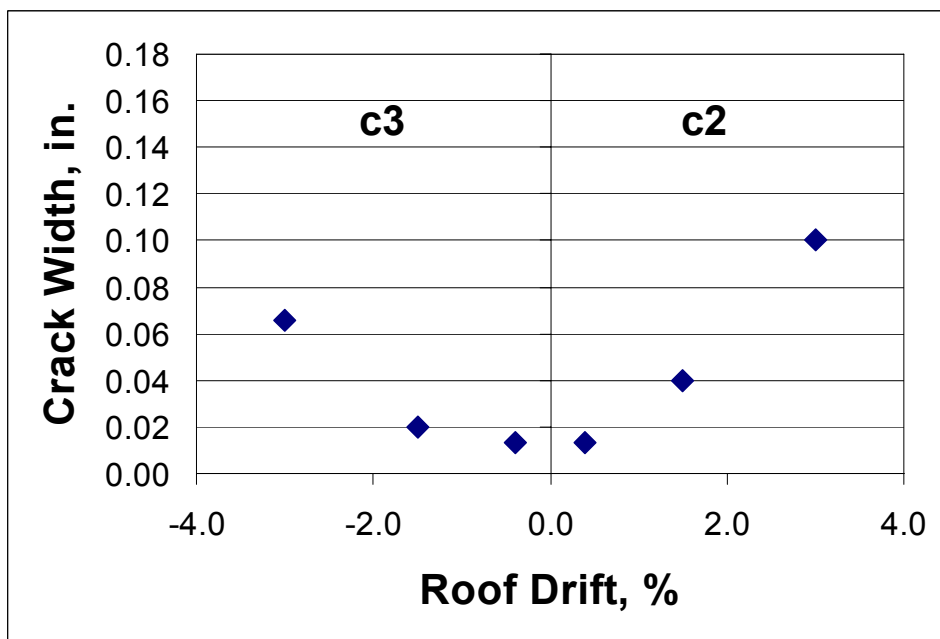


Figure 3-43 Level 2-2A Crack-Width vs. Roof Drift

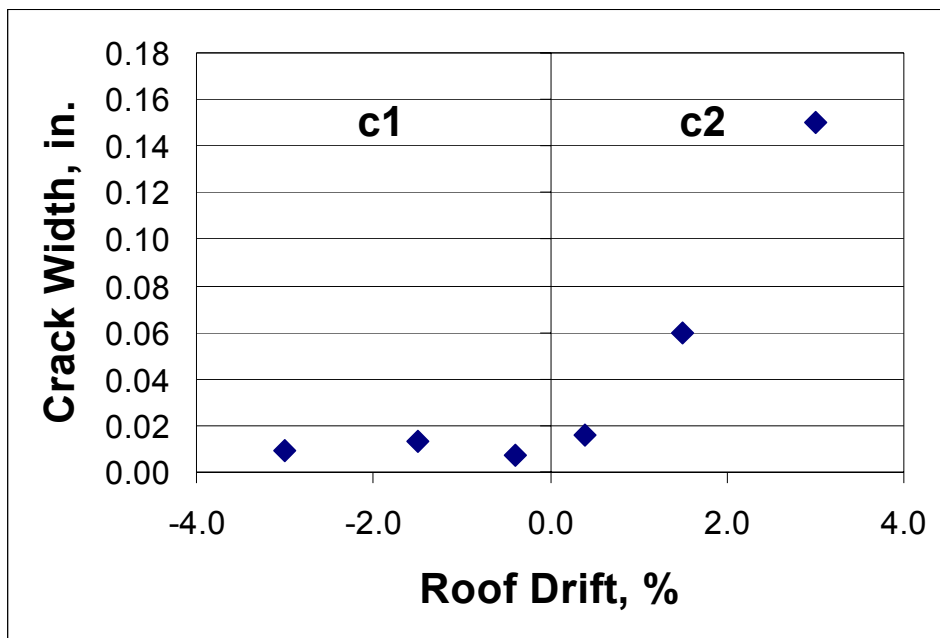


Figure 3-44 Level 2-3A Crack-Width vs. Roof Drift

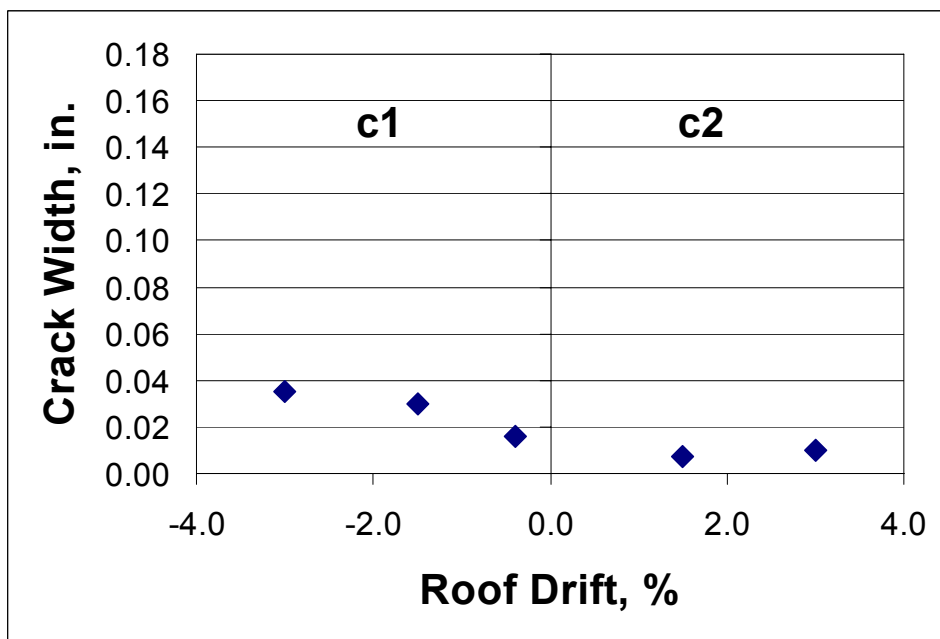


Figure 3-45 Level 2-1B Crack-Width vs. Roof Drift

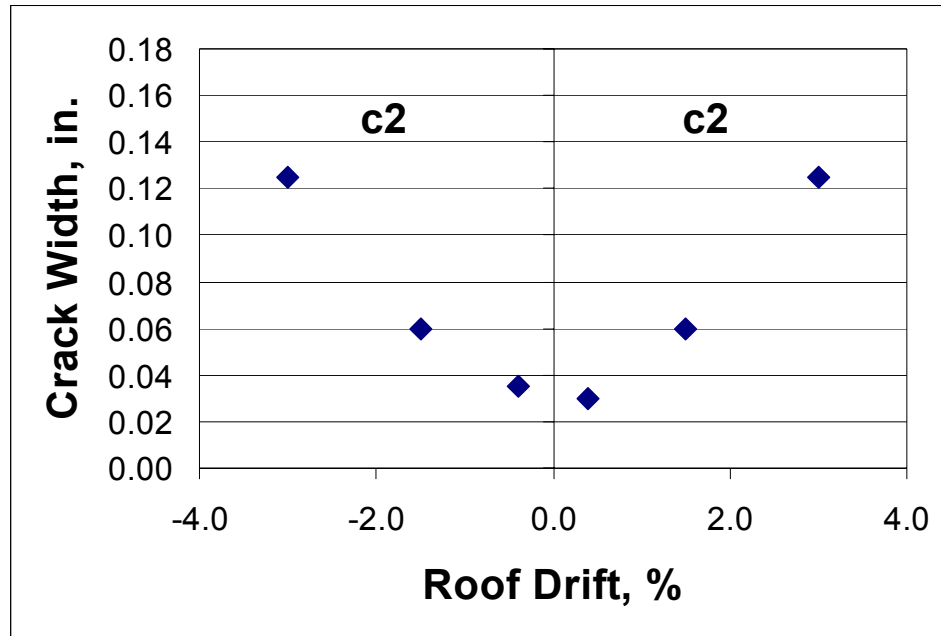


Figure 3-46 Level 2-2B Crack-Width vs. Roof Drift

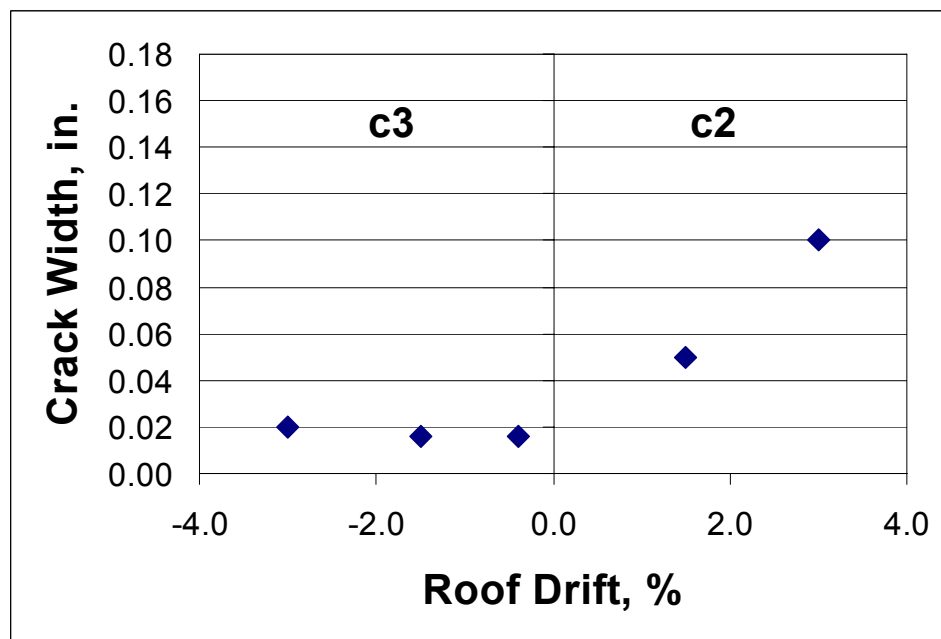


Figure 3-47 Level 2-3B Crack-Width vs. Roof Drift

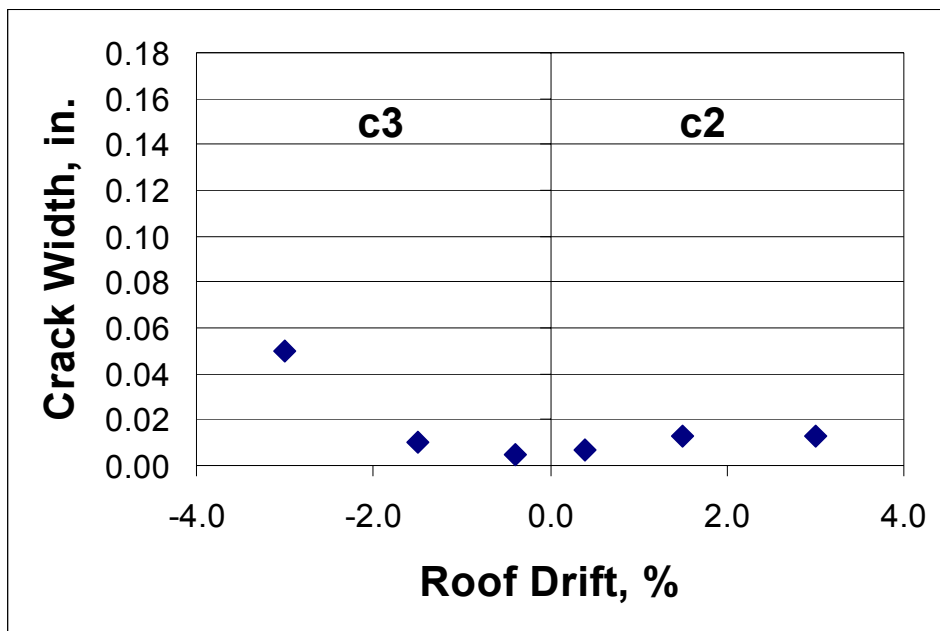


Figure 3-48 Level 3-1A Crack-Width vs. Roof Drift

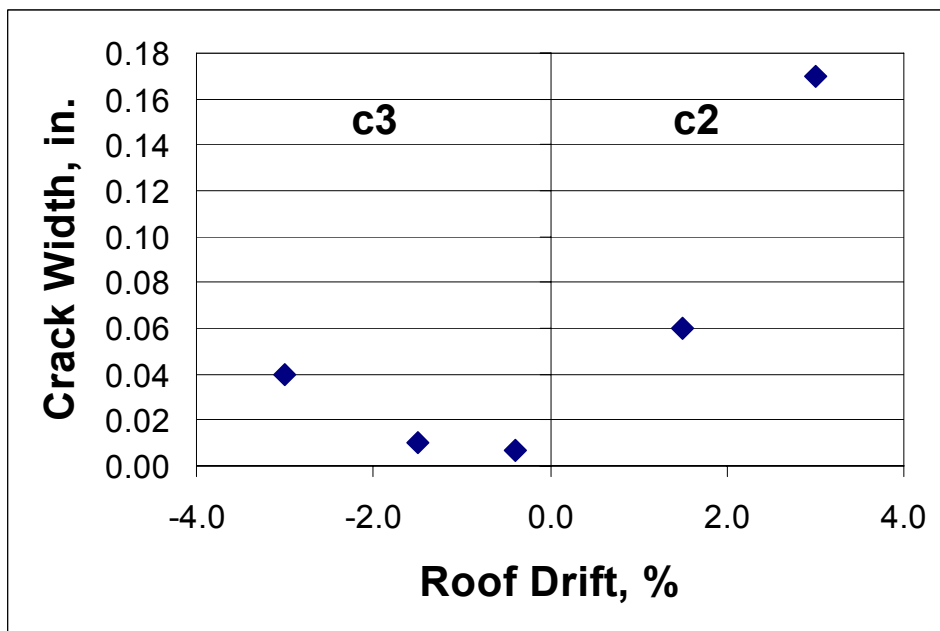


Figure 3-49 Level 3-2A Crack-Width vs. Roof Drift

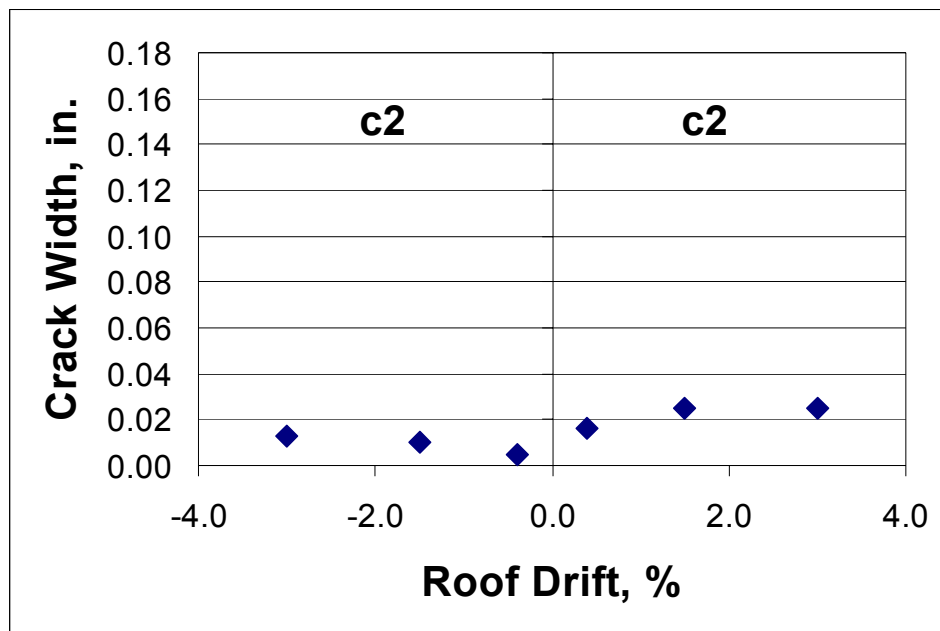


Figure 3-50 Level 3-3A Crack-Width vs. Roof Drift

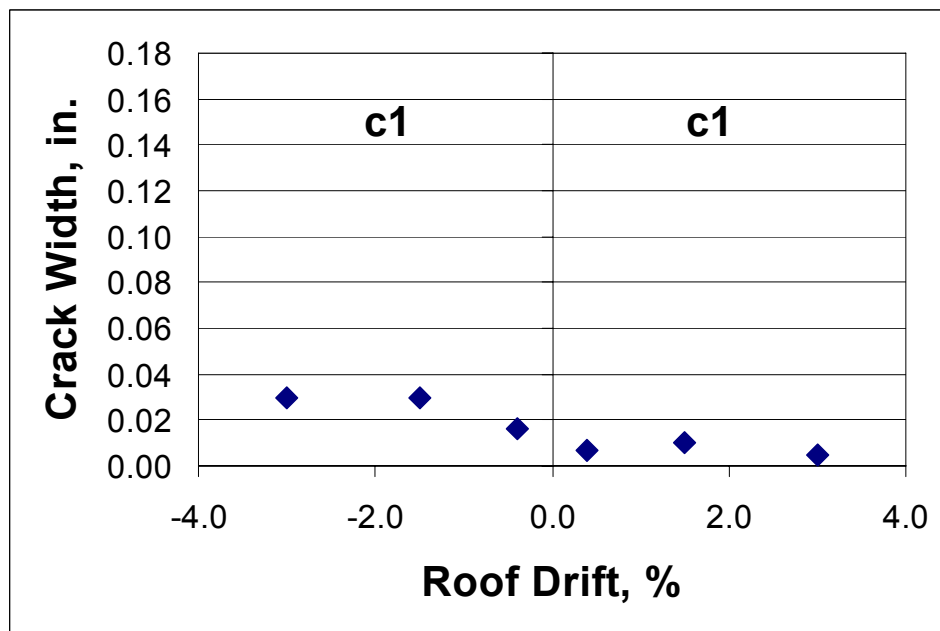


Figure 3-51 Level 3-1B Crack-Width vs. Roof Drift

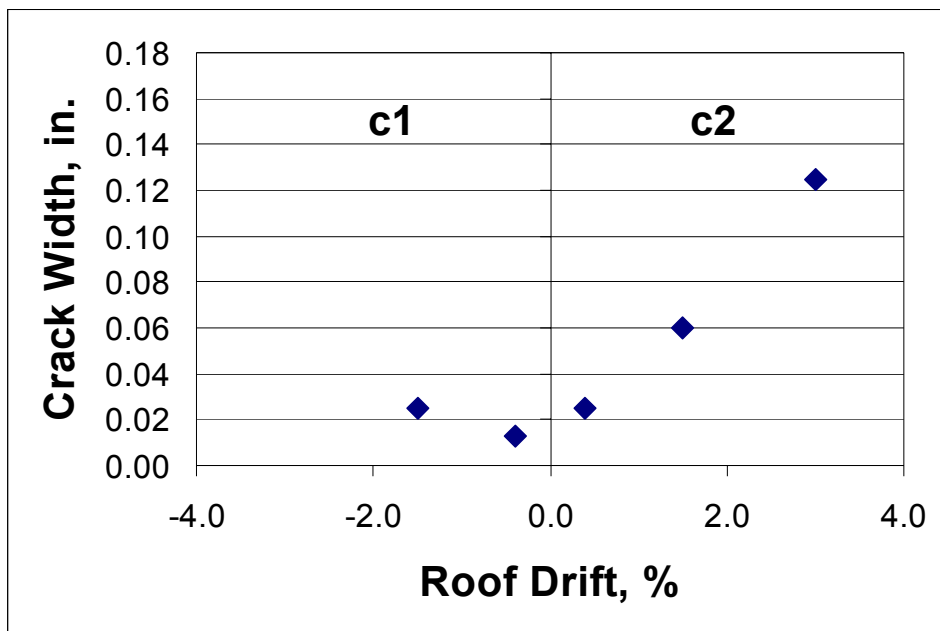


Figure 3-52 Level 3-2B Crack-Width vs. Roof Drift

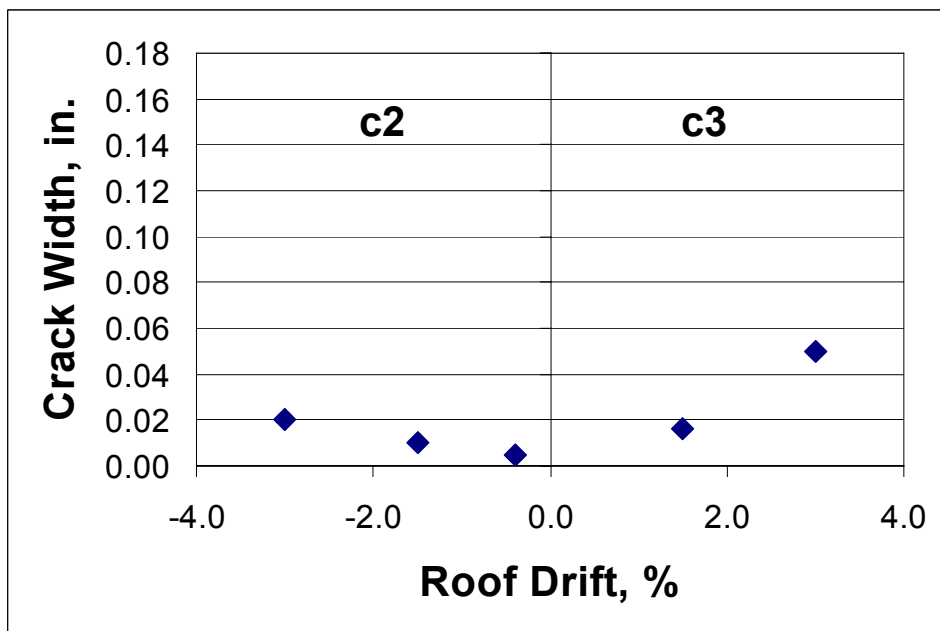


Figure 3-53 Level 3-3B Crack-Width vs. Roof Drift

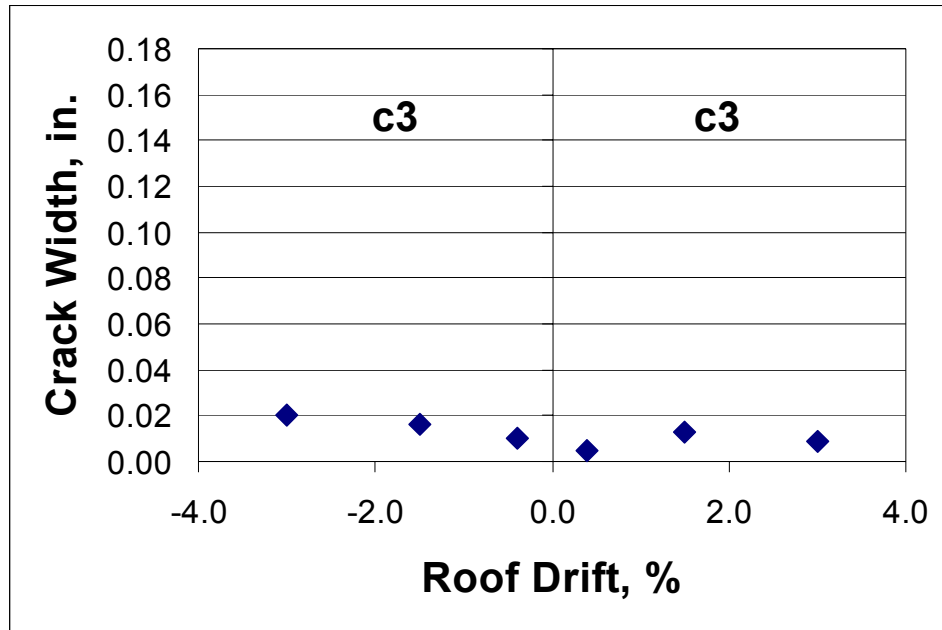


Figure 3-54 Level R-1A Crack-Width vs. Roof Drift

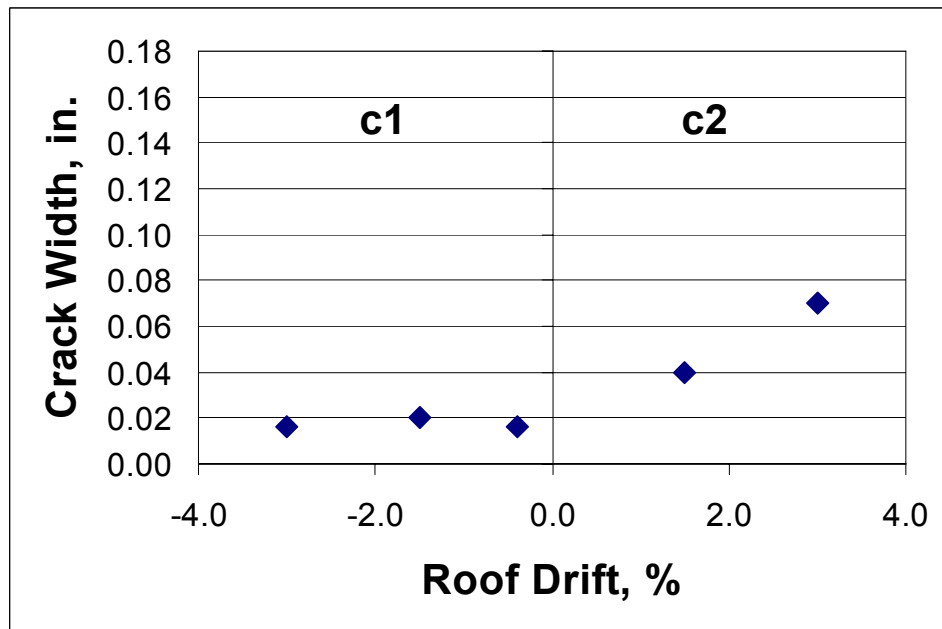


Figure 3-55 Level R-2A Crack-Width vs. Roof Drift

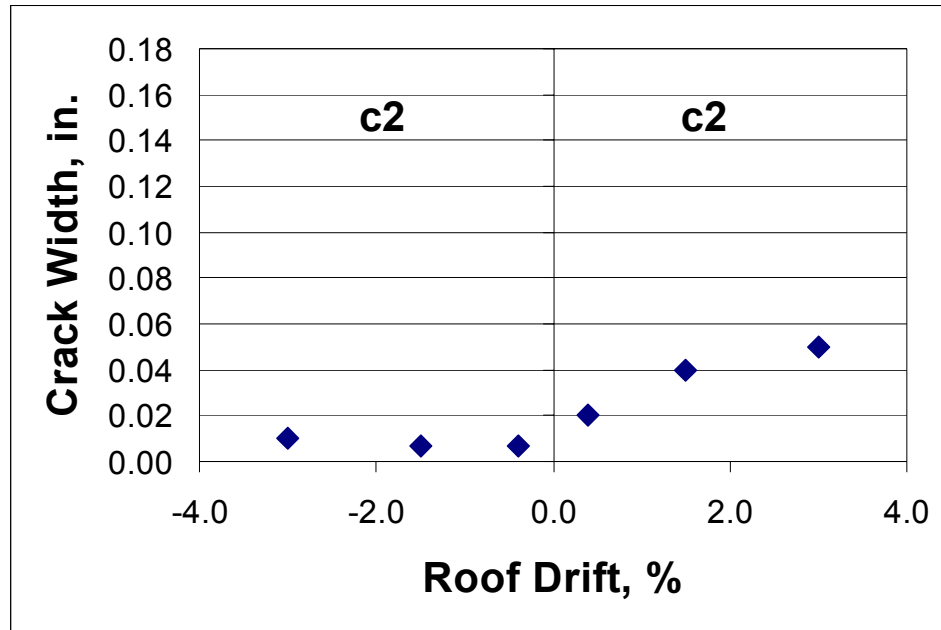


Figure 3-56 Level R-3A Crack-Width vs. Roof Drift

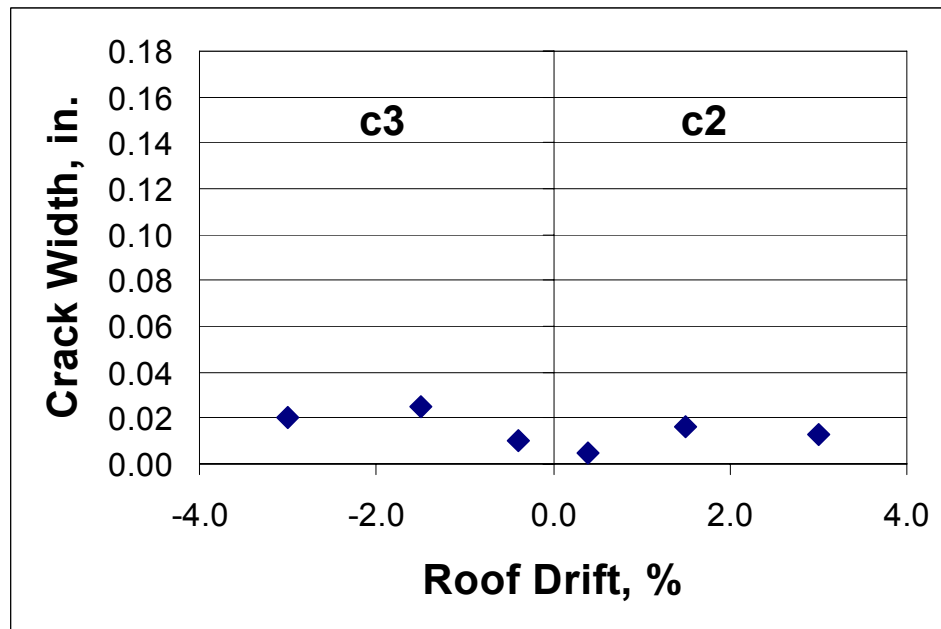


Figure 3-57 Level R-1B Crack-Width vs. Roof Drift

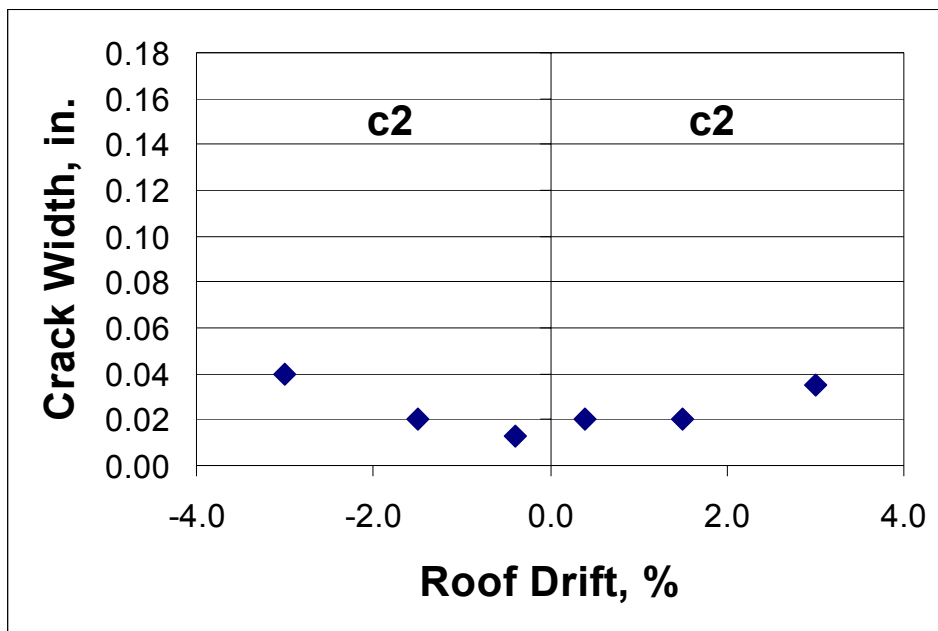


Figure 3-58 Level R-2B Crack-Width vs. Roof Drift

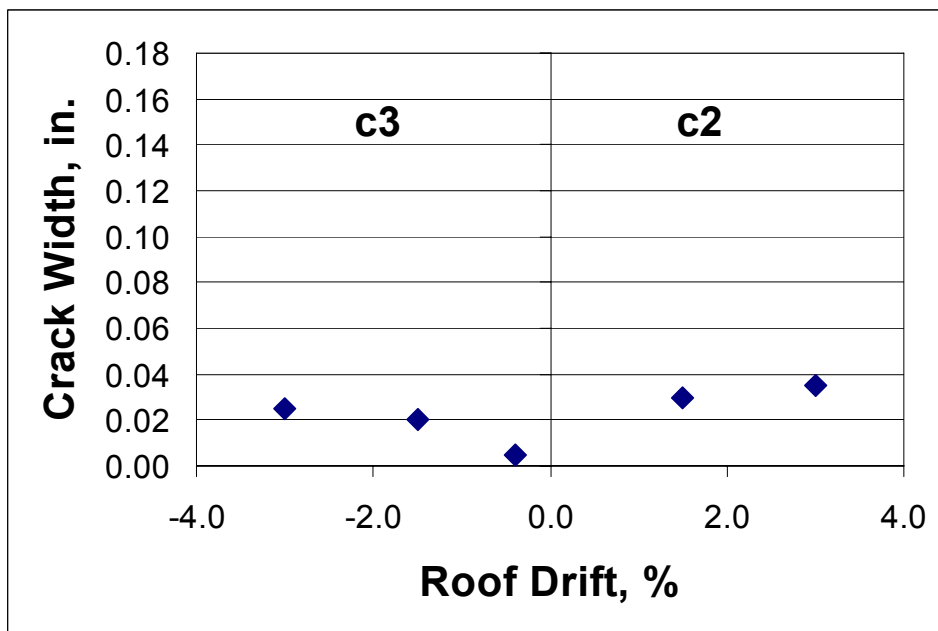


Figure 3-59 Level R-3B Crack-Width vs. Roof Drift

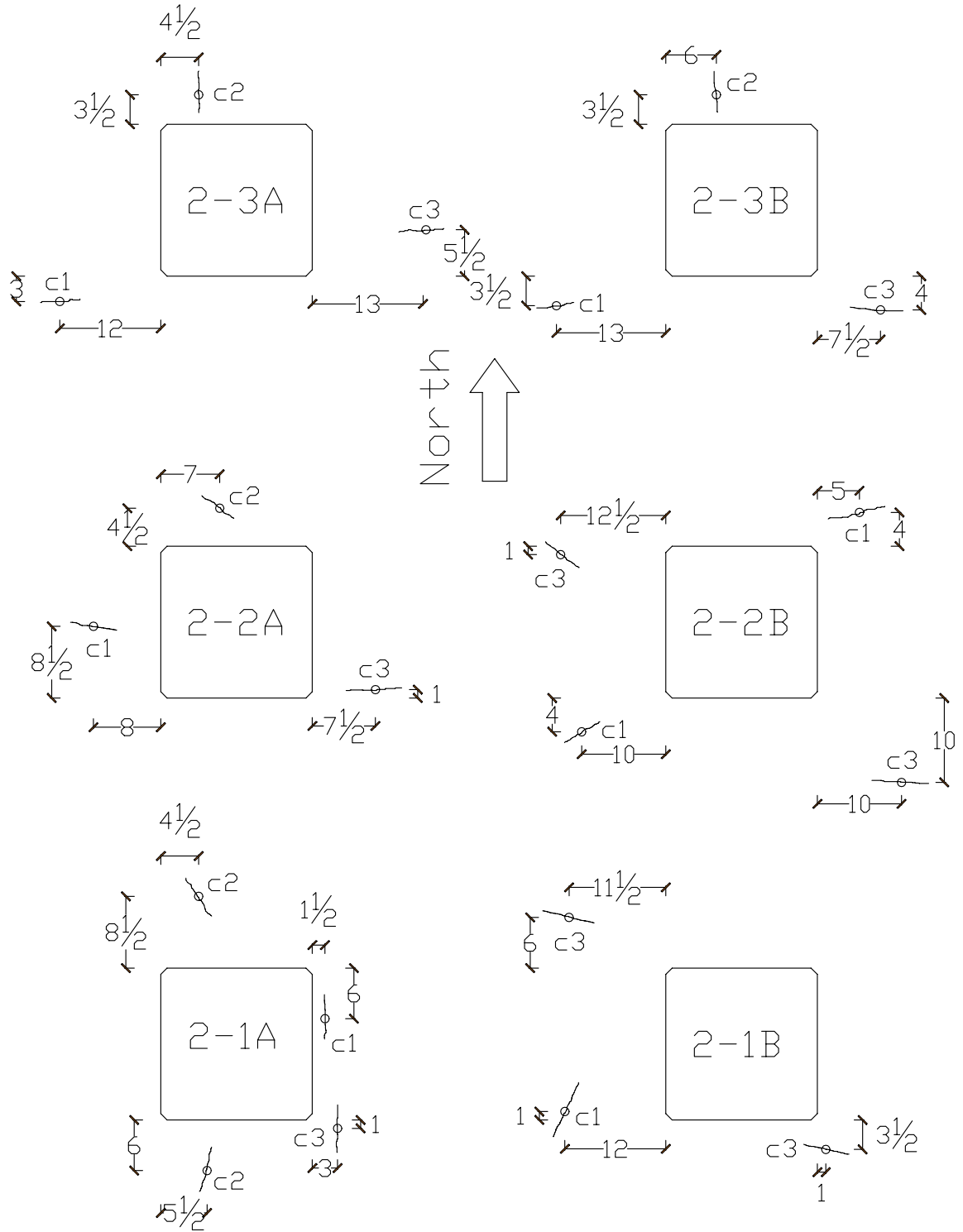


Figure 3-60 Locations of Measured Crack Widths (Level 2)
(Dimensions in Inches)

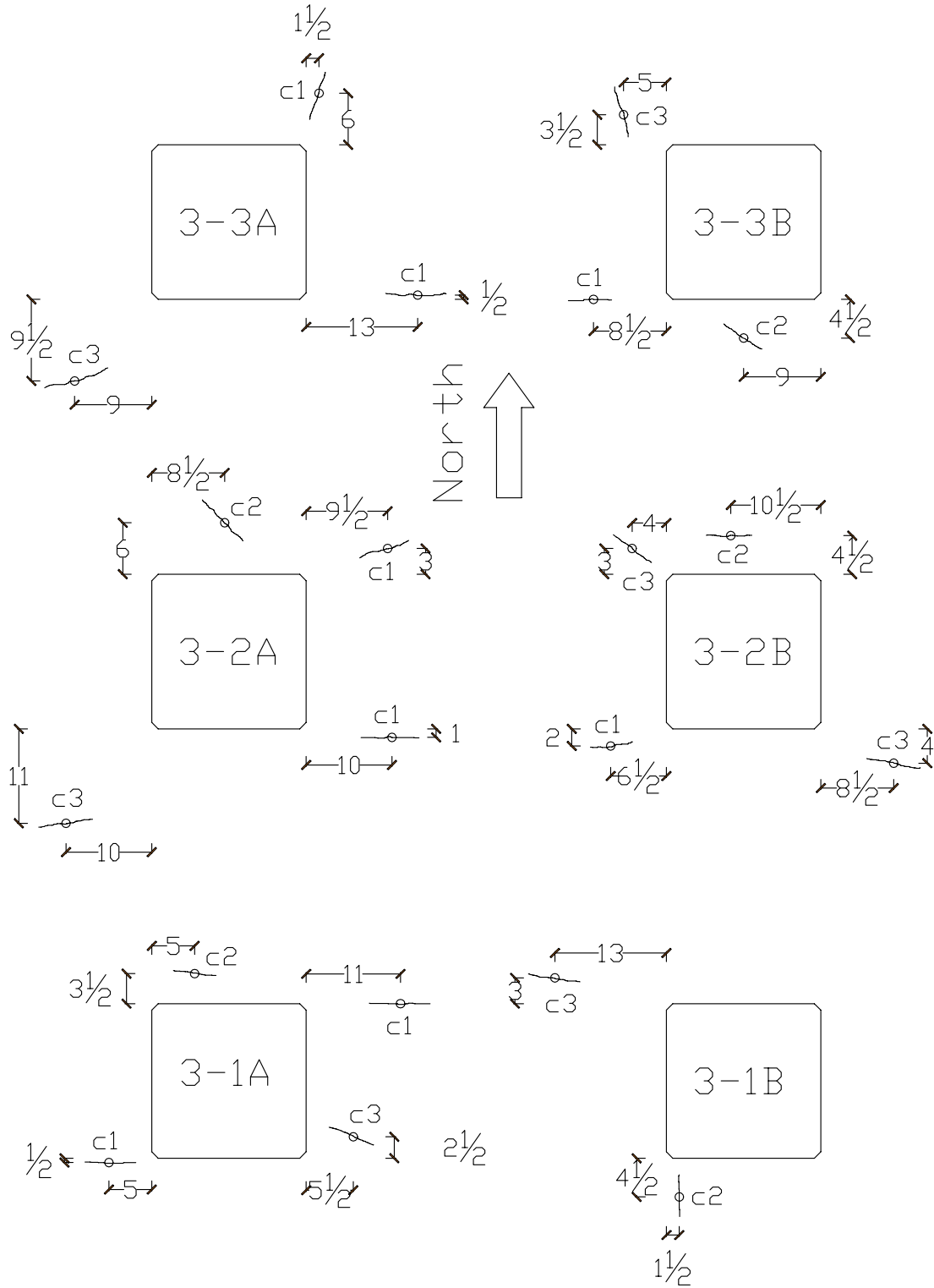


Figure 3-61 Locations of Measured Crack Widths (Level 3)
(Dimensions in Inches)

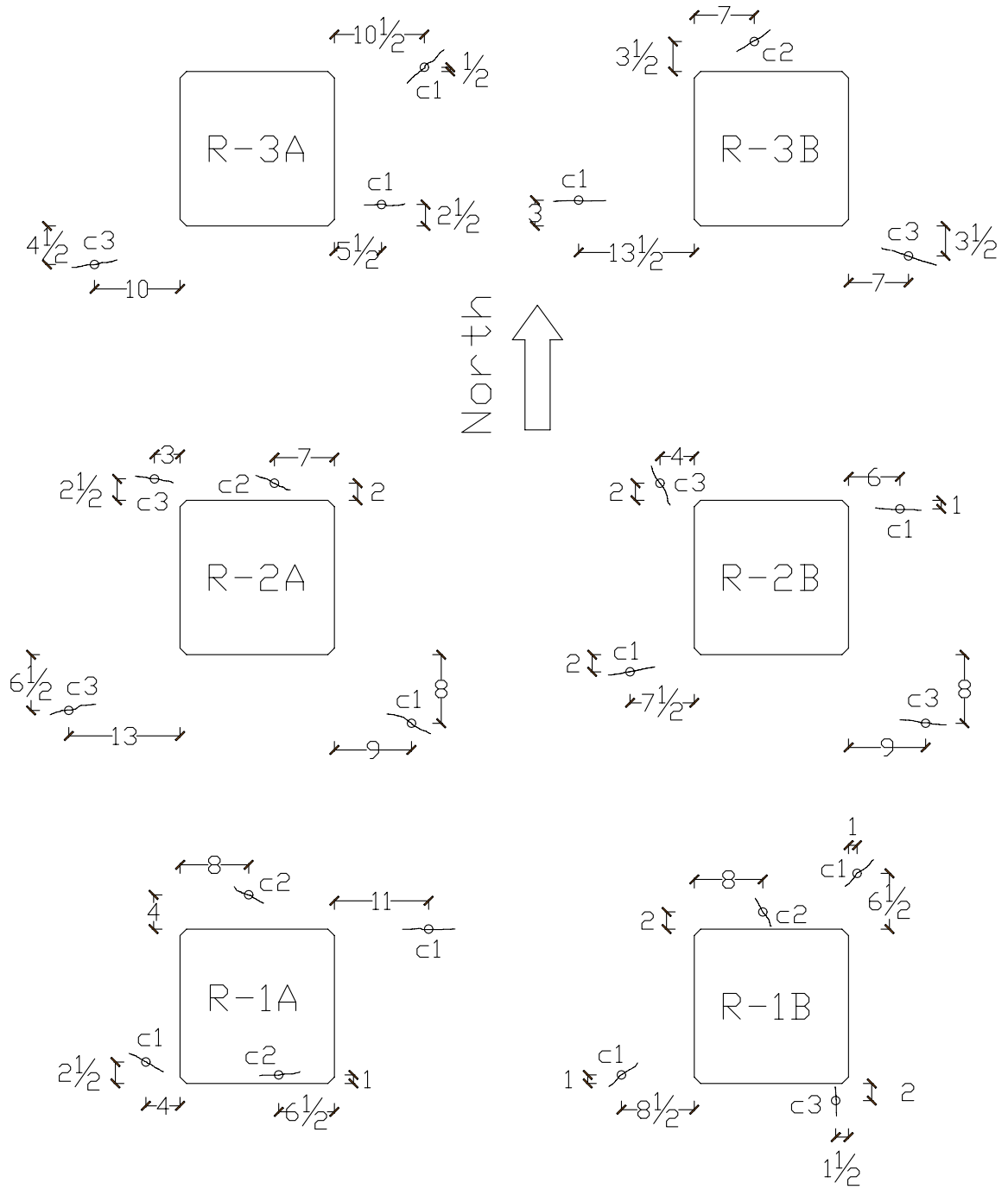


Figure 3-62 Locations of Measured Crack Widths (Roof)
(Dimensions in Inches)

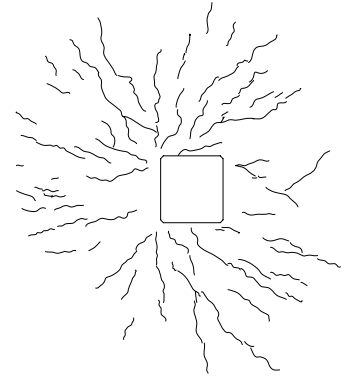
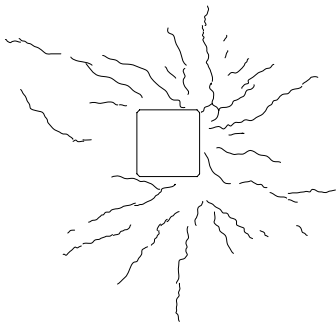


Figure 3-63 Level 3-2A and 2B Initial Top of Slab Cracks

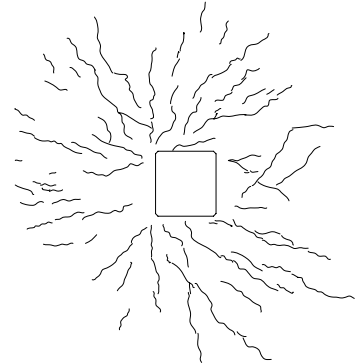
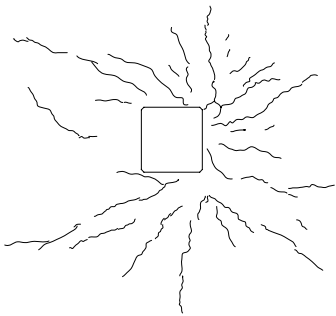


Figure 3-64 Level 3-2A and 2B Top of Slab Cracks (North 0.4% Roof Drift)

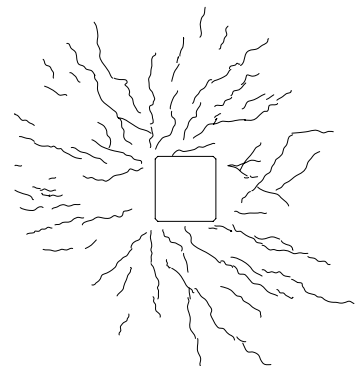
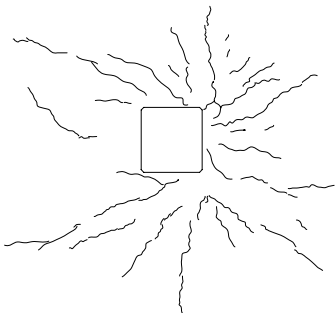


Figure 3-65 Level 3-2A and 2B Top of Slab Cracks (South 0.4% Roof Drift)

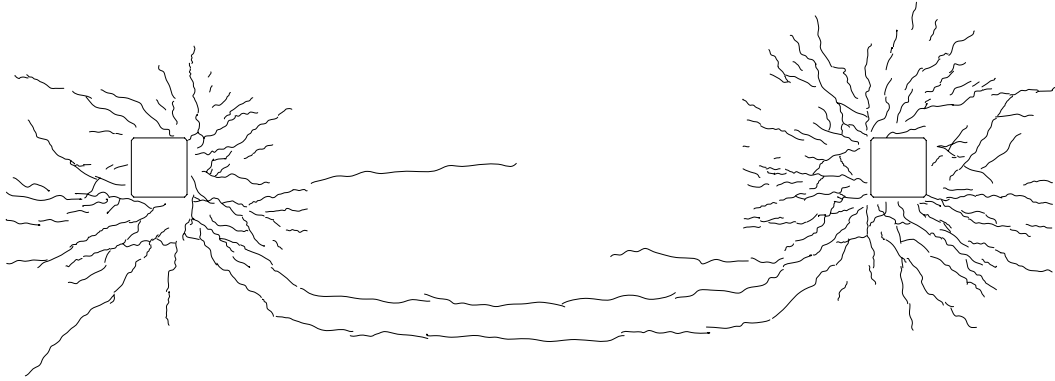


Figure 3-66 Level 3-2A and 2B Top Slab Cracks (North 1.5% Roof Drift)

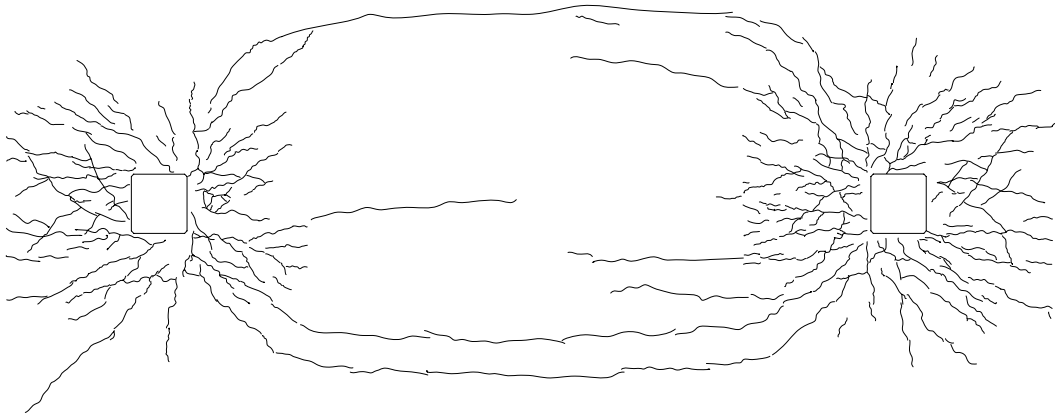


Figure 3-67 Level 3-2A and 2B Top Slab Cracks (South 1.5% Roof Drift)

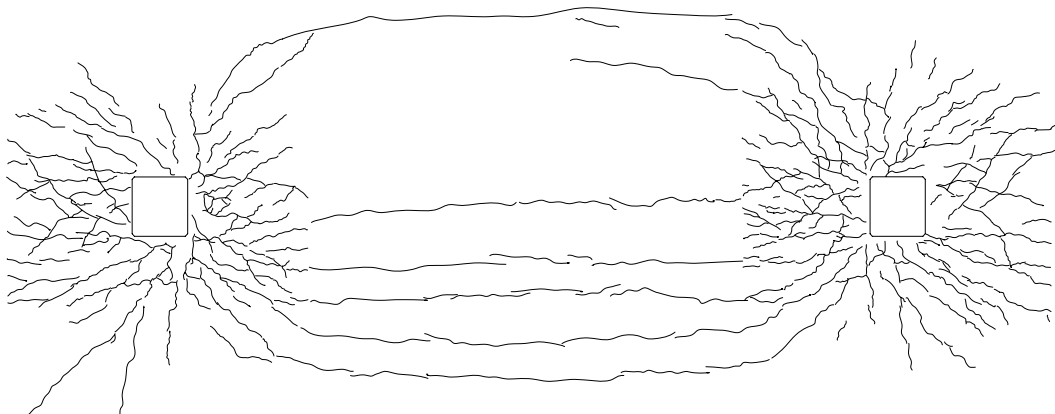


Figure 3-68 Level 3-2A and 2B Top Slab Cracks (North 3% Roof Drift)

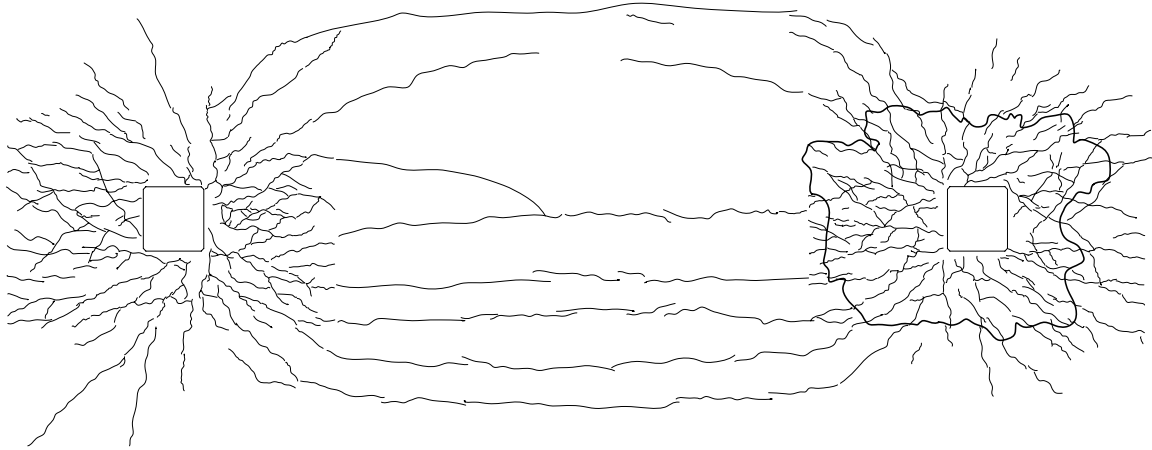


Figure 3-69 Level 3-2A and 2B Top Slab Cracks (South 3% Roof Drift)



Figure 3-70 Level 3-2A and 2B Bottom Slab Cracks (North 1.5% Roof Drift)

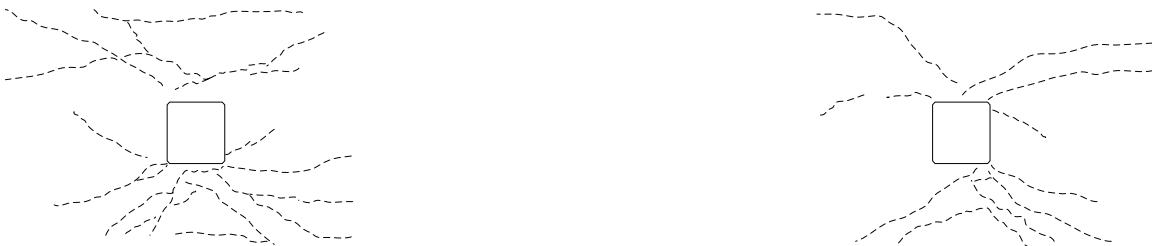


Figure 3-71 Level 3-2A and 2B Bottom Slab Cracks (South 1.5% Roof Drift)

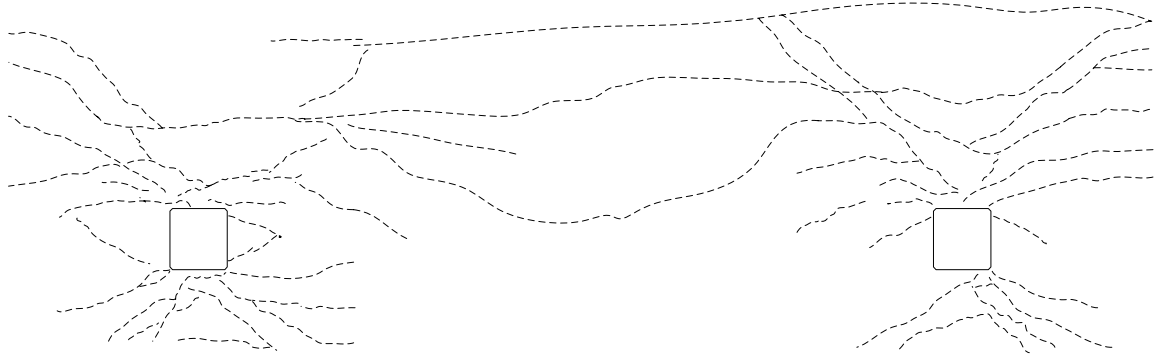


Figure 3-72 Level 3-2A and 2B Bottom Slab Cracks (North 3% Roof Drift)

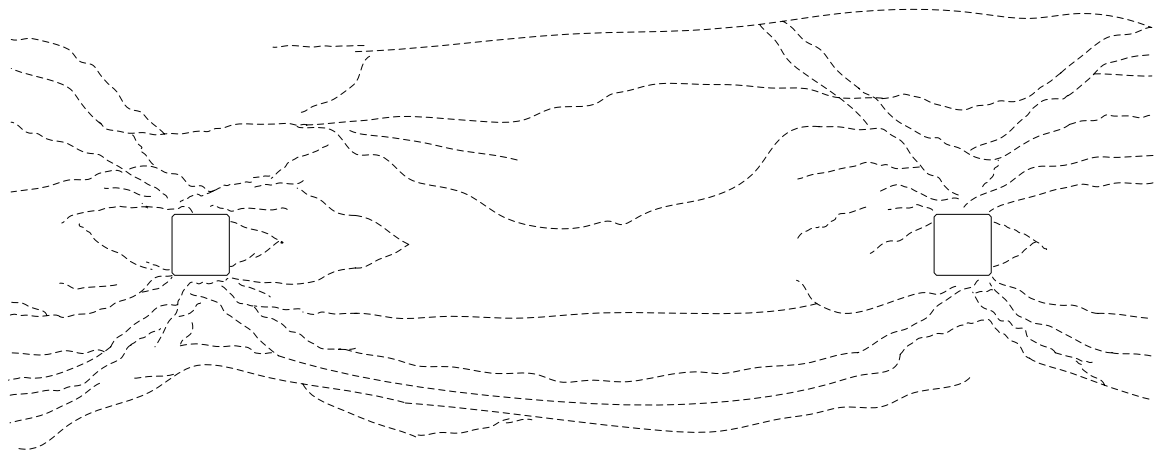


Figure 3-73 Level 3-2A and 2B Bottom Slab Cracks (South 3% Roof Drift)



Figure 3-74 Level 2 Column 2A South Initial Cracks



Figure 3-75 Level 2 Column 2A South Final Cracks



Figure 3-76 Level 2 Column 3A South Initial Cracks



Figure 3-77 Level 2 Column 3A South Final Cracks



Figure 3-78 Level 2 Column 2B South Initial Cracks



Figure 3-79 Level 2 Column 2B South Final Cracks



Figure 3-80 Level 2 Column 3B South Initial Cracks



Figure 3-81 Level 2 Column 3B South Final Cracks



Figure 3-82 Level 3 Column 2A South Initial Cracks



Figure 3-83 Level 3 Column 2A South Final Cracks



Figure 3-84 Level 3 Column 3A South Initial Cracks



Figure 3-85 Level 3 Column 3A South Final Cracks



Figure 3-86 Level 3 Column 2B South Initial Cracks



Figure 3-87 Level 3 Column 2B South Final Cracks



Figure 3-88 Level 3 Column 3B South Initial Cracks



Figure 3-89 Level 3 Column 3B South Final Cracks

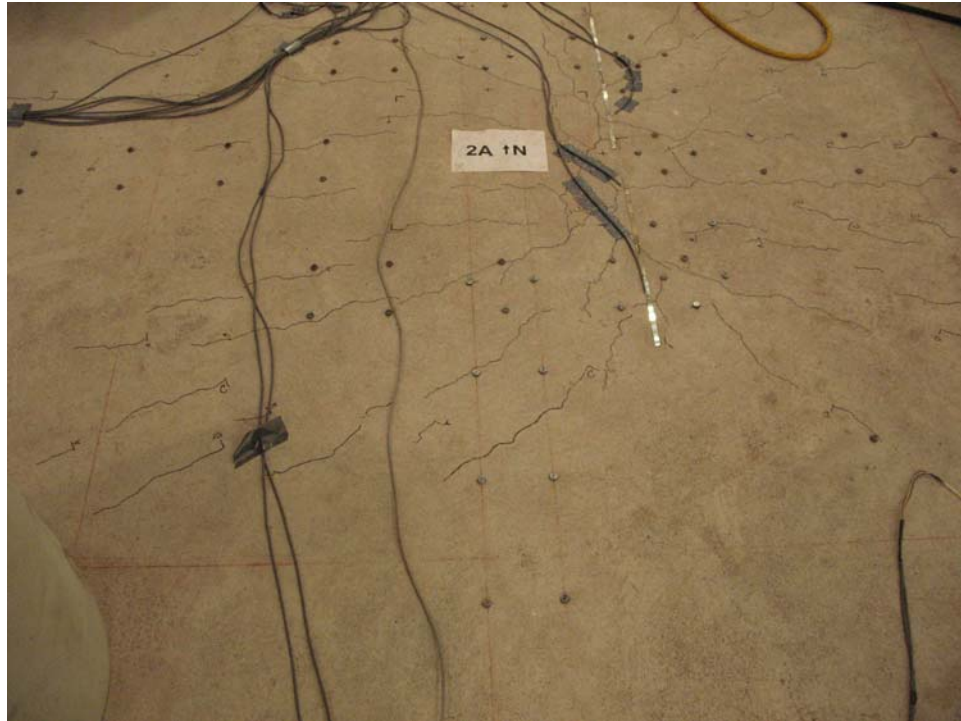


Figure 3-90 Roof Column 2A South Initial Cracks

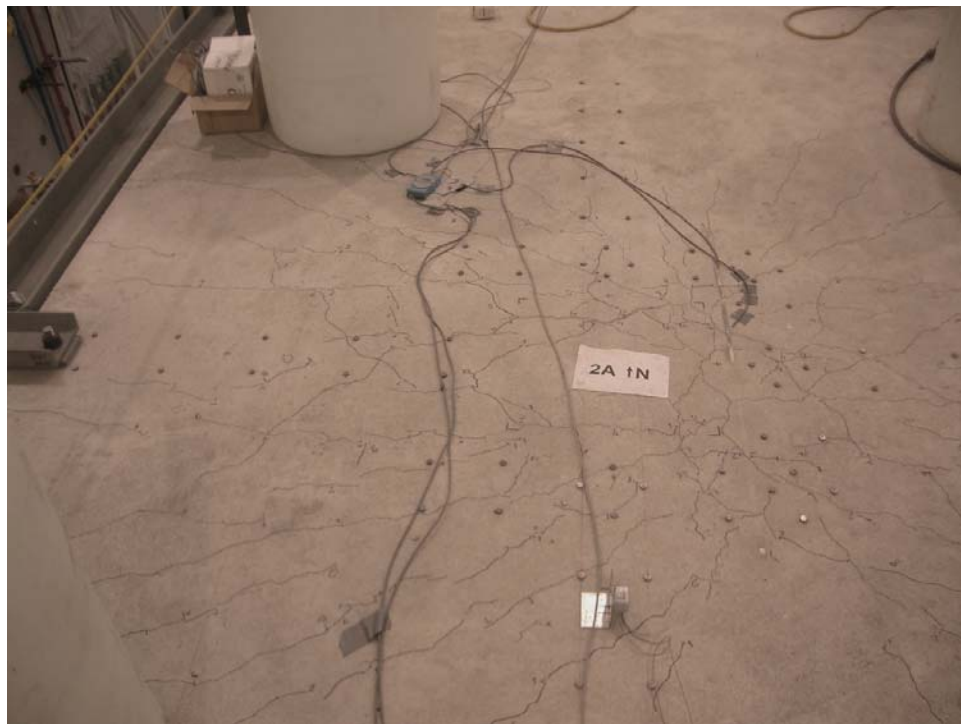


Figure 3-91 Roof Column 2A South Final Cracks

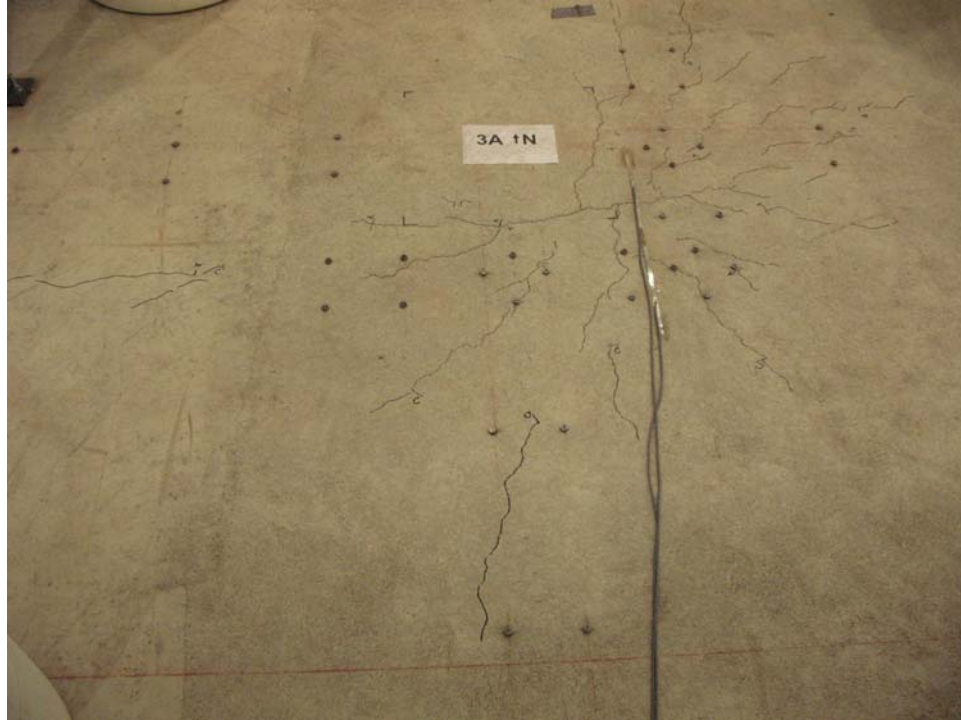


Figure 3-92 Roof Column 3A South Initial Cracks

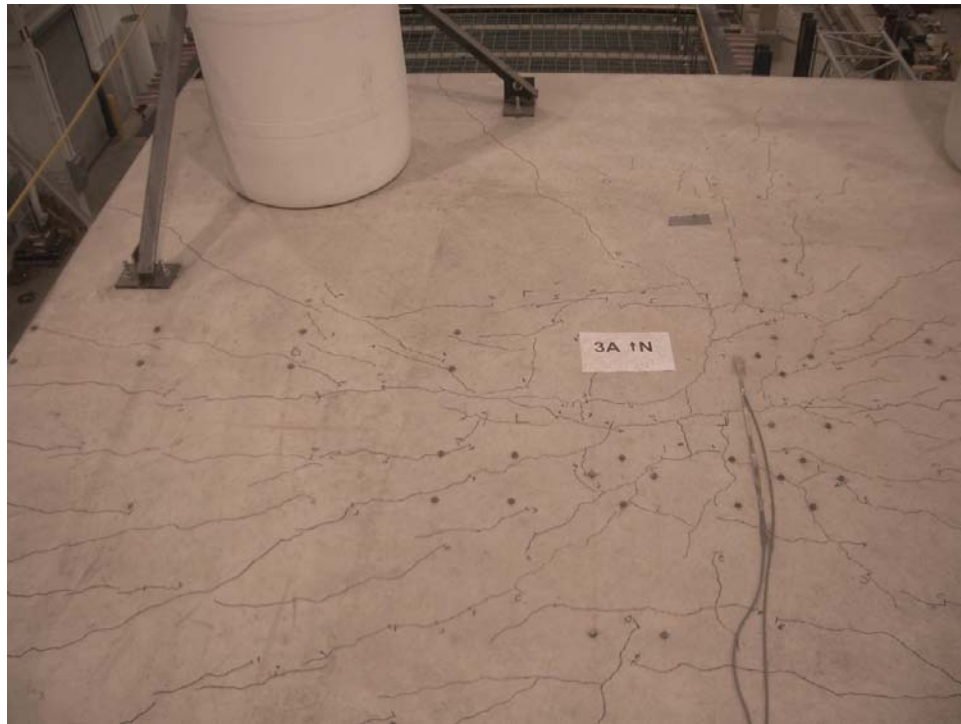


Figure 3-93 Roof Column 3A South Final Cracks

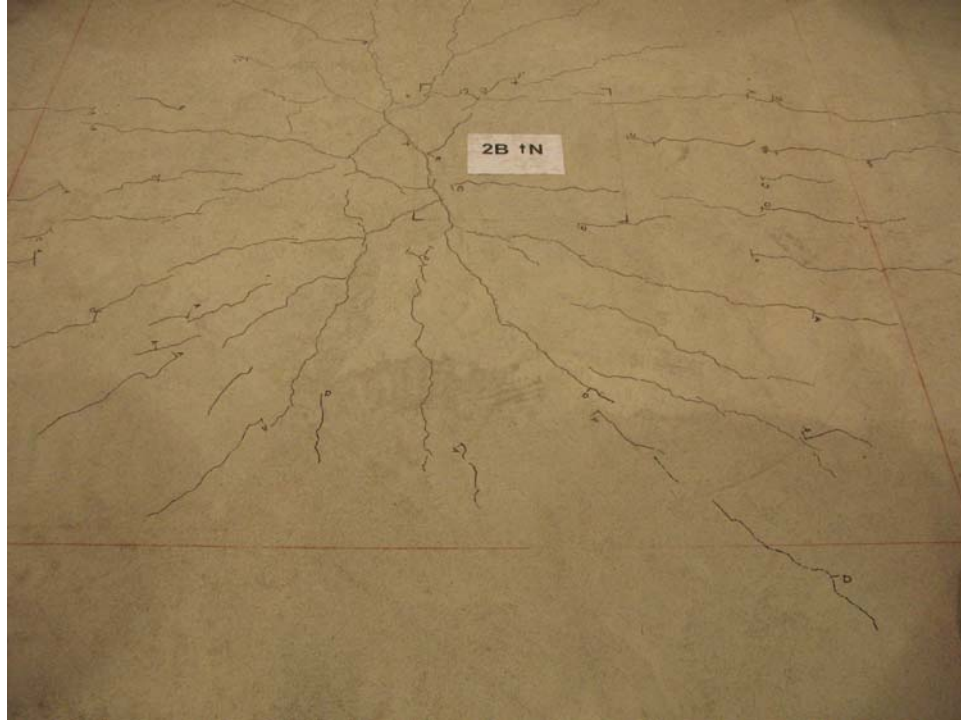


Figure 3-94 Roof Column 2B South Initial Cracks

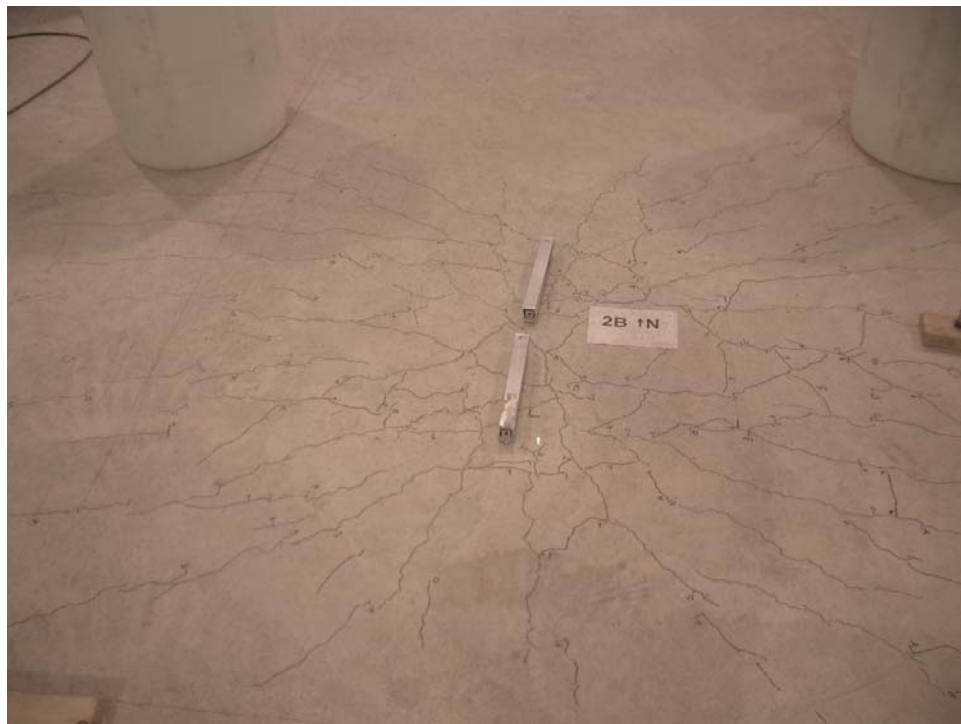


Figure 3-95 Roof Column 2B South Final Cracks

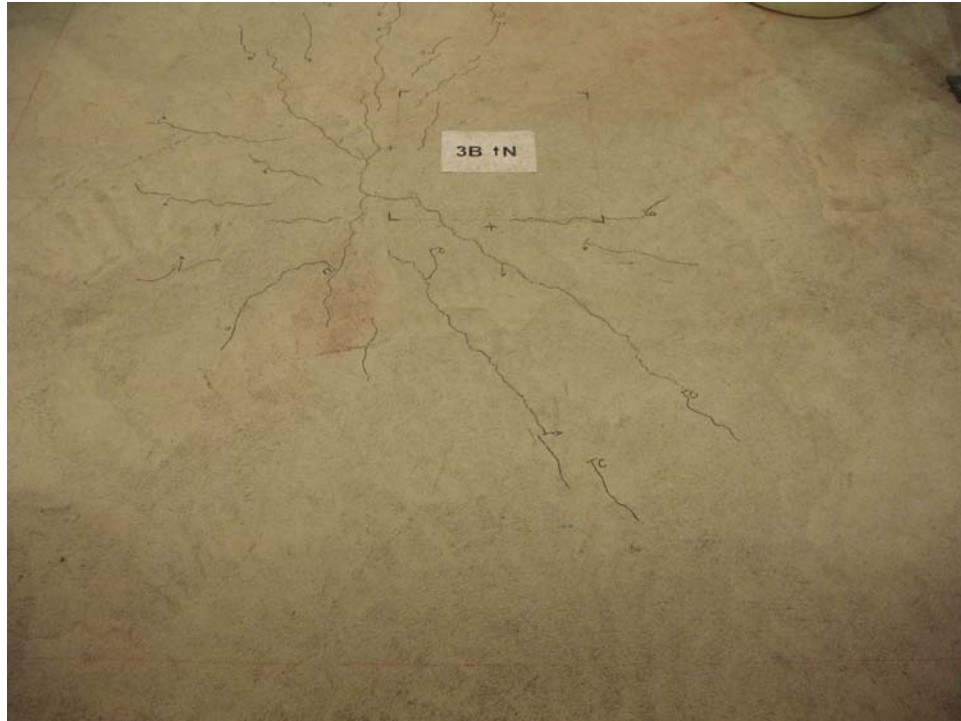


Figure 3-96 Roof Column 3B South Initial Cracks

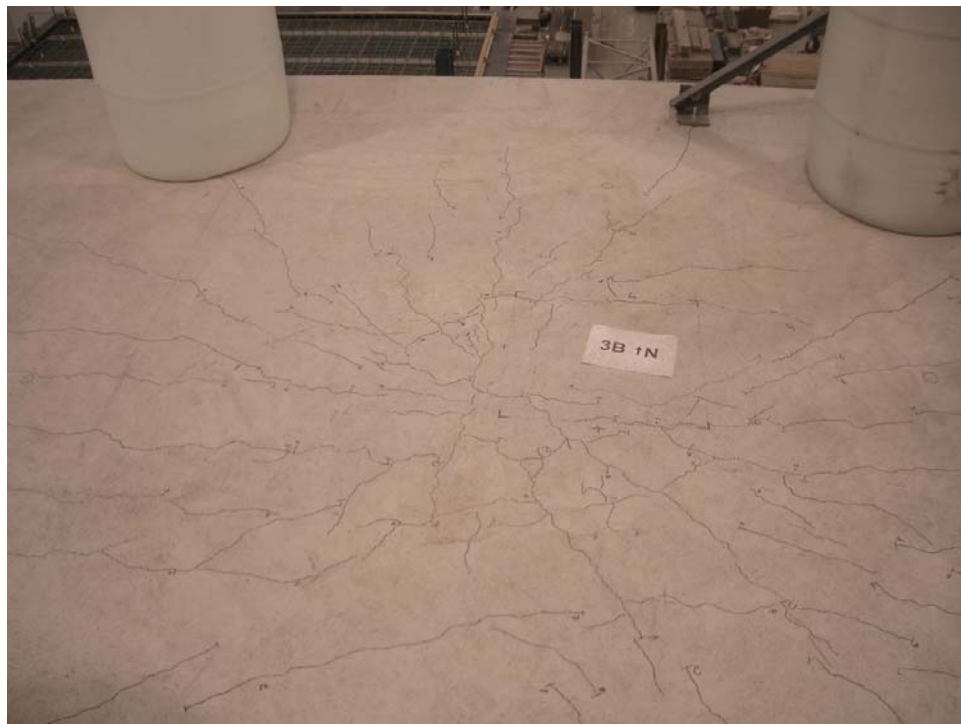


Figure 3-97 Roof Column 3B South Final Cracks



Figure 3-98 Level 2 Column 1A North Initial Cracks



Figure 3-99 Level 2 Column 1A North Final Cracks



Figure 3-100 Level 2 Column 2A North Initial Cracks



Figure 3-101 Level 2 Column 2A North Final Cracks



Figure 3-102 Level 2 Column 1B North Initial Cracks



Figure 3-103 Level 2 Column 1B North Final Cracks



Figure 3-104 Level 2 Column 2B North Initial Cracks



Figure 3-105 Level 2 Column 2B North Final Cracks

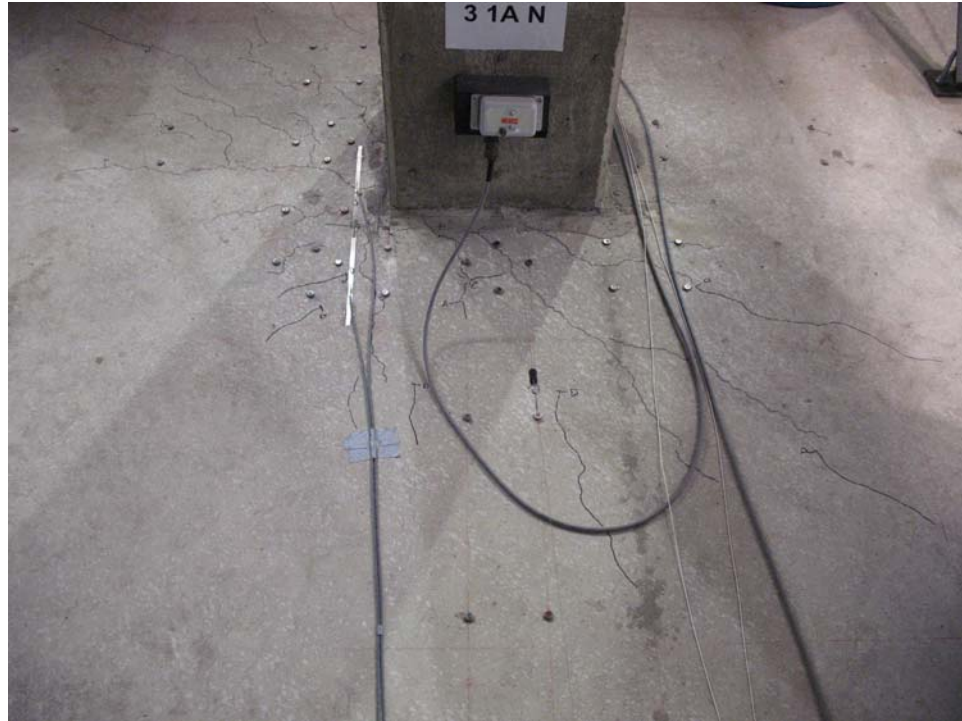


Figure 3-106 Level 3 Column 1A North Initial Cracks



Figure 3-107 Level 3 Column 1A North Final Cracks



Figure 3-108 Level 3 Column 2A North Initial Cracks



Figure 3-109 Level 3 Column 2A North Final Cracks



Figure 3-110 Level 3 Column 1B North Initial Cracks



Figure 3-111 Level 3 Column 1B North Final Cracks



Figure 3-112 Level 3 Column 2B North Initial Cracks



Figure 3-113 Level 3 Column 2B North Final Cracks

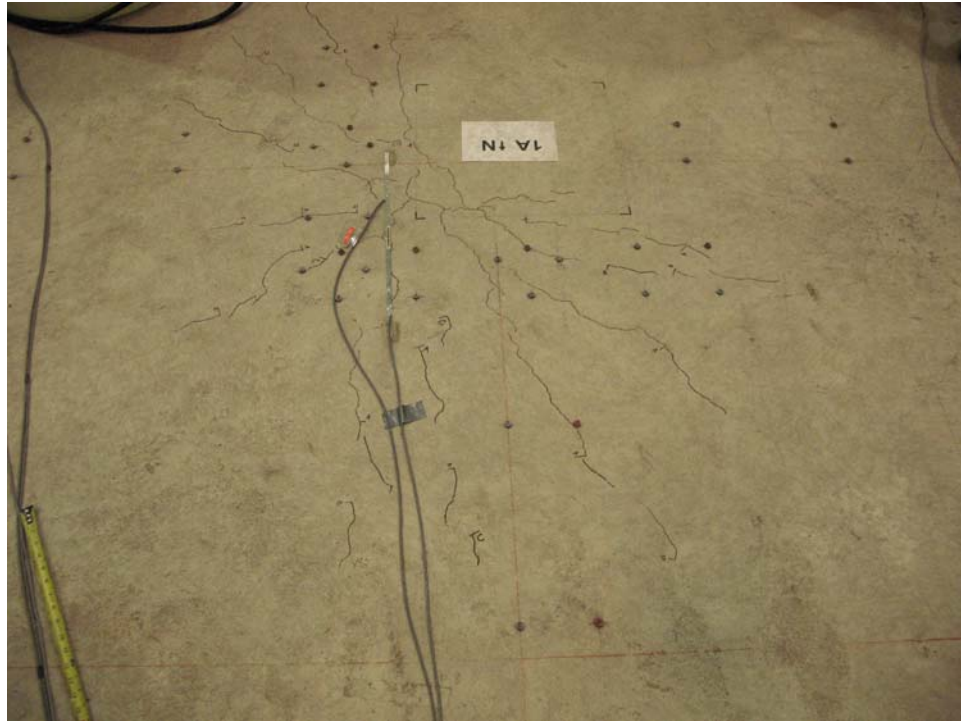


Figure 3-114 Roof Column 1A North Initial Cracks

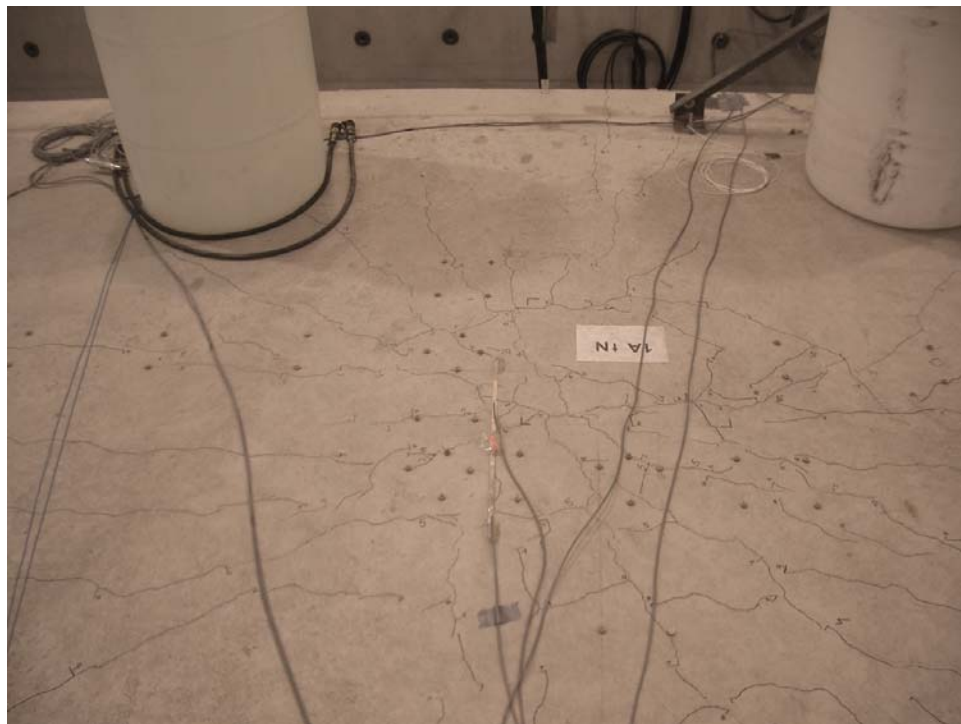


Figure 3-115 Roof Column 1A North Final Cracks

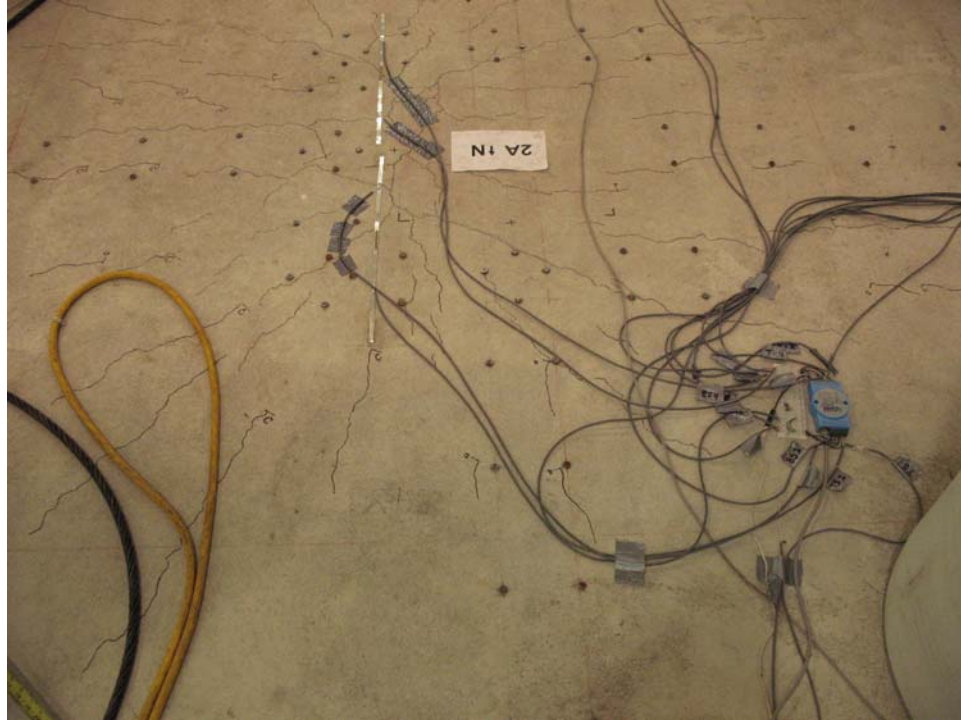


Figure 3-116 Roof Column 2A North Initial Cracks

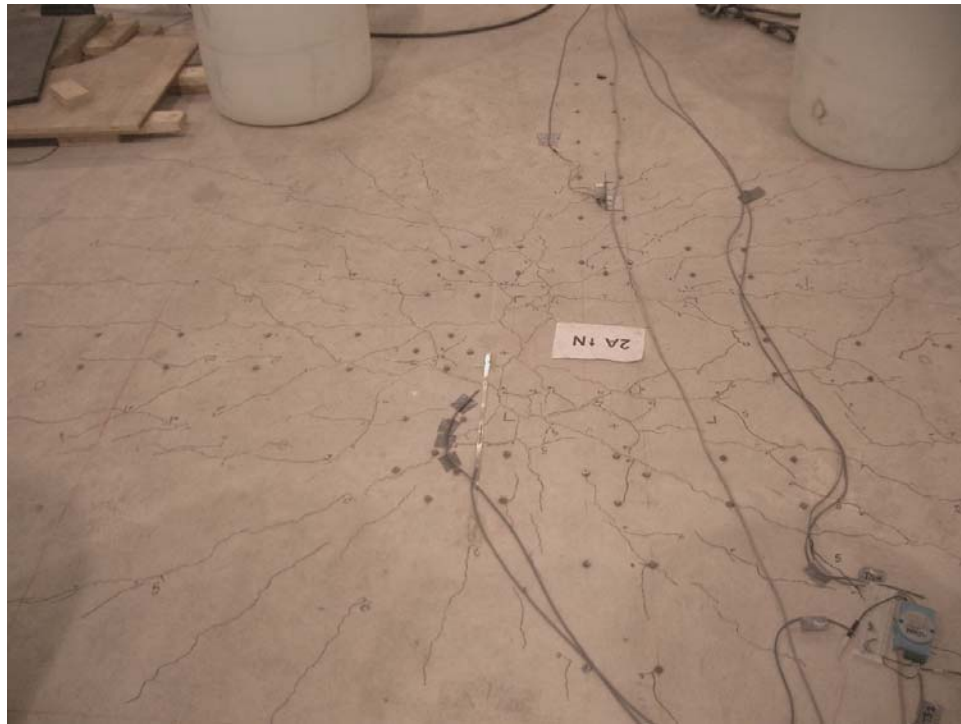


Figure 3-117 Roof Column 2A North Final Cracks

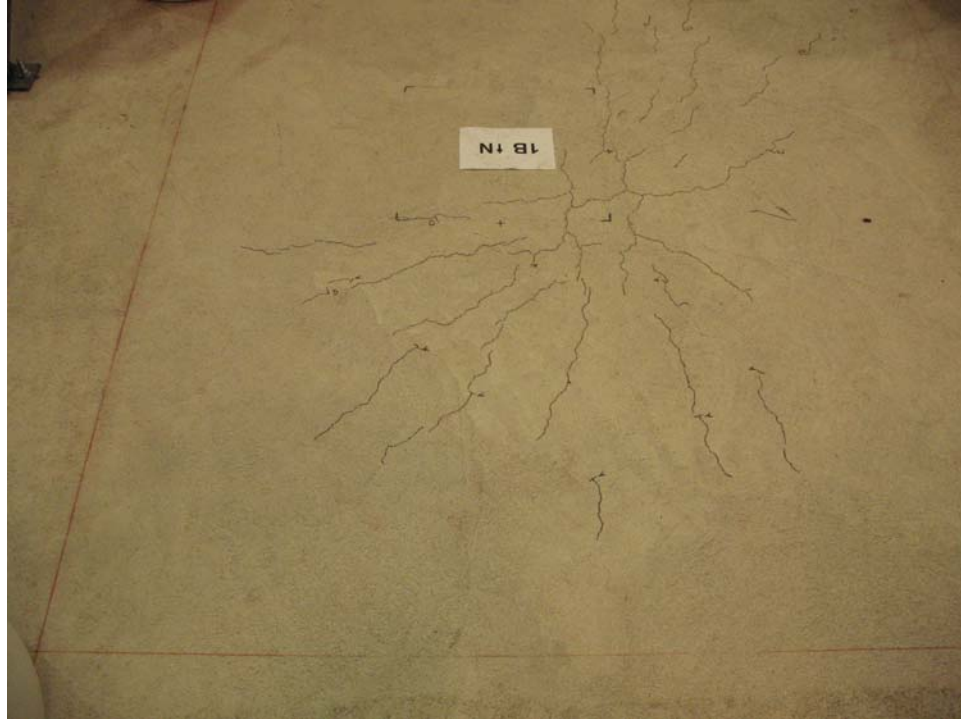


Figure 3-118 Roof Column 1B North Initial Cracks

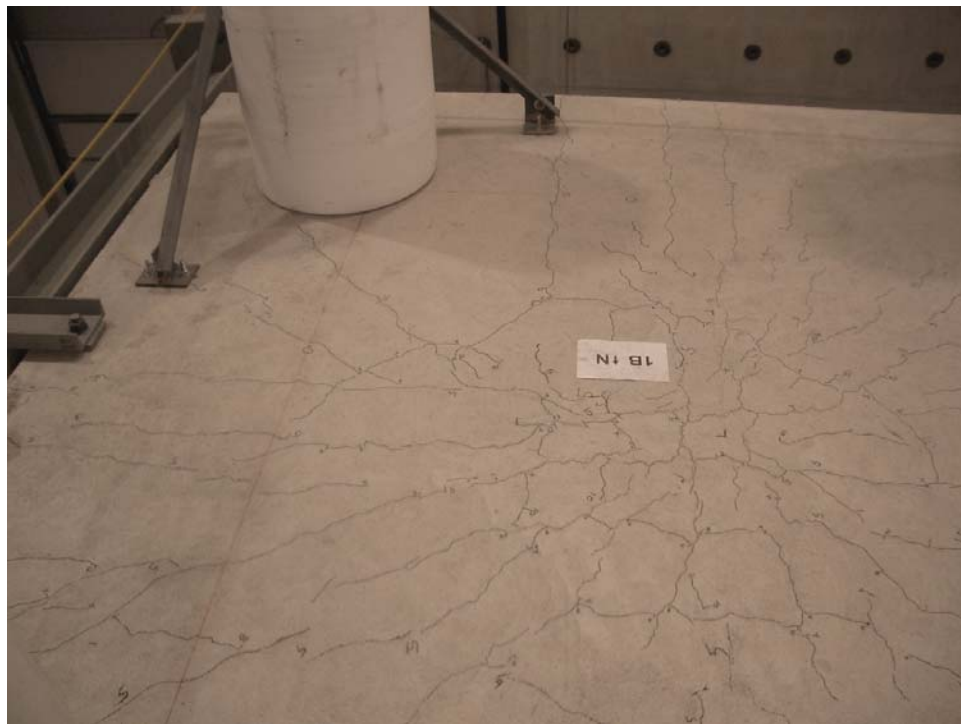


Figure 3-119 Roof Column 1B North Final Cracks

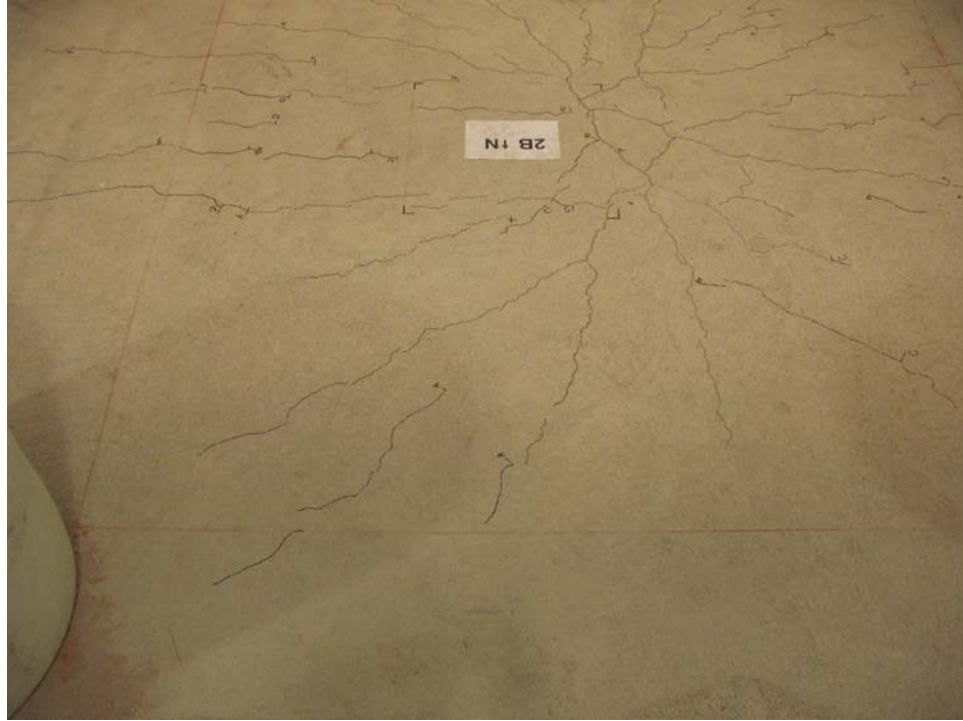


Figure 3-120 Roof Column 2B North Initial Cracks



Figure 3-121 Roof Column 2B North Final Cracks

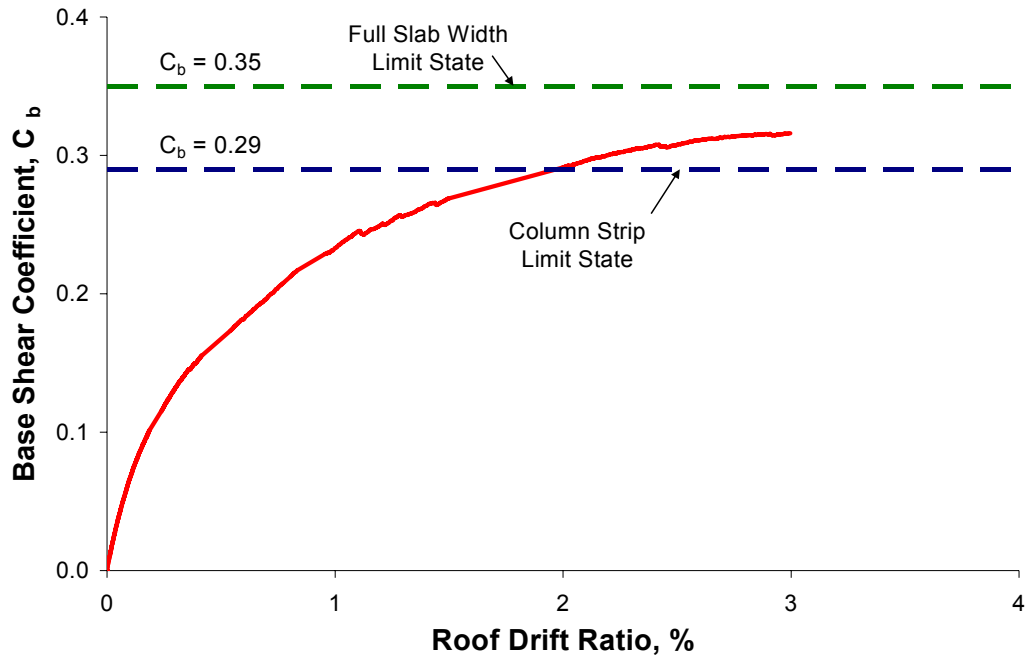


Figure 4-1 Limit State Analysis Results

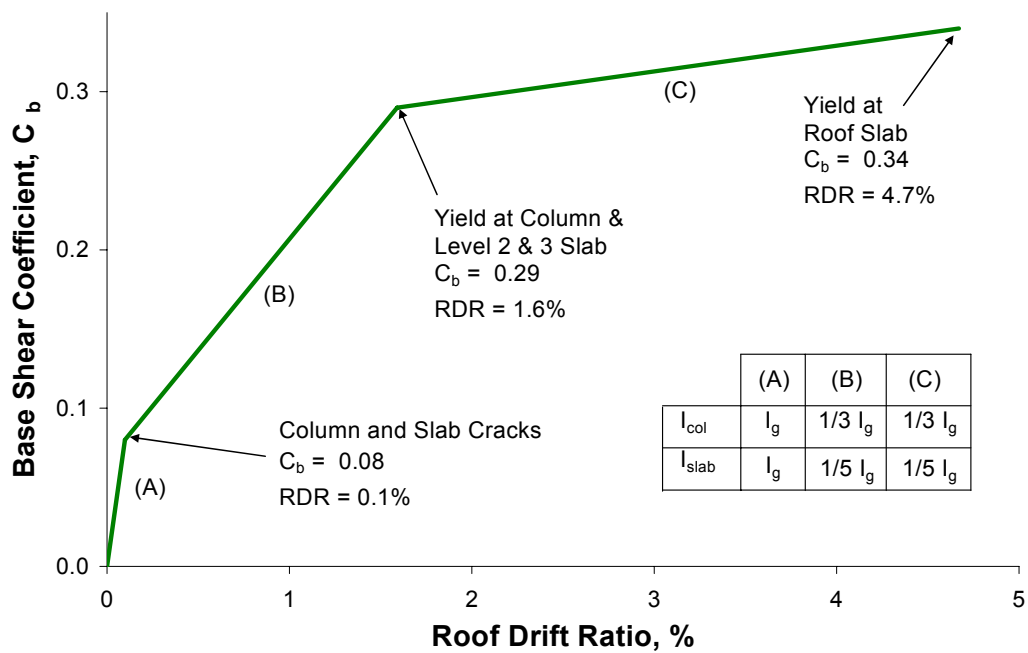


Figure 4-2 Trilinear Model Segments

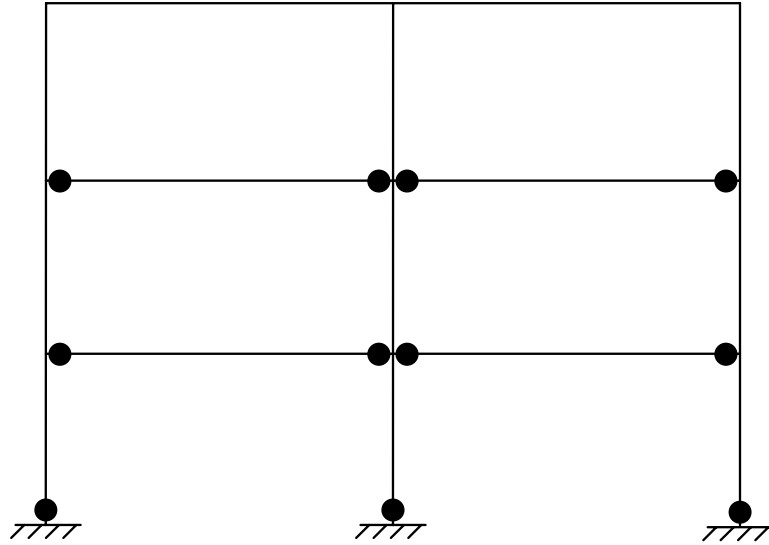


Figure 4-3 Trilinear Model with Hinges

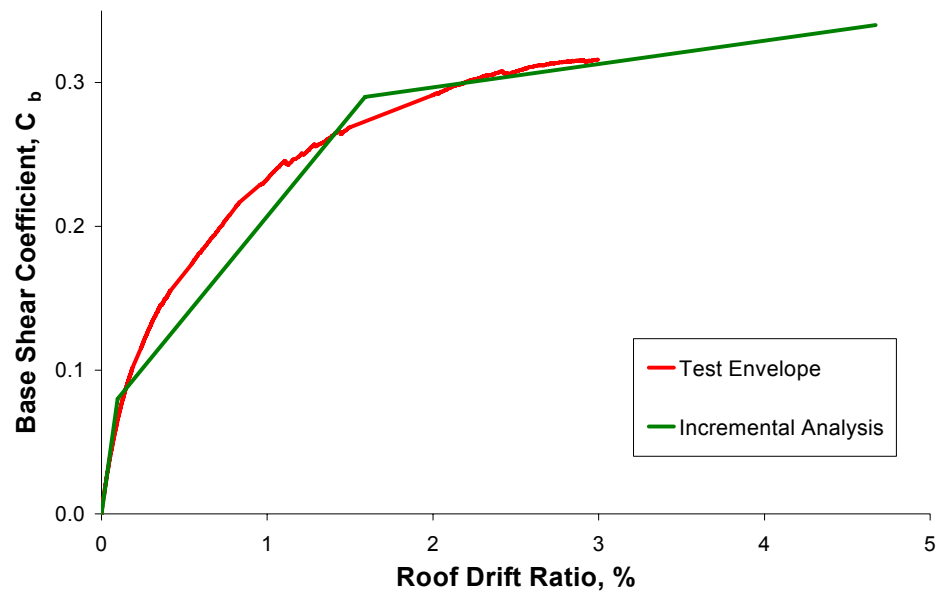


Figure 4-4 Trilinear Model Comparison

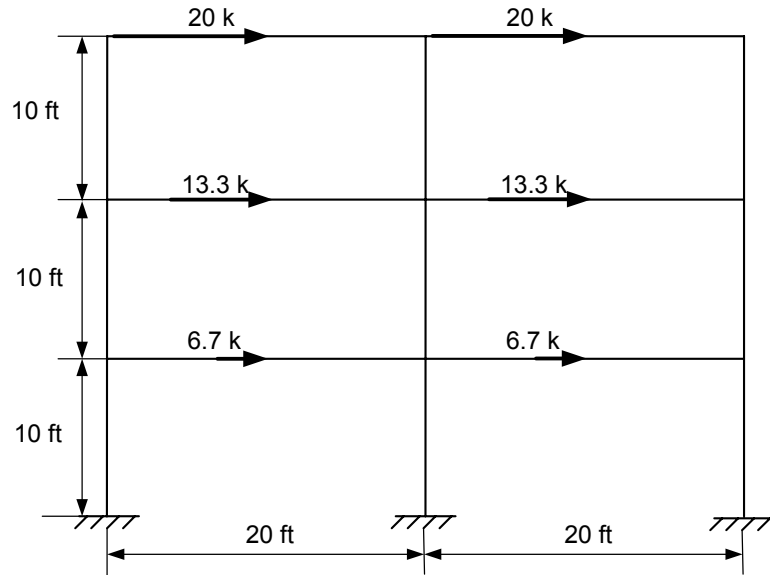


Figure 4-5 Nonlinear Analysis Frame Dimensions and Loading

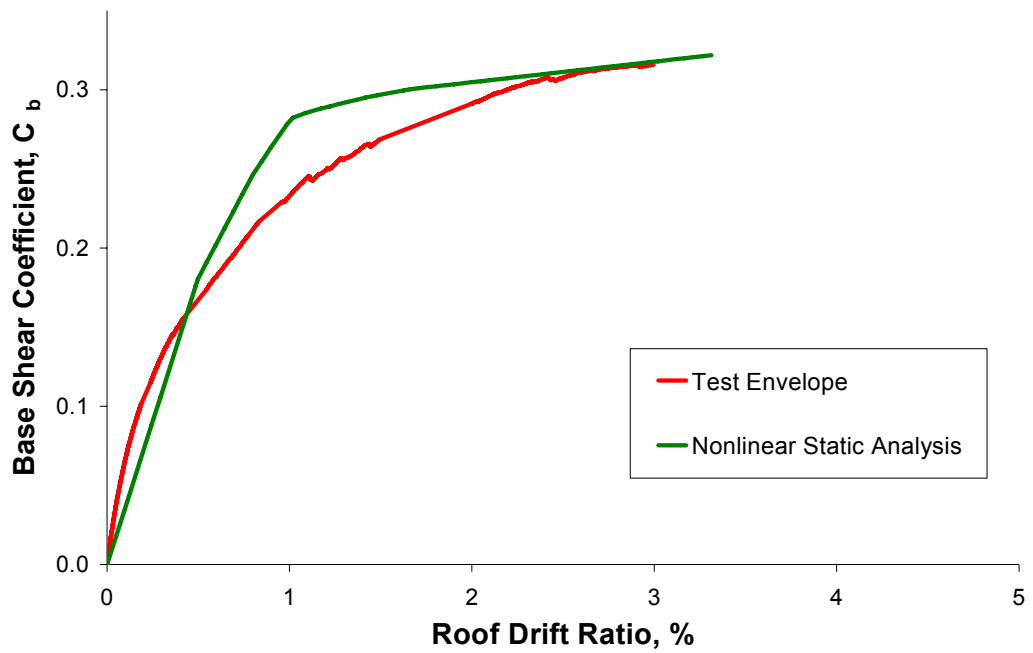


Figure 4-6 Nonlinear Static Analysis Comparison

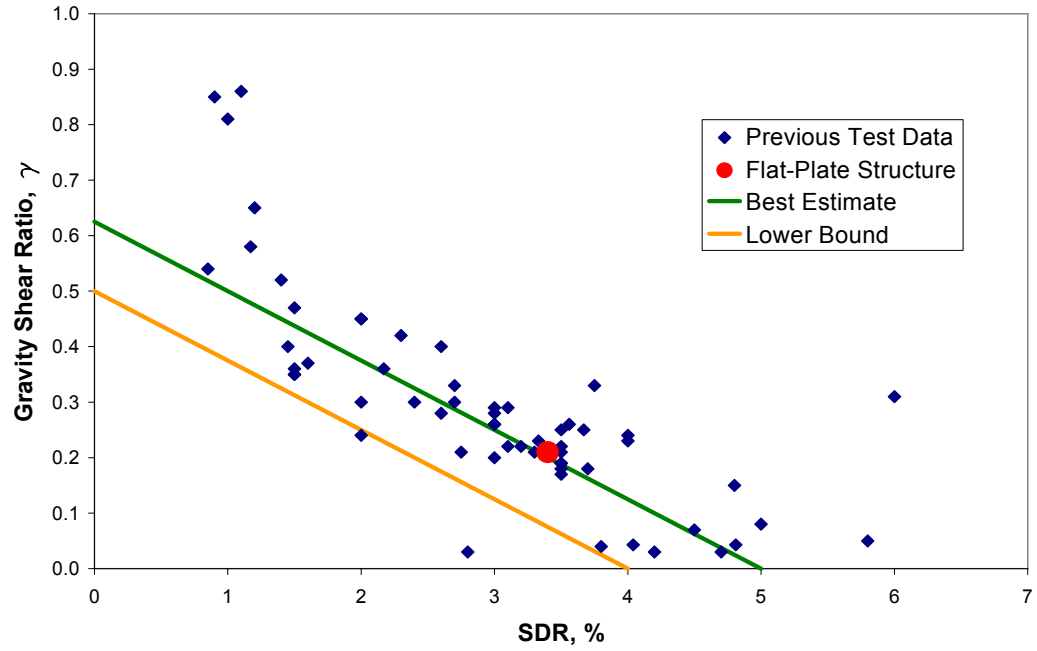


Figure 4-7 Flat-Plate Comparison with Previous Data

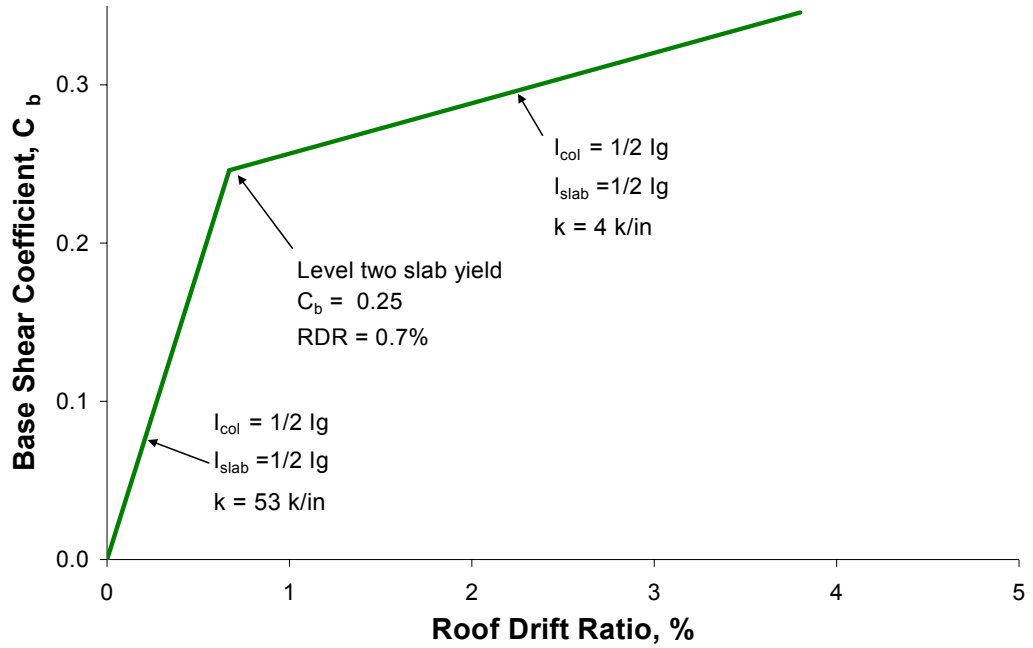


Figure 5-1 Bilinear Model Segments

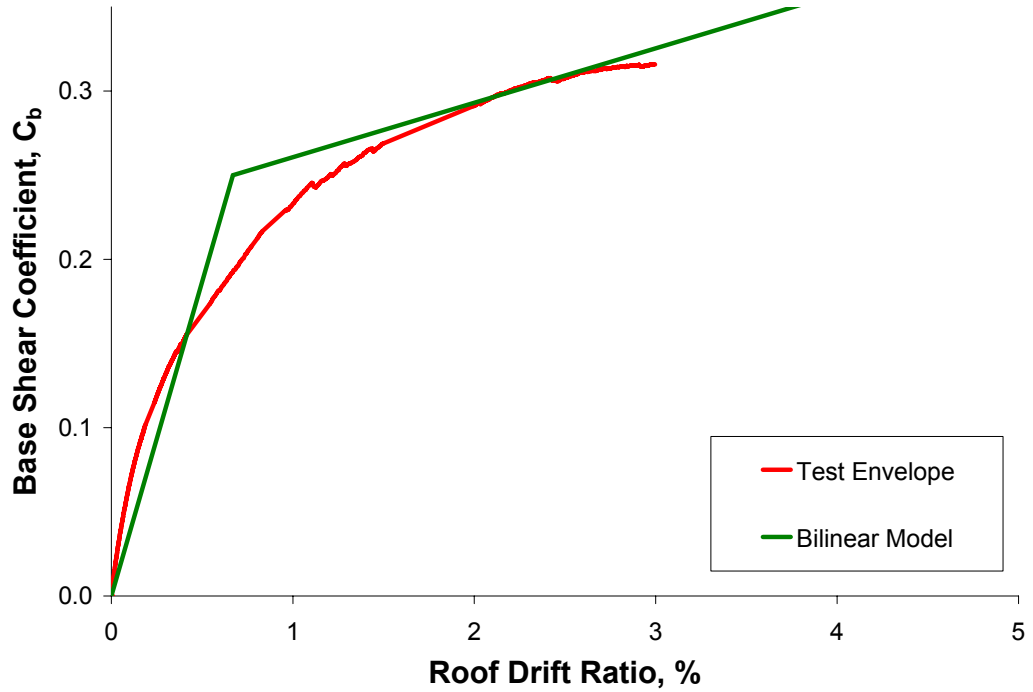


Figure 5-2 Bilinear Model Comparison

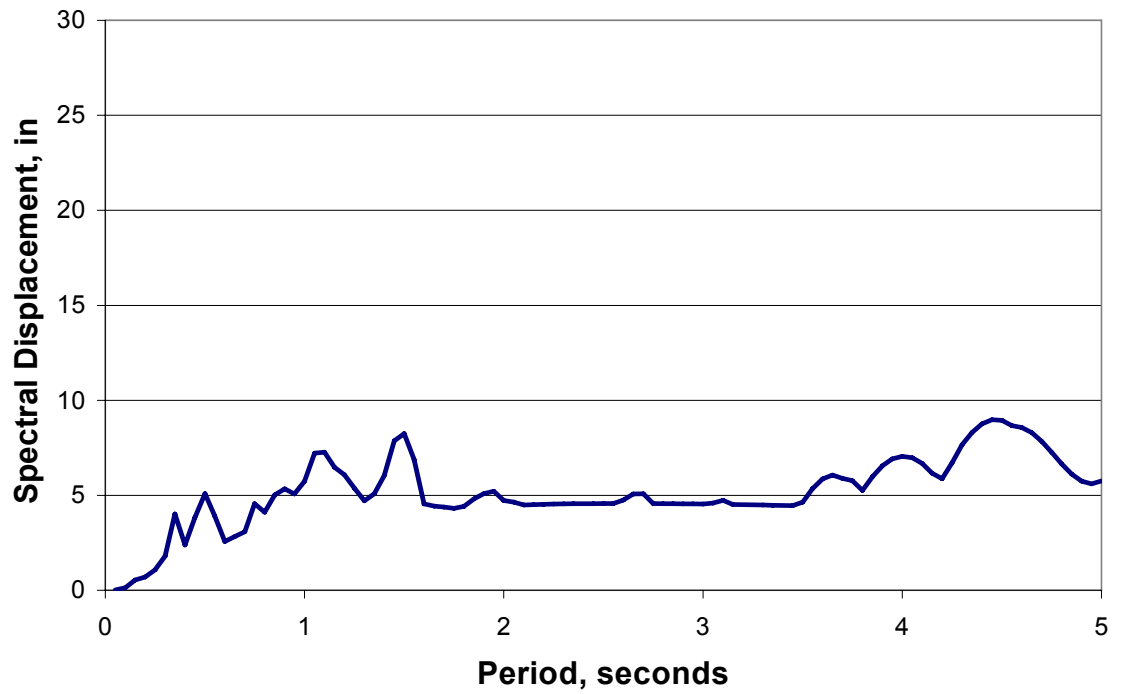
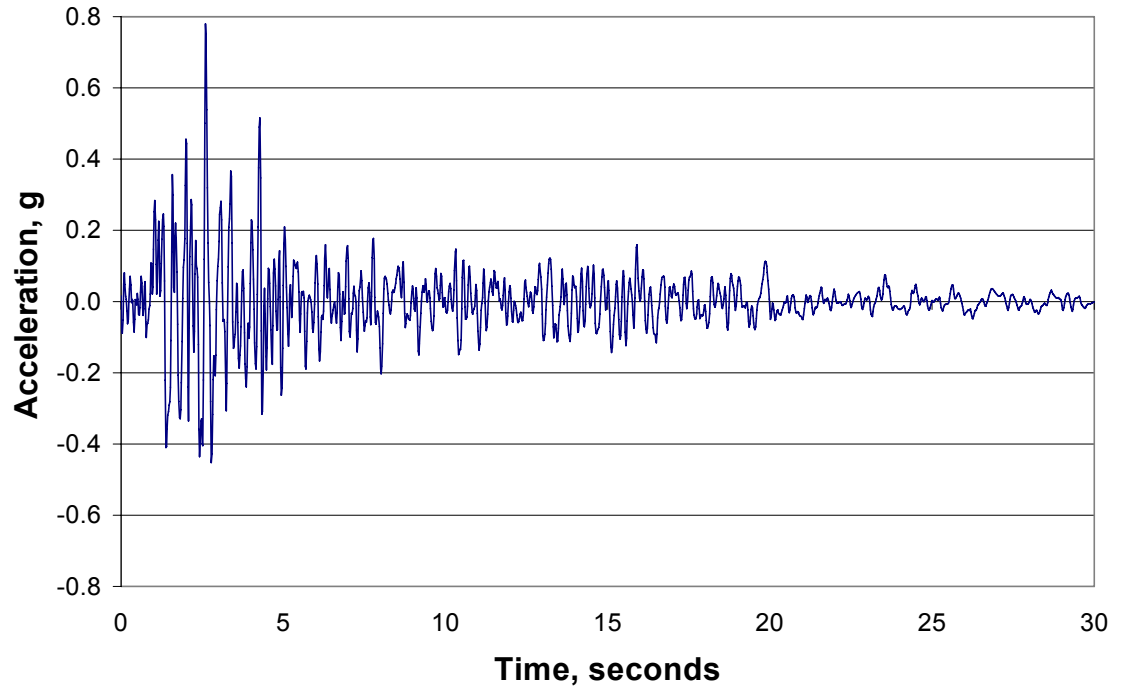


Figure 5-3 Castic N21E Acceleration History and Displacement Spectrum

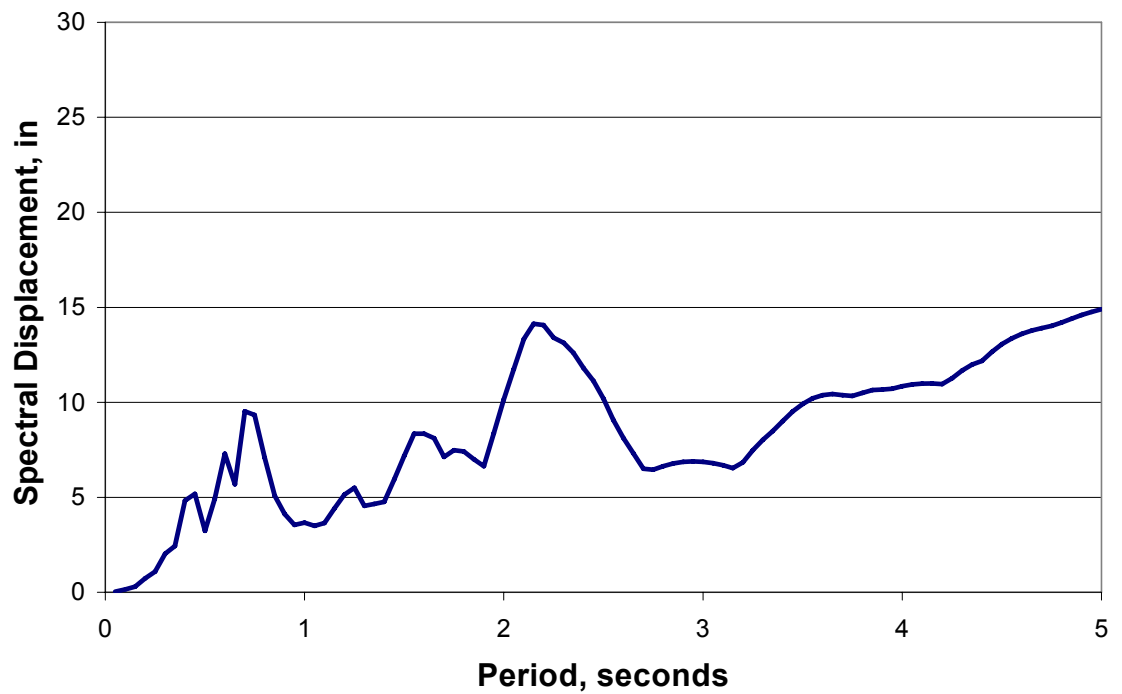
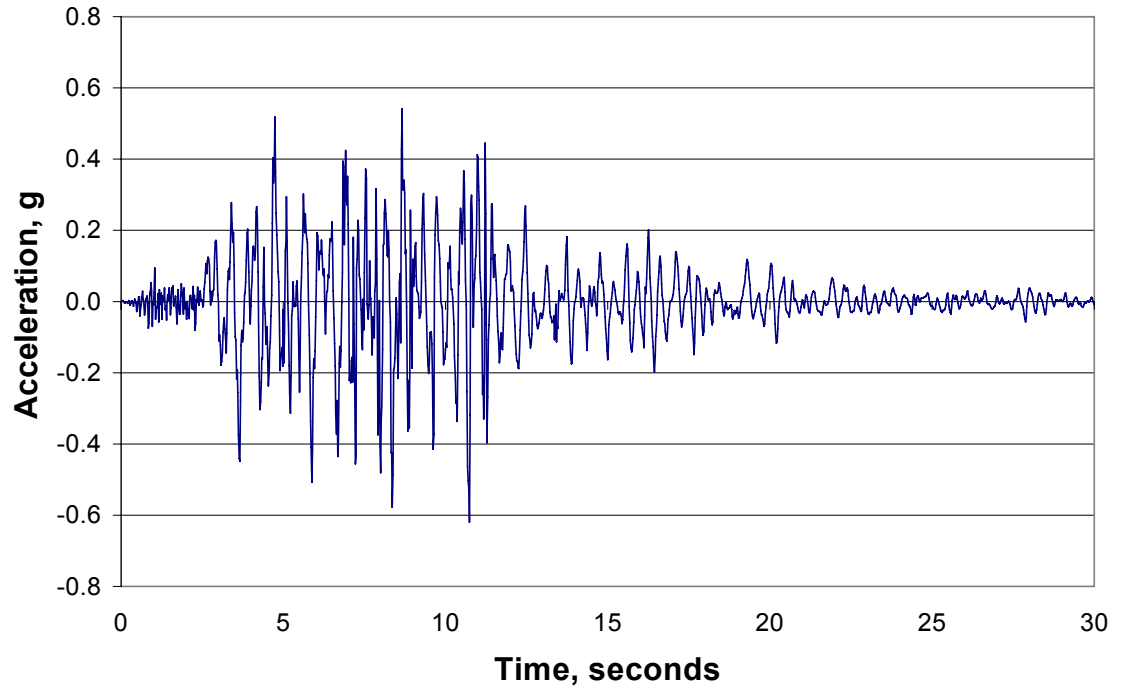


Figure 5-4 Tarzana NS Acceleration History and Displacement Spectrum

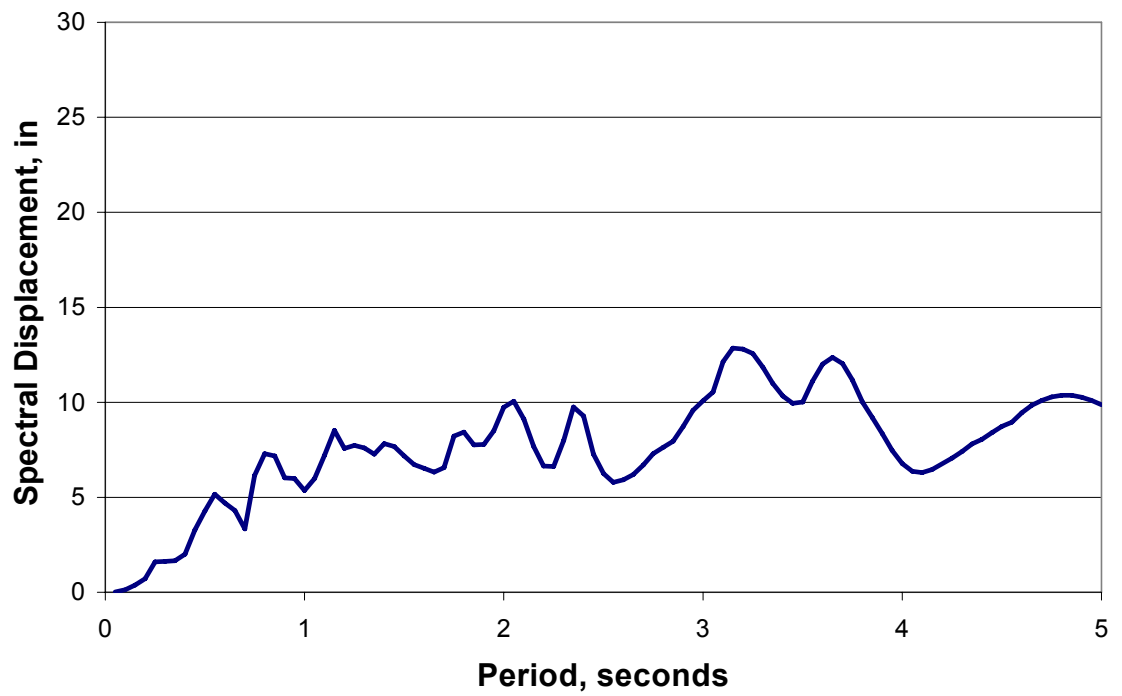
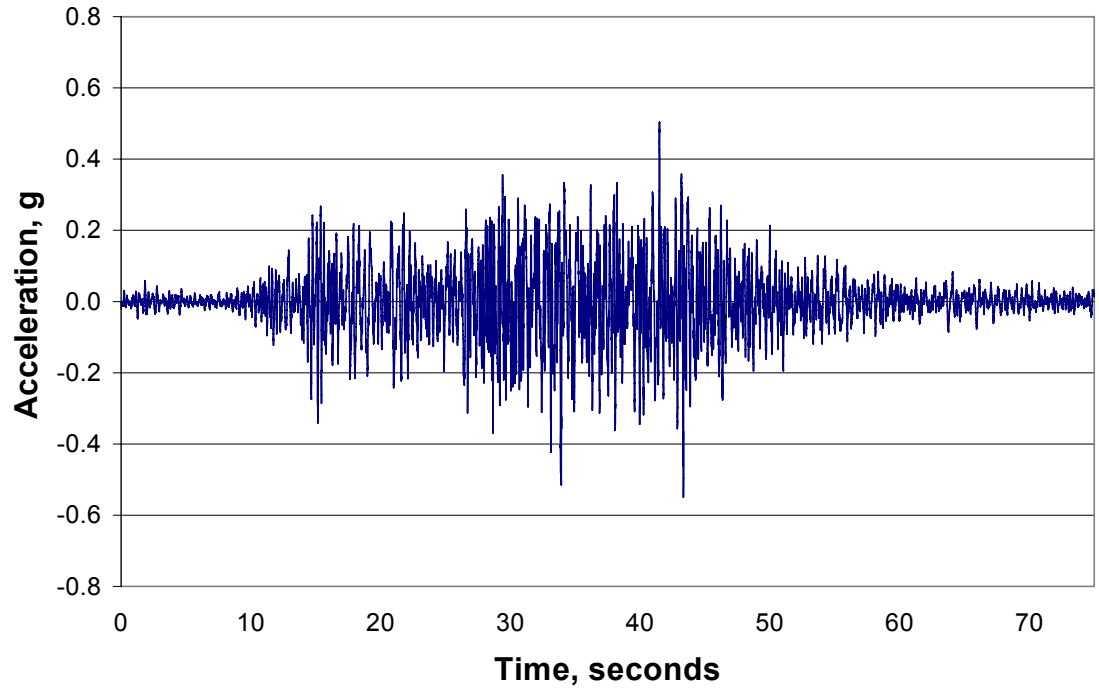


Figure 5-5 Lolloe N10E Acceleration History and Displacement Spectrum

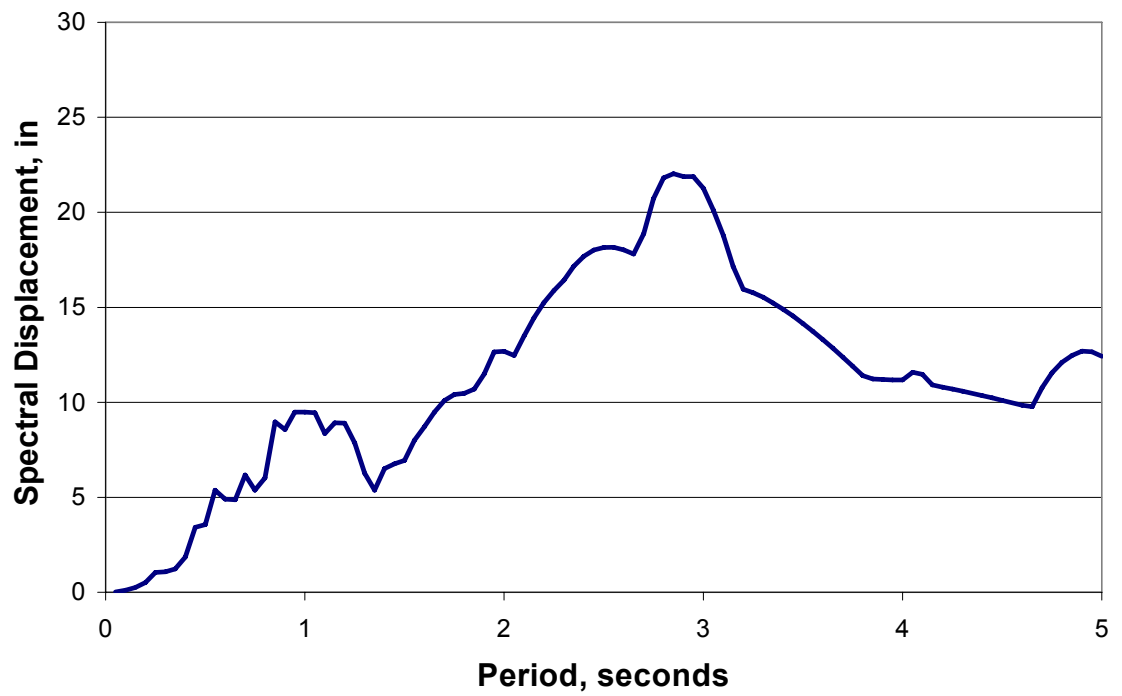
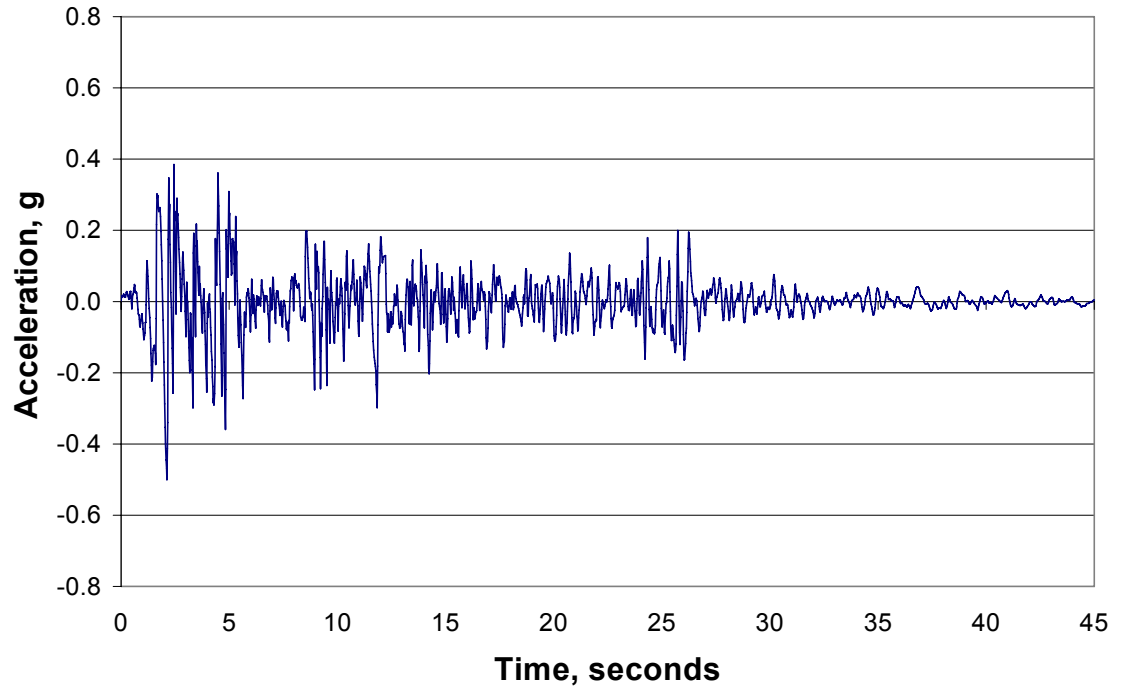


Figure 5-6 El Centro NS Acceleration History and Displacement Spectrum

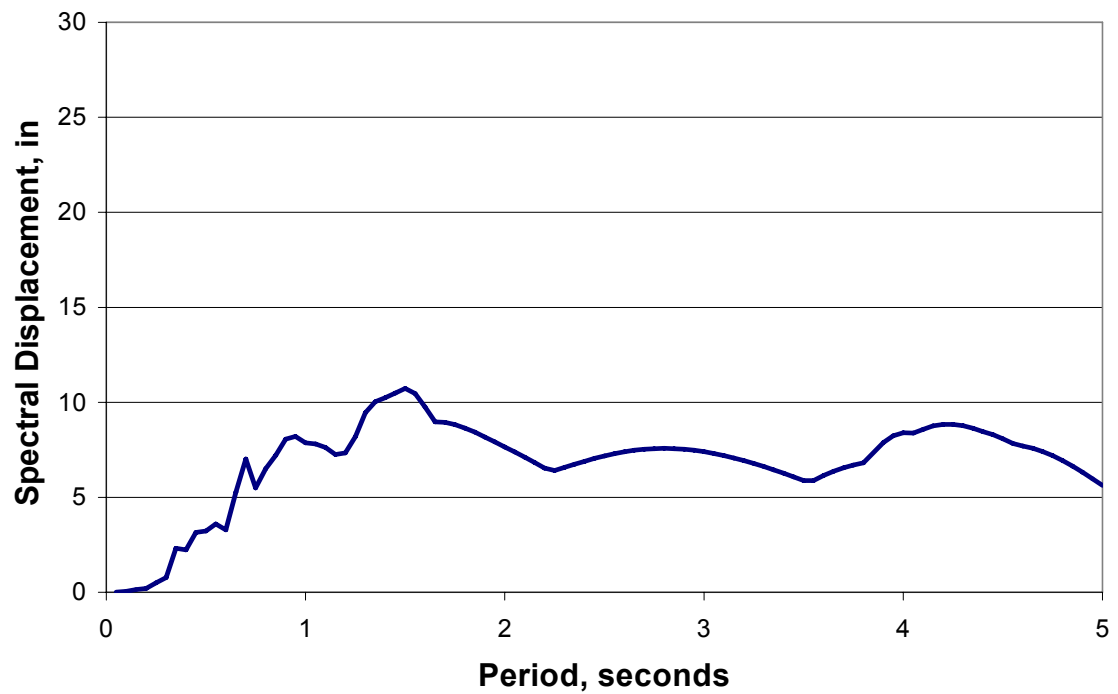
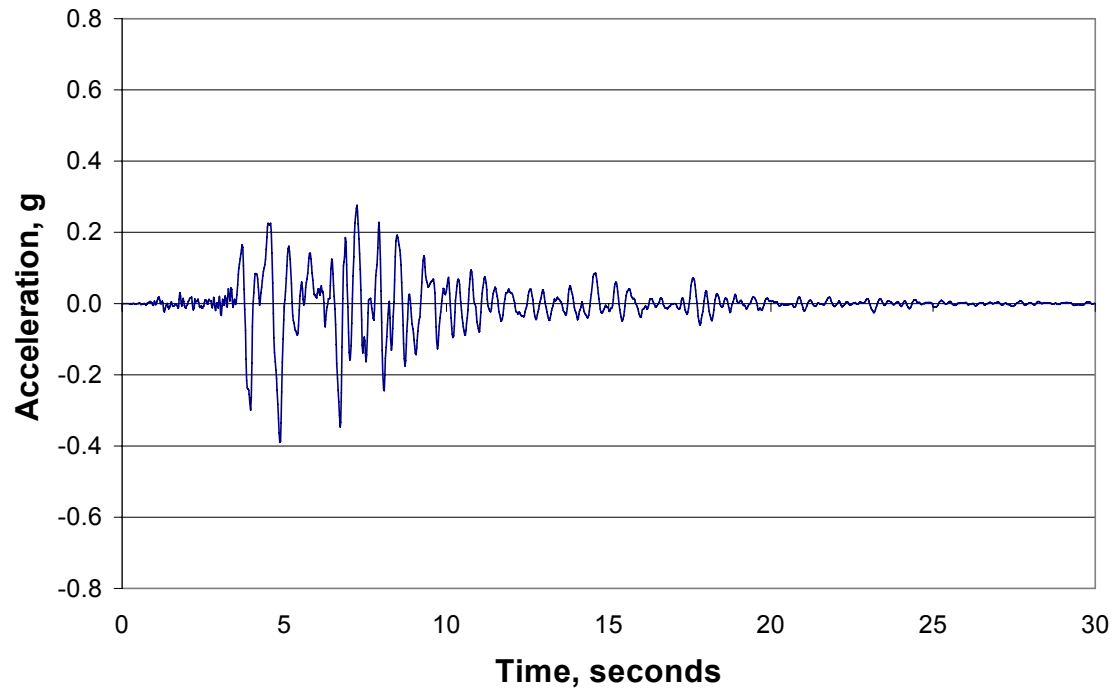


Figure 5-7 Kobe NS Acceleration History and Displacement Spectrum

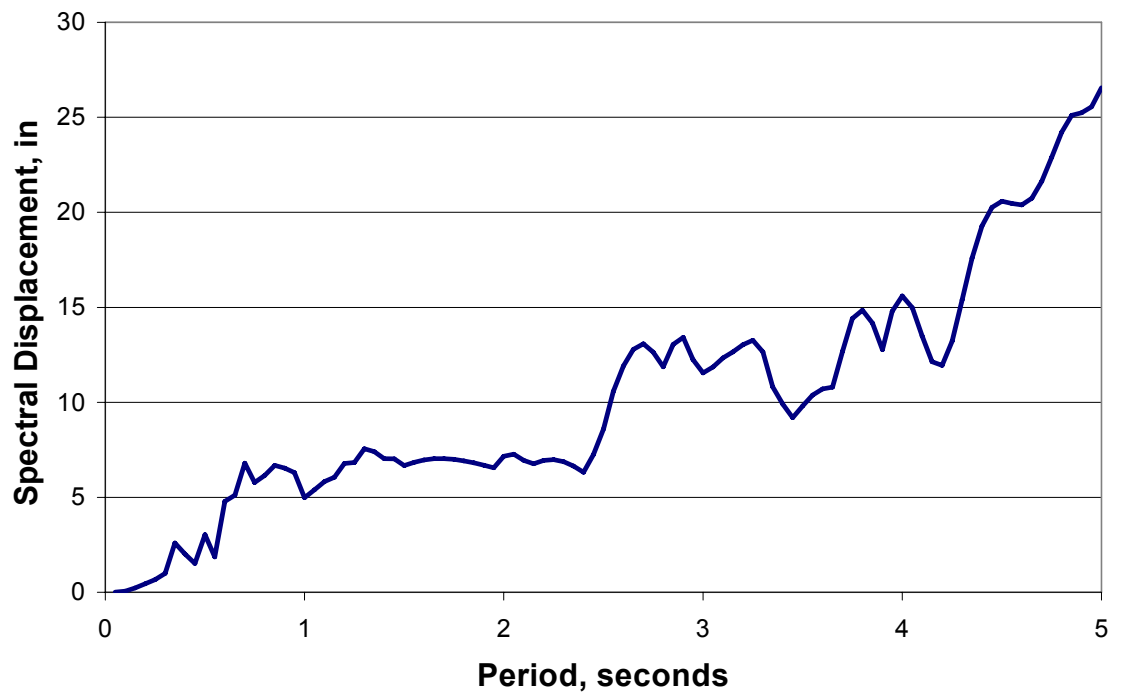
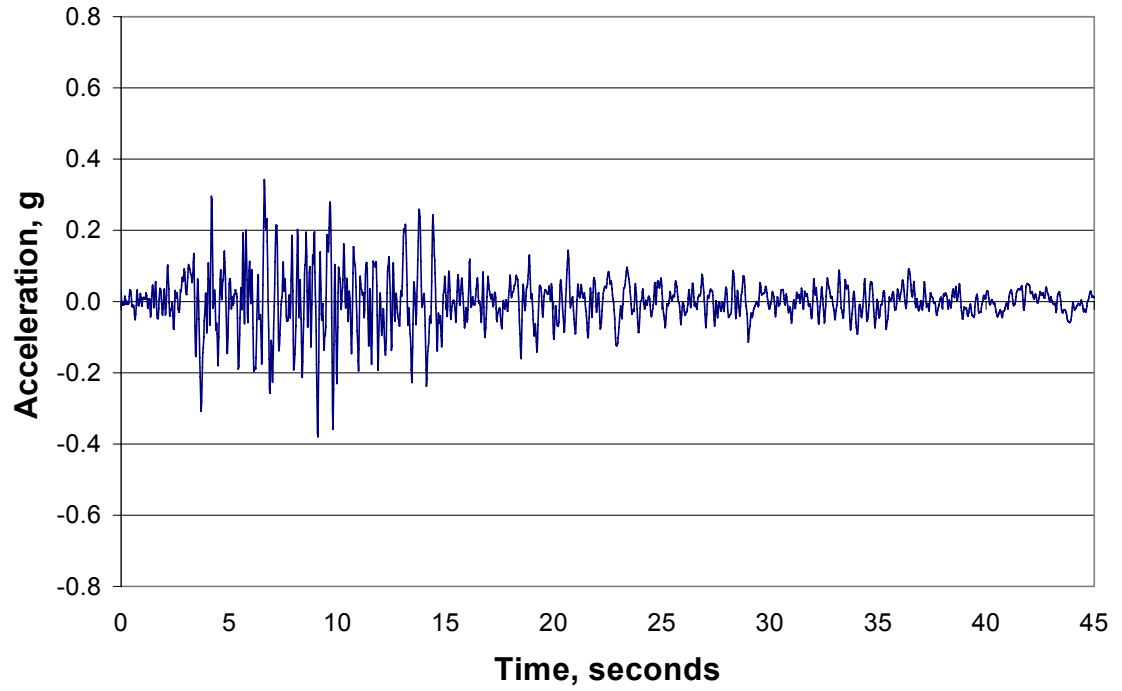


Figure 5-8 Taft N21E Acceleration History and Displacement Spectrum

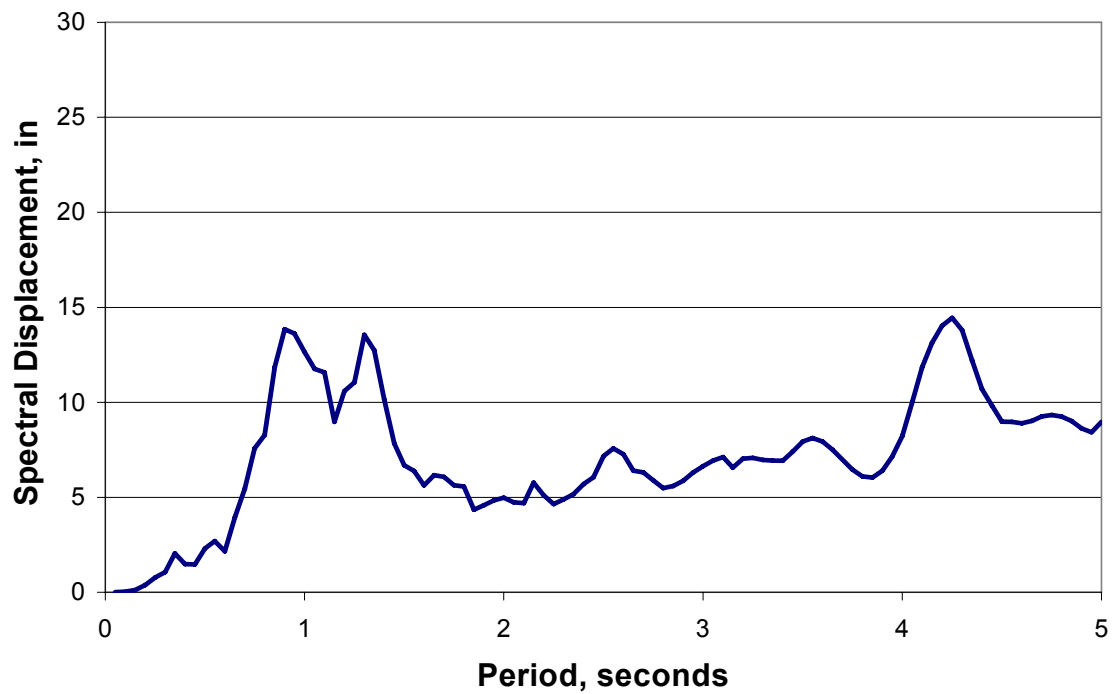
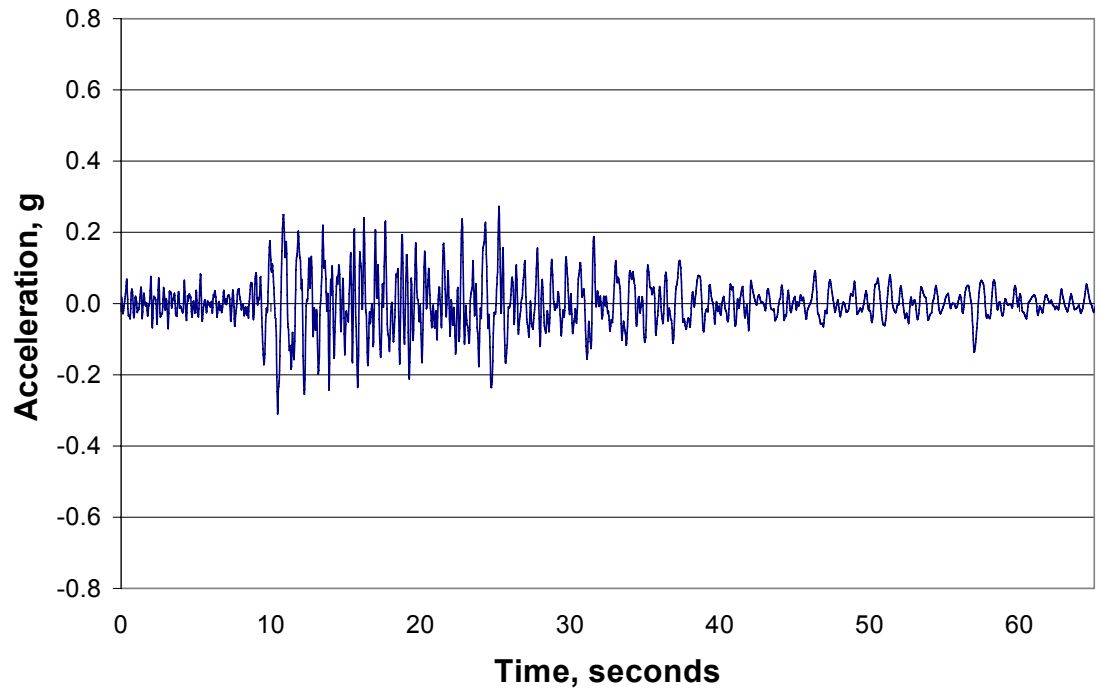


Figure 5-9 Seattle S02W Acceleration History and Displacement Spectrum

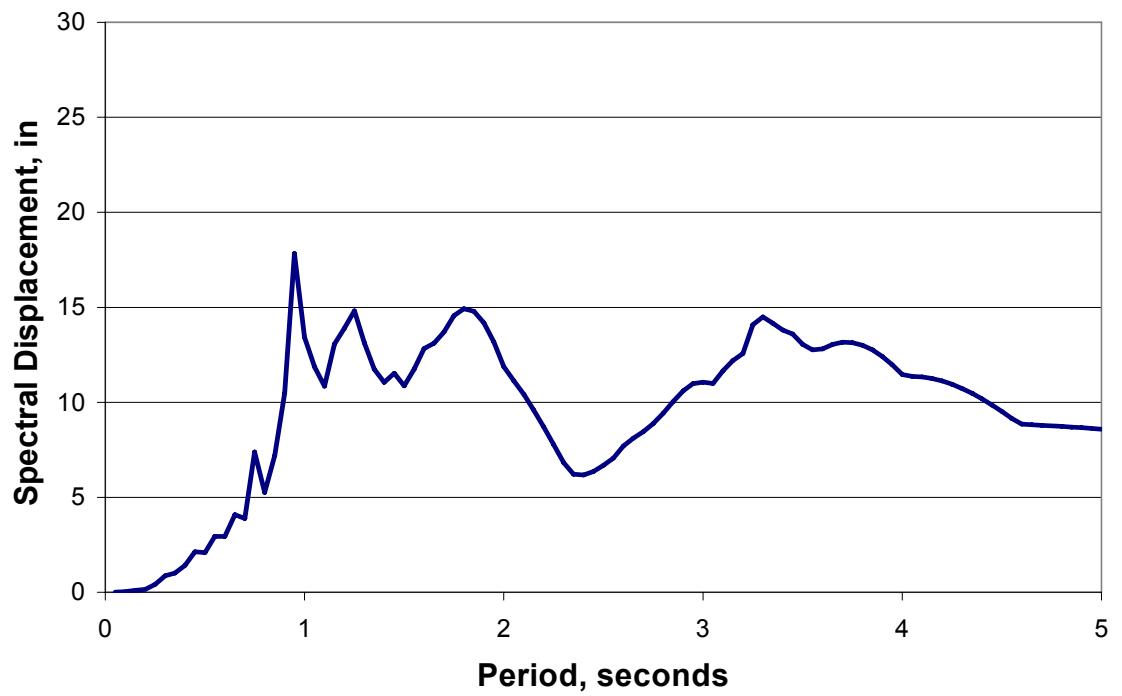
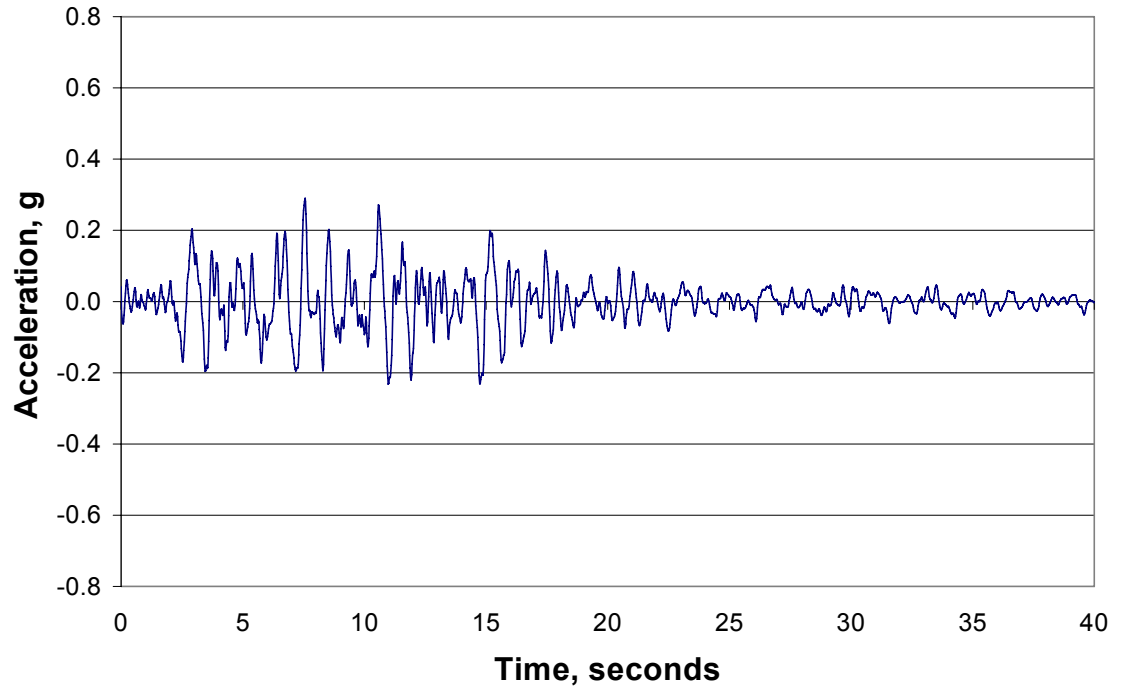


Figure 5-10 Sendai NS Acceleration History and Displacement Spectrum

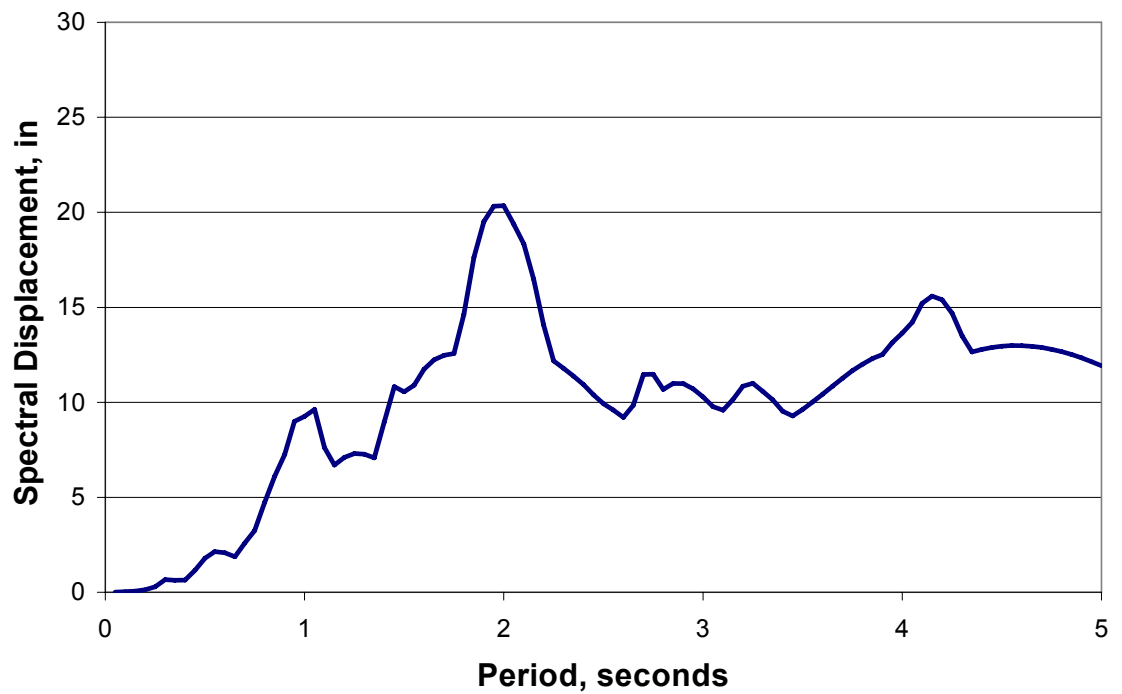
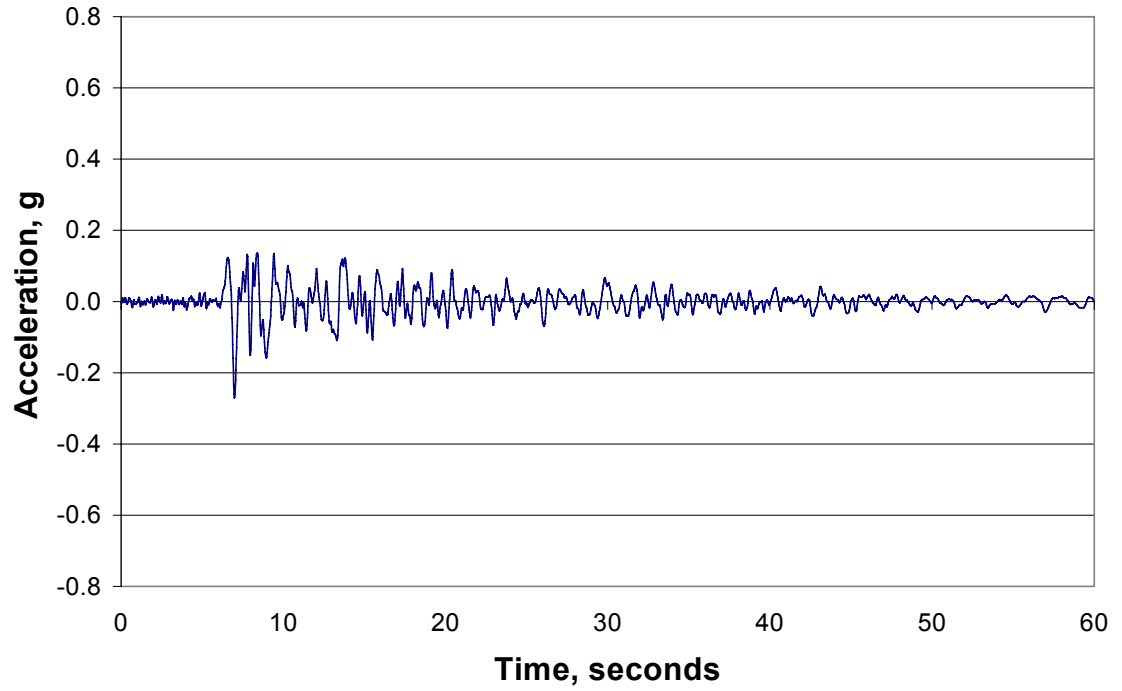


Figure 5-11 Santa Barbara S48E Acceleration History and Displacement Spectrum

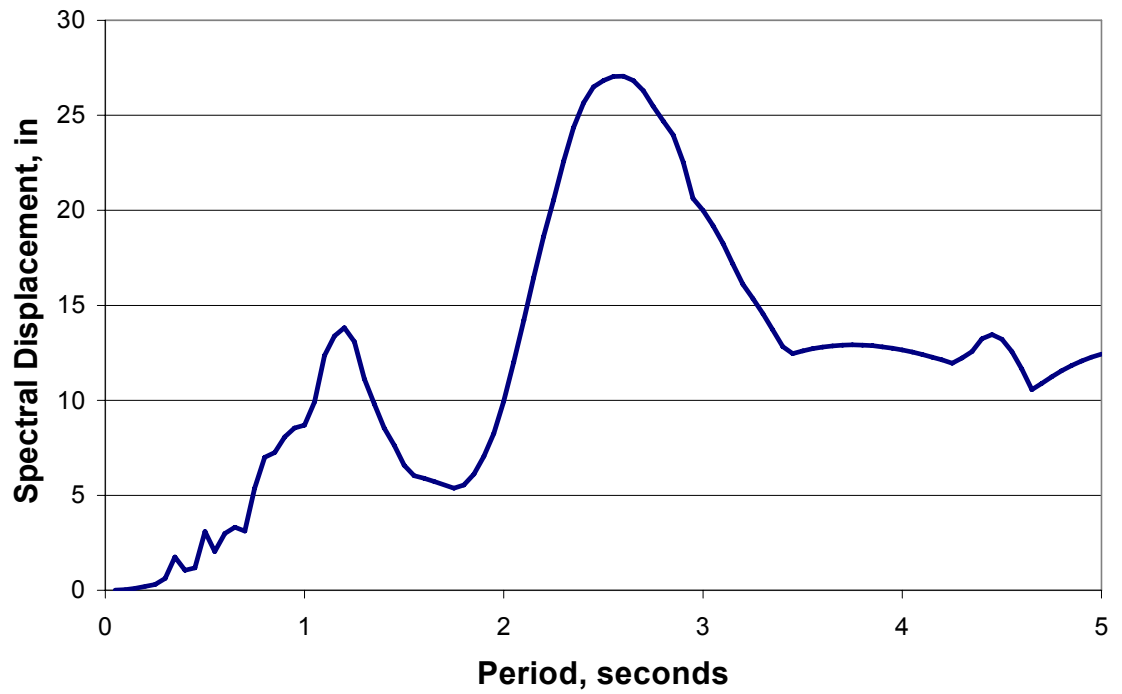
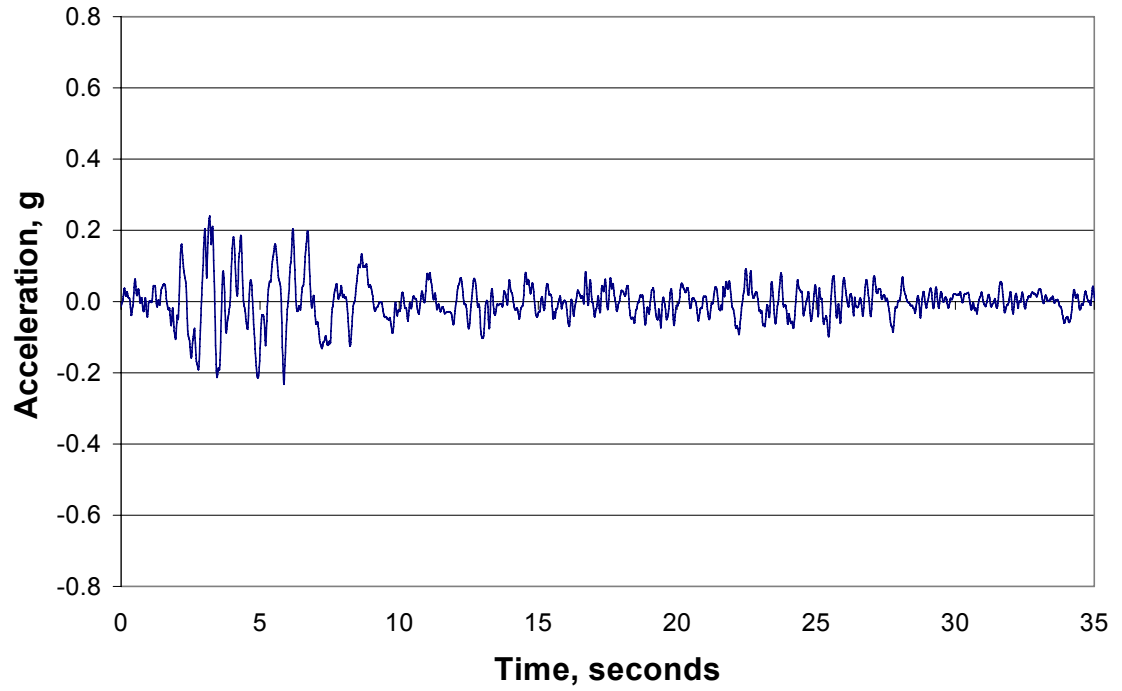


Figure 5-12 Hachinohe EW Acceleration History and Displacement Spectrum

LIST OF REFERENCES

- Durrani, A. J., Du, Y., and Luo, Y. H. (1995). "Seismic Resistance of Nonductile Slab-Column Connections in Existing Flat-Slab Buildings." *ACI Structural Journal*, 92(4), 479-487.
- Elgabry, A. A., and Ghali, A. (1987). "Tests on Concrete Slab-Column Connections with Stud-Shear Reinforcement Subjected to Shear-Moment Transfer." *ACI Structural Journal (American Concrete Institute)*, 84(5), 433-442.
- Farhey, D. N., Adin, M. A., and Yankelevsky, D. Z. (1993). "RC Flat Slab-Column Subassemblages Under Lateral Loading." *Journal of Structural Engineering*, 119(6), 1903-1916.
- Ghali, A., Elmasri, M. Z., and Dilger, W. (1976). "Punching of Flat Plates Under Static and Dynamic Horizontal Forces." *Journal of The American Concrete Institute*, 73(10), 566-572.
- Hanson, J. M., and Hanson, N. W. (1968). "Shear and Moment Transfer Between Concrete Slabs and Columns." *Portland Cement Association -- Research and Development Laboratories -- Journal*, 10(1), 2-16.
- Hawkins, N. M. (1974). "Shear Strength of Slabs with Moments Transferred to Columns." *Shear in Reinforced Concrete*, American Concrete Institute, Detroit, MI, 785-816.
- Hawkins, N. M., and Corley, W. G. (1971). "Transfer of Unbalanced Moment and Shear From Flat Plates to Columns." *Cracking, Deflection and Ultimate Load of Concrete Slab Systems*, American Concrete Institute, Detroit, MI, 147-176.
- Hawkins, N. M., Mitchell, D., and Sheu, M. S. (1974). "Cyclic Behavior of Six Reinforced Concrete Slab-Column Specimens Transferring Moment and Shear." *Progress Report, NSF Project GI-38717*, University of Washington, Seattle, WA.
- Hognestad, E. (1953). "Shearing Strength of Reinforced Concrete Column Footings." *American Concrete Institute -- Journal*, 25(3), 189-208.
- Hueste, M. B. D., Browning, J., Lepage, A., and Wallace, J. W. (2007). "Seismic Design Criteria for Slab-Column Connections." *ACI Structural Journal*, 104(4), 448-458.
- Hwang, S.-J., and Moehle, J. P. (2000). "Vertical and Lateral Load Tests of Nine-Panel Flat-Plate Frame." *ACI Structural Journal*, 97(1), 193-203.

- International Code Council., Building Officials and Code Administrators International., International Conference of Building Officials., and Southern Building Code Congress International. (2000). "International Building Code." The Council, Falls Church, Va., v.
- Islam, S., and Park, R. (1976). "Tests on Slab-Column Connections with Shear and Unbalanced Flexure." 102(3), 549-568.
- JMA. (1995). "Strong Motion Accelerograms." Japan Meteorological Agency.
- Lepage, A. (1997). "A Method for Drift-Control in Earthquake-Resistant Design of RC Building Structures," Dissertation, University of Illinois, Urbana-Champaign, IL.
- Luo, Y. H., and Durrani, A. J. (1995). "Equivalent Beam Model for Flat-Slab Buildings - Part I: Interior Connections." *ACI Structural Journal*, 92(1), 115-124.
- Matamoros, A. B. (1999). "Study of Drift Limits for High-Strength Concrete Columns," Dissertation, University of Illinois, Urbana-Champaign, IL.
- Megally, S., and Ghali, A. (1994). "Design Considerations for Slab-Column Connections in Seismic Zones." *ACI Structural Journal (American Concrete Institute)*, 91(3), 303-314.
- Megally, S., and Ghali, A. (2000). "Punching of Concrete Slabs Due to Column Moment Transfer." *Journal of Structural Engineering*, 126(2), 180-189.
- Moe, J. (1961). "Shearing Strength of Reinforced Concrete Slabs and Footings Under Concentrated Loads."
- Mori, A. W., and Crouse, C. B. (1981). "Strong Motion Data from Japanese Earthquakes." SE-29, National Geophysical Data Center, Boulder, Colorado.
- Morrison, D. G., Hirasawa, I., and Sozen, M. A. (1983). "Lateral-Load Tests of R/C Slab-Column Connections." *Journal of Structural Engineering*, 109(11), 2698-2714.
- Newmark, N. M. (1959). "Method of Computation for Structural Dynamics." *ASCE -- Proceedings -- Journal of the Engineering Mechanics Division*, 85(EM3, Part 1), 67-94.
- Pan, A., and Moehle, J. P. (1989). "Lateral Displacement Ductility of Reinforced Concrete Flat Plates." *ACI Structural Journal (American Concrete Institute)*, 86(3), 250-258.

- Pan, A. D., and Moehle, J. P. (1992). "Experimental Study of Slab-Column Connections." *ACI Structural Journal (American Concrete Institute)*, 89(6), 626-638.
- Rayleigh, J. W. S. (1945). *Theory of Sound*, Dover, New York.
- Robertson, I., and Durrani, A. J. (1990). "Seismic Response of Connections in Indeterminate Flat-Slab Subassemblies." 41, Rice University, Houston, TX.
- Robertson, I., and Johnson, G. (2006). "Cyclic Lateral Loading of Nonductile Slab-Column Connections." *ACI Structural Journal*, 103(3), 356-364.
- Robertson, I. N., Kawai, T., Lee, J., and Enomoto, B. (2002). "Cyclic Testing of Slab-Column Connections with Shear Reinforcement." *ACI Structural Journal*, 99(5), 605-613.
- Saragoni, R., Gonzalez, P., and Fresard, M. (1985). "Análisis de los Acelerogramas del Terremoto." *Publicacion SES-1-4/1985(199)*, Universidad de Chile.
- Schultz, A. E. (1992). "Approximating Lateral Stiffness of Stories in Elastic Frames." *Journal of Structural Engineering*, 118(1).
- Symonds, D. W., Mitchell, D., and Hawkins, N. M. (1976). "Slab-Column Connections Subjected to High Intensity Shears and Transferring Reversed Moments." *Progress Report on NSF Project GI-38717*, University of Washington, Seattle, WA.
- Tasker, H. E. (1963). "Shear in Flat-Plate Construction Under Uniform Loading." Australian Commonwealth Experimental Building Station, Sydney, Australia.
- Wey, E. H., and Durrani, A. J. (1992). "Seismic Response of Interior Slab-Column Connections with Shear Capitals." *ACI Structural Journal (American Concrete Institute)*, 89(6), 682-691.
- Whitney, C. S. (1937). "Design of Reinforced Concrete Members Under Flexure or Combined Flexure and Direct Compression." *American Concrete Institute -- Journal*, 8(4), 483-498.
- Zaghlool, E. E. R. (1973). "Strength Analysis of Corner Column-Slab Connections." *Journal of the Structural Division, Proceedings of the American Society of Civil Engineers*, 99(No. ST1), 53-70.

Zee, H. L., and Moehle, J. P. (1984). "Behavior of Interior and Exterior Flat Plate connections Subjected to Inelastic Load Reversals." *Earthquake Engineering Research Center No.UCB/EERC-84/07*, University of California, Berkeley, CA.

APPENDIX

Appendix A. Experimental Program

A.1. Introduction

Appendix A contains information about the materials, design, construction, and instrumentation of the full-scale three-story flat-plate reinforced concrete test specimen. Information about the loading frame and testing sequence is also included.

A.2. Materials

A.2.1. Concrete

Three different concrete mixture designs were provided by Irving Materials, Inc. of West Lafayette, IN for the construction of the test specimen. The mixture proportions and their placement locations are listed in Table A.1

Table A.1 Concrete Mix Designs

Concrete cylinders were cast on the days of concrete placement. The 6 in. x 12 in. cylinders were capped with neoprene pads and tested with a Forney F-60C-DFM/I Compression Testing Machine with a loading rate of 1 kip/sec. Compression tests were conducted 28 days after casting and during lateral-load testing. Measured strengths are reported in Table A.2 and Table A.3. A plot of the cylinder strength data vs. age is shown in Figure A-1.

A.2.2. Steel

Three different ASTM A615 reinforcing bar sizes were used in the construction of the flat-plate structure. Sizes were No. 3 bars (3/8 in. nominal diameter) for the

column ties, No. 4 bars (1/2 in. nominal diameter) for all slab reinforcement, and No. 7 bars (7/8 in. nominal diameter) for all column longitudinal steel.

Tensile tests were performed on a representative sample of the bottom and top reinforcement and the column longitudinal bars. An MTS Series 311 220-kip load frame with an MTS 445 Servo Controller was used to apply axial tension on the bars at a rate of .014 in. /sec. Elongations were measured with an MTS 634.25 Axial Extensometer with a 2 in. gage length. Results of the tensile tests are summarized in Table A.4 and the stress-strain plots are shown in Figure A.2 through Figure A-4.

A.3. Design

A gravity design was performed for the flat-plate structure using the ACI Building Code (ACI 318-2002). In addition to the self weight, a superimposed dead load of 5 psf and live load of 40 psf were used. These loads meet the requirements of the International Building Code (International Code Council. et al. 2000) for residential-building occupancy. A 7-in. slab was chosen based on the minimum slab thicknesses shown in Table 9.5(c) of the 2002 ACI Building Code. The slab reinforcement was determined using the Direct Design Method for 10-ft column and middle strips. For the negative moment column strip, 18 - No. 4 bars were selected and resulted in a reinforcement ratio of 0.5%. Nine No. 4 bars (0.25%) were selected for the negative and positive moment regions of the middle strip and the positive moment region of the column strip. The resulting slab reinforcement is shown in Figure A-5 and Figure A-6. Nominal depths of the slab reinforcement are shown in Figure A-7, which were spot-checked during construction. Shear stresses were checked and found to be adequate for one-way and two-way action under gravity loading.

The primary intent of the research program was to investigate slab behavior and therefore the desired failure mechanism is one in which the slab reinforcement yields on all levels and the columns yield only at their connections to the footings. This structural mechanism is shown in Figure A-8 where the solid circles indicate the assumed plastic hinge locations. The columns were proportioned so this failure mode occurs at the smallest base shear value in comparison to mechanisms that include column yielding at the upper stories.

For the limit-state analysis the lateral-load distribution shown in Figure A-9 was assumed. The slab and column capacities were based on 4000-psi concrete and reinforcement yield strength of 70-ksi. To determine the negative and positive moments, the 10-ft column strips were used. The column capacities were calculated including the axial load due to the structure self weight and a test load of 15 psf.

The results of this analysis suggested a column size of 18 x 18 in. with a reinforcement ratio of 1.5 % would result in the structural mechanism. Figure A-10 shows the arrangement of the No. 7 longitudinal reinforcement and No. 3 ties in the columns. The column section corners were chamfered 3/4-in.

A.4. Construction

Construction of the flat-plate specimen began on November 15, 2004. The first two days involved forming the footings, placing the reinforcement, and casting the concrete. Figure A-11 is a photo of the footing reinforcement. Placing the column cages over the dowels and building the column forms typically took two days. Figure A-12 is a photo showing the installed column cages and forms. After the columns were cast, shoring for the slab was erected and reinforcement was placed. The process lasted one week. Level-one shoring and slab reinforcement are shown in Figure A-13 and Figure A-14. The slab was cast using two laboratory cranes to lift concrete buckets to the elevation of the slab.

The concrete was consolidated with several hand-held vibrators and screeded by hand to the correct elevation. A laser level was installed on the laboratory catwalk and provided a reference to the correct elevation. After the concrete was screeded, a bull-float was used to level the surface. Finishing operations began after the bleed water was absorbed back into the concrete and the surface had set sufficiently to sustain very small depressions under foot traffic. Hand trowels were used along the edges and a mechanical finisher was used on the interior of the slab. The methods of placing and finishing the concrete are shown in Figure A-15 and Figure A-16. A curing compound was applied to the surface of the concrete after finishing.

The sequence of construction events described was repeated for levels 2 and 3 of the structure. The final slab was cast on December 14 and forms were removed the week of December 27. Construction was completed December 30, 2004. Table A.5 is a timeline of the construction events and a completed photograph of the flat-plate structure is shown in Figure A-17.

A.5. Instrumentation

Instrumentation used to measure displacements during the static loading cycles of the flat-plate structure included optical encoders and Linear Variable Differential Transformers (LVDT). One of the encoders was damaged before testing and was replaced by a UniMeasure PA-25-DS string potentiometer. Concrete surface strains were measured with an electronic Whittemore gage and vertical slab displacements were measured with a surveying level. Crack-width measurements were made with a crack comparator. The accuracy and precision of the Instrumentation are shown in Table A.6. The survey accuracy and precision values account for instrument error and rod precision. Electronic Whittemore accuracy and precision is based on the LVDT and measurement variations due to noise and recording consistency.

A.5.1. Encoders

The primary displacement measuring devices on the flat-plate structure are UniMeasure's HX-EP-50-H5 incremental encoders. They are well suited for full-scale testing applications because of their accuracy over large measurement ranges. Due to the long lengths of cables (up to 75 ft) the encoders were calibrated with their final cables connected to the data-acquisition system used for the test. Calibration constants provided by the manufacturer were found to be within 0.01 in. of an LVDT calibration device that was used to extend and release the wire ropes of the encoders. Labels and locations of the encoders are shown in Figure A-18 through Figure A-22. Details of the diagonal encoder connections to the upper and lower columns are shown in Figure A-23 and Figure A-24. Photographs of the lateral and diagonal encoders are shown in Figure A-25 and Figure A-26

A.5.2. LVDT Measurements

Schaevitz DC operated LVDTs were used to measure column rotations, load frame connection displacements, and sliding movement of the footings. All devices were calibrated with final cable lengths and data acquisition using an Instron Extensometer Calibrator with a measurement stroke of one in. and a precision of .0001 in. LVDT models used for column rotation and load frame connections were DC-E-500 (1 in. full scale span). Sliding of the footing was measured using model DC-E-250 (0.5 in. full span). Labels and locations of the LVDTs are shown in Figure A-18 through Figure A-22. Details of the LVDT attachments are shown in Figure A-27 through Figure A-29 and photographs are shown in Figure A-30 through Figure A-32.

A.5.3. Concrete Surface Strains

Concrete surface strains were measured in both the transverse and longitudinal direction of the slab. Longitudinal strains were measured on four sides of all first-

story columns near the base. Two electronic Whittemore gages, modeled after the original mechanical Whittemore strain gage (Matamoros 1999) were used for the strain measurements. The electronic Whittemore consists of a Schaevitz DC-E-250 LVDT mounted inside an aluminum tube. The LVDT housing is fixed to one end of the tube and the core is mounted to a low friction sliding table. Outside the aluminum tube are two tapered drill-rod pins spaced at 5 in. One of these pins is attached to the sliding table to which the core is connected. Measurements are made when the pins are inserted into steel disks (3/16" thick, 1/2 in. diameter) with holes in the center that are epoxy glued to the surface of the concrete. The distance between measurement points was approximately 5 in. for the slab and 11-1/4 in. for the column. The LVDTs inside the gages were calibrated using the same method described above. The locations of slab surface strain measurements are shown in Figure A-33 and Figure A-34. The measurement locations on each side of the level one columns are shown in Figure A-35. Photographs of the electronic Whittemore gages are shown in Figure A-36 and Figure A-37.

A.5.4. Actuator Load and Displacement

Load cells attached to the Shore Western actuators were used to record the load applied to the flat-plate structure. The Interface load cells (model 123ACK-100K-B) were shunt calibrated with the actual cables and electronics of the controller.

Displacements from the actuators were used internally by the control program during the test. All lateral displacements of the flat-plate structure were recorded by the encoders.

A.5.5. Data Acquisition

Voltage signals were conditioned and recorded with Vishay-Measurements Group Model 5100 scanners and SCXI modules from National Instruments. The

digital signal of the encoders was recorded with a National Instruments PCI counting board. All instruments were recorded at a rate of 2 samples per second.

A.6. Load Frames

Steel load frames were used to transfer the load from the hydraulic actuators to the concrete slabs at each level of the flat-plate test specimen. The connections to the slab were designed and detailed to minimize interaction between rotation of the slab and bending of the load frame. A wide flange shape (W8x48) oriented about its weak axis and connected at the mid span of the slab was selected to minimize this interaction.

The connection consists of two steel channels fastened with threaded rods through the slab and high strength bolts to the load frame (Figure A-38). To prevent the rotation of the slab from transferring bending moment to the load frames a 1/2 in. space was left between the flanges and channel. Without this load path, moment transfer could only occur between the bolts and the web. Because the web thickness is small (1/2 in.) and a bearing-only connection exists between the bolts and the web, it is believed minimal bending moment was transferred to the steel load frame. Details of the load frame and connection to the slab are shown in Figure A-39.

A.7. Test Sequence

Testing of the flat-plate specimen began by measuring initial concrete strains, slab deflections with the survey level, marking cracks, and photo documentation. Due to time constraints, only one half of a loading cycle was completed each day. Because the first cycle of loading was used primarily to check functionality of the equipment and new crack formation was minimal, cracks were not mapped or measured. Measurements for cycle two were made at the north and south

peak displacements. Intermediate measurements for cycles 3 and 4 in addition to the peak displacements were made. The hydraulic pressure was turned off from the actuators and the controller and data acquisition was stopped at the end of each half cycle test. Table 3-1 is a summary of the dates each test was performed and the measurements recorded.

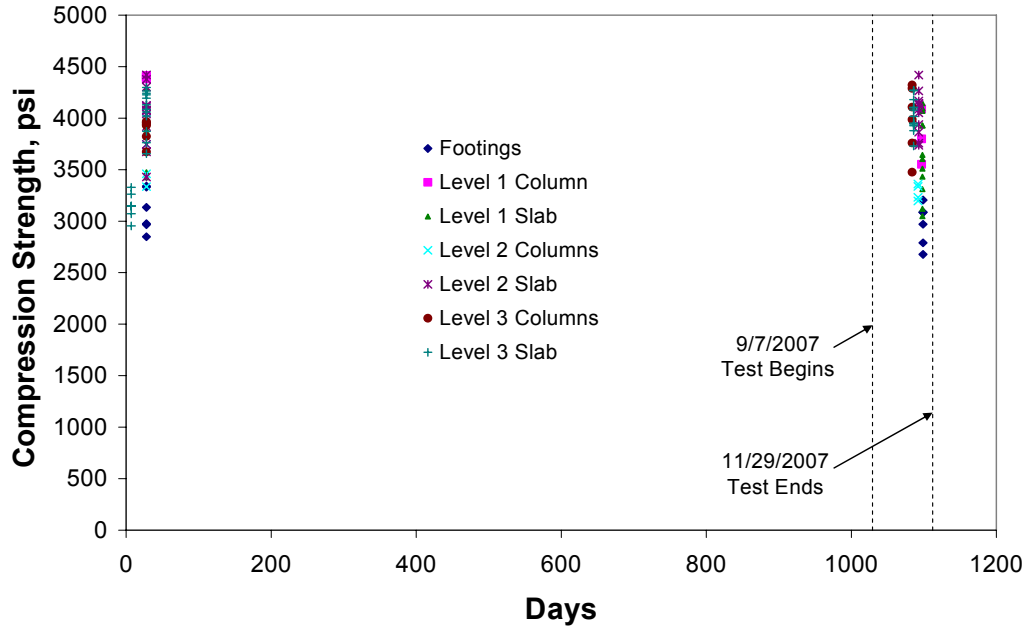


Figure A-1 Concrete Cylinder Strength Data.

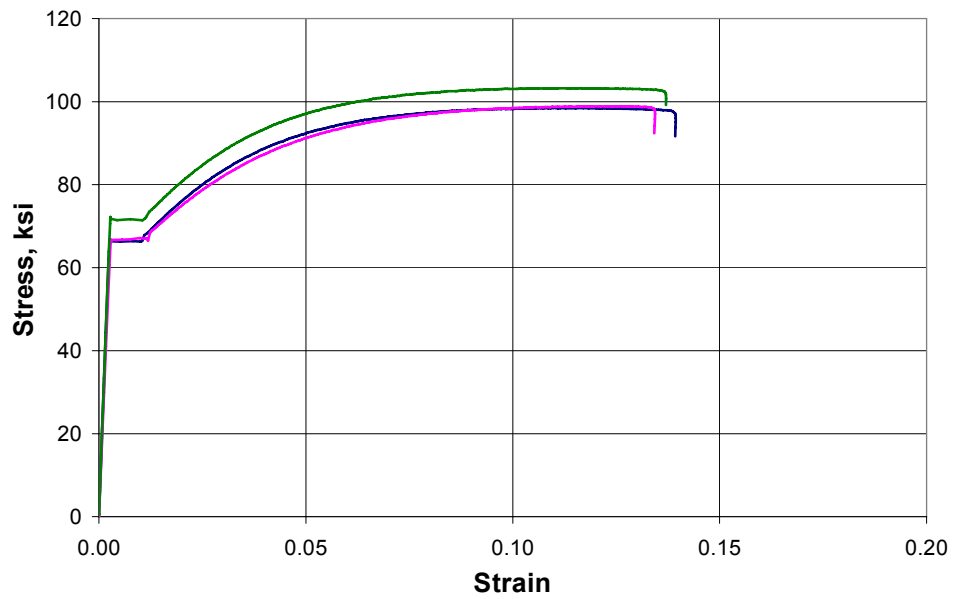


Figure A.2 Stress Strain Plot, No. 4. Bottom Reinforcing Bars.

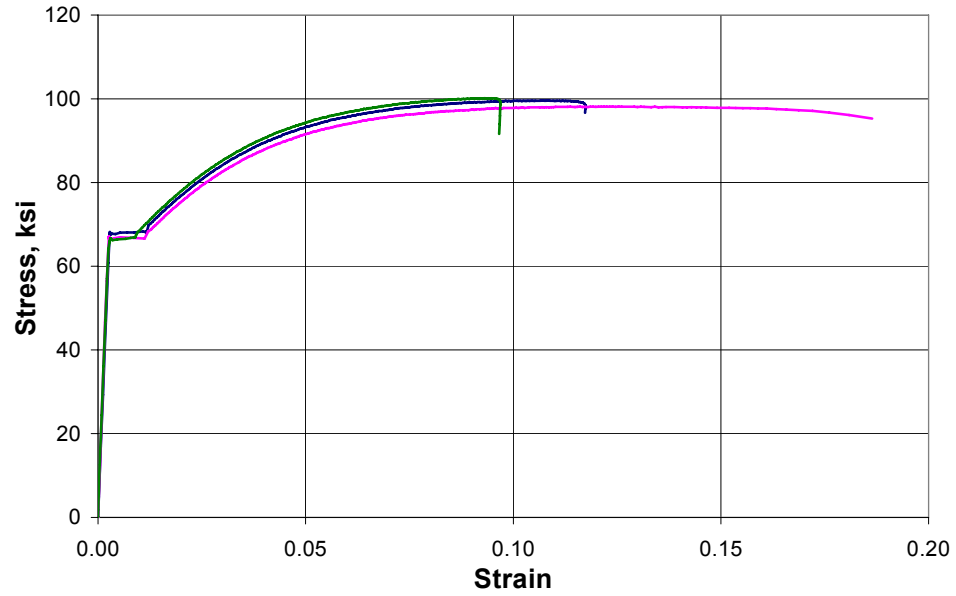


Figure A-3 Stress Strain Plot, No. 4 Top Reinforcing Bars

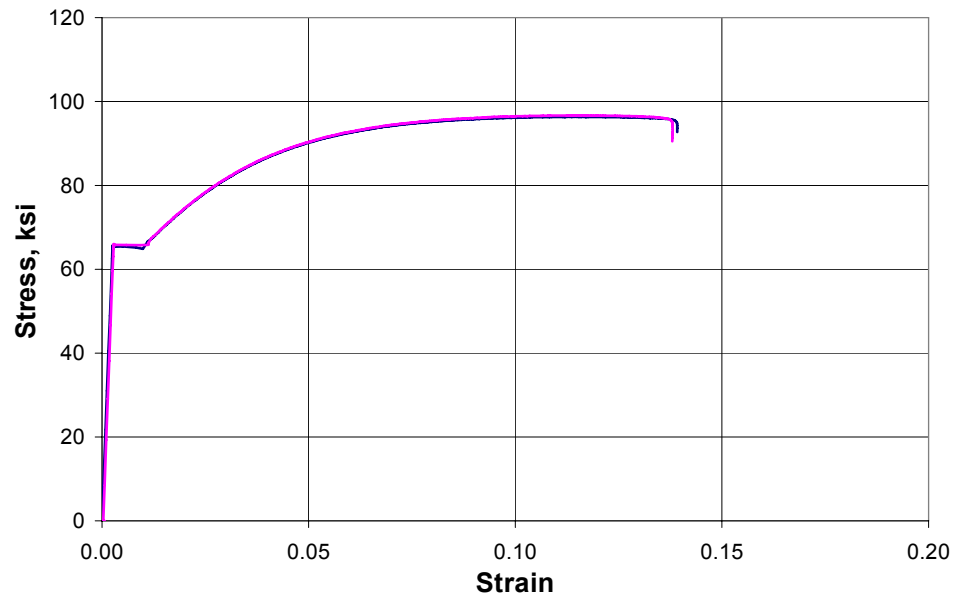
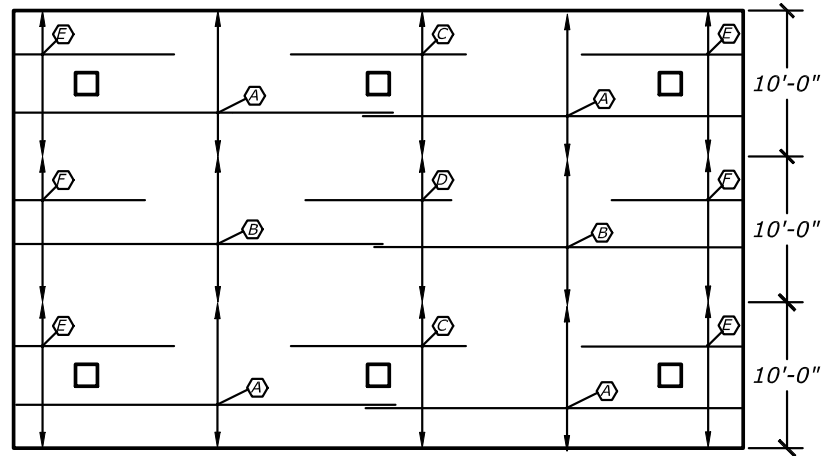
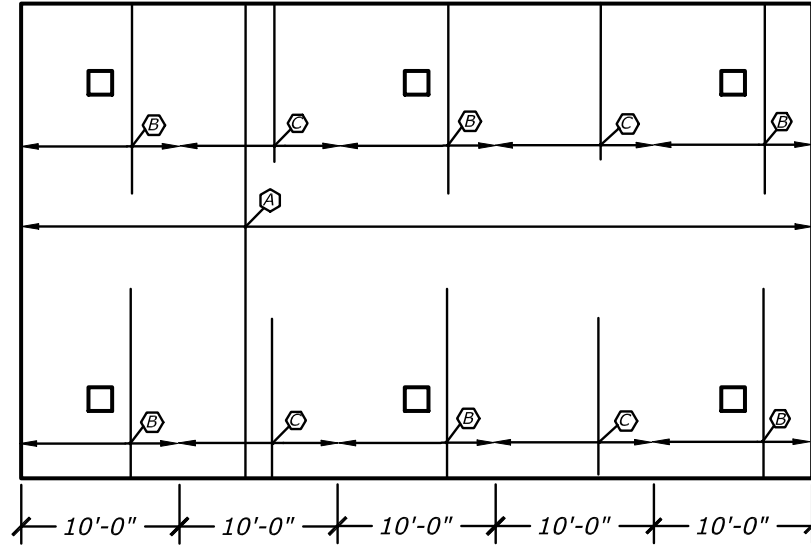


Figure A-4 Stress Strain Plot, No. 7 Column Longitudinal Bars



| MARK | REINFORCEMENT |
|------|----------------------|
| | 9-#4 x 26'-0" BOTTOM |
| | 9-#4 x 26'-0" BOTTOM |
| | 18-#4 x 13'-0" TOP |
| | 9-#4 x 10'-0" TOP |
| | 18-#4 x 12'-0" TOP |
| | 9-#4 x 10'-0" TOP |

Figure A-5 Longitudinal Reinforcement



| MARK | REINFORCEMENT |
|------|-----------------------|
| (A) | 45-#4 x 29'-8" BOTTOM |
| (B) | 18-#4 x 12'-0" TOP |
| (C) | 9-#4 x 10'-0" TOP |

Figure A-6 Transverse Reinforcement

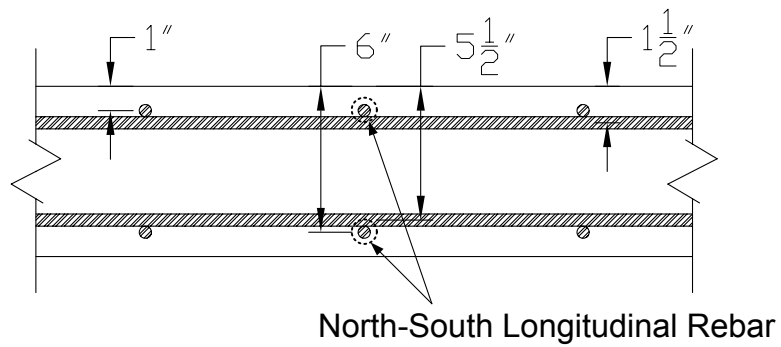


Figure A-7 Reinforcement Depths

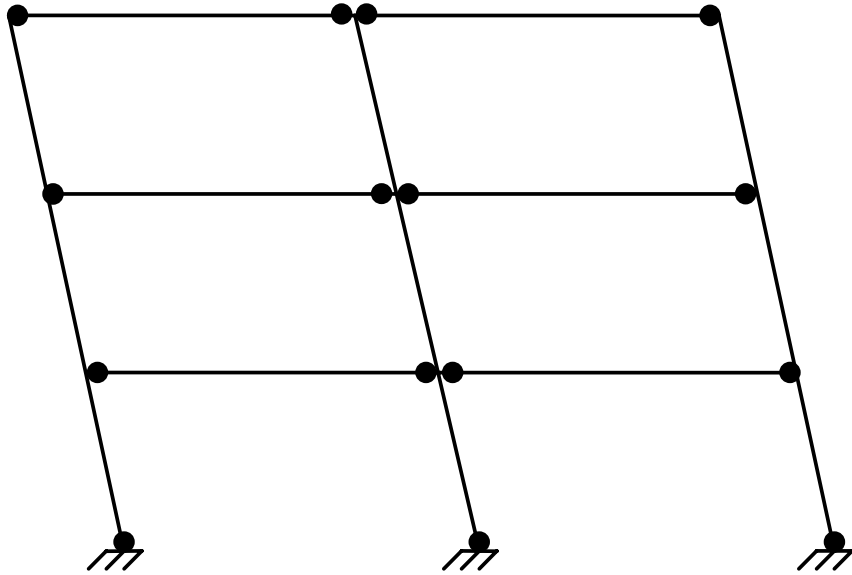


Figure A-8 Structural Mechanism

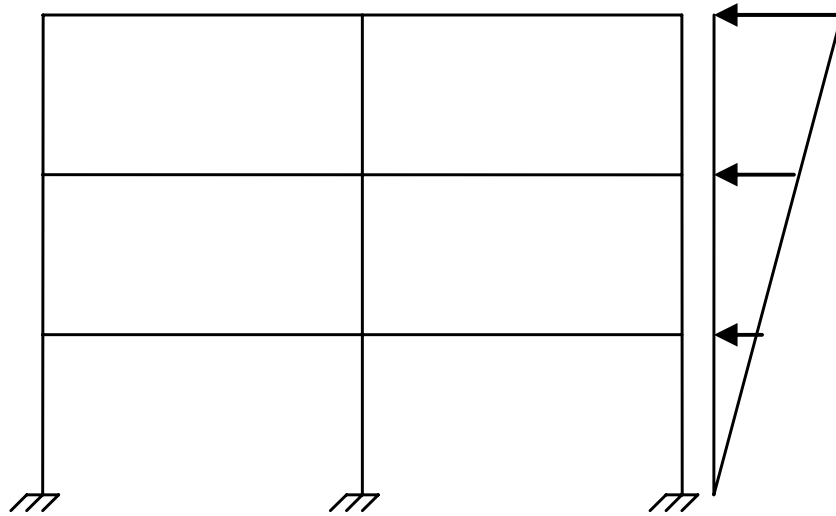


Figure A-9 Loading Distribution

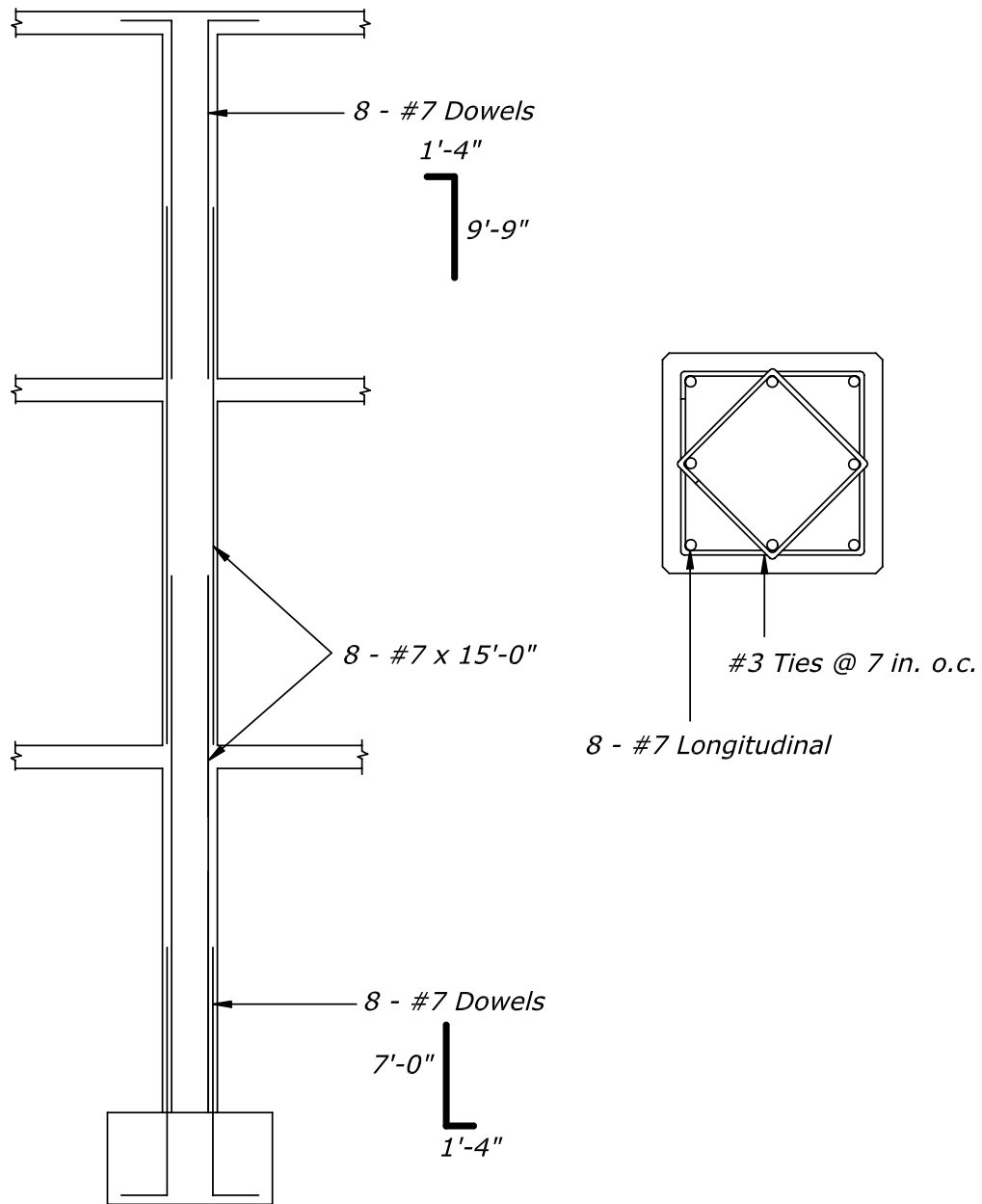


Figure A-10 Column Reinforcement



Figure A-11 Footing Reinforcement



Figure A-12 Level 1 Column Cage and Forms



Figure A-13 Level 1 Slab Shoring



Figure A-14 Slab Reinforcement



Figure A-15 Concrete Placement



Figure A-16 Concrete Finishing



Figure A-17 Completed Specimen

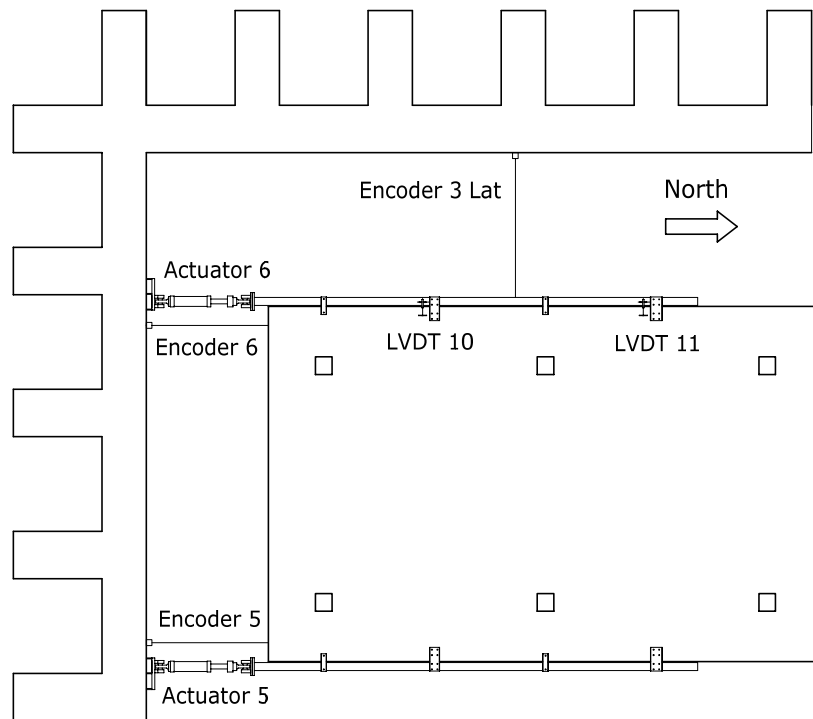


Figure A-18 Roof Instrumentation Plan

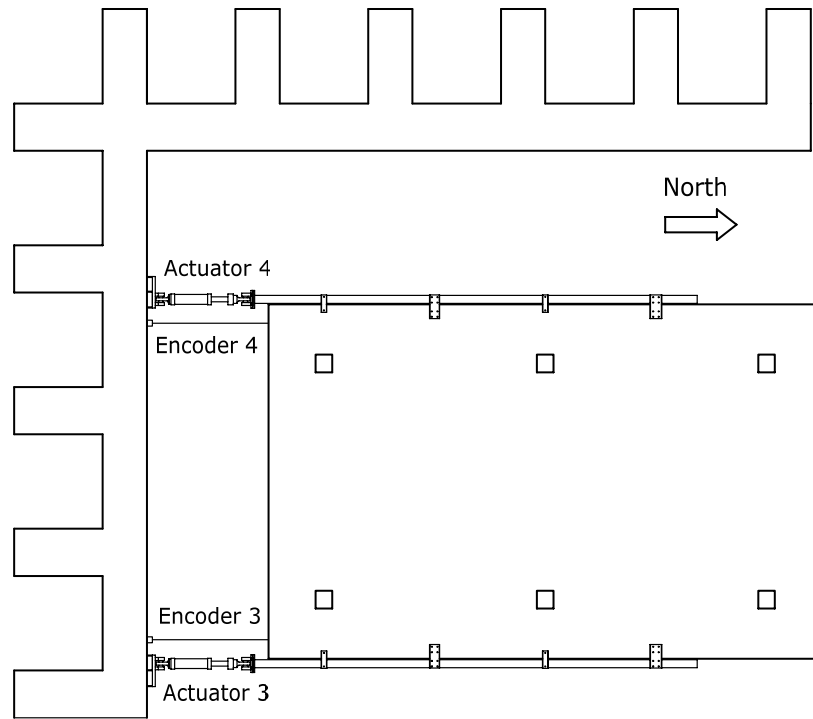


Figure A-19 Level 3 Instrumentation Plan

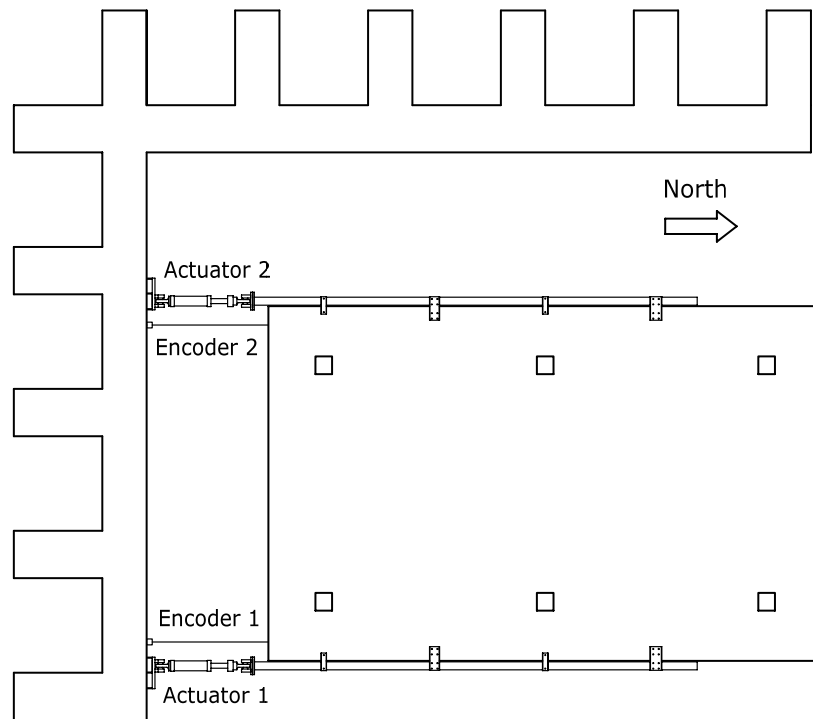


Figure A-20 Level 2 Instrumentation Plan

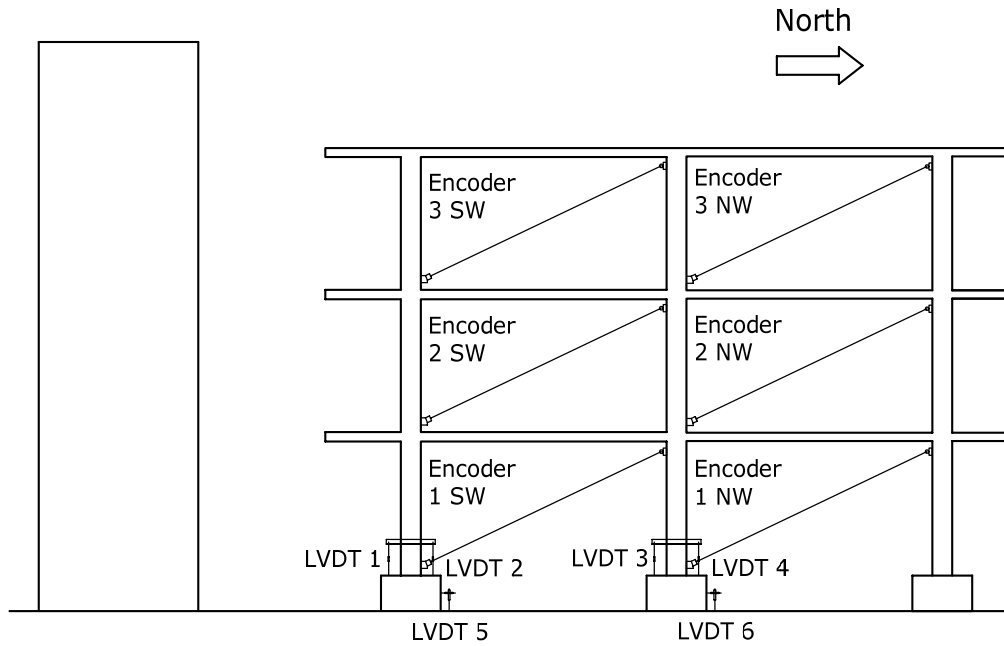


Figure A-21 Frame A Instrumentation Elevation

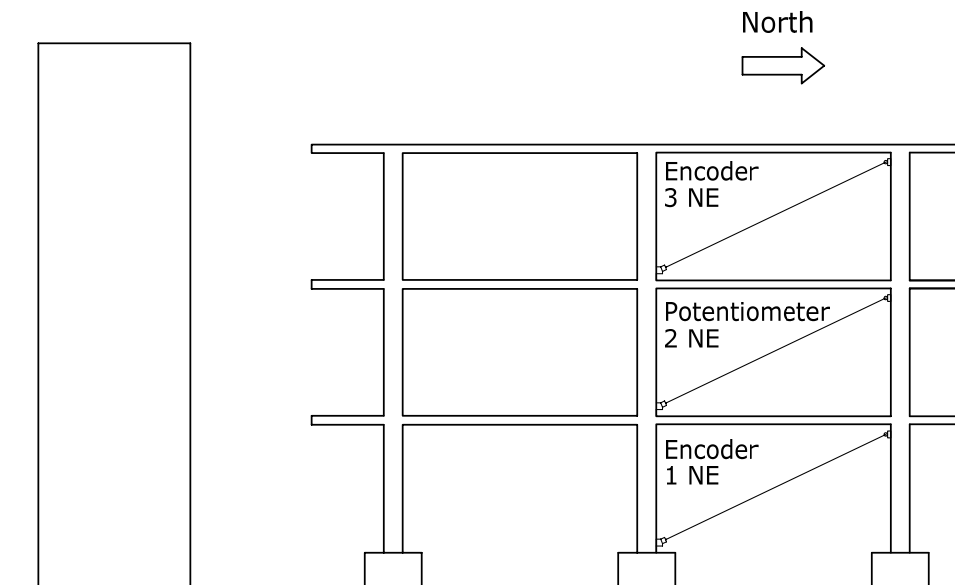


Figure A-22 Frame B Instrumentation Elevation

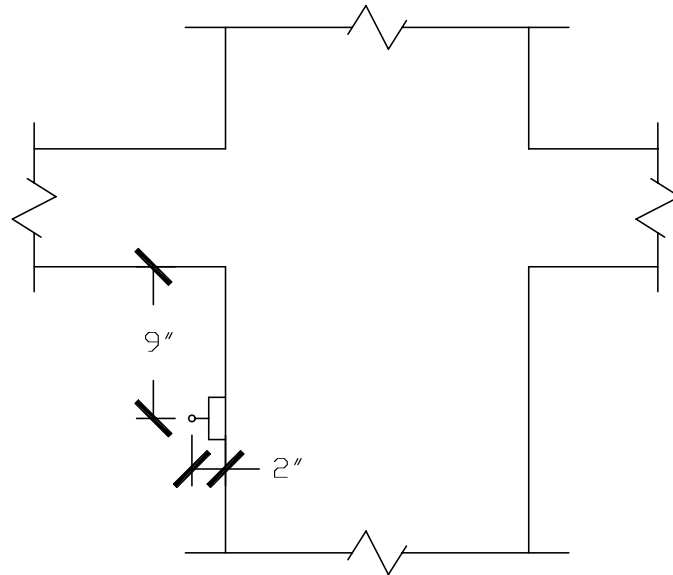


Figure A-23 Upper Diagonal Encoder String Connection

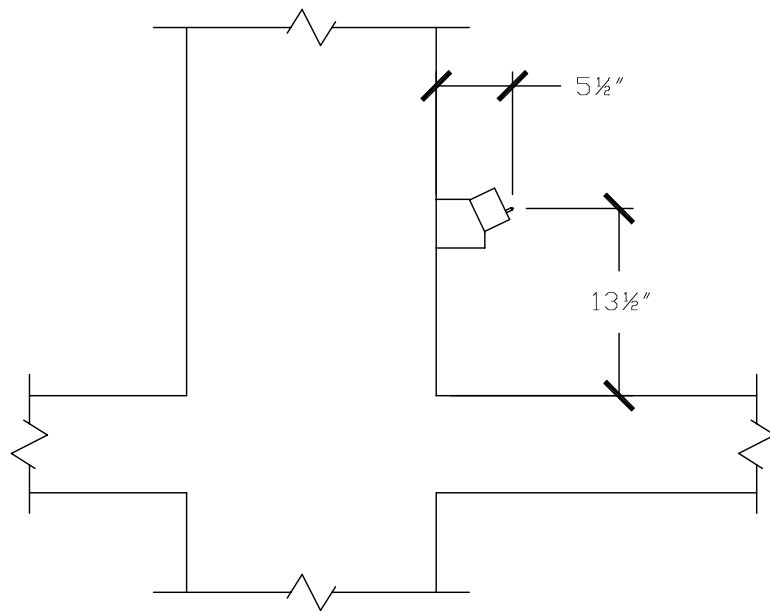


Figure A-24 Lower Diagonal Encoder Connection

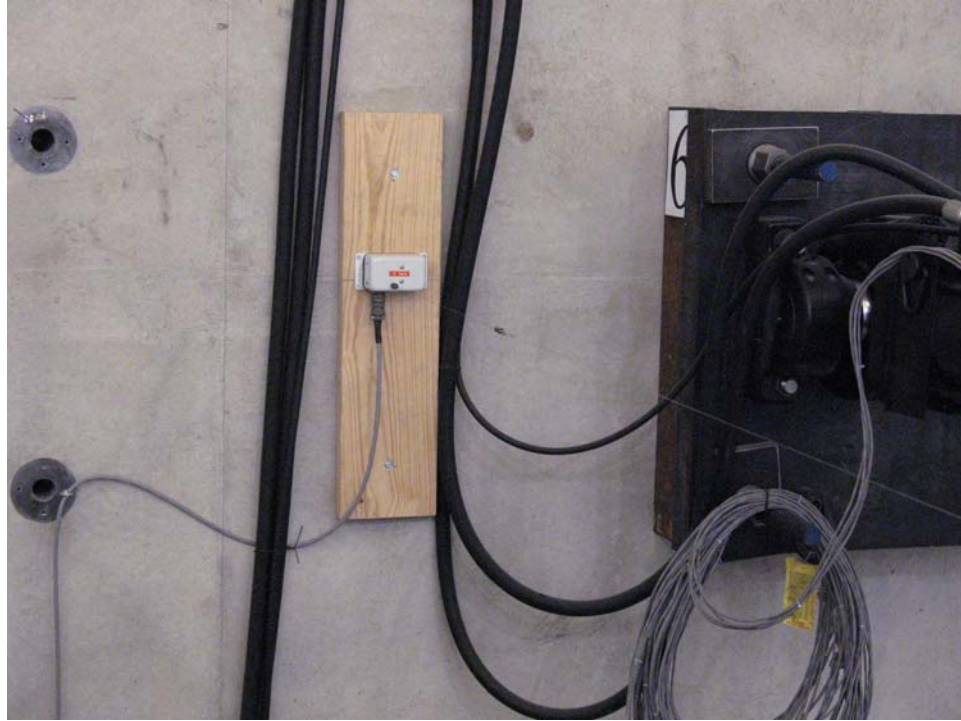


Figure A-25 Lateral Displacement Encoder



Figure A-26 Diagonal Displacement Encoder

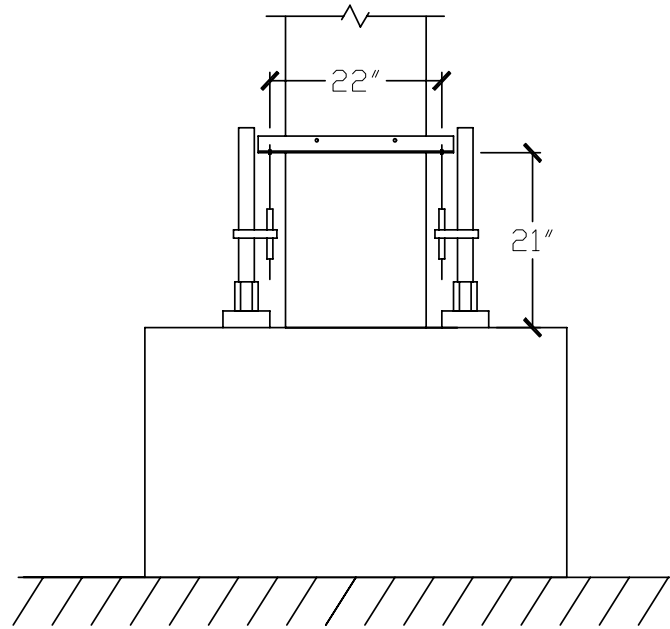


Figure A-27 Column Rotation LVDTs

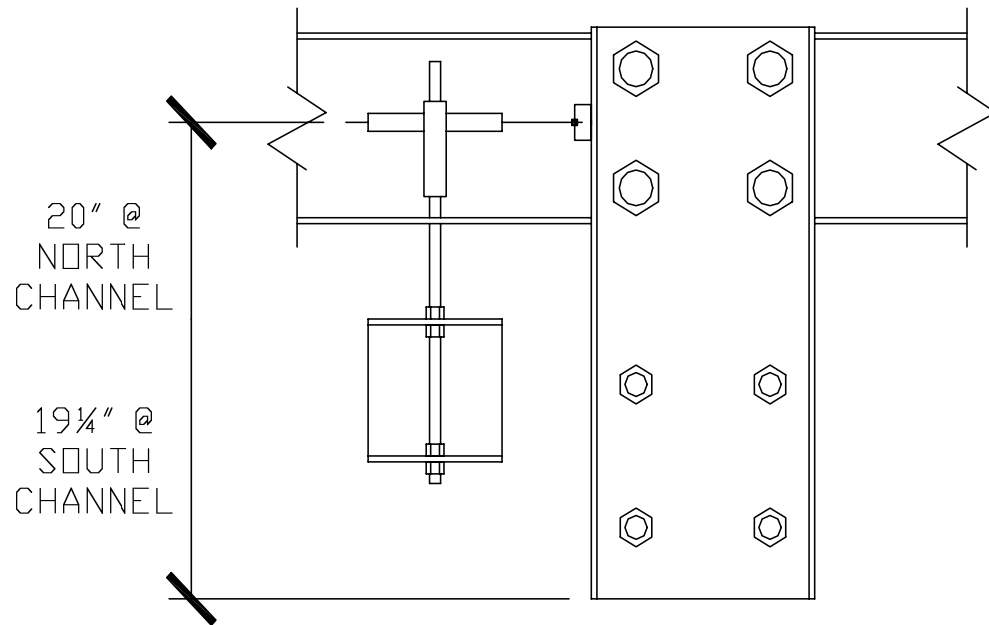


Figure A-28 Load Frame Channel-Slab Connection LVDT

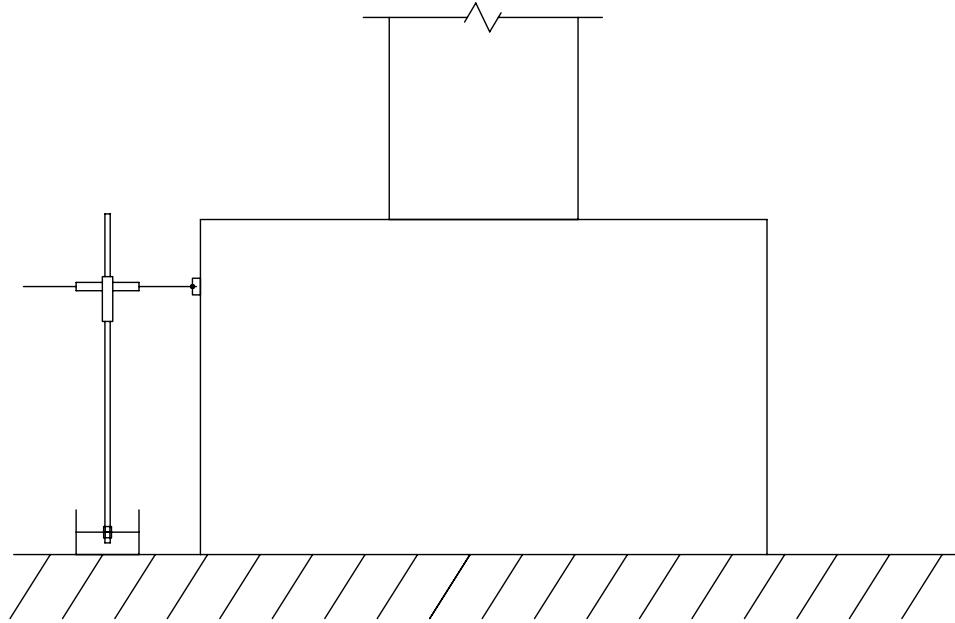


Figure A-29 Footing Movement LVDT



Figure A-30 Column Rotation LVDT



Figure A-31 Footing Movement LVDT

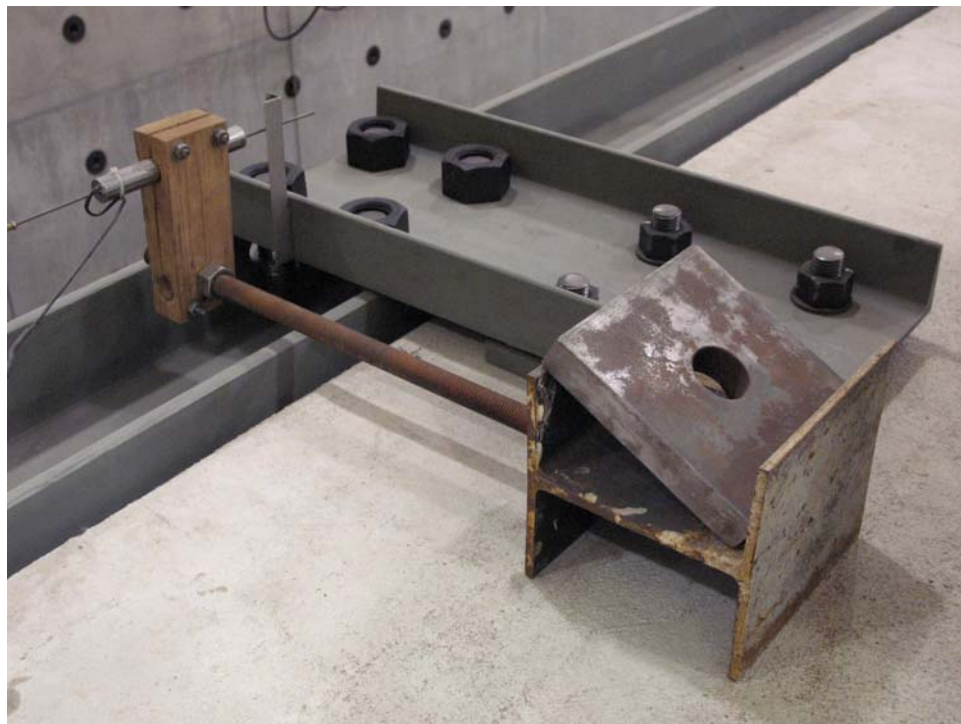


Figure A-32 Load Frame Channel-Slab Connection LVDT Photo

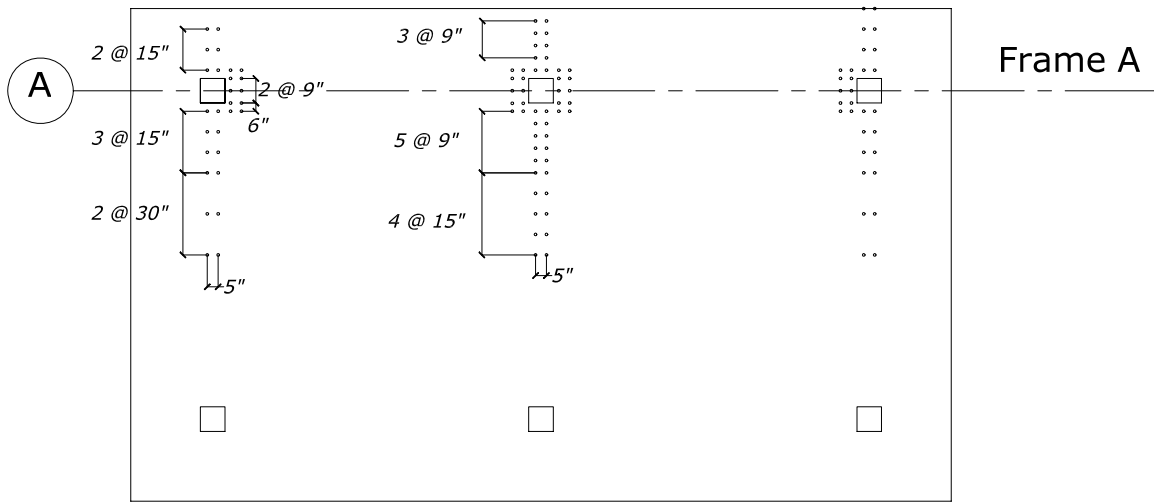


Figure A-33 Longitudinal Concrete Surface Strain Measurements

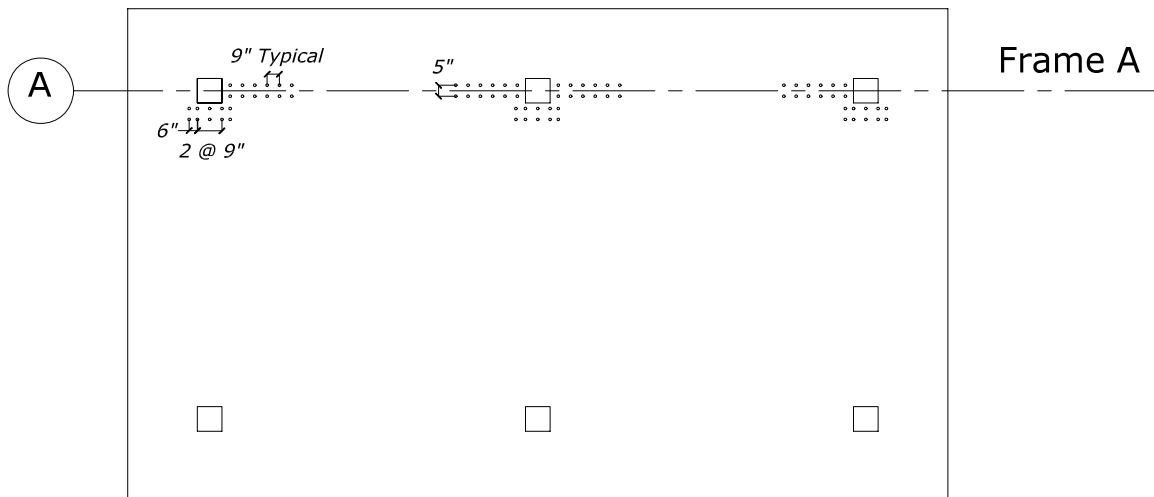


Figure A-34 Transverse Concrete Surface Strain Measurements

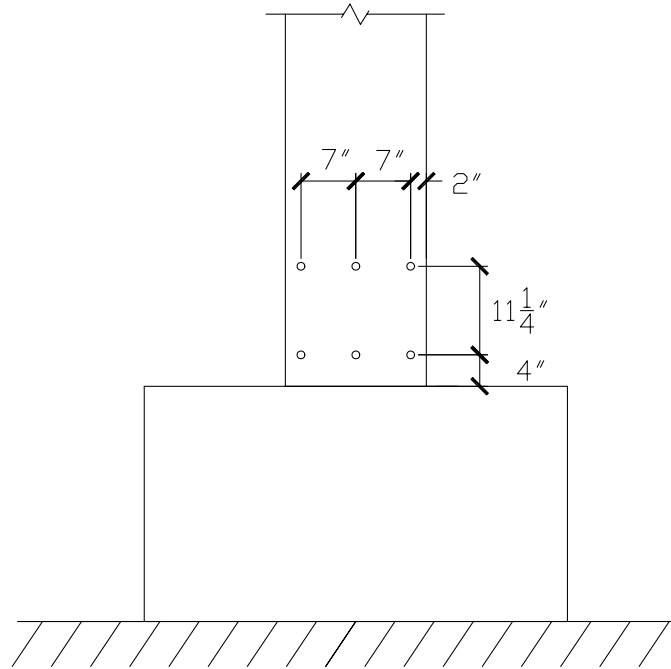


Figure A-35 Column Surface Strain Measurements



Figure A-36 Electronic Whittemore Gage



Figure A-37 Electronic Whittemore Measurement

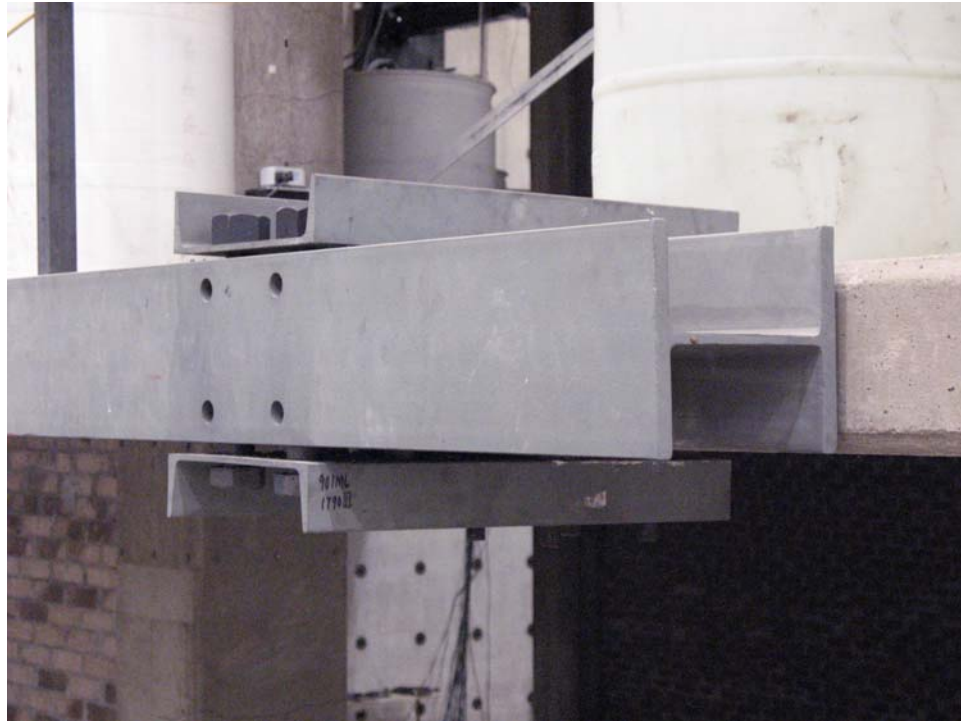


Figure A-38 Load Frame Connection

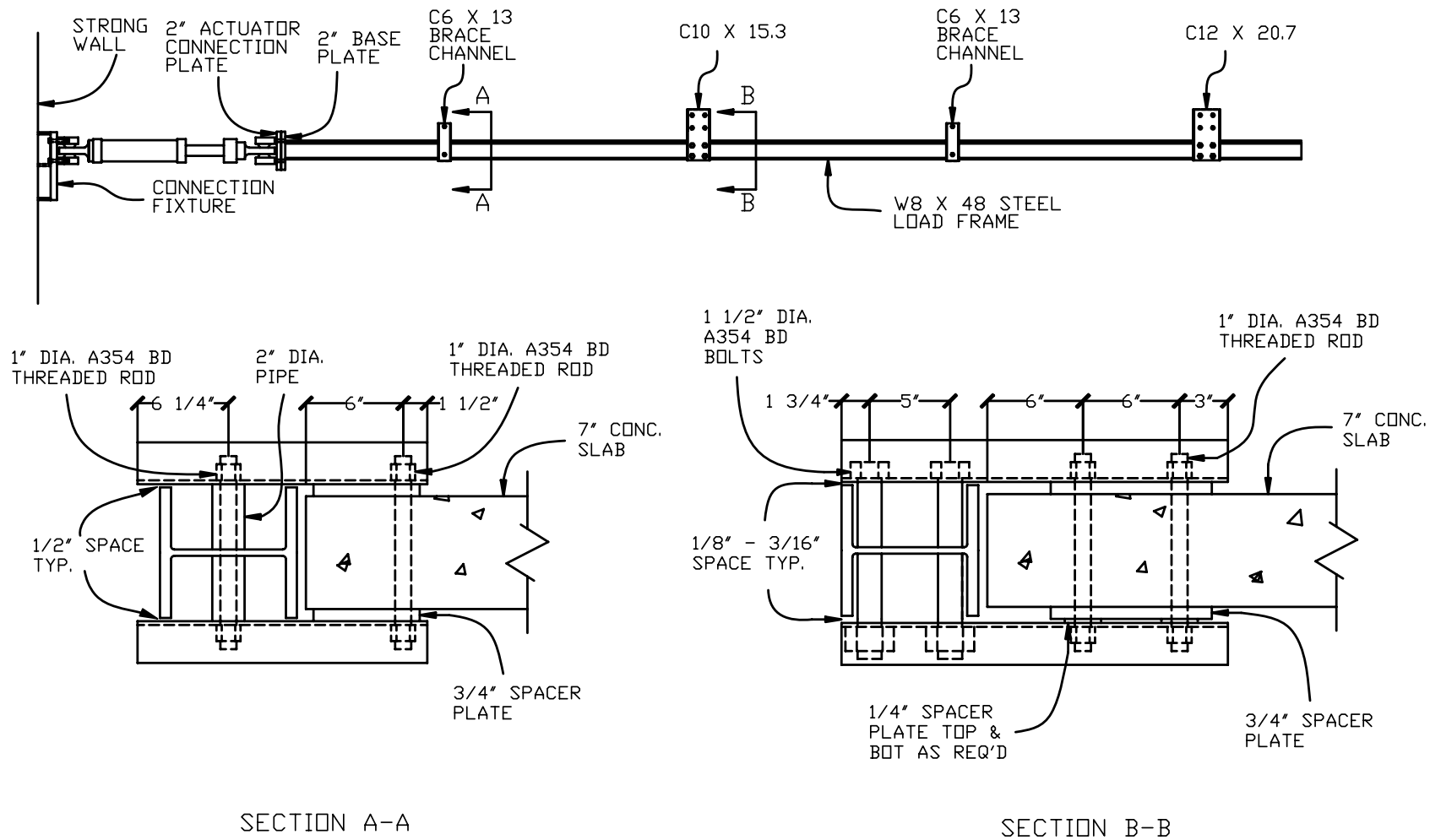


Figure A-39 Load Frame Connection Details

Table A.1 Concrete Mix Designs

| | Footings | Level 1 Columns | Level 2 & 3 Columns, Slabs |
|------------------|-----------------|----------------------------|---|
| Nominal Strength | 3000 psi | 4000 psi | 3500 psi |
| Cement | 423 lb | 517 lb | 470 lb |
| Sand | 1560 lb | 1485 lb | 1523 lb |
| Gravel | 1850 lbs | 1850 lb | 1850 lb |
| Water | 203 lb | 232 lb | 211 lb |
| Mid Range W/R | 17 oz/yd | 17 oz/ yd | 19 oz/ yd |
| W/C Ratio | 0.48 | 0.45 | 0.45 |
| Slump | 4 - 6 in. | 4 - 6 in. | 4 - 6 in. |

Table A.2 Concrete Cylinder 28-Day Strengths

| Level | Truck 1 | Truck 2 | Truck 3 | Truck 4 | Mean |
|-----------------------|---------|---------|---------|---------|-------------|
| Roof Slab | 4270 | 3870 | 4130 | 4230 | 4070 |
| | 3660 | 4190 | 4080 | 4240 | |
| | 3760 | 4060 | 4300 | 4020 | |
| Mean | 3900 | 4040 | 4170 | 4160 | |
| Level 3 Column | 3820 | 3970 | | | 3880 |
| | 3670 | 3940 | | | |
| | 3950 | 3930 | | | |
| Mean | 3810 | 3950 | | | |
| Level 3 Slab | 3430 | 4420 | 4040 | 4380 | 4030 |
| | 3670 | 4110 | 4080 | 3920 | |
| | 3750 | 4070 | 4130 | 4300 | |
| Mean | 3620 | 4200 | 4080 | 4200 | |
| Level 2 Column | 3750 | 3460 | | | 3640 |
| | 4000 | 3340 | | | |
| | | | | | |
| Mean | 3880 | 3400 | | | |
| Level 2 Slab | 4110 | 3990 | 3930 | 3450 | 3920 |
| | 3890 | 4120 | 3950 | 3940 | |
| | 3820 | 4290 | 4120 | 3430 | |
| Mean | 3940 | 4130 | 4000 | 3610 | |
| Level 1 Column | 4410 | | | | 4400 |
| | 4400 | | | | |
| | 4380 | | | | |
| Mean | 4400 | | | | |
| Footing | 3340 | 2970 | | | 3100 |
| | 3330 | 2850 | | | |
| | 3130 | 2980 | | | |
| Mean | 3270 | 2930 | | | |

Table A.3 Concrete Cylinder Test Strengths, psi

| Level | Testing Concrete Cylinder Strength (psi) | | | | Mean |
|-----------------------|--|---------|---------|---------|-------------|
| | Truck 1 | Truck 2 | Truck 3 | Truck 4 | |
| Roof Slab | 4180 | 4080 | 4270 | 4270 | 4040 |
| | 3940 | 3930 | 3880 | 3950 | |
| | 4020 | 4110 | 3730 | 4100 | |
| Mean | 4050 | 4040 | 3960 | 4110 | |
| Level 3 Column | 3480 | 4290 | | | 3990 |
| | 3760 | 4110 | | | |
| | 3990 | 4320 | | | |
| Mean | 3740 | 4240 | | | |
| Level 3 Slab | 3760 | 4130 | 3940 | 4420 | 4060 |
| | 3860 | 4140 | 4050 | 4090 | |
| | 3740 | 4260 | 4140 | 4170 | |
| Mean | 3790 | 4180 | 4040 | 4230 | |
| Level 2 Column | 3200 | 3230 | | | 3290 |
| | 3340 | 3360 | | | |
| | | | | | |
| Mean | 3270 | 3300 | | | |
| Level 2 Slab | 4070 | 3930 | 3600 | 3120 | 3650 |
| | 3430 | 4090 | 3640 | 3310 | |
| | 4150 | 3930 | 3500 | 3050 | |
| Mean | 3880 | 3980 | 3580 | 3160 | |
| Level 1 Column | 3550 | | | | 3810 |
| | 4090 | | | | |
| | 3800 | | | | |
| Mean | 3810 | | | | |
| Footing | 3090 | 2790 | | | 2970 |
| | 3090 | 2670 | | | |
| | 3210 | 2970 | | | |
| Mean | 3130 | 2810 | | | |

Table A.4 Reinforcement Tensile Tests, ksi

| | Fy | Fu |
|---------------------|-----------|------------|
| #4 Bot. Slab | 66 | 99 |
| | 67 | 99 |
| | 72 | 103 |
| Mean | 68 | 100 |
| #4 Top Slab | 68 | 100 |
| | 67 | 98 |
| | 66 | 100 |
| Mean | 67 | 99 |
| #7 Column | 65 | 96 |
| | 66 | 97 |
| Mean | 66 | 97 |

Table A.5 Concrete Placement Dates

| | |
|------------------------|-------------------|
| Footings | November 16, 2004 |
| Level 1 Columns | November 18, 2004 |
| Level 2 Slab | November 24, 2004 |
| Level 2 Columns | November 30, 2004 |
| Level 3 Slab | December 6, 2004 |
| Level 3 Columns | December 8, 2004 |
| Roof Slab | December 14, 2004 |

Table A.6 Instrumentation Accuracy

| | Precision | Accuracy |
|-------------------------------|-------------------|-------------------|
| Optical Encoders | 0.001 in. | 0.008 in. |
| DC-E-500 LVDT | 0.001 in. | 0.003 in. |
| DC-E-250 LVDT | 0.001 in. | 0.001 in. |
| Wire Potentiometer | 0.001 in. | 0.04 in. |
| Actuator Load Cells | 25 lbs | 25 lbs |
| Survey Readings | .06 in. | 0.1 in. |
| Slab Surface Strains | 600 $\mu\epsilon$ | 600 $\mu\epsilon$ |
| Column Surface Strains | 100 $\mu\epsilon$ | 100 $\mu\epsilon$ |

VITA

VITA

Damon R. Fick was born in Fargo, North Dakota on September 2, 1973. He received his B.S. and M.S. degrees in Civil Engineering from the University of Minnesota in 1997 and 1998. Research for his master's thesis included the instrumentation and vibration monitoring of a steel truss bridge.

Upon completion of his M.S. degree, the author went to work for Opus Architects and Engineers, Inc. as a structural engineer in Minneapolis, MN. In 2004 the writer started the Ph.D. program at Purdue University.